3-31-2015 12:00 AM

Static and Dynamic Response of Silty Toyoura Sand with PVA Fibre and Cement Additives

Colin J.R. Schmidt
The University of Western Ontario

Supervisor
Timothy Newson
The University of Western Ontario

Graduate Program in Civil and Environmental Engineering
A thesis submitted in partial fulfillment of the requirements for the degree in Master of Engineering Science

STATIC AND DYNAMIC RESPONSE OF SILTY TOYOURA SAND WITH PVA FIBRE AND CEMENT ADDITIVES

Thesis format: Monograph

by

Colin Schmidt

Graduate Program in Engineering Science
Department of Civil and Environmental Engineering

A thesis submitted in partial fulfillment
of the requirements for the degree of
Master of Engineering Science

The School of Graduate and Postdoctoral Studies
The University of Western Ontario
London, Ontario, Canada

Abstract

After the Great East Japan Earthquake of 2011, nearly 24 million tons of disaster debris such as concrete products, natural and polymeric fibres, and tsunami deposits remained on the coast of Japan. Much of this debris was recycled and repurposed in engineering projects such as embankments, park restoration, and agricultural field restoration around Tokyo Bay, one of the hardest hit regions of the country. Such a major disaster developed a need for the stabilization of the liquefaction susceptible regions of the reclaimed Tokyo Bay coastline. This thesis specifically focuses on the stabilization against liquefaction of Toyoura sand with the typical silt contents found in the Tokyo Bay region using polyvinyl alcohol (PVA) fibres and Ordinary Portland Cement (OPC). A link between the large strain static and dynamic behavior of the silty sand and the microstructural elements controlling the mechanical response of the amended soil was developed.

On a macro scale (Rowe cell, bender element, & cyclic triaxial tests), trends based on cement content, fibre content, silica flour content, and cyclic stress ratio were developed to aid the prediction of the mechanical response of the soil mixture. On a micro scale (SEM and CT scans, mercury intrusion porosimetry), the pore structure, soil structure and soil fabric were visualized to understand the mechanisms underlying these trends. Results from the many tests performed confirmed that the addition of polymer fibres and cement improve the liquefaction resistance, undrained shear strength, and stiffness of silty and clean Toyoura sand. In general, the results suggest that the addition of silica flour is beneficial until a threshold percentage of 28-35% is reached, after which the soil becomes mechanically unstable and more susceptible to static and cyclic liquefaction. The addition of 0-2% fibres provides minimal improvement in all tests. Cement, as expected, improves the soils stiffness and liquefaction resistance proportional to the addition percentage.

Keywords

The Great East Japan Earthquake, Tokyo Bay, liquefaction, soil stabilization, Toyoura sand, silica flour, silty sand, recycled, Ordinary Portland Cement, PVA fibres, Rowe cell, bender element, cyclic triaxial, computerized tomography, scanning electron microscopy, mercury intrusion porosimetry, cyclic stress ratio, microstructure, macrostructure, critical state line, phase transformation line, permeability.

Abbreviations and Symbols:

Abbreviations:

CRR	Cyclic resistance ratio
CSL	Critical state line
CSR	Cyclic stress ratio
CT	Computerized Tomography
LCC	Limiting compression curve
MIP	Mercury intrusion porosimetry
OPC	Ordinary Portland Cement
PSD	Particle size distribution
PTL	Phase transformation line
PVA	Polyvinyl alcohol
PWP	Pore water pressure
SEM	Scanning Electron Microscopy

Symbols

a_{max}	Peak ground acceleration (L/T^2)
A_L, A_T	Area of the hysteresis loop in cyclic load vs. displacement graph; area of the right triangle within the hysteresis loop
α	Shear wave velocity at mean effective stress of 1 kPa (L/T)
b	Exponent representing curvature of the exponential best fit (Pestana & Whittle, 1995)
B	Skempton's saturation parameter; ratio of change in pore water pressure to change in confining pressure
β	Dimensionless material constant for 1D compression modelling
β_0, β_0*	Exponent related to the sensitivity of the sample to changes in stress, exponent calculated from sample compressibility C_c
β_1	Fitting exponent
c_1	Ratio of constrained modulus/P_a at σ_v'/P_a=1
C_b	Constant that controls elastic stiffness (600-1000)

C_c	Coefficient of curvature, sample compressibility
C_u	Coefficient of uniformity
c_u	Undrained shear strength (F/L^2)
c_v	Coefficient of consolidation (L^2/T)
γ	Surface tension of mercury (0.484 N/m)
γ_b	Bulk density of mercury intrusion porosimetry samples (M/L^3)
Γ	Specific volume of the critical state line at unit pressure
D_{10}, D_{30}, D_{50}, D_{60}	Particle diameters representing 10-60% finer (L)
D_{li}, D_{si}	Diameter of larger and smaller sieves from PSD testing (L)
D	Damping ratio (percentage)
D_r	Relative density
e, e_0, e_{min}, e_{max}, e_{sk}	Void ratio, initial void ratio, minimum and maximum void ratio, skeletal void ratio
E, E_{sec}	Young's modulus, secant Young's modulus from cyclic triaxial testing (F/L^2)
ε_f, ε_a,	Strain to failure for monotonic shearing, axial strain
g	Gravitational constant (9.81 m/s^2)
G, G_{max}, G_{sec}	Shear modulus, maximum shear modulus from bender element testing, secant shear modulus from cyclic triaxial testing (F/L^2)
G_s	Specific gravity
H, H_f, H_0	Sample height, sample height after consolidation, initial sample height (L)
θ, θ_0	Contact angle between sand and mercury (135°), elasto-plastic transition point (0.2-0.7)
I_{total}	Total intrusion volume (L^3)
k	Permeability (L/T)
K_0	Coefficient of lateral earth pressure at rest
κ	Slope of swelling line in e:ln p' space
L_{max}, L_{char}	Length and which conductance is maximum, characteristic length (L)
λ	Slope of normal compression line in e:ln p' space
m	Fitting exponent
m_v	Coefficient of volume compressibility (L^2/F)
M	Earthquake magnitude
M	Slope of the critical state line
M_0	Constrained modulus (F/L^2)
M_{fines}, M_{total}	Mass of fines (<0.075 mm), total mass of solids (M)

n	Porosity
N, N_L	Number of cycles, number of cycles to failure
ν	Poisson's ratio
N	Specific volume of the normal compression line at unit pressure
p'	Cambridge mean effective stress (F/L^2)
P, P_{10}, P_{30}, P_{50}, P_{60}	Pore diameter, pore diameter representing 10-60% finer (L)
P_a,	Atmospheric pressure (100 kPa)
ρ, ρ_{max}, ρ_{min}, ρ_{exp}	Density, maximum and minimum dry density, density used experimentally (M/L^3)
ρ_c	Slope of the NCL in log e-logσ_v' space
q, q_{peak}, q_{res}	Deviator stress (σ_1-σ_3), peak deviator stress, residual deviator stress (F/L^2)
r_d	Stress reduction coefficient
r_u	Excess pore water pressure ratio
SF	Shape factor for Carrier (2003) permeability equation
S_{Lmax}	Fractional volume of connected pore space involving pore widths >L_{max}
σ	Applied intrusion pressure for MIP (F/L^2)
σ_v', σ_c'	Vertical effective stress, effective confining pressure (F/L^2)
σ_{v0}, σ_{v0}', σ_1, σ_3	Total vertical stress, effective vertical stress, major principal stress, minor principal stress,
σ'_{vr}	Reference pressure where the void ratio equals unity (F/L^2)
t_{90}, t_{50}, t_f	Time for 90% and 50% primary consolidation, time to fail in monotonic shearing (T)
T_v	Theoretical time factor for vertical drainage (0.379 for t_{50}, 1.031 for t_{90}) (Head, 1986)
τ	Tortuosity
τ_{static}, τ_{cyclic}	Initial shear stress, applied cyclic shear stress (F/L^2)
u	Pore water pressure (F/L^2)
ϕ', ϕ'_{cs}, ϕ'_i	Internal friction angle, critical state friction angle, instability line angle
φ	Dilation angle
V_{hp}, V_{voids}, V_{solids}, V_b,	Volume of hydration products, void volume, volume solids, back volume
V_0	Initial volume of sample (L^3)
V_s	Shear wave velocity (L/T)
V_p	P-wave velocity (L/T)

Acknowledgements

First and foremost I would like to thank my supervisor, Dr. Timothy Newson, for his unwavering support and encouragement as I progressed through my degree. It has been a challenging and enlightening journey and his guidance and expertise has been wholly appreciated.

To my colleagues in Fukuoka University, Kenichi Sato, Miho Nakamichi, and Takuro Fujikawa, thank you for your time and effort. Your help, guidance, support, and lab work has been of incalculable help.

Many thanks to the laboratory technicians and staff at Western for their help and guidance: Whitney Barrett, Brad Kobe, Stephanie Lawrence, Melodie Richards, Tim Stephens, Erol Tas, and Joseph Umoh.

To all my friends at Western that have stayed by my side over the last six years of my education here, I could not have done it without you. My basement lab would have been sad and lonely without your visits, and you have definitely kept my spirits up and my mind motivated.

I would of course also like to thank my parents for their constant love and support throughout my two and a half years as a master's student. Their belief in my success was my motivation to persist and without them I would not be where I am today.

Contents

List of Tables

List of Figures

CHAPTER 1: Introduction

1. Introduction

1.1. Background

Natural disaster mitigation and management is a massive and complex field in engineering. Every year, earthquakes, tsunamis, and floods etc. cause catastrophic loss of life, homes and other societal infrastructure, and billions of dollars, especially in susceptible regions such as Japan (Japan MOE, 2014). Mitigation techniques involving the reuse of debris and waste from these disasters, have attempted to reduce the volume of material incinerated and sent to landfills, and have been successfully adapted to help prevent liquefaction of soils, destabilization of foundations, and flow failures of earth structures (Bhattacharya et al., 2011). Primarily, in terms of geotechnical engineering in Japan, the focus has been on the recycling of concrete and wood products during rebuilding phases. These waste products have been used for roadbeds, embankments, dikes, and stabilizing the 35,000 km Tokyo Bay coastline against liquefaction after the 2011 Great East Japan Earthquake (The World Bank, 2014). On a smaller scale, the aforementioned recycled waste products can also be used to stabilize dynamically susceptible soils beneath structures subjected to any dynamic or vibratory load such as roads, train tracks, generators, and skyscrapers.

Reclamation of the Tokyo Bay region of Japan began in the 17th century, reaching completion in the late 20th century (Yasuda, Haradai, Ishikawa, & Kanemaru, 2012). Soils were dredged from the bottom of the sea and consisted primarily of Toyoura sand and 3-42% silt (Yasuda, Haradai, Ishikawa, & Kanemaru, 2012). The silty sand mixtures in the Tokyo Bay region are susceptible to liquefaction caused by seismic loads, and the stabilization of these soils provides the basis for experimentation in this thesis.

1.2. Seismicity in Japan

Japan has seen more than 47 earthquakes of magnitude 6.3 or greater since 1891 when their official recordings began, of which ten have been greater than magnitude 8.0 (Richter magnitude) (USGS 2012). Only seven earthquakes worldwide have been recorded as magnitude 9.0 or greater, the largest of which occurred in Chile 1960 (M=9.5), Alaska 1964 (M=9.2), Sumatra 2004 (M=9.1), Kamchatka 1952 (M=9.0), and Japan 2011 (Great East Japan Earthquake M=9.0) (USGS, 2012). Since Japan lies in the Pacific Ring of Fire, a region that sees around 80% of the world's largest earthquakes, it is one of the most seismically active countries in the world. The number and magnitude of earthquakes from 1900 to 2012 can be seen in Figure 1.1. Recent studies suggest that slow-motion tectonic slips along the coast of Japan can lead to further increases in annual quakes, and since the frequency of earthquake occurrences already is nearly triple that of pre-2011; the likelihood of another large earthquake in the near future has increased to nearly 17% (Hecht, 2014).

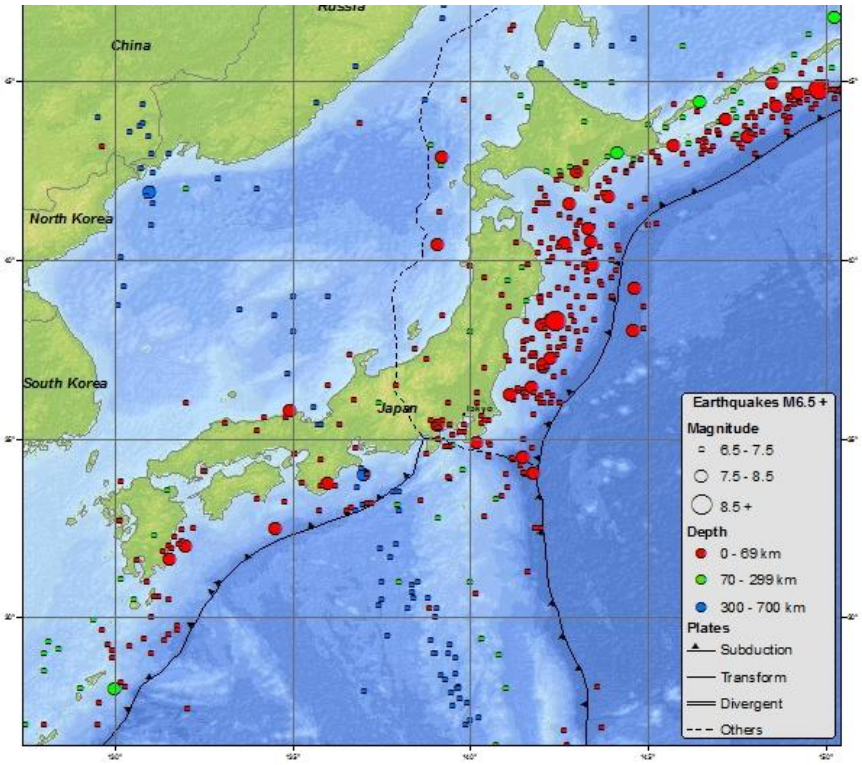

Figure 1.1. Seismicity map of Japan (USGS, 2012)

1.2.1. The Great East Japan Earthquake

On March 11, 2011, 2:46pm JST the Great East Japan Earthquake occurred at a depth of 32 km. The epicenter of this magnitude 9.0 earthquake was located at 38.297°N, 142.372°E, just 72 km east of the Tohoku region of Japan. Peak ground accelerations hit 3.18 g (31.2 m/s^2) in some areas of Japan (Figure 1.2). However, the feature that made the Great East Japan Earthquake so destructive and catastrophic was the nearly six minute duration of the initial earthquake and immediate aftershocks, caused primarily by the 80 m translation of the crustal plates and massive energy releases (World Health Organization, 2012). The tremor itself released enough energy (1.9×10^{17} Joules) to shift the earth's rotational axis 10 cm and the whole of Honshu Island 2.4 m east (Aon Benfield, 2011). This convergence of two major crustal plates as shown in Figure 1.3 caused a major up-thrust and the resulting 10 m high tsunami was the primary cause of destruction in northeastern Japan, during which over 18,500 people were killed with over 6,100 reported injured and 2,600 more missing (World Bank, 2014). Economic losses were of the order of $210 Billion USD (¥16.9 trillion) (Japan MOE, 2014). Over 1,200 aftershocks occurred in the first six months after the earthquake, with nearly seventy of them being magnitude six or higher (Aon Benfield, 2011).

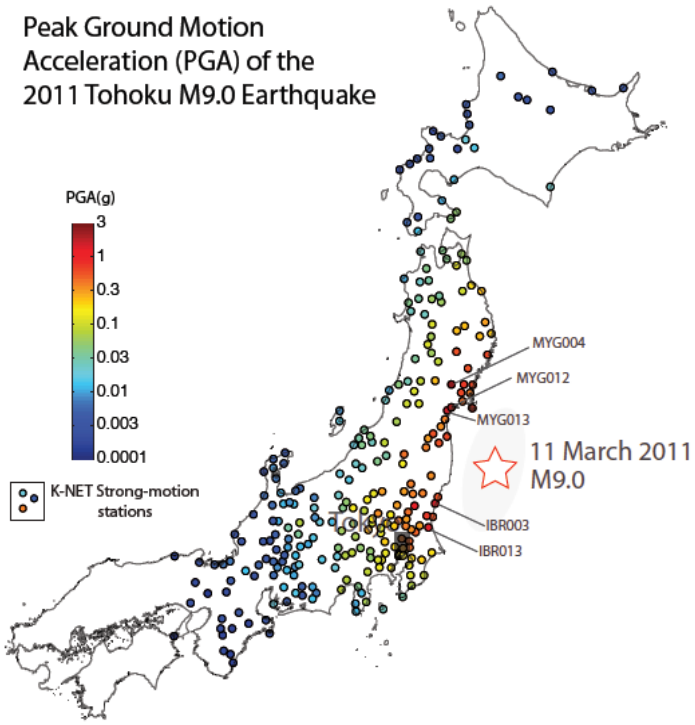

Figure 1.2. Peak ground acceleration map during the 2011 Great East Japan Earthquake (Kalkan, 2011)

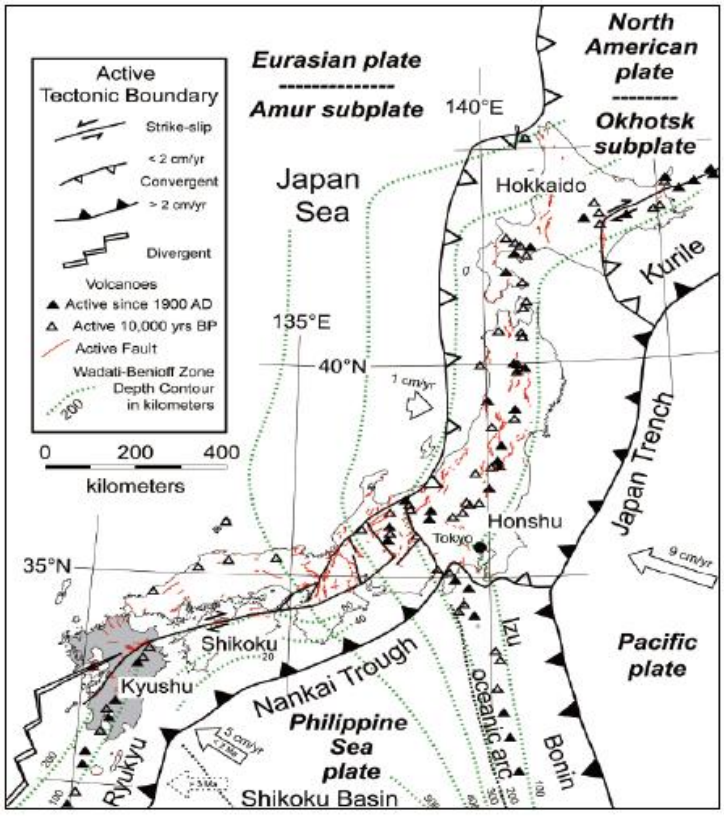

Figure 1.3. Active tectonic plates near Japan (Aon Benfield, 2011)

1.2.2. Structural Damage and Waste

The Great East Japan Earthquake led to over 197 separate landslides and many incidents of building subsidence due to liquefaction (mostly of non-engineered buildings or structures built prior to 1981). The liquefied materials were mainly engineered fills and geologically young alluvia such as silty Toyoura sand, which exhibited liquefaction in the form of slope failures, sand boils, water spouting, and excessive settlement. Actual liquefaction zones around Tokyo Bay and maps of liquefied and damaged regions of Japan are shown in Figure 1.4 and 1.5 respectively (Yasuda et al., 2012; Aon Benfield, 2011). Nearly 85% of Urayasu City's coast was liquefied; the worst hit city in Japan. Specifically in the Tokyo Bay region, scientists were shocked at the severity and extent of liquefaction of the silty sand and fill materials after the Great East Japan earthquake, despite previous compaction efforts and liquefaction mitigation methods (Yasuda, Haradai, Ishikawa, & Kanemaru, 2012).

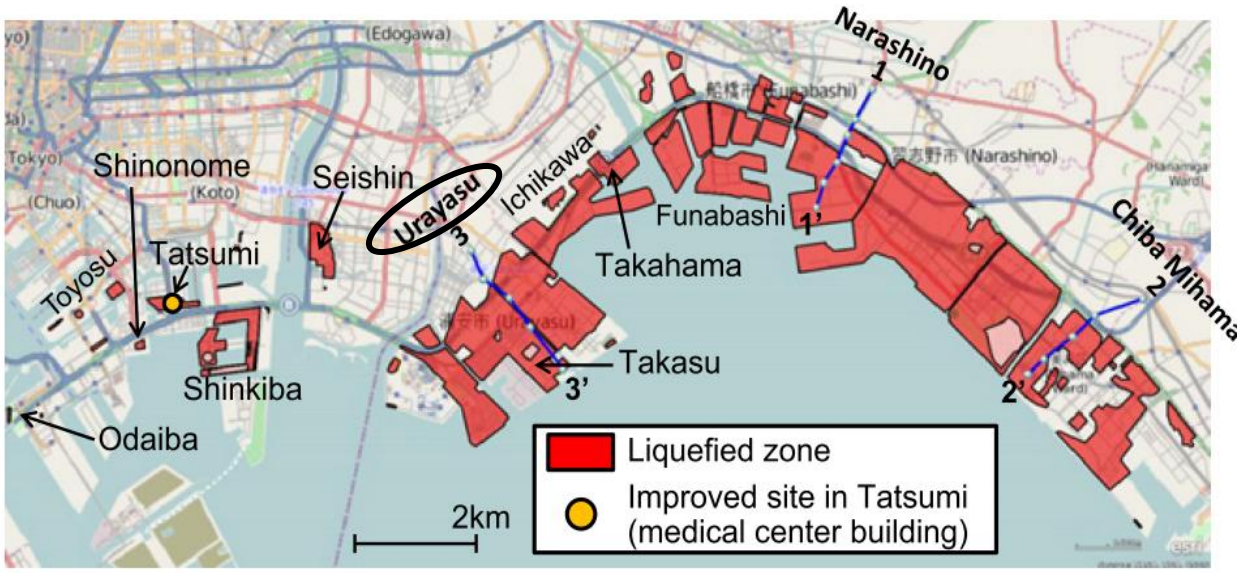

Figure 1.4. Liquefied regions around Tokyo Bay (Yasuda et. al, 2012)

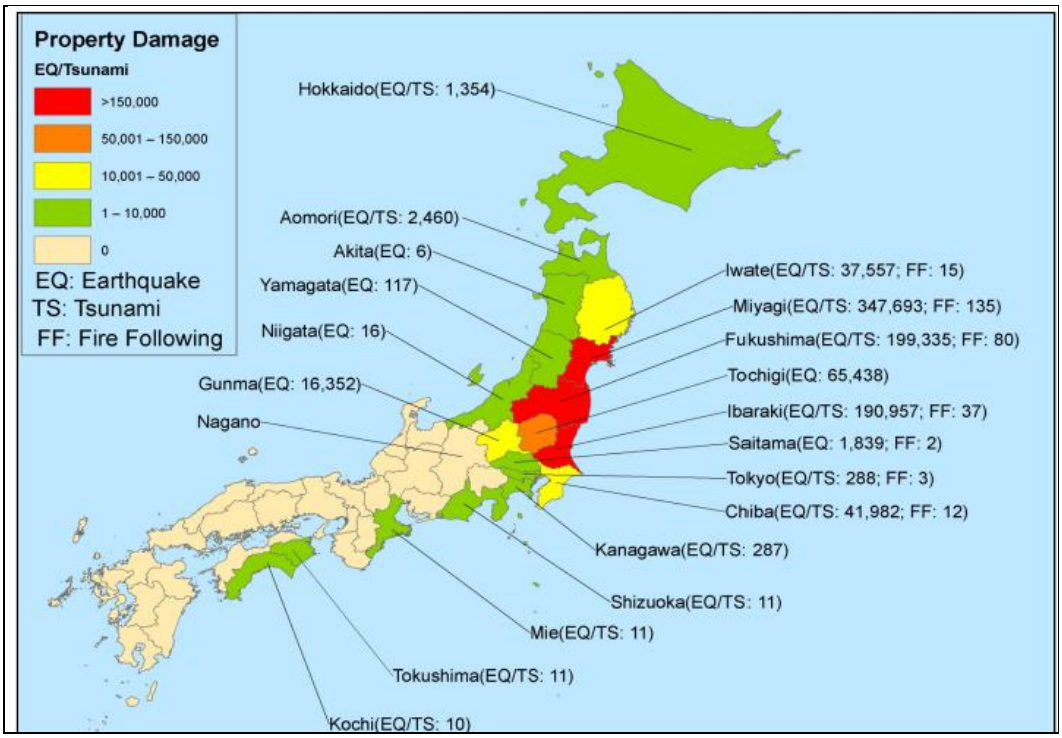

Figure 1.5. Post-earthquake property damage in Japan (Aon Benfield 2011)

The most heavily damaged prefectures were Iwate, Miyagi, Fukushima, and Ibaraki (Figure 1.5), much of which will never be rebuilt. Nearly 300,000 buildings were destroyed, and over 1 million more damaged, which created over 24 million tons of debris including 9.59 million tonnes of tsunami deposits (Japan MOE, 2014). Wood, concrete, and plastic products have been recycled and reused whenever possible to limit how much of this waste was sent to landfills. As of February 28, 2014, nearly 96% of the debris had been cleared from the four heaviest hit prefectures and much of this debris will be used in various engineering projects. Waste audits (Figure 1.6) estimated that the repurposed debris consisted of approximately 59% construction materials, 8% raw cement fuel, and 14% metal products, with the remaining 20% being incinerated (Azuma, 2013). Some of this recycled material has been used as stabilization for various earth works projects and to reduce instances of liquefaction throughout the country (see Figure 1.7).

Figure 1.6. Great East Japan Earthquake tsunami debris and waste audits (Johnston, 2013)

	Project	Recycled Material	Amount (including planned use) (x10,000 tons)
Iwate Prefecture	Coastal or river embankment restoration	Tsunami deposits Concrete debris	30
	Coastal disaster-prevention forest restoration	Tsunami deposits Concrete debris	16
	Agricultural field restoration	Tsunami deposits Concrete debris	64
	Park construction	Tsunami deposits Concrete debris	43
	Fishing port projects	Concrete debris	17
	Construction of temporary storage sites	Concrete debris	48
	Other projects	Tsunami deposits Concrete debris	77
Miyagi Prefecture	Coastal or river embankment restoration	Tsunami deposits Concrete debris	103
	Coastal disaster-prevention forest restoration	Tsunami deposits Concrete debris	110
	Agricultural field restoration	Tsunami deposits Concrete debris	15
	Park construction	Tsunami deposits Concrete debris	262
	Fishing port projects	Concrete debris	29
	Construction of temporary storage sites	Tsunami deposits Concrete debris	89
	Other projects	Tsunami deposits Concrete debris	114
Fukushima Prefecture	Coastal or river embankment restoration	Concrete debris	9
	Coastal disaster-prevention forest restoration	Concrete debris	9
	Park construction	Tsunami deposits	14
	Other	Concrete debris	16

Figure 1.7. Recycled debris used in Japanese engineering projects in Iwate, Miyagi, and Fukushima prefectures (Japan MOE 2014)

1.3. Liquefaction Mechanisms and Phenomena

Liquefaction of soil is a common geotechnical engineering problem and has been studied continuously since the late 1910s, with a large engineering focus in the 1960s after the Niigata and Alaska earthquakes of 1964 (C.A.C., 2012). It can be precisely defined as "…a phenomenon wherein a mass of soil loses a large percentage of its shear resistance when subjected to monotonic, cyclic, or shock loading, and flows in a manner resembling a liquid until the shear stresses acting on the mass are as low as the reduced shear resistance" (Sladen et. al. 1985). Relevant phenomena are classified as flow liquefaction, cyclic softening, cyclic liquefaction, or cyclic mobility, all of which are associated with the different methods and stages of excess pore water pressure build-up in granular soils (Robertson & Fear, 1995). Accumulation of this excess pore water pressure in saturated, undrained (or poorly drained) soil samples is associated with the deterioration of the soil structure and large reductions in undrained shear strength. As the pore pressure approaches the confining pressure, stress begins to transfer from the soil skeleton to the pore water, which does not offer shear resistance (Equation 1.1):

$$\boldsymbol{r_u = \frac{\Delta u}{\Delta \sigma_3'}} \qquad \textbf{[1.1]}$$

where r_u is the excess pore water pressure ratio, u is the pore water pressure, and σ_3' is the effective confining pressure. When there is no longer enough interparticle friction, the soil structure collapses and experiences flow deformation that can cause settlement, translation of earth structures, slope failures, sand boils, and sinkholes, all of which are evidence of cyclic mobility and liquefaction. In the case of dense granular materials, initial dilation of particles tends to expedite drainage and improve liquefaction resistance (Idriss & Boulanger, 2006). Liquefaction phenomena seen across much of Japan following the 2011 earthquake have been related to the engineering properties of the soil, and methods of preventing future liquefaction of these soils have been frequently proposed and studied.

1.4. Laboratory Determination of Liquefaction Susceptibility

The most common measure of liquefaction resistance, the cyclic resistance ratio (CRR), is the CSR required to develop a pore water pressure ratio (r_u) of 1.0 or reach a certain strain percentage (often defined between 1-10% axial strain) in 15 cycles for an equivalent magnitude 7.5 earthquake (e.g. Youd & Idriss, 2001; Boulanger & Idriss, 2006). Other criteria for liquefaction susceptibility include the "Chinese Criteria" proposed by (Wang, 1979) and modified by (Andrews and Martin, 2000; Seed et. al., 2003; Bray et. al., 2004) based on the fines content of the soil, the liquid and plastic limits of the fines, and the initial moisture content of the soil.

1.4.1. Effects of Silty Fines on Liquefaction

It is commonly known that the soils most susceptible to liquefaction are loose to medium dense sands, silts, and silty sands. However, some unique soils such as Leda Clay may also liquefy due to increases in pore water pressure that cause structural collapse (Rasmussen, 2012). Studies of regions that liquefied during major earthquakes such as San Francisco, U.S.A. (1989), Adapazari, Turkey (1999), Christchurch, New Zealand (2011), and Tokyo Bay, Japan (2011) have shown silt contents as high as 50%. Data gathered from these sites and other similar sites has caused an increase in research into the static and dynamic behavior of silty sands, especially with regard to liquefaction during earthquakes.

1.4.2. Effects of Soil Amendments on Strength and Liquefaction

Soil improvements and stabilization techniques have been studied since the early 1900s, with cement being used to improve roadbeds in the United States as early as 1935 (C.A.C., 2012). The use of fibers is a more recent development in soil stabilization, and dozens of materials from natural plant fibers to engineered polymeric fibers have been examined (e.g. Freitag, 1986; Gray, 1986-88; Michalowskia et. al., 1990; Ghiassian & Ghazi, 2009) and more. These amendments can improve the ultimate undrained shear strength of soils (Figure 1.8), reduce the likelihood of shearing planes developing in slopes, and increase the liquefaction resistance of soils during static or dynamic loading events.

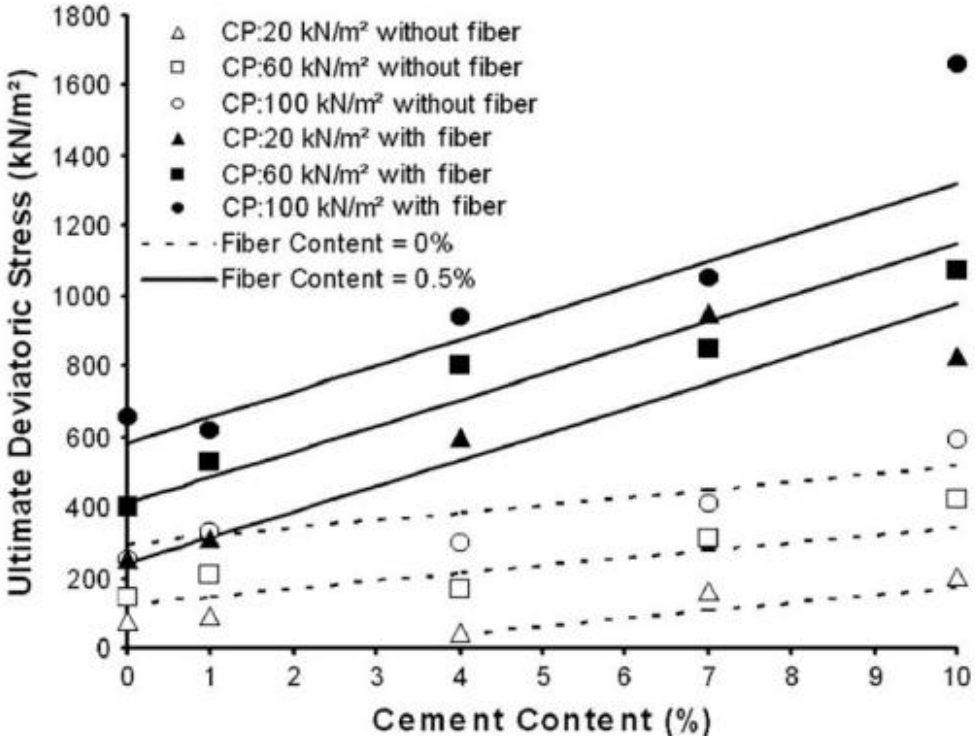

Figure 1.8. Peak deviator stress vs. cement content from consolidated undrained triaxial tests on cement and fibre reinforced Osorio Sand from southern Brazil at various confining pressures (Consoli, Vendruscolo, Fonini, & Dalla Rosa, 2009)

Despite the wide range of fibre contents and cement contents that have been studied in various sand behavioural studies, minimal research has been performed on the effects of these additives in mixed soils such as silty sands.

1.5. Aims of Study

Limiting the effects of flow failure and liquefaction of silty sands has become an important task for geotechnical engineers especially in seismically prone regions such as Japan. Although extensive research has been performed on the mechanical behaviour of Toyoura sand, silty sands, and stabilized pure sands, the effect of OPC and PVA fiber stabilizers on the liquefaction resistance and flow properties of Toyoura sand and silt mixtures is minimal. This thesis will explore the effects of varying non-plastic silt content in stabilized and unstabilized Toyoura sand on the soil's microstructure, shear wave velocity, shear modulus, compressibility, permeability, and liquefaction resistance. It will also evaluate the links between the microstructural properties found from CT scanning, MIP testing, and SEM imaging, and the mechanical responses from large and small strain testing under monotonic and cyclic loading. This thesis is intended to determine how these stabilizers work, and how and why their effectiveness may be altered by the addition of silty fines.

Overall, the aims of this thesis are:

- to investigate the basic geotechnical properties of sand and silt mixtures stabilized with Ordinary Portland Cement (OPC) and Polyvinyl Alcohol (PVA) fibre;
- to develop a database of the mechanical behaviour of these mixtures when subjected to static and dynamic loads;
- to determine the permeability, compressibility, shear deformation responses of the mixtures;
- to determine the resistance to flow failure, cyclic mobility, and liquefaction of the mixtures;

- to explore the links between the microstructure of the stabilized silty Toyoura sand and the mechanical behavior of these mixtures during monotonic and dynamic loading.

1.6. Thesis Objectives

To achieve the aims outlined in Section 1.5., experimental tests on the micro and macrostructural behaviour of the Toyoura sand mixtures were performed. The objectives were met as follows:

- Direct shear, oedometer, constant head permeability, sieve analysis, and hydrometer were conducted,
    - to determine the engineering properties of Toyoura sand and silica flour;
    - to provide comparison with values found in the literature;
    - to validate the results of the cyclic, monotonic, and one dimensional shearing testing.
- Scanning electron microscopy, computerized tomography, and mercury intrusion porosimetry were conducted,
    - to characterize the microstructure of the stabilized, silty Toyoura sand and the mechanical behavior of the mixtures;
    - to understand the pore and skeletal structure of the stabilized samples;
    - to provide qualitative information regarding the sand, silt, cement, and fiber interaction after cement hydration;
    - to enable estimation of the void volumes;
    - to explain why cement and fibres have a stabilizing effect on the Toyoura sand mixtures.
- Rowe cell, bender element, and cyclic triaxial were conducted,
    - to evaluate the effectiveness of recycled OPC and PVA fibres as soil stabilizers;

- to characterize small and large strain behavior of the Toyoura sand with varied silt and stabilizer percentages.

Overall, these tests have been done to establish insight into the stabilized behavior of Toyoura sand during relevant static and dynamic loading events.

1.7. Collaboration with Fukuoka University

Through collaboration with Fukuoka University, the effects of silt, cement and fibre addition have been further documented. Shared research between Western University and our colleagues in Japan has allowed the analysis of broader ranges of silt percentages, fibre lengths, and materials, cement contents, and cyclic stress ratios (CSR). The upper range of silt content found in Tokyo Bay (21-42%) was analyzed in this thesis, whereas 0-14% silt content was analyzed at Fukuoka University in Japan. Some of these results were combined to achieve a more complete data set and will be combined in subsequent publications by the two laboratory groups.

1.8. Chapter Summary

This thesis contains five chapters, organized in a monograph format as follows:

Chapter 2: This chapter explains the geological history of Toyoura sand, and its basic engineering properties. It outlines the current knowledge of the large and small strain behavior of sands on a macro and micro scale, and the effects of cementitious and fibrous materials on the stabilization of granular soils against dynamic and static loading.

Chapter 3: Chapter 3 describes the properties of the materials used for the laboratory testing and the tests that were performed. It explains the rationale behind each testing method and the phases of sample preparation and sample sizes used for the SEM tests, CT scans, MIP tests, Rowe cell, oedometer, direct shear, bender element, and cyclic triaxial tests.

Chapter 4: This chapter contains all of the qualitative soil structure imagery obtained from SEM and CT scans, as well as the quantitative data from MIP testing. All of the results obtained from large (>1%) and small strain (~0.001%) laboratory mechanical tests are analyzed and presented graphically to determine the trends and the effectiveness of PVA fibre and OPC additives as soil stabilizers.

Chapter 5: The final chapter draws conclusions from the results of Chapter 4 and explains why Toyoura sand behaves as it does when mixed with silica flour, Ordinary Portland Cement, and PVA fibres and how these trends can be used in various engineering applications. The suitability of these materials as stabilizers against static and dynamic loads, specifically in the Tokyo Bay region of Japan, is critically evaluated.

CHAPTER 2: Literature Survey

2. Literature Survey

2.1. Introduction

Toyoura sand has become a benchmark sand for geotechnical engineers. Its properties have been well defined and documented with respect to static and dynamic load response, and its behavior is well understood (Meneses-Loja, Ishihara, & Towhata, 2000). One aim of this thesis is to further explore how Toyoura sand behaves in response to cyclic and static loads when combined with silt, cement, and fibre additives. In particular, the flow properties and liquefaction resistance of stabilized silty sands will be explored. The intent of the following literature survey is to provide an overview of Toyoura sand specifically, including its origin and engineering properties, its micro- and macrostructure, and its large and small strain behavior. The effect of cement and fibre additives on the behaviour of this sand when subjected to static and dynamic loads will also be examined.

2.2. Geological History of Toyoura Sand

Japan has been dominated by the subduction of the Pacific plate along with the Eurasia, Amur, Okhotsk, and the Philippine Sea plates. The interaction between these plates makes Japan prone to seismic and volcanic activity. Toyoura sand can be found near the coastal rim of the Pacific Ocean. Sea floor spreading and weathering due to the constant presence of water are all contributing factors that lead to the formation of Toyoura sand, which is primarily composed of 75% quartz, 22% percent feldspar and 3% percent magnetite (Tarnawski, Momose, & Leong, 2011).

2.3. Basic Properties of Toyoura Sand

Toyoura sand is a sub-angular to angular sand (Lam & Tatsuoka, 1988; De & Basudhar, 2008). It is characterized as a poorly graded sand (SP) under the Unified Soil Classification System. The peak friction angle of Toyoura sand ranges from 33.5-43.7° for very loose and very dense states respectively. Toyoura sand has a D_{10} ranging from 0.12-0.17 mm, a D_{30} between 0.14-0.18 mm and a D_{50} from 0.16-0.206 mm, which indicates that it is very fine sand. Using this data, the coefficient of uniformity (C_u) and coefficient of curvature (C_c) were found to range from C_u=1.29-1.7 and C_c=0.95-1.0 respectively (e.g. Bellotti et. al. 1997, HongNam, Koseki & Sato, Hyodo et. al. 1994, Koseki et. al. 1999, Oda 1977, Wang et. al 2002, & Whitlow 2001). These values suggest a poorly graded sand with very uniform distribution. The specific gravity (G_s), like many silicate sands, ranges from 2.64-2.65; the addition of silica flour lowers this value slightly.

There is some discrepancy between the recorded minimum and maximum void ratio of Toyoura sand, which ranges from e_{min}=0.635-0.597 and e_{max}=0.990-0.954, corresponding to dry densities of ρ_{max} of 1.619-1.65 g/cm^3 and ρ_{min} of 1.330-1.355 g/cm^3 respectively (Koseki et al., 1999; Oda, Takemura, & Takahasi, 2004). This suggests that the method of sample preparation (air pluviation versus funneling) and compaction (vibration table versus hand compaction), as well as the origin of the sand, can alter the recorded void ratios.

These engineering properties of Toyoura sand make it quite susceptible to liquefaction, posing a threat to any structures built on this soil. In the Tokyo Bay region of Japan, for example, this soil was found to have liquefied in multiple locations and is commonly studied due to this susceptibility.

2.4. Critical State Parameters of Toyoura Sand

The critical state friction angle (ϕ_{cs}) of Toyoura sand has been found to be between 33° and 35.1° (De & Basudhar 2008; Pradhan, Tatsuoka & Horii, 1988). The critical state parameters of Toyoura sand are as follows: the specific volume of the normal compression line at unit pressure N=0.87, the slope of the compression line λ=0.02-0.05, the slope of the swelling line κ=0.0064, the specific volume of the CSL at unit pressure Γ=0.83-0.86 (Cam Clay model), the slope of the critical state line M=1.30 and Poisson's ratio υ=0.30 (Yang, Li, & Yang, 2008). A graph of the critical state void ratio (e_c) versus normalized effective mean stress (p'/p_a) showing the critical state line of various sands can be seen in Figure 2.1.

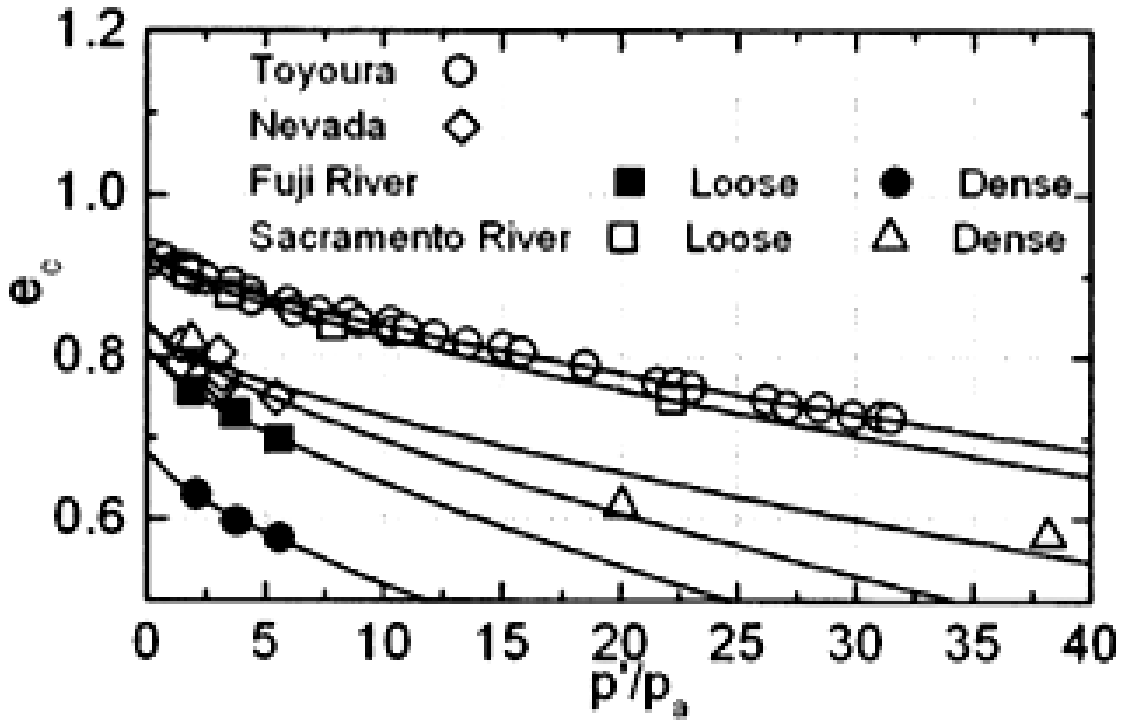

Figure 2.1. Critical state line (CSL) of Toyoura sand compared to Nevada, Fuji, and Sacramento River sand (Ling & Yang, 2006)

2.5. Microstructure of Unstabilized and Stabilized Sand

Tatsuoka et. al. (1979) verified through twenty one methods that the liquefaction potential of sand is unrelated to the sample preparation method if it is performed correctly and consistently. Through x-ray computed tomography, accurate models, and images of Toyoura sand, shear bands during testing have been visualized as shown in Figure 2.2. These images show that the microstructure of the Toyoura sand changes dramatically, while non-elastic deformation accumulates in shear bands (Oda, Takemura & Takahasi 2004). Large voids are produced in the sand as a result of dilatancy and changes in particle orientation at the shear band boundaries. These large voids allow for the rapid destabilization of loose sands, increasing the likelihood of liquefaction and reducing the effective bearing capacity of the sand.

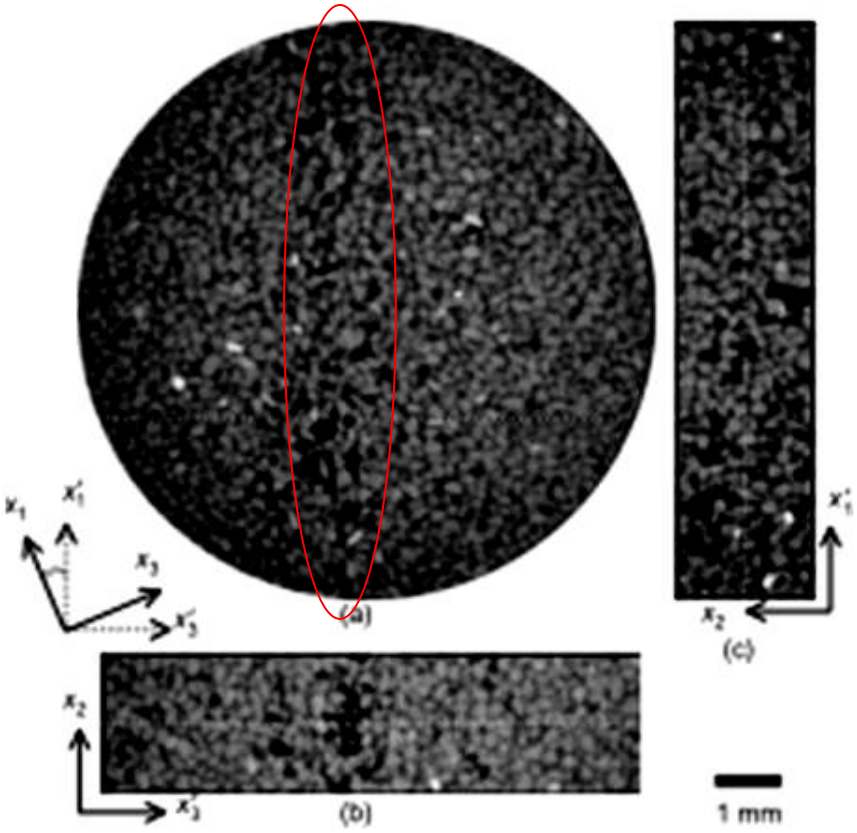

Figure 2.2. CT image of shear banding in Toyoura sand (Oda, Takemura, & Takahasi, 2004)

Toyoura sand's moderate liquefaction resistance and high undrained shear strength are caused, in part, by the roughness and surface angularities of the sand grains. This has been supported by the microstructural imaging of the shear band initiation and development, and through discrete element modeling. Many other researchers have also examined the microstructure of cement stabilized sands to determine the mechanisms of chemical and mechanical bonding between the sand particles (Figure 2.3) due to cement hydration (Bullard, et al., 2010). The effects of the addition of polymer, natural, or steel fibres on the microstructure of cemented sands has been less thoroughly examined, though a significant amount of work has been done on the effects of these fibres on concrete strength and stiffness (Uygunoglu, 2008; Mehta & Monteiro, 2013).

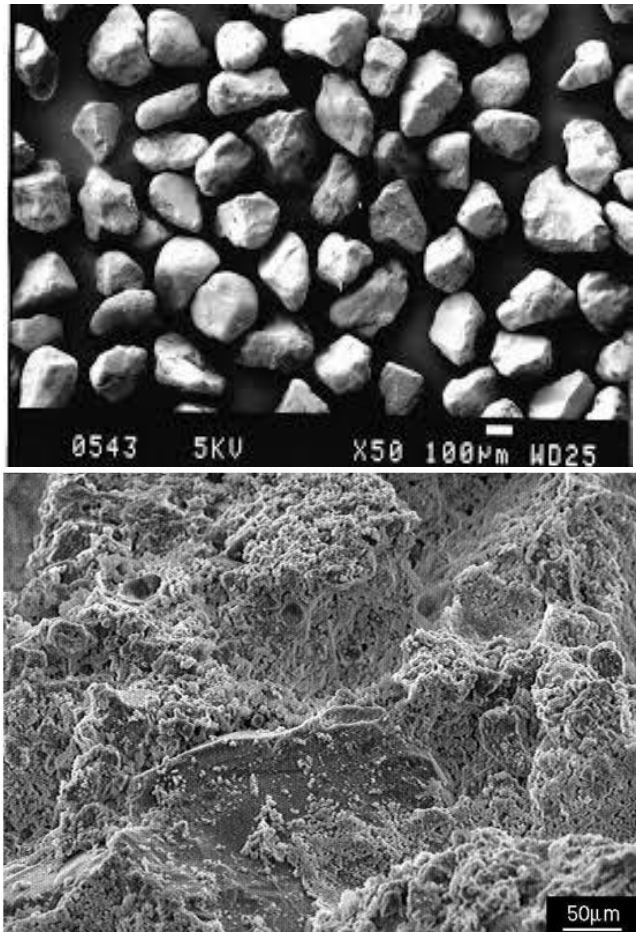

Figure 2.3. Microstructure of a) sand b) cemented sand (SEM/EDC of Cement and Concrete, 2014)

2.6. Large and Small Strain Behaviour of Sand and Silty Sand

Toyoura sand will contract continually when packed loosely and subjected to monotonic shearing, but will experience an initial period of contraction followed by dilation when packed densely (Hyodo, Tanimizu, Yasufuku, & Murata, 1994). At the same initial void ratio and various confining pressures, the yield surface will grow but the same steady state point will eventually be reached in q-p' space (Figure 2.4a). The same behaviour can be seen for low plasticity silt, though the stress-strain behaviour and pore pressure generation is quite different from that of the sand (labeled Silt #1 in Figure 2.4b).

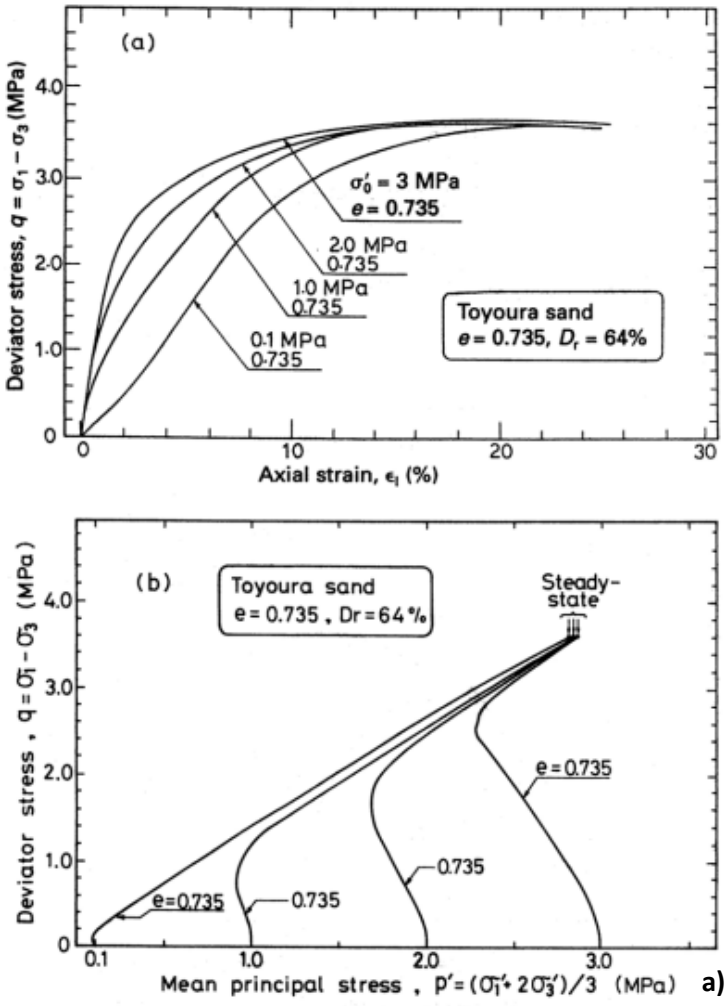

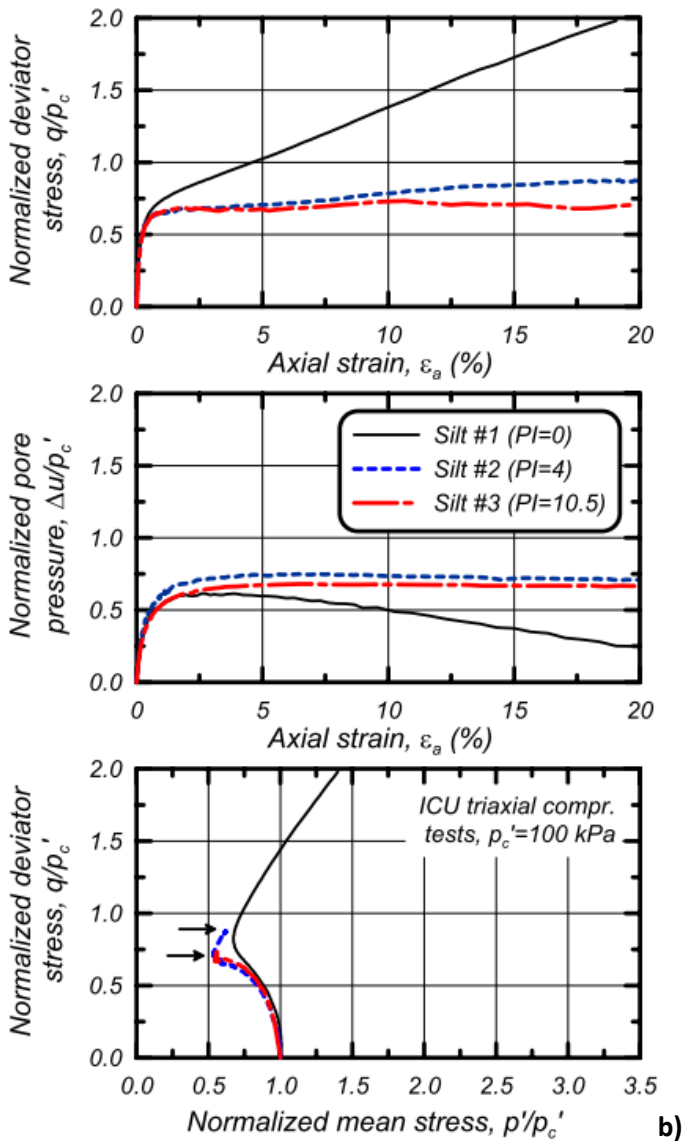

Figure 2.4. Stress-strain behaviour of a) Toyoura sand; b) medium dense silt with varied plasticity (Boulanger & Idriss, 2004)

When sheared, granular materials tend to exhibit elastic behaviour until reaching an initial yield surface (Schofield & Wroth, 1968). Each soil has a unique critical state line that the effective stress path will approach regardless of initial confining pressures, above which the soil is contractive and below which the soil is dilative (Been et al., 1991; Ishihara, 1993; Verdugo & Ishihara, 1996). At low pressures medium dense sand has minimal contractiveness, thus dilation dominates the soil behaviour after passing the phase transformation line (PTL) and the stress path drifts toward higher effective stress

values and the deviator stress increases toward a steady state. At medium stress levels, contraction behaviour tends to dominate, and positive excess pore pressure increases causing the stress path to approach and track along the plastic yield surface and with the pore pressure continuing to increase, the sample reaches the PTL (Ishihara et al. 1975). At this point, the suppressed dilation causes negative pore pressures and the stress path increases linearly until steady state conditions are reached. Finally, at high confining pressures, continuously increasing pore pressure causes the effective stress path to constantly track to the left, reach a peak deviator stress, and then decline until it reaches steady state along the failure surface. At the point in the shearing phase where no further stress or volume changes occur with changing axial displacement, there exists the critical state line (CSL) (Yamamuro & Lade, 1998).

In the case of low and medium confining stresses at the point where the failure surface is reached, either strain hardening or strain softening behaviour can be seen due to the soil's instability (Yamamuro & Lade, 1998). During strain hardening, wet of the critical state line, the yield surface expands and the soil is only able to deform plastically if the deviator stress continues to increase. At this stage, deformation occurs without any significant change in sample volume or shear stress. Dry of the critical state line, softening behaviour (i.e. the loss of strength and stiffness and shrinking of the yield surface with increasing strain (Coduto, Yeung, & Kitch, 2011)) is seen accompanied by volume dilatancy at the point when the stress path reaches the yield surface. At this point the phase transformation line in stress space has been encountered, where the soil behaviour transitions from compressive to expansive (Lade & Ibsen, 1997) for a certain stress ratio. This phase transformation line has also been derived in q vs. p' plots from cyclic triaxial testing in Section 4.7. These key behaviours can be documented using triaxial monotonic or cyclic shearing.

From bender element tests, the characteristic frequency of Toyoura sand was found to range from 2444-3443Hz, again dependent on void ratio and confining pressure (Youn, Choo, & Kim, 2008;

Whitlow, 2001). Youn, Choo, & Kim (2008) also determined that the shear wave velocity (V_s) of Toyoura sand ranged from 220-360 m/s when dry, and 170-340 m/s when fully saturated (B value > 0.96). Using bender elements, the P-wave velocity (V_p) was found to be dependent on sample porosity (n), soil skeleton, Poisson's ratio (ν), and saturation level (Wang et. al. 2002), and ranged from 500-2000 m/s for Toyoura sand. Again from bender element tests, the small strain shear modulus G_{max} was determined to range from 50-250 MPa. This value was found to be a function of confining pressure, relative density of the sample, and the isotropy conditions (Bellotti et. al. 1997, Wang et. al. 2002). The shear modulus was found to drop to between 60-200 MPa when anisotropy was considered (Builes, Garcia & Riveros 2008).

In terms of large strain cyclic triaxial testing (e.g. Nakamichi & Sato, 2013), Toyoura sand is weaker in extension than compression, has a phase transformation line with a slope of roughly 1.33 in compression and 1.0 in extension, and follows the expected transformed sinusoidal curve for excess pore water pressure as shown in Figure 2.5c below. When stabilized with cement and polymer fibres (as will be discussed in Section 2.9) the liquefaction resistance clearly improves as shown in Figure 2.5d. Cement and polymer fibres have most commonly been used at dosage rates of 0-12% and 0-6% respectively in the literature (Ingles & Metcalf, 1973; Gray D. H., 1988). Cement addition of 2% can more than triple the liquefaction resistance depending on curing time and initial density, as shown in Figure 2.5d.

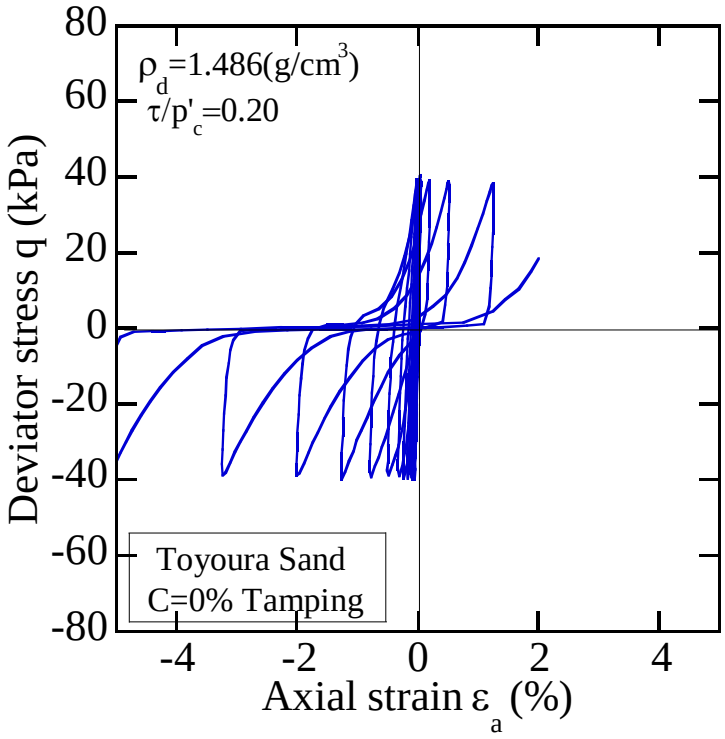
80
60
40
20
0
-20
-40
-60
-80
-4
-2
0
2
4
ρd=1.486(g/cm3)
τ/p'c=0.20
Toyoura Sand
C=0% Tamping
Deviator stress q (kPa)
Axial strain εa (%)

a)

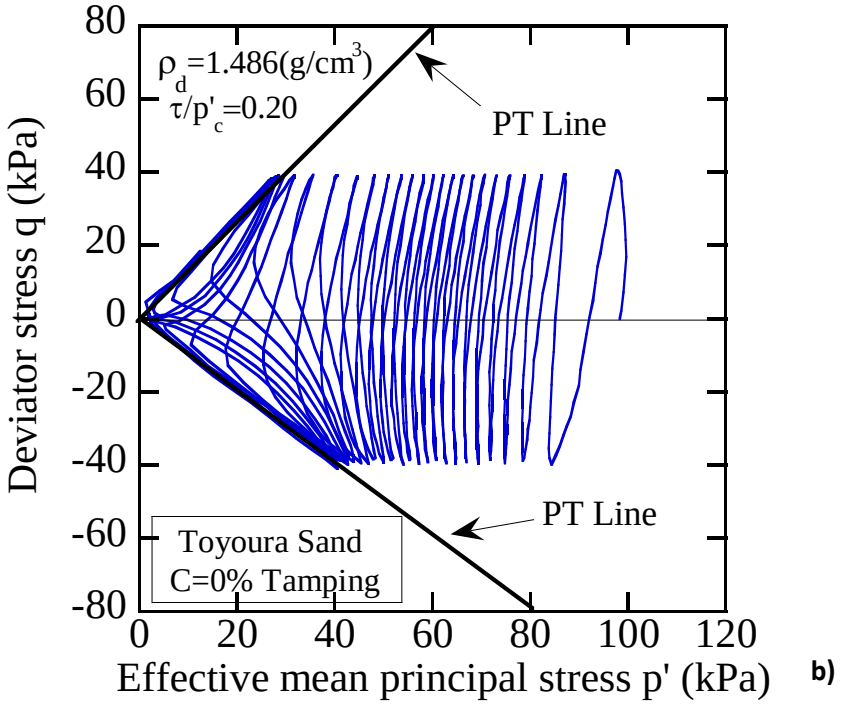
80
60
40
20
0
-20
-40
-60
-80
0
20
40
60
80
100
120
ρd=1.486(g/cm3)
τ/p'c=0.20
PT Line
PT Line
Toyoura Sand
C=0% Tamping
Deviator stress q (kPa)
Effective mean principal stress p' (kPa)

b)

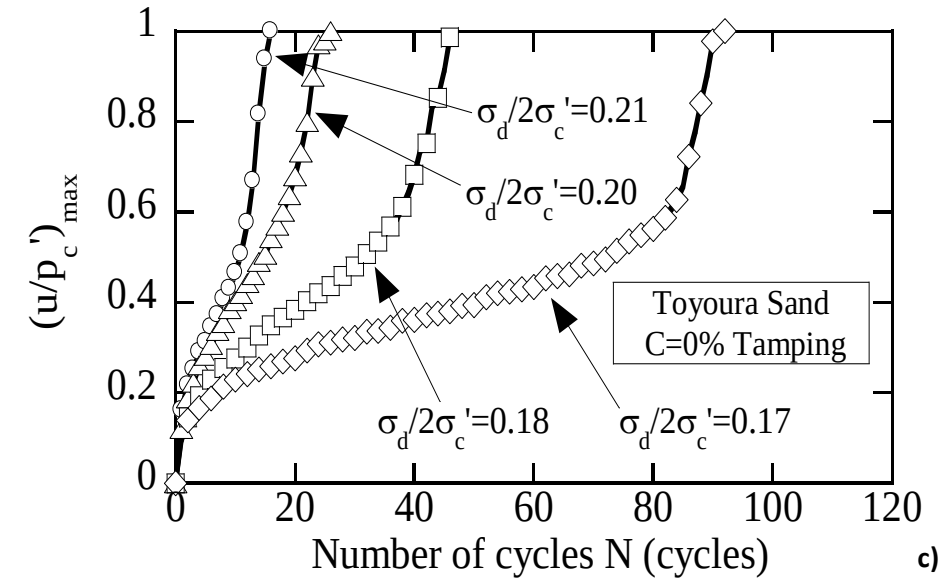

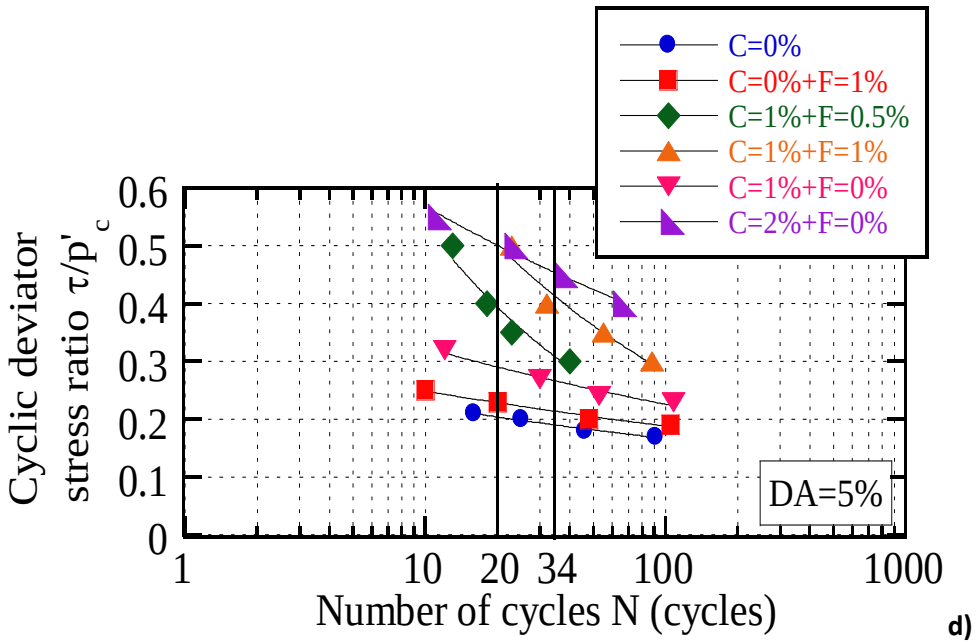

Figure 2.5. Large strain cyclic behavior of Toyoura sand at 60% relative density, σ_c'=100k Pa a) q vs. ε_a ; b) q vs. p' c) r_u vs. N; d) CSR vs. N for various stabilizer concentrations (Nakamichi & Sato, 2013)

2.7. Typical In-Situ Properties & Liquefaction Susceptibility in the Tokyo Bay Region

To quantify the phenomenon of liquefaction there are two critical values that must be calculated: the cyclic stress ratio (CSR), which represents the seismic stress to strain ratio to cause soil failure, and cyclic resistance ratio (CRR), which represents the soil's capacity to resist liquefaction.

Seed and Idriss, 1971 developed the most commonly used in-situ quantification of the CSR:

$$\boldsymbol{CSR = 0.65 * \frac{a_{max}}{g} * \frac{\sigma_{v0}}{\sigma'_{v0}} * r_d} \qquad \textbf{[2.1]}$$

where a_{max} is the peak ground acceleration, g is the gravitational constant (9.81 m/s^2), σ_{v0} and σ'_{v0} are the total and effective stress, and r_d is a stress reduction coefficient (Youd, & Idriss, 2001).

The CRR can be calculated from many in situ tests including standard penetration tests (SPT) and cone penetrometer tests (CPT) and has been correlated to parameters such as blow count, cone tip resistance, and shear wave velocity. Japanese data for typical SPT blow counts (typically N<20) and liquefaction zones around Tokyo Bay can be seen in Figure 2.6. Sand boils were seen specifically in regions where the sand yielded low SPT blow counts (fewer than 10 for 1.5') suggesting loose deposits. This blow count has been correlated to the CRR of the soil and has a clear positive relationship; the higher the SPT blow count, the higher the CRR of the sand (Youd & Idriss, 2001).

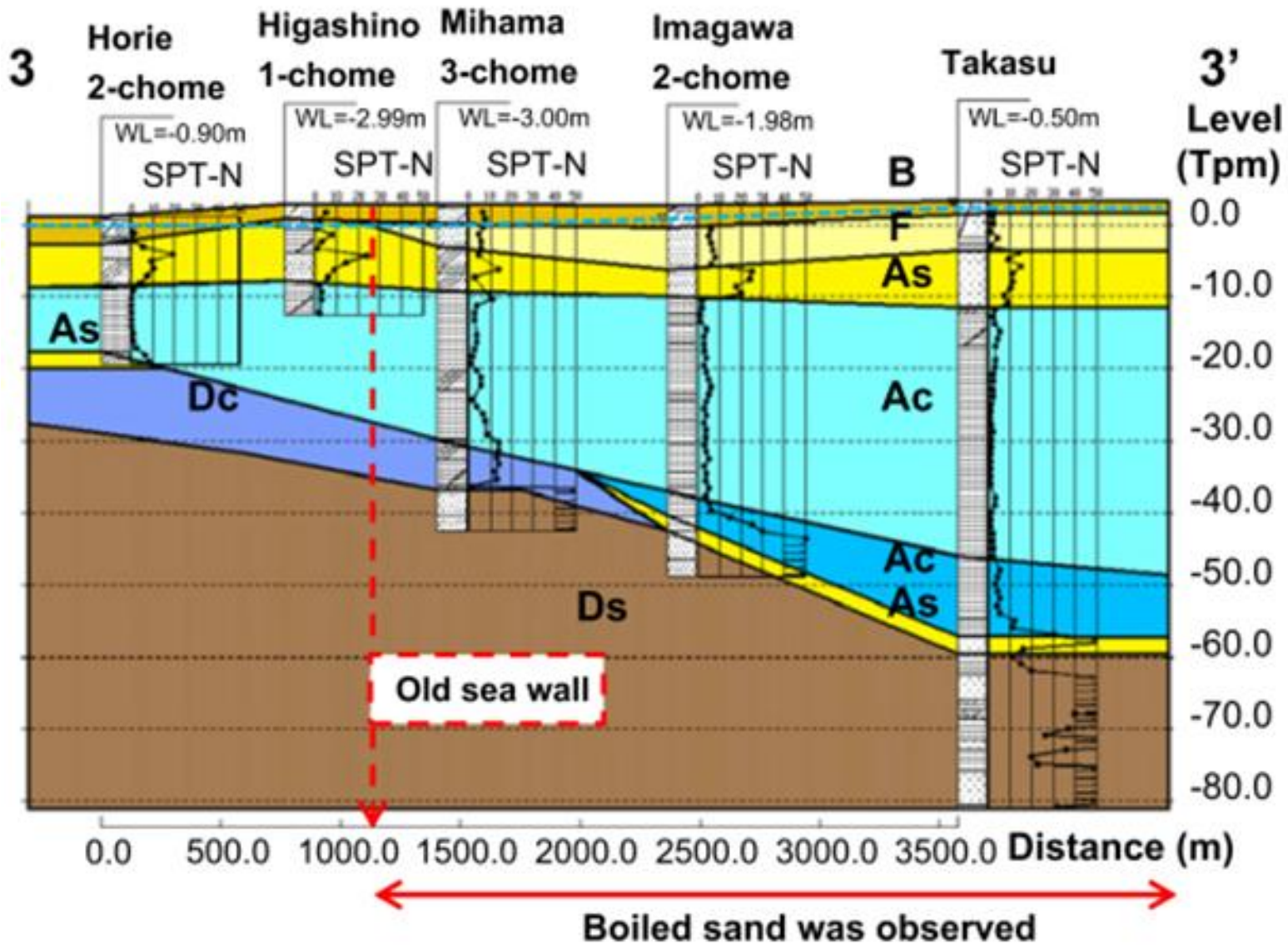

Figure 2.6. SPT results from liquefied zones in the Tokyo Bay region (Yasuda et al., 2012)

This cyclic resistance ratio can be improved in many ways, including the addition of cement and recycled polymer or wood fibres. In the Tokyo Bay region, many liquefaction countermeasures have been applied both before and after the Great East Japan Earthquake (Figure 2.7). It is evident that the lattice type deep mixing method using stabilizing additives is an effective method of countering liquefaction (Derakhshani et al., 2011). Figure 2.7 shows that although the most common stabilizing technique is the sand compaction pile method, the deep mixing method has been used in similar circumstances.

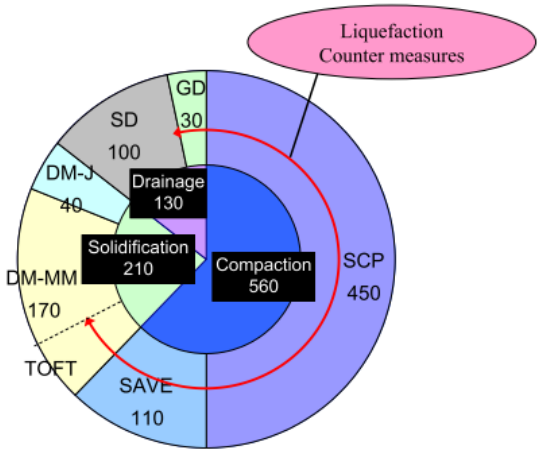

SCP : Vibratory Sand Compaction Pile method
SAVE : Non-vibratory Sand Compaction Pile method
DM-MM : Deep Mixing method (mechanical mixing)
TOFT : Lattice type Deep Mixing method
DM-J : Deep Mixing method (jetting)
SD : Sand Drain method
GD : Gravel Drain method

Figure 2.7. Commonly used liquefaction countermeasures (Yasuda et al., 2012)

Figure 2.8 and Table 2.1 clearly show that many of the soils that were studied due to their liquefaction during the Great East Japan Earthquake have a fines fraction (silt content) between 10% and 42.5% (Nakamichi & Sato, 2013). As shown in the literature, increasing the silt content consequently decreases the liquefaction resistance of a soil, suggesting the need for stabilization of these weak soils especially if the silt content is high.

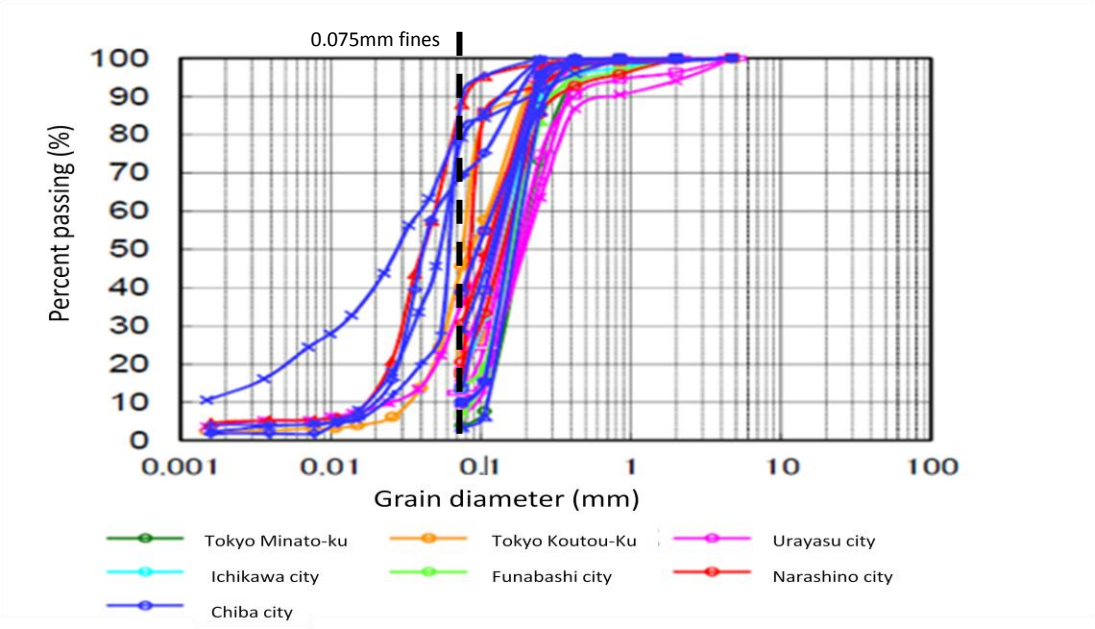

Figure 2.8. Particle size distribution of soil in Japan 2011 (Nakamichi & Sato, 2013)

Table 2.1. Gradation of sand with liquefaction boils in Tokyo Bay after the Great East Japan Earthquake (Nakamichi and Sato 2013)

Sampling point	No. of samples	Gravel content (%)	Sand content (%)	Fine fraction (%)	D_{50} (mm)	U_c	I_p
Tokyo Koutou-ku	4	0	70.4	29.6	0.121	3.49	NP
Urayasu city	9	1.2	83.0	15.8	0.164	3.29	NP
Ichikawa city	1	0.1	82.2	17.7	0.150	-	NP
Funabasi city	2	0.1	89.1	10.5	0.175	2.26	NP
Narashino city	5	0.2	66.7	33.1	0.098	2.81	NP
Chiba city Mihama-ku	10	0.1	57.4	42.5	0.106	2.61	NP ～5.7

2.8. Liquefaction of Sand and Silty Sand

The process of liquefaction in Japan is a very important subject due to the frequent seismic activity along the Pacific Ring of Fire. Through laboratory tests done by (Skempton, 1954; Sherif et al., 1977; Chaney, 1978; Jafarzadeh & Sadeghi, 2010; & Yoshimi et al., 1989) a positive relationship between liquefaction resistance of sands and the degree of saturation was previously determined, suggesting saturated sands are significantly more liquefiable than unsaturated sands (Figure 2.9). Damping (D) increases sharply above 90% saturation, whereas the shear modulus tends to decrease, and liquefaction resistance at 70% saturation is nearly triple that at 100% saturation (Yoshimi et al., 1989).

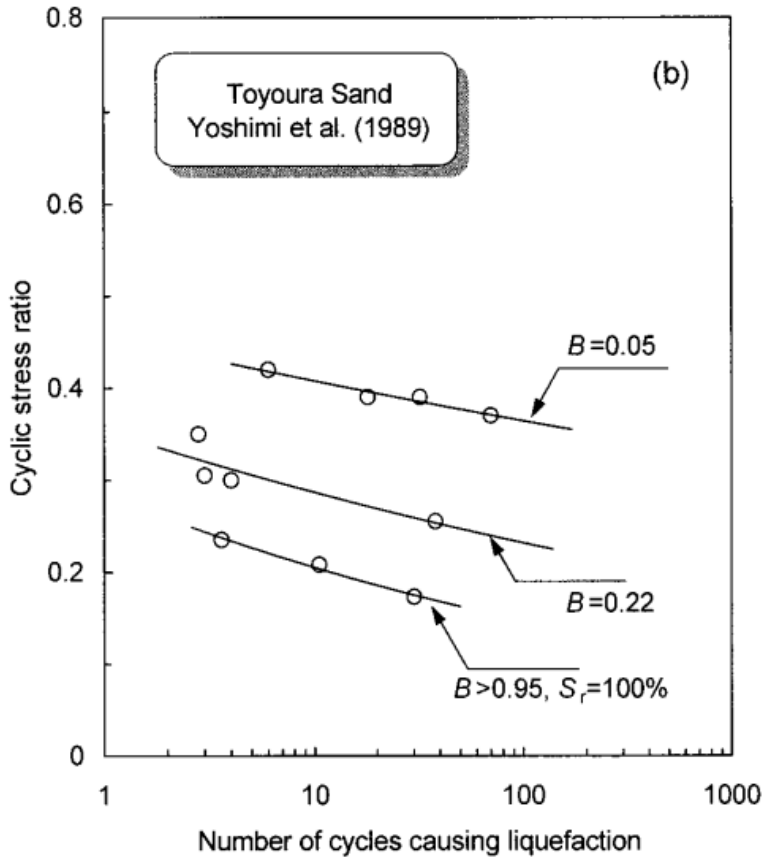

Figure 2.9. CSR vs. # cycles to failure (liquefaction resistance) of Toyoura Sand at various saturation levels (Yang et. al. 2004)

Overall, shear strain amplitude, confining pressure, and number of load cycles are the most important external factors when considering liquefaction potential, and in undrained conditions the importance of internal characteristics such as relative density, particle size distribution, overconsolidation ratio, and K_0 conditions increases (Jafarzadeh & Safeghi, 2012). Liquefaction resistance is also dramatically affected by the sand, gravel, and silt content of the soil as shown in Figure 2.10. The dashed line in Figure 2.10 represents the approximate limiting concentrations of sand and gravel, silt, and clay of liquefaction susceptible soils. It suggests that soils with sand and gravel contents from 80-100%, silt contents from 0-100%, and clay contents from 0-20% are all susceptible to liquefaction during dynamic load events.

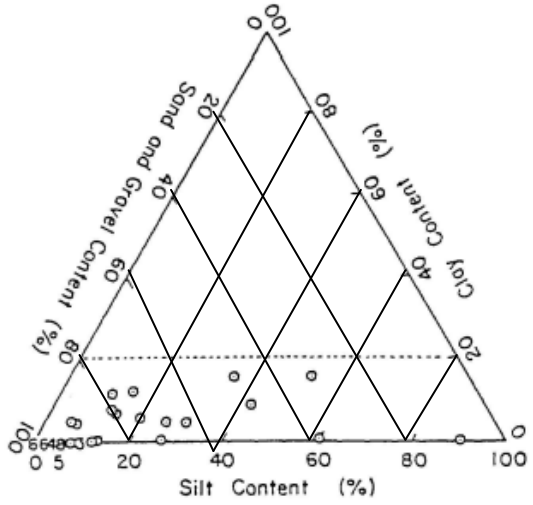

Figure 2.10. Liquefaction susceptibility based on sand, silt, and clay content (Andrews & Martin, 2000)

In general, the liquefaction susceptibility of a soil is based on the soil's historical records of liquefaction occurrence, deposition method, composition, gradation, angularity, and density.

Data for liquefaction resistance of sand, silt, and silty sand has been quite thoroughly analyzed by many researchers (e.g. Robertson & Fear, 1995; Xenaki & Athanasopolous, 2003; Andrews & Martin, 2000; Vucetic et al., 1998; Sitharam et al., 2013; Andrus & Stokoe, 2000; Yamamuro & Lade, 1998; Zhou & Chen, 2005; Vaid & Sivathayalan, 1995; Builes et al., 2008; Chiaro et al., 2012). They have since determined that there are three major causes for the vulnerability of fine grained cohesionless materials to liquefaction (Towhata, 2008):

a. There is nothing that prevents or reduces particle dislocation and dilatancy;
b. The reduced particle sizes work to reduce permeability and inhibit drainage;
c. During cyclic loading the deposit becomes looser due to Stokes Law.

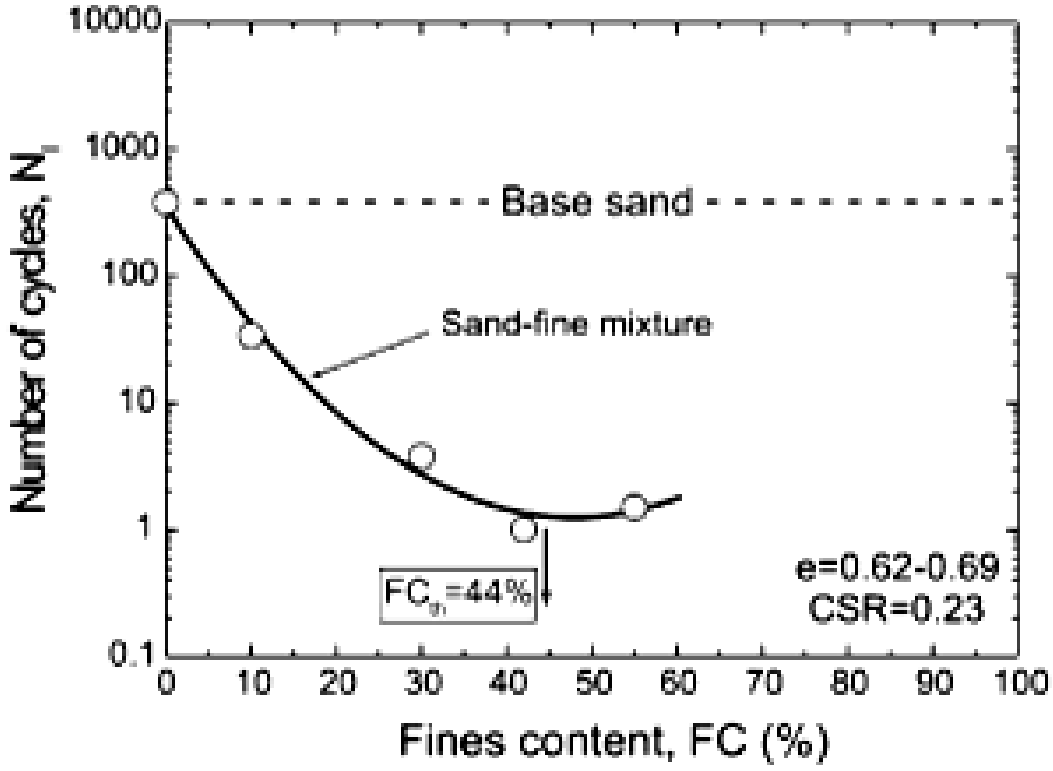

Figure 2.11. Effect of fines content on liquefaction resistance at a constant void ratio (Xenaki and Athanasopolous, 2003)

As shown in Figure 2.11, the addition of fines to sand can initially decrease the liquefaction resistance until about 40% silt content is reached, after which the resistance begins to increase slightly (Xenaki & Athanasopolous, 2003). Other research suggests that as little as 15% fines can half the liquefaction resistance of sand (Troncoso, 1986). The results of liquefaction resistance of silty sands overall tend to conflict with each other, with some researchers suggesting a decrease in resistance up to 10% silt content, then an increase in resistance to an asymptote at 60% (Chang, 1982). Others suggest a decrease until 35%, with a large increase after 75% fines (Askari, Dabiri, Shafiee, & Jafari, 2011). These trends are often dependent on what the author has decided to keep constant (e.g. the void ratio, the density, the relative density etc.). Despite these discrepancies, it is agreed upon that the addition of non-plastic silts negatively affects the overall resistance of sand to dynamic loading.

2.9. Soil Stabilization and Cementitious Admixtures

Many soils do not make adequate foundations or building materials for geotechnical engineering projects and can liquefy during seismic events. This leads engineers to the decision of whether to design the structure to withstand the poor soil conditions, remove and replace the poor quality soil, or, as will be discussed in this thesis, to stabilize the soil such that it can support the structure more effectively.

Of primary concern to geotechnical engineers are the volume stability, strength, permeability, and durability of the silty Toyoura sand found around the Tokyo Bay region in Japan (Ingles & Metcalf, 1973). The three main forms of stabilizer used as countermeasures are physical (e.g. electricity, heat which are not discussed in this thesis), chemical (e.g. Ordinary Portland Cement, gypsum, and lime), and mechanical (e.g. PVA fibres, and geofabrics) (Ingles & Metcalf, 1973). The decision to use these stabilizers is based on several important criteria, as outlined in Figure 2.12.

I. Characteristics of Hardening Agent 1. Type of hardening agent 2. Quality 3. Mixing water and additives
II. Characteristics and conditions of soil 1. Physical, chemical, and mineralogical properties of soil 2. Organic content 3. pH of pore water 4. Water content
III. Mixing conditions 1. Degree of mixing 2. Time of mixing/remixing 3. Quantity of hardening agent
IV. Curing conditions 1. Temperature 2. Curing Time 3. Humidity 4. Wetting/Drying/Freezing/Thawing etc.

Figure 2.12. Factors affecting the strength increase of a soil using the deep mixing method (Terashi & Juran, 2000)

There are also many possible ground improvement methods for sands and silty sands as seen in Figure 2.13

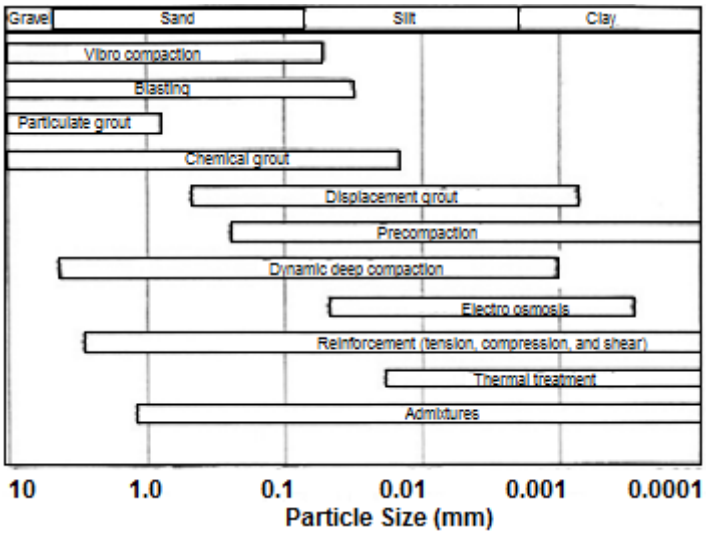

Figure 2.13. Optimal ground improvement methods based on soil type (Terashi & Juran, 2000)

Of particular interest for earthquake mitigation is the dry deep mixing method, a common technique used to add cementitious stabilizers to saturated sands and soft soils. This can be executed as a square grid of grouting or columnar grouting, both of which reduce the excess pore water pressure build-up, deformation and displacement of earth structures, and liquefaction susceptibility of sands and silts (Derakhshani et al., 2011). This method also increases soil density and unconfined compressive strength, and adds cohesion to poor quality granular materials when a cementitious material is used (Terashi & Juran, 2000). For well and poorly graded sands the recommended cement dosage varies from 2-6% by mass for pavement construction, however this content can increase to nearly 20% depending on the intended use of the soil, the silt content, and the overall initial soil quality (Ingles & Metcalf, 1973; Department of the Army Corps of Engineers, 1984). There is, however, an absence of data for sands with high silt concentrations stabilized with cementitious and fibrous additives.

2.10. Additives and Cementation

Tests have been conducted with regards to adding stabilizers to the Toyoura sand to improve liquefaction resistance. The results taken from (Nakamichi & Sato, 2013) with regards to adding Ordinary Portland cement and recycled Bassanite from waste plasterboard demonstrate how additives reduce liquefaction potential. They increase liquefaction resistance due to the change in the inter-particle forces and increased cohesion. Overall, the use of recycled cementitious materials has been proven to be successful in reducing liquefaction.

2.10.1. Fibre Addition

The addition of fiber stabilizers in sand has been studied extensively by (Freitag 1986; Gray 1986-88; Michalowskia et. al. 1990; Ghiassian & Ghazi, 2009) and many others. Many types of fibers have been considered, ranging from polyamide fibers and steel fibers (Michalowskia et. al., 1990), polymer fibers and reclaimed high density polyethylene (HDPE), carpet waste fibers (Ghiassian & Ghazi, 2009), plant roots and geotextiles (Gray, 1986-88), vakka, date and bamboo fibers (Rao & Rao, 2007), and Coir fibers (Babu & Vasudevan, 2008). The fiber contents studied have generally ranged from 0.5-6%, which is the highest feasible weight fraction proposed by (Gray, 1988) based on an asymptotic upper limit to strength gain. Tests have most commonly examined the fiber aspect ratio, tensile strength and concentration, results of which indicate an increase in ultimate strength proportional to an increase in each respective property. A random fiber orientation has also been deemed most effective as it will not create planes of weakness in the sample during shearing. These fibres also incrementally improve liquefaction resistance, increasing the CSR to cause failure in 15 cycles (equivalent magnitude 7.5 earthquake) by between 0.02 and 0.04 (Nakamichi & Sato, 2013).

Regardless of the aforementioned properties, the addition of fibers has been shown to inhibit dilatancy and cause the soil's apparent cohesion to increase with no significant change to the internal friction angle (Michalowskia et. al., 1990).

2.10.2. Cement Addition

The effects of cement addition with and without fiber stabilization have also been tested comprehensively by several authors (e.g. Maher et. al., 1994; Dano et. al., 2004; Pantazopolous & Atmatzidis, 2012; Fernandez & Santamarina, 2001; Consoli et. al. 1998, 2009-10; Nakamichi & Sato, 2013) with several other papers published on the effects of cement with silty sands. Cementing is associated with an obvious decrease in liquefaction potential, and an increase in small strain stiffness by up to an order of magnitude (Fernandez & Santamarina, 2001). Jafarzadeh & Sadeghi (2012) showed that an increase in dynamic shear modulus of cemented sands occurs during the first ten loading cycles. Tests have shown that cement content, curing time, curing temperature, and relative density all dramatically affect the compressive strength of cemented sands, indicating that an increase in any of the aforementioned parameters improves the ultimate strength of the soil. The strength gain is caused by one of two mechanisms: creation of a nucleated structure or development of a hydrated cement skeleton structure (Ingles & Metcalf, 1973).

What has yet to be evaluated critically is the combined effect of cement and PVA fiber on the liquefaction potential of silty sand. Since silt is known to increase the liquefaction potential of granular soils, but cement and fibers are known to decrease it, the combined effects should be critically analyzed with regard to the cyclic mechanical performance and in-situ stabilization practices. One-dimensional consolidation and permeability data is also lacking for stabilized sands used in cyclic applications where partial drainage under cyclic loading may occur.

As shown in Figure 2.5d in Section 2.6, the addition of various cement contents can nearly triple the CSR required to cause liquefaction. When combined with the fibres discussed in Section 2.10.1, the slope of the liquefaction resistance curve steepens, but still indicates an improvement over the samples with only the cement.

Practically speaking, fibers and cementitious materials are often mixed into soil columns as stabilizers using methods such as deep mixing (Section 2.1). Gray (1988) evaluated some of the mixing methods used, including blade and paddle mixers (which ball up the fibers), vibratory mixers (which float fibers to the top of the samples), and oscillatory and helical mixers, which were considered to be the most effective. Several in-situ methods, especially the deep mix method, have also been analyzed critically by Kazemian & Huat (2009) and Terashi & Juran (2000). Experimentally, fiber addition has been mainly performed experimentally using the moist tamping method to avoid separation. Other uses for fiber and cement addition include underground pipeline stabilization, embankments, earth dams, and other small scale earthworks for both static and cyclic loading including earthquakes.

2.11. Summary

The focus of this chapter was the micro- and macrostructural properties and behaviour of Toyoura sand when subjected to static and dynamic loads. Research done on large scale and micro scale liquefaction (cyclic triaxial testing), monotonic shearing (consolidated, undrained shearing), and very small strain shearing (bender element testing) behaviour of Toyoura sand was investigated.

The effects of the addition of silt, fibres, and cementitious materials on poorly graded, uniform Toyoura sand were also examined individually and in conjunction with each other. The mixture of all three of the additives to the Toyoura sand has not been examined thoroughly, though the implementation of each stabilizing additive individually via deep mixing, grouting, vibro-compaction etc. and the resulting effects has been extensively studied. The literature suggests that the addition of silt has an initially beneficial effect on the liquefaction resistance of sand by improving gradation, followed by a negative effect, though the exact transition point varies. In the Tokyo Bay region of Japan, the silt contents generally ranged from 0-42%, which was within the general range of transition points found in the literature. Cement has an obvious positive effect on the strength and stiffness of sand, and is further enhanced by the addition of fibres.

Overall, the effects of stabilizing additives have been well documented in the literature for pure sands, though research is lacking in the area of the stabilization of silty sands. This literature survey summarizes the behaviour of Toyoura sand with and without these additives, and identifies some of the gaps in the research.

CHAPTER 3: Materials and Experimental Methods

3. Materials and Experimental Methods

3.1. Introduction

The silty sand mixtures in the Tokyo Bay region are extremely susceptible to liquefaction caused by seismic loads, and the stabilization of these soils provides the basis for experimentation in this thesis. Tests on samples of pure Toyoura sand and pure silica flour were performed to establish upper and lower bound conditions and explain the soil mixture behaviors with respect to these boundaries.

Using the aforementioned Toyoura sand and silica flour (silt) with Ordinary Portland Cement (OPC) and PVA fibres as stabilizers, a testing regimen was designed to first determine the basic geotechnical properties of each soil constituent (e.g. specific gravity, particle size distribution (PSD), internal friction angle, etc.). Following this, the microstructure and fabric of the soils was visualized using scanning electron microscopy (SEM), computerized tomography (CT), and mercury intrusion porosimetry (MIP). A link between the microstructure and the flow properties, shear modulus, and liquefaction resistance of the specimens was established using oedometer and Rowe cells tests, bender element tests, and cyclic triaxial tests respectively. Bender element, monotonic, and cyclic triaxial tests subject specimens to small (~0.001%) and large strains (>5%) respectively and have provided strength, stiffness, shear modulus reduction, and liquefaction behaviour of the materials. This chapter provides a further detailed description of the materials and methods used in this study.

3.2. Material Properties

Four main materials were used in the testing regimen to replicate the in-situ and stabilized conditions of the Tokyo Bay region: Toyoura sand, silica flour, Ordinary Portland cement (OPC), and polyvinyl alcohol (PVA) fibres.

Toyoura sand is composed of 75% quartz, 22% feldspar, and 3% magnetite and can be found primarily on the coastal rim of the Pacific Ocean in Japan (Lam & Tatsuoka 1988, De & Basudhar 2008). It is an angular to sub-angular, fine grained and poorly graded sand - confirmed by a low coefficient of uniformity and coefficient of curvature - classified as SP by the Unified Soil Classification System (USCS) (Bellotti et. al., 1997; HongNam, Koseki & Sato; Hyodo et. al., 1994; Oda, 1977; Wang et. al., 2002; Whitlow, 2001). The peak internal friction angle (ϕ') ranges from 33.5° in a very loose state to 43.7° when dense. The peak dilation angle (φ) ranges from 5°-10° at normal stresses of 25-300 kPa.

The sub-angular silica flour (Bell & McKenzie, Sil-Co-Sil #106) used for these tests consists of 100% ground quartz and is fine grained and well-graded, based on the high coefficient of uniformity and coefficient of curvature. It is classified as ML according to the USCS and has a peak internal friction angle of 41° at 90% relative density, and a peak dilatancy angle that ranges from 6°-14° at normal stresses of 25-300 kPa. The choice to use silica flour versus natural silt was for experimental repeatability and consistency in the particle size distribution and shape. The engineering properties of Toyoura sand and silica flour can be found in Table 3.1 below.

Table 3.1. Engineering properties of Toyoura sand and silica flour

	Specific Gravity	D_{60} (mm)	D_{10} (mm)	ρ_{dry} (min) (g/cm^3)	e_{max}	ρ_{dry} (max) (g/cm^3)	e_{min}	C_u	C_c
Toyoura Sand	2.647	0.21	0.17	1.346	0.946	1.640	0.614	1.24	0.91
Silica Flour	2.641	0.025	0.0009	1.015	1.602	1.440	0.834	27.78	2.84

Type I Ordinary Portland Cement (OPC) from Ube-Mitsubishi Cement Corporation and PVA fibre stabilizers RECS100L from Kuraray Co. Ltd. were added as a percent by mass in each specimen. The OPC has a specific gravity of 3.15 and a composition consisting of approximately 63% tricalcium silicate, 12% dicalcium silicate, 5% tricalcium aluminate, 11% tetracalcium aluminoferrite (ASTM C150/C150M-12). The PVA fibres have a specific gravity of 1.3, an average length of 12 mm and a diameter of 0.11-0.12 mm. They have a Young's Modulus of 28 GPa and a tensile strength of 1,200 MPa (Kuraray Co. Ltd). These additives have been used to model recycled gypsum and bamboo fibres.

The mass of all sample constituents was calculated as a percentage of the total dry mass required to produce the desired relative density (e.g. a 100 g sample of 42% silt, 2% cement, 1% fibre, and 55% Toyoura sand contains 42 g of silt, 2 g of cement, 1 g of fibre, and 55 g of Toyoura sand). For all cemented samples, the final relative density varied a little due to hydration and expansion of the cementitious material. The relative density of the Toyoura sand or the silty sand was used and increased slightly when cement was added to account for this change in soil fabric. Also, at the higher initial densities required for the silty sand samples the mass of cement to reach the same additive stabilizer percentage increases, which can have obvious improvement effects on the soil. Despite this fact, cement was added as a percentage by mass of the total sample and is later commented on in the results section. This issue is still debated in the literature, and no definitive conclusion as to the best way to address this has been agreed upon (Bullard et al., 2010; Clough et al., 1989; Dvorkin & Yin, 1995).

All of the cemented samples were allowed to cure for 3 days in a laboratory environment with 100% relative humidity to match the procedure used by researchers at Fukuoka University. The three day curing time was also used to simulate the occurrence of an earthquake during the implementation of the soil stabilization and determine the behaviour of the partially hydrated soil and cement mixture. After three days, an average degree of hydration of 88% was assumed based on empirical data from (Shafiq & Nuruddin, 2010; CEB/FIB, 2000). From this data the volume of hydrated cement products was roughly 2.1 times the volume of the initially added dry cement as shown below:

$$\boldsymbol{V_{hp} = 2.1 * M_{cement}/G_{s-cement}} \quad \textbf{[3.1]}$$

$$\boldsymbol{e = \frac{V_{voids}}{V_{solids}+V_{hp}}} \quad \textbf{[3.2]}$$

Void ratios were then calculated based on the volume of voids, solids, and hydrated cement products (V_{hp}). The addition of fibers was assumed not to alter the initial void ratio.

3.3. Basic Properties & Scanning Electron Microscopy

3.3.1. Basic Properties of Toyoura sand and silica flour

The specific gravity, particle size distribution (PSD), minimum and maximum density, and internal friction angle were all determined for each soil mixture.

Specific gravity tests were performed on clean Toyoura sand and silica flour according to ASTM D854-10. The goal of these tests was to determine the specific gravity of each stabilized soil specimen using a weighted average of each individual material listed in Section 3.1.

Particle size distributions for clean Toyoura sand and silica flour were performed to determine the D_{10}, D_{30}, D_{50}, and D_{60} particle sizes in millimeters. The #40, #45, #60, #80, #100, #120, #140, #170, and #200 sieve sizes were used for Toyoura sand and silica flour. A hydrometer test was performed on silica

flour to determine the particles size distribution of the - #200 particles (<0.075 mm) (ASTM D422-2007). The particle size distribution for all silty sand mixtures was calculated using the percent retained on each sieve and the results of the hydrometer test. Each particle size distribution can be seen in Figure 3.1.

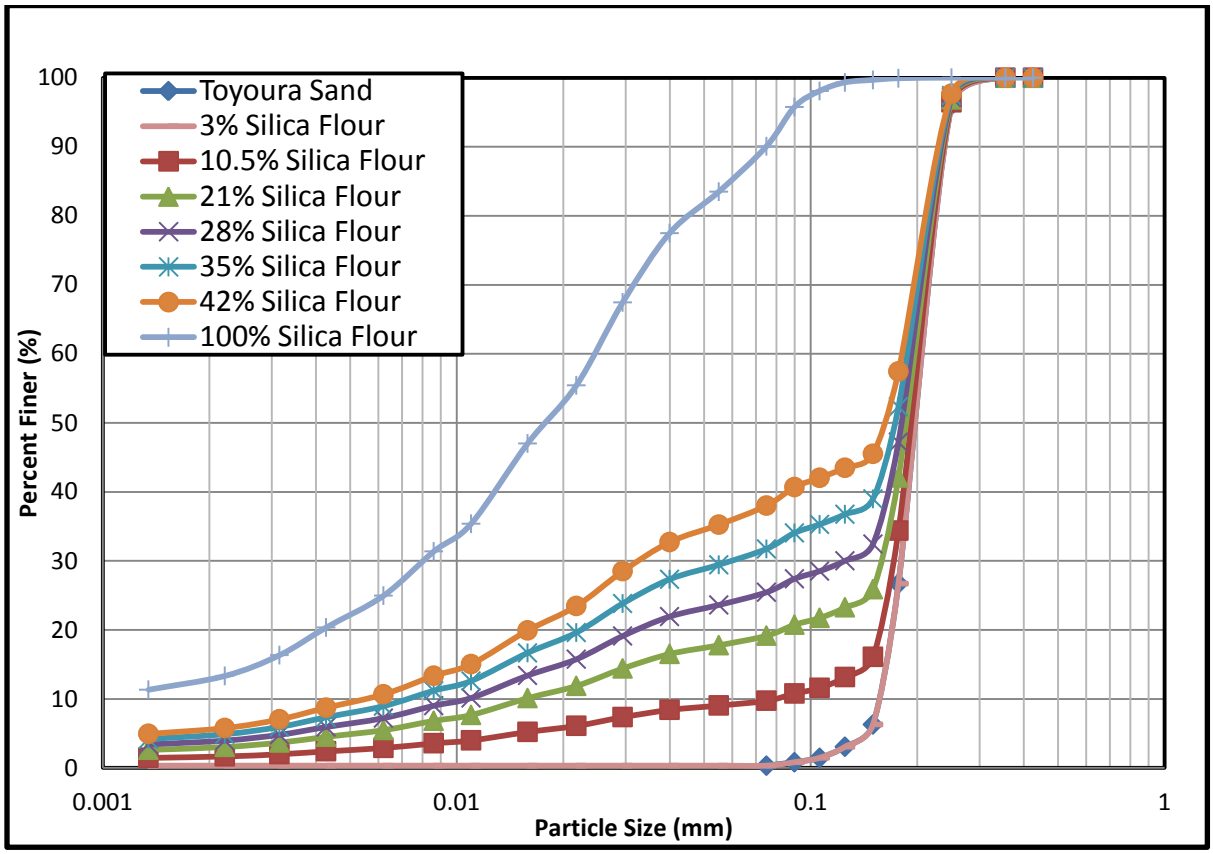

Figure 3.1. Particle size distribution of Toyoura sand with various percentages of silica flour

Minimum and maximum dry density tests were performed on Toyoura sand and silica flour according to ASTM D4254-06 (poured from a graduated cylinder) and D4253-06 (vibrating table with a 14 kPa surcharge) (Figure 3.2). Tests were also performed on 10.5-42% silica flour (with the remaining 58-89.5% being Toyoura sand) to determine each mixture's 60% relative dry density and corresponding initial void ratio. The results were graphed and fit with a quadratic best fit line with an R^2 value of 0.967.

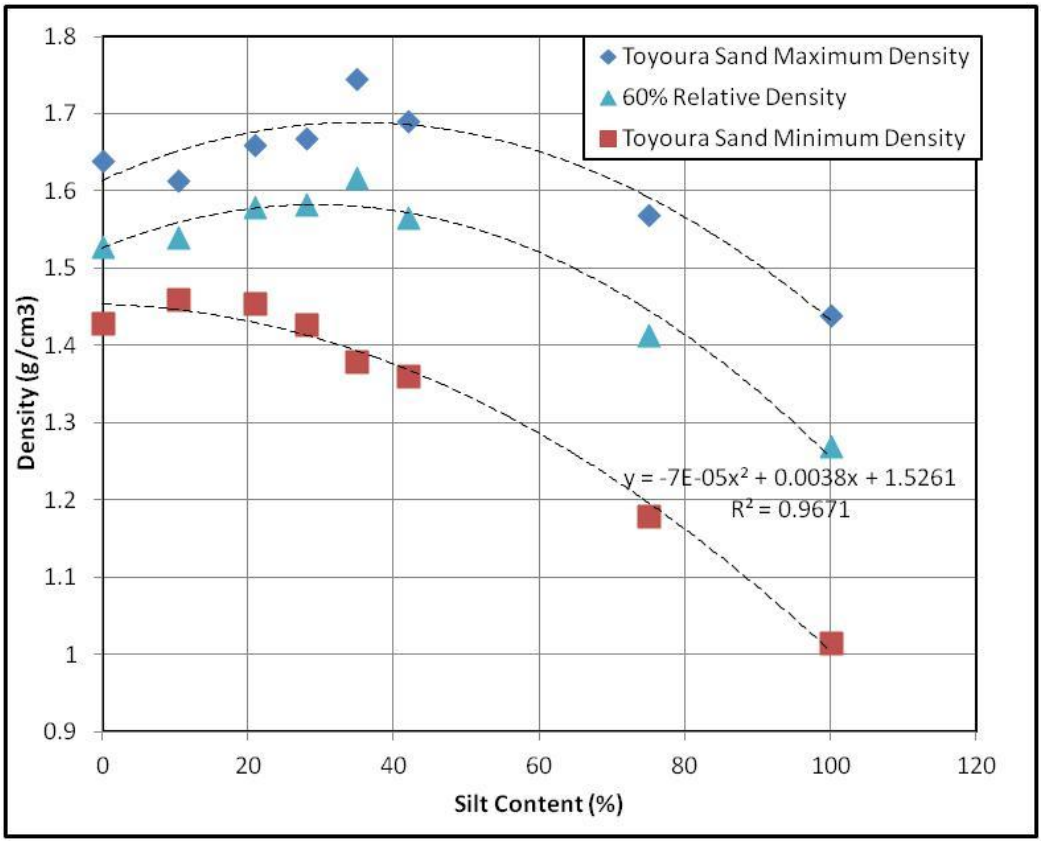

Figure 3.2. Relative density of Toyoura sand with varied percentages of silica flour

3.3.2. Scanning Electron Microscopy

Five Scanning Electron Microscopy (SEM) tests were performed on roughly 0.1 g samples taken from mercury intrusion porosimetry specimens: Toyoura Sand, Silica Flour, PVA fibres, and two representative mixtures of 42% silica flour, 2% cement, 1% fibre. The SEM images were used to supplement CT scans by providing a microscopic view of the interaction between the soil and the stabilizers. Images were captured at magnifications ranging from 100-30,000x to view the surface angularity of soil particles, the striations along the PVA fibres, and visualize the hydrated cement products. SEM scans were performed on a Hitachi S-4500 field emission scanning electron microscope using a Quartz Xone EDX system, gold sputtering, and imaging software at The Alan D. Edgar Laboratory, in Surface Science Western. The accuracy and resolution of the SEM scans were ±5% and 2 nm respectively.

3.4. Computerized Tomography and Mercury Intrusion Porosimetry

3.4.1. Computerized Tomography

Six specimens of Toyoura sand with silt, cement, and fibre additives were tested (Table 3.2). The goal of the CT scans was to visualize the homogeneity and consistency of stabilized and un-stabilized specimens with respect to isotropy and dispersion of the stabilizers.

Table 3.2. Testing regimen for CT scans

% Sand	% Silt	% Cement	% Fibre	Density (g/cm^3)
100	0	0	0	1.52
99	0	0	1	1.52
98	0	2	0	1.53
97	0	2	1	1.53
58	42	0	0	1.57
55	42	2	1	1.58

Specimens for CT scanning were constructed with a 50 mm diameter and 100 mm height (in five lifts of 20 mm) using the moist tamping method (Ladd, 1978). Each specimen was prepared with 10% initial moisture content in a rubber membrane and then wrapped in bubble wrap and sealed completely to avoid loss of moisture. Transportation of the specimens was conducted carefully to minimize disturbance. All CT scans were performed at Robarts Imaging in London Ontario, using a machine with voxel resolution of 50 μm. Specimens were analyzed using GE HealthCare Microview 2.2 to improve the pixel contrast and visualize the location and orientation of the PVA fibres, the volume of hydrated cement products, and the homogeneity of the silt content.

3.4.2. Mercury Intrusion Porosimetry

Mercury intrusion porosimetry (MIP) is used to determine pore sizes, ranging from 0.003-360 μm, of various materials. The theory behind MIP is based on the non-wetting properties of mercury and the interfacial contact angle between the mercury and the studied material. When an external pressure is applied to the mercury it is forced into the pores, the diameters of which are calculated using correlations determined by Washburn, 1921 (see Equation 3.3). There are a number of uncertainties for MIP testing on soil samples (Lawrence, 1977):

- The applicability of the Washburn equation to pore shapes that are not cylindrical
- Ink bottle effects
- Pore collapse during measurement
- Uncertainty regarding the surface tension and contact angle of mercury
- Void ratio values determined using MIP are significantly larger than those calculated from 1D compression tests
- Permeability values are calculated based on pore diameter, regardless of pore structure

MIP on cemented cohesionless soils has rarely been studied in the literature though plenty of data exists on the pore size distribution (PSD) of clays, silty clays, cemented clays and cement mortars (Fies, 1992; Qi et al., 1996; Peneumander & Dean, 2000; Fies & Bruand, 2002; Sasanian, 2011; Karimi, 2012).

A series of 12 mercury intrusion porosimetry tests were performed on a Micromeritics AutoPore IV Mercury Porosimeter (Table 3.3). The objective of these tests was to obtain the pore size distribution of each specimen and relate it to the permeability found from the Rowe cell and oedometer testing. Specimens were prepared using the moist tamping method (Ladd, 1978) in two lifts of 1 cm each, at densities ranging from 1.34-1.67 g/cm^3. The initial 10% moisture content was removed from each specimen by vacuum desiccation (Galle, 2011) for at least 24 hours or until the mass of the sample became constant. Within the porosimeter a vacuum of less than 50 μmHg was applied to verify that no

moisture was present during the testing, after which stringently controlled pressures ranging from 0-345 kPa (±1%, 69 Pa resolution) and 345 kPa-414 MPa (±0.1%, 689-2070 Pa resolution) were applied in stages, allowing intrusion to occur for at least 10 seconds in each stage to ensure complete pore penetration. Intrusion was accurate to ±1% of the stem volume and had a resolution finer than 1 μL.

Table 3.3. Testing regimen for mercury intrusion porosimetry

% Sand	% Silt	% Cement	% Fibre	Density (g/cm^3)
100	0	0	0	Loose
0	100	0	0	Loose
98	0	2	0	1.51
97	0	3	0	1.41
96	0	4	0	1.43
97.5	0	2	0.5	1.34
97	0	2	1	1.34
96	0	2	2	1.34
87.5	10.5	2	0	1.67
77	21	2	0	1.67
56	42	2	0	1.67
55	42	2	1	1.42

Representative samples for MIP testing (0.69-3.5 g) were taken from each specimen by carefully using a scoopula to minimize disturbance. The documented initial dry density was based on the mass and volume of the overall specimen rather than the retrieved sample.

Pore sizes were calculated by the AutoPore software using the Washburn equation (Washburn, 1921) (Equation 3.3):

$$\boldsymbol{P = -\frac{4\gamma cos\theta}{\sigma}} \qquad \textbf{[3.3]}$$

Where P is the pore diameter, γ is the surface tension of mercury (0.484 N/m), θ is the contact angle (135°), σ is the applied intrusion pressure (ranging from 0-414 MPa). Based on data from Diamond

(1970) and Sills et al. (1973) on clays, a contact angle of 135° was chosen for all samples. In the absence of prior research in this field, this assumption was made and kept consistent throughout testing.

Permeability was calculated using the Katz-Thompson equation (Katz & Thompson, 1986) (Equation 3.4):

$$\boldsymbol{k = \frac{1}{89} L_{max}^2 \frac{L_{max}}{L_{char}} I_{total} \gamma_b S_{LMax}} \quad \textbf{[3.4]}$$

Where k is the permeability (millidarcys), L_{Max} is the length at which the conductance is maximum, L_{char} is the characteristic length, I_{total} is the total intrusion volume, γ_b is the bulk density of the sample, and S_{LMax} is the fractional volume of connected pore space involving pore widths of size L_{Max} and larger.

Three graphs were plotted for each test:

1. Cumulative intrusion (mL) vs. pore diameter (μm)
2. Log differential intrusion (mL) vs. pore diameter (μm)
3. Percent finer (%) vs. pore diameter (μm)

From the pore size distribution curve, a "P_{50}" and "P_{10}" value were extracted, representing the median pore size (50% finer) and the 10% finer pore size respectively.

3.5. Compression and Flow Parameters

3.5.1. Rowe Cell

A series of 27 Rowe cell tests was performed on a GDS Consolidation Testing System (Rowe Type, S/N 13309) to determine the one dimensional flow properties and compressibility of each sample (Table 3.4). To achieve this, 32 mm tall, 100 mm diameter samples at 60% relative density were prepared. Back and vertical pressure measurements were accurate to ±0.5% of the full range (2,000 kPa) with a resolution of 1 kPa. Pore pressure measurements were accurate to 0.5% of the full range (500 psig) with a resolution of 0.01 kPa (S/N 85407). Water volumes were accurate to 0.25% of the measured value,

with a resolution of 1 mm^3. Axial displacement was measured using a linear variable displacement transducer (LVDT) accurate to ±0.5% full range (50 mm) with a resolution of 0.1 μm (S/N 04L00715).

Sample preparation was performed using the moist tamping method (Ladd, 1978) at 10% initial moisture content in three lifts of 10.6 mm each for a total height of 32 mm. This method was designed to mimic the work of (Nakamichi & Sato, 2013) from Fukuoka University, who used a similar method for cyclic triaxial specimen preparation. A 745 g tamper with a 60 mm diameter and 20 mm thick head was used to compact each layer to the correct height, which was measured using markings on the tamper head (Figure 3.3).

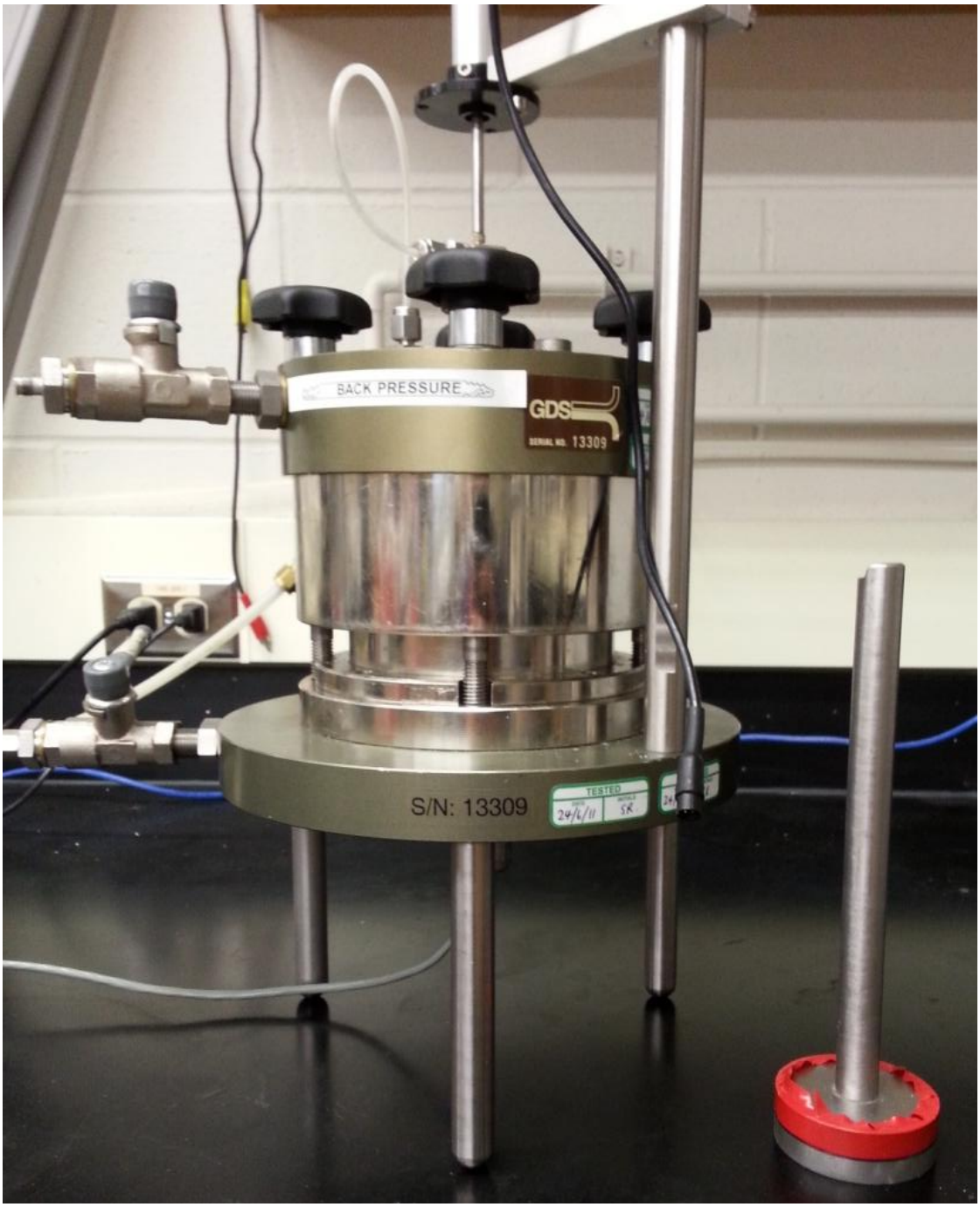

Figure 3.3. Rowe cell apparatus and tamping hammer

Table 3.4. Testing regimen for Rowe cell tests

% Sand	% Silt	% Cement	% Fiber	ρ_{max} (g/cm^3)	ρ_{exp} (g/cm^3)	ρ_{min} (g/cm^3)
100	0	0	0	1.640	1.528	1.346
99.75	0	0	0.25	1.640	1.528	1.346
99.5	0	0	0.5	1.640	1.528	1.346
99	0	0	1	1.640	1.528	1.346
98	0	0	2	1.640	1.528	1.346
99	0	1	0	1.640	1.520	1.346
98	0	2	0	1.640	1.530	1.346
97	0	3	0	1.640	1.540	1.346
96	0	4	0	1.640	1.542	1.346
89.5	10.5	0	0	1.651	1.559	1.445
79	21	0	0	1.680	1.520	1.431
72	28	0	0	1.692	1.528	1.418
65	35	0	0	1.699	1.528	1.400
58	42	0	0	1.699	1.520	1.379
0	100	0	0	1.440	1.272	1.015
88.5	10.5	0	1	1.651	1.556	1.445
78	21	0	1	1.680	1.579	1.431
71	28	0	1	1.692	1.573	1.418
64	35	0	1	1.699	1.520	1.400
57	42	0	1	1.699	1.520	1.379
0	99	0	1	1.478	1.272	1.015
86.5	10.5	2	1	1.651	1.560	1.445
76	21	2	1	1.680	1.582	1.431
69	28	2	1	1.692	1.589	1.418
62	35	2	1	1.699	1.589	1.400
55	42	2	1	1.699	1.582	1.379
0	97	2	1	1.478	1.275	1.015

As the Rowe cell was assembled, each part was checked for cleanliness and damage. Lines were de-aired prior to use and vacuum grease was applied to all O-rings and interfaces from which water may escape. Carbon dioxide was bubbled through each sample for one hour, after which distilled de-aired water was slowly flushed through the sample from the bottom until no more bubbles came out. Vertical and base pressures were then increased to 200-400 kPa with a constant effective stress of 10 -15 kPa to dissolve any remaining CO_2. A B-value of 0.95 or higher was achieved before consolidation began to ensure complete saturation and consistent results between tests.

The vertical pressure was increased in the following effective stress increments: σ_v'=15, 25, 50, 100, 200, 400, 800, 1000 kPa. Swelling occurred along the same stress decrements. Consolidation and swelling were considered to be complete when the back volume change was less than 5 mm^3 over a period of 5 minutes, as calculated by the GDS software.

Values of t_{90} were calculated using data from consolidation graphs when possible according to ASTM D2435-04, and a coefficient of consolidation (c_v) was calculated using Equation 3.5 (Head, 1986).

$$\mathbf{c_v = 0.526 \frac{T_v H^2}{t}} \qquad \textbf{[3.5]}$$

where c_v the coefficient of consolidation (m^2/yr), T_v=0.379 based on t_{50} values, and T_v=1.031 based on t_{90} values, H is the sample drainage height (mm), and t is the time until 50% or 90% of primary consolidation is complete (mins).

For a number of low silt content samples the loading and drainage rate was limited by the slow time of response of the laboratory equipment (i.e. the sample end filters and the volume-pressure devices) and was therefore not representative of instantaneous loading or the natural drainage rate required to accurately calculate t_{90} for sand. For these tests, a t_{90} value was back calculated from the results of three permeameter tests and it was assumed that there was a linear decrease in permeability between different silt concentrations.

The coefficient of volume compressibility was calculated using Equation 3.6 (Head, 1986).

$$\mathbf{m_v = \frac{e_0 - e}{\Delta \sigma_v'} * \frac{1000}{1 + e_0}} \qquad \textbf{[3.6]}$$

Where m_v is the coefficient of volume compressibility (m^2/MN), $\Delta\sigma_v$' is the change in the vertical effective stress during the consolidation stage (kPa), e_0 is the void ratio at the start of the consolidation stage and e is the current void ratio.

Using these values, permeability (k) was calculated in m/s using Equation 3.7:

$$\boldsymbol{k = c_v m_v} \quad \textbf{[3.7]}$$

Using Microsoft Excel, the following graphs were plotted for all Rowe cell tests:

1. Back volume (mm^3) vs. Square root of time (mins) for each stress increment
2. Void ratio vs. Vertical effective stress (kPa)
3. Constrained modulus (kPa) vs. Vertical effective stress (kPa)
4. Permeability (m/s) vs. Vertical effective stress (kPa)

Note that the back volume graphs were used only to calculate t_{90} values when possible and are not shown in this thesis.

Permeability was also calculated with six different equations as shown in Table 3.5 for comparative purposes, though only results from Equation 3.7 and K_3 from Table 3.5 are discussed in this thesis. The shape factors (SF) for Carrier (2003) were assumed based on the particle angularity of each constituent material, which was qualitatively determined from SEM scans in Section 4.1. Values were based on Fair & Hatch (1933) and Loudon (1956) and chosen as follows: SF=7.5 for clean Toyoura sand, SF=7.7 for silica flour, SF=7.6 for sand and silica flour mixtures, SF=8.2 for cemented samples.

Permeability was confirmed via three constant head permeability tests (ASTM D2434-68, 2006) performed on each of Toyoura sand, silica flour, and a mixture of 42% silica flour and 58% Toyoura sand. Each constant head test was performed with a sample at 60% relative density, and was performed at three different head levels to ensure accuracy. Results for all other tests were compared to these experimental permeability values for validation.

Table 3.5. Permeability calculations for Rowe cell tests

Reference #	Equation	Units
K	$k = c_v m_v \gamma_w$	k (m/s), c_v (m^2/s), m_v (m^2/kN)
K_1 (Hazen, 1911)	$k_1 = CD_{10}^2$	k (cm/s), D_{10} (cm), C=110
K_2 (Fine, 2014)	$k_2 = 100 D_{10}^2 e^2$	k (m/s), D_{10} (cm)
K_3 (Carrier, 2003)	$k_3 = 1.99x10^4 \left(\frac{100}{\sum \frac{f_i}{D_{li}^{0.404} D_{si}^{0.595}}} \right)^2 (\frac{1}{SF})^2 \left(\frac{e^3}{1+e} \right)$	k (cm/s), D_{li} & D_{si} (cm), SF=6-8.4*
K_4 (Chapuis, 2004)	$k_4 = 2.4622 \left(D_{10}^2 \frac{e^3}{1+e} \right)^{0.7825}$	k (cm/s), D_{10} (mm)
K_5 (Amer & Awad, 1974)	$k_5 = D_{60}^{0.6} D_{10}^{1.72} \left(\frac{e^3}{1+e} \right)$	k (m/s), D_{10} (mm), D_{60} (mm)

*(Fair & Hatch, 1933), (Loudon, 1956)

3.5.2. Oedometer

Five oedometer tests were performed on clean Toyoura sand, Toyoura sand with 28, 50, and 75% silica flour, and pure silica flour according to ASTM D2435-04 to compare with the results of the Rowe cell. These tests were performed on a Wykeham Farrance Eng. Ltd. oedometer, using a Schaevitz 14.7 mm Linear Variable Displacement Transducer (LVDT) (S/N PCA 116-200) accurate to 0.2% of the full scale output with a resolution of 0.001 mm (Figure 3.4). These 50 mm diameter samples were built using the moist tamping method (Ladd, 1978) in two lifts of 7.5 mm for a final thickness of 15 mm, at 50-60% relative density and with an initial moisture content of 10%. Specimens were left to saturate for 24 hours prior to incremental stress increases (0, 25, 50, 100, 200, 400, 800, 1600 kPa). Each consecutive stress increase was left for 24 hours with readings taken at the following time intervals (in minutes): 0.08, 0.25, 0.5, 1, 2, 4, 8, 15, 30, 60, 120, 240, 480, 1440.

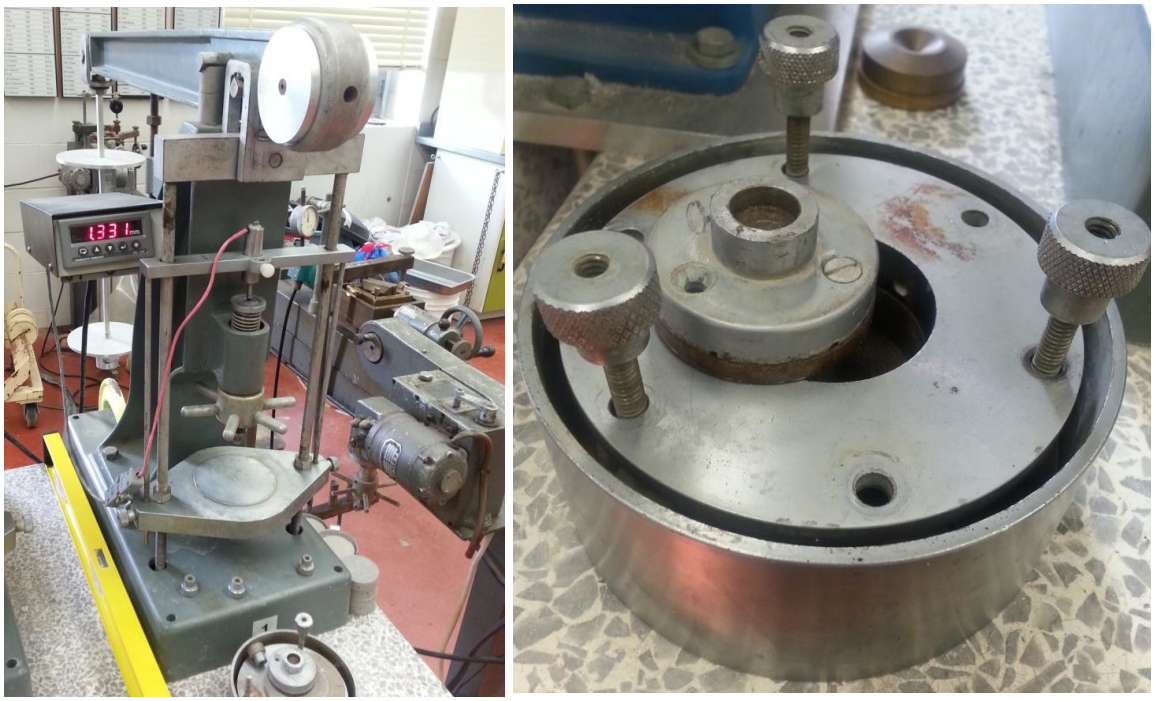

Figure 3.4. Oedometer apparatus and sample chamber

The goal of these tests was to determine the one dimensional compression behavior of the sand and silt mixtures and compare these results to the Rowe cell tests. Graphs of e vs. σ_v', k vs. σ_v', and m_v vs. σ_v' were plotted to acquire the one dimensional critical state parameters M (slope of the CSL), λ (compression index), and Γ (intercept).

3.6. Direct Shear

Five direct shear tests each were performed on clean Toyoura sand and silica flour according to ASTM D3080 to determine the internal friction angle and peak dilation angle of each material. The dilation angle was determined from the maximum slope of the vertical displacement versus horizontal displacement curves and using Equation 3.8.

$$\boldsymbol{\varphi = \phi'_{pk} - \phi'_{cs}} \qquad \textbf{[3.8]}$$

All samples were created with a dry density of 1.40 g/cm^3, with dimensions of 60 x 60 x 19.9 mm for a volume of 70,036 mm^3 excluding the ribbed plates. Tests were performed on a Wykeham Farrance Eng. Ltd. direct shear box with a 13 lb 1.5 oz hanger (Figure 3.5) and stress increments of 25.0, 41.4, 58.4, 152.4, 200.0 and 302.3 kPa. The load cell (S/N 015560) had a resolution of 0.001 kN and the LVDT had a resolution of 0.001 mm. For Toyoura sand and silica flour a shear rate of 0.182 mm/min was used to achieve a 10% strain in 60 minutes (Head, 1986).

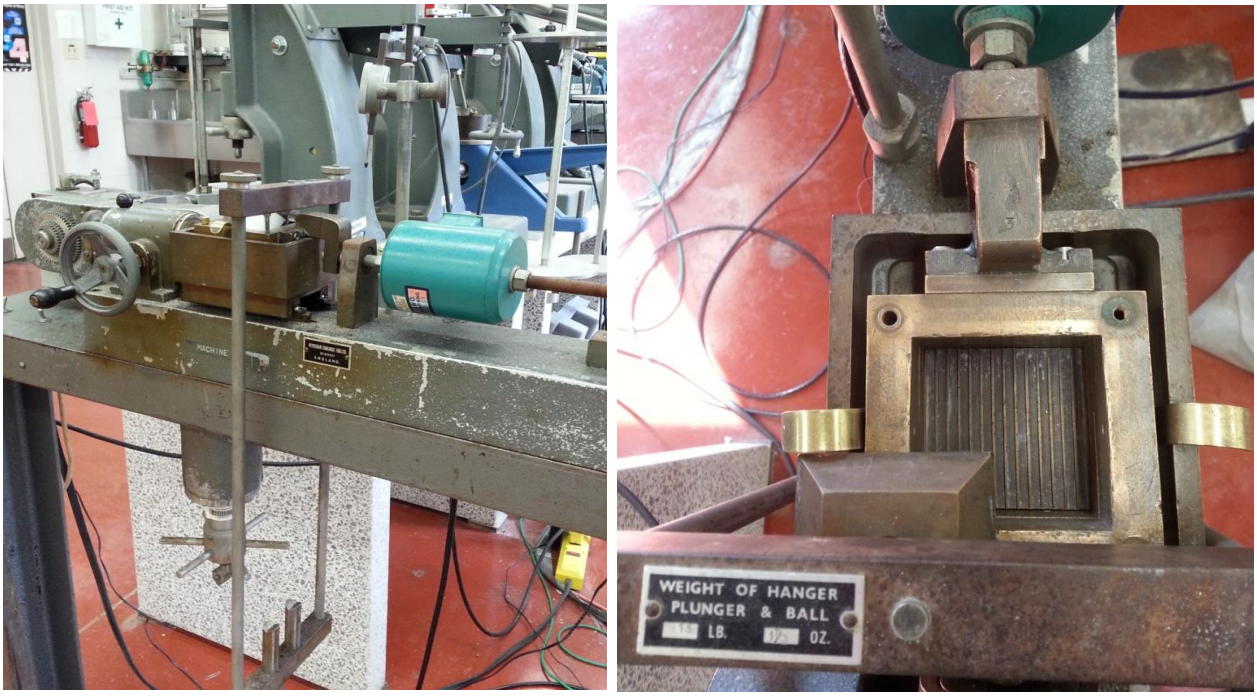

Figure 3.5. Direct shear apparatus, sample box, and hanger

3.7. Bender Element Testing

3.7.1. Shear and P-wave Velocity Measurements

A series of 16 bender element tests were performed with varying silt, cement and fibre contents to determine the shear wave velocity, P-wave velocity, and shear modulus of each sample (Table 3.6). Tests were performed according to ASTM D4767-04 for triaxial testing in a 2 MPa Bishop and Wesley triaxial cell (S/N 13301) (Figure 3.6). The 5 kN load cell (S/N 36186) was accurate to 0.1% of the full scale output with a resolution of 0.0001 kN. Back and vertical pressure measurements were accurate to ±0.5% of the full range (2000 kPa) with a resolution of 1 kPa. Pore pressure measurements were accurate to 0.5% of the full range (3447 kPa) with a resolution of 0.01 kPa (S/N 85407). Water volumes were accurate to 0.25% of the measured value, with a resolution of 1 mm^3. The axial displacement was measured using an LVDT (S/N 10C00009) accurate to ±0.5% full range (50 mm) with a resolution of

0.0001 mm. Bender elements were 2.3 mm long cantilever type, piezoceramic plates (GDS Instruments Internal Product Testing).

Table 3.6. Testing regimen for bender element tests

% Sand	% Silt	% Cement	% Fiber	ρ_{max} (g/cm^3)	$\rho_{experiment}$ (g/cm^3)	ρ_{min} (g/cm^3)
0	100	0	0	1.440	1.272	1.015
100	0	0	0	1.640	1.490	1.346
0	99	0	1	1.440	1.272	1.015
99	0	0	1	1.640	1.520	1.346
0	99	2	0	1.440	1.280	1.015
98	0	2	0	1.640	1.530	1.346
97	0	2	1	1.640	1.530	1.346
86.5	10.5	2	1	1.651	1.560	1.445
76	21	2	1	1.680	1.579	1.431
69	28	2	1	1.692	1.590	1.418
62	35	2	1	1.699	1.590	1.400
55	42	2	1	1.699	1.582	1.379
0	97	2	1	1.440	1.280	1.015
99	0	1	0	1.640	1.530	1.346
97	0	3	0	1.640	1.531	1.346
96	0	4	0	1.640	1.533	1.346

Cylindrical samples were prepared using the moist tamping method in five lifts of 20 mm each (for a total height of 100 mm), 50 mm diameter, to a relative density of 50-60%. Carbon dioxide was bubbled through each sample for 1.5 hours, after which distilled de-aired water was slowly flushed through the sample from the bottom until no more bubbles exited. Vertical and base pressures were then increased to 200-400 kPa with a constant effective stress of 10 -15 kPa to dissolve any remaining CO_2. A B-value of 0.95 or higher was achieved before consolidation began to ensure complete saturation and consistent results between tests. The vertical pressure was increased in the following effective stress increments: σ'=15, 25, 50, 100, 200, 400 kPa. Consolidation was considered to be complete when the back volume change was less than 5 mm^3 over a period of five minutes, as

calculated by the GDS software. After consolidation was achieved for each stress increment, a shear wave and P-wave were pulsed through the sample and responses were measured.

Bender element shear and P-wave propagations were analyzed using GDS Bender Element Analysis Tool (BEAT) software, with the distance travelled being measured from the tip of each bender element (Dyvik & Madshus, 1985; Viggiani & Atkinson, 1995; Lee & Santamarina, 2005). The first arrival time was determined using the BEAT software using peak-to-peak response for shear waves to avoid near field effects and side-reflected compression waves (Youn, Choo, & Kim, 2008), and the first maxima for the P-waves.

Using Microsoft Excel, the following graphs were plotted for all bender element tests:

1. Back volume (mm^3) vs. Square root of time (mins) for each stress increment
2. Bender element output signal vs. Time (ms) for each stress increment
3. Shear modulus (MPa) vs. Cambridge effective stress (kPa)

3.7.2. Consolidated Undrained Shearing

At 400 kPa effective stress, samples were sheared to a maximum strain of between 15% and 25% for silty sand and dense sand respectively. All tests were failed in 2-5 hours; the minimum time suggested for cohesionless samples. The rate of strain was calculated from Equation 3.9 below (Head, 1986):

$$\boldsymbol{Rate\ of\ strain} = \frac{\boldsymbol{\varepsilon_F H}}{\boldsymbol{100 t_f}} \qquad \textbf{[3.9]}$$

Where ε_f is the failure strain (%), H is the sample height at the onset of shearing (mm), and t_f is the time to failure (mins).

Undocked sample heights were calculated using Equation 3.10. (Head, 1986):

$$H_f = H_0\left(1 - \frac{1}{3} * \frac{\Delta V_b}{V_0}\right) \quad \textbf{[3.10]}$$

Where H_f is the sample height after consolidation (mm), H_0 is the initial sample height (mm), ΔV_b is the change in back volume during consolidation (mm^3), and V_0 is the initial sample volume (mm^3).

Using Microsoft Excel, the following graphs were plotted for all undrained shearing tests:

1. Deviator stress (kPa) vs. Axial Strain (%)
2. Pore water pressure (kPa) vs. Axial strain (%)
3. Deviator stress (kPa) vs. Cambridge effective stress (kPa)→ phase transformation line (PTL)
4. Deviator stress (kPa) vs. Cambridge effective stress (kPa) → critical state line (CSL)

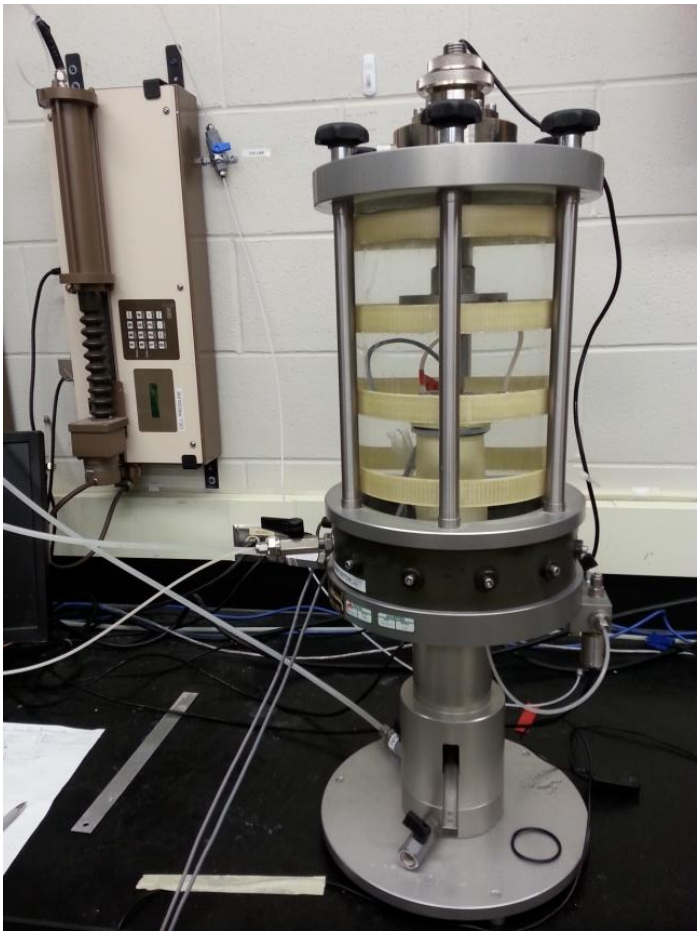

Figure 3.6. Bishop and Wesley triaxial cell for bender element testing

3.8. Cyclic Triaxial Testing

A series of 44 cyclic triaxial tests were performed with varying silt, cement and fibre contents (Table 3.7) to determine the liquefaction resistance of each sample and observe the behaviour during undrained cyclic shearing. Tests were performed according to ASTM D3999-11 in a 2 MPa triaxial cell Figure 3.7. The 5 kN load cell (S/N 25652) was accurate to 0.1% of the full scale output with 0.0001 kN resolution. Back and cell pressures were accurate to ±0.5% of the full range (2000 kPa) with 1 kPa resolution. Pore pressure was accurate to 0.5% of the full range (500 psig) with 0.01 kPa resolution (S/N 85407). Water volumes were accurate to 0.25% of the measured value, with 1 mm^3 resolution. Axial displacement was accurate to ±0.5% full range (50 mm) with 0.0001 mm resolution using an LVDT (S/N 05F01389).

Fifty millimeter diameter samples were prepared using the moist tamping method in five lifts of 20 mm each (for a 100 mm sample height) to a relative density of 50-60%. Carbon dioxide was flushed through each sample for 1.5 hours, after which distilled, de-aired water was slowly flushed through the sample from the bottom until no more bubbles came out. The back pressure was then increased to between 200-500 kPa with a constant effective stress of 10 to 15 kPa to maintain the sample's form. A B-value of 0.96 or higher was achieved before consolidation began to ensure complete saturation and consistent results between tests (Toki et al., 1986). Specimens were cycled at an effective stress of 100 kPa, a frequency of 1 Hz (though the effect of frequency from 0.05-1Hz has been found to be negligible (Toki et al., 1986), and stiffness estimates ranging from 0.4-1.0 kN/mm for un-cemented and cemented samples respectively. The initial stiffness estimate was lowered to more accurately acquire data during the rapid stiffness reduction caused by cyclic liquefaction.

Table 3.7. Testing regimen for cyclic triaxial tests

% Sand	% Silt	% Cement	% Fiber	ρ_{max} (g/cm^3)	$\rho_{experiment}$ (g/cm^3)	ρ_{min} (g/cm^3)	# Tests
100	0	0	0	1.640	1.490	1.346	4
99.5	0	0	0.5	1.640	1.490	1.346	1
99	0	0	1	1.640	1.490	1.346	1
88.5	10.5	0	1	1.651	1.556	1.445	1
79	21	0	1	1.680	1.570	1.431	1
71	28	0	1	1.692	1.586	1.418	1
64	35	0	1	1.699	1.586	1.400	1
57	42	0	1	1.699	1.579	1.379	4
0	99	0	1	1.440	1.272	1.015	1
98	0	2	0	1.640	1.530	1.346	4
49	49	2	0	1.699	1.582	1.379	1
0	98	2	0	1.440	1.280	1.015	4
97	0	2	1	1.640	1.53	1.346	4
86.5	10.5	2	1	1.651	1.56	1.445	1
79	21	2	1	1.680	1.570	1.431	1
69	28	2	1	1.692	1.590	1.418	1
62	35	2	1	1.699	1.590	1.400	1
55	42	2	1	1.699	1.582	1.379	1
0	97	2	1	1.440	1.280	1.015	4
89.5	10.5	0	0	1.651	1.560	1.445	1
79	21	0	0	1.680	1.570	1.431	1
72	28	0	0	1.692	1.586	1.418	1
65	35	0	0	1.699	1.586	1.400	1
58	42	0	0	1.699	1.579	1.379	4
0	100	0	0	1.440	1.272	1.015	4
97	0	3	0	1.640	1.532	1.346	1
96	0	4	0	1.640	1.532	1.346	1

Using Microsoft Excel, the following graphs were plotted for all cyclic triaxial tests:

1. Load (kN) vs. Axial displacement (mm)
2. Double amplitude axial strain (%) vs. Number of cycles
3. Secant shear modulus (MPa) vs. Double amplitude shear strain (%)
4. Excess pore water pressure (kPa) vs. Number of cycles
5. Peak cyclic stress (kPa) vs. Number of cycles
6. Deviator stress (kPa) vs. Cambridge effective stress (kPa)
7. CSR vs. Number of cycles (for samples with more than one test performed)

The cyclic stress ratio (CSR) was calculated for each sample (Equation 3.11):

$$\mathbf{CSR} = \frac{\mathbf{q}}{\mathbf{2\sigma_{3'}}} \quad \textbf{[3.11]}$$

Where q is the deviator stress (kPa) and σ_3' is the effective confining pressure (kPa). The CSR and the number of cycles to failure were plotted against each other to develop a liquefaction resistance curve.

The damping ratio was calculated using Equation 3.12 from ASTM D3999-11 below:

$$\boldsymbol{D}(\%) = \frac{\boldsymbol{A_L}}{\boldsymbol{4\pi A_T}} \boldsymbol{x100}\% \quad \textbf{[3.12]}$$

where D(%) is the damping ratio, A_L is the area of the hysteresis loop of the load vs. displacement graph, and AT is the area of the right triangle within the hysteresis loop.

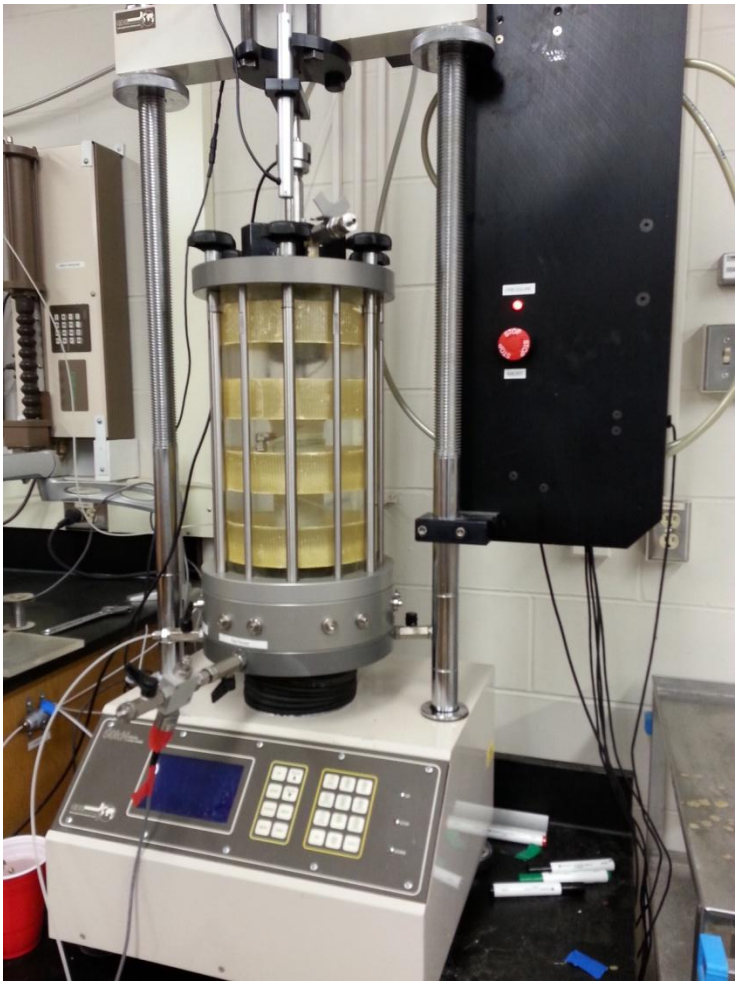

Figure 3.7. Pneumatic cyclic triaxial apparatus

CHAPTER 4: Results and Discussion

4. Results and Discussion

4.1. Introduction

The study of the dynamic and flow properties of sands and silty sands is extensive in the literature. The effect of cement and fibre stabilization, specifically on liquefiable silty sands, is less well understood. To understand the failure mechanisms of stabilized silty Toyoura sand, computerized tomography (CT), scanning electron microscopy (SEM), and mercury intrusion porosimetry (MIP) has been first used to develop a qualitative and quantitative description of the small scale (micro-fabric) characteristics and behavior. The interaction between the particles, fibres, and cement was analyzed and pore size distributions were identified. Subsequently, oedometer and Rowe cell tests were performed to determine the one dimensional compressibility and consolidation behaviour and parameters; allowing comparison of the effects of silica flour, cement, and PVA fibre on the response of Toyoura sand. To obtain the stress-strain responses of Toyoura sand with these additives, a series of bender element tests and monotonic and cyclic triaxial tests were performed at small and large strain levels respectively.

4.2. Scanning Electron Microscopy

A scanning electron microscope uses a focused beam of electrons in a raster scan pattern to produce and detect signals that indicate surface topography and composition. The narrow electron beam allows for high resolution images from 10-500,000x magnification, which allows the visualization of depth and contours of microscopic elements (Atteberry, 2009). Using this technique on stabilized soil produces a microscopic image of the soil structure, fabric, shape, angularity, and most importantly the mechanical bonds between each soil element.

To get representative images of the soil and additives, five samples were tested in the Hitachi S-4500 field emission scanning electron microscope using a Quartz Xone EDX system and gold sputtering. Each sample was viewed at magnifications between 100-30,000x as shown below.

- Toyoura sand
- Silica flour
- PVA fibre
- 98% Toyoura sand and 2% cement
- 55% Toyoura sand, 42% silica flour, 2% cement, and 1% fibre

Microscopically, Toyoura sand can be clearly seen to be angular to sub-angular and fairly uniform in size (at 100x magnification), which confirmed results from USGS classification and sieve analyses and findings from other researchers (e.g. Lam & Tatsuoka, 1988; De & Basudhar, 2008), as seen in Figure 4.1a. At 10,000x magnification (Figure 4.1b), the microfines - representing 1.1% of the sample by mass passing the #200 (75μm) sieve - became visible. The mineralogical composition of Toyoura sand - 75% quartz, 22% feldspar and 3% magnetite - has a rating of 5.5 or higher on the Moh's scale of mineral hardness, and has brittle and angular cleavage, explaining the soil's angularity. Evident surface textures of the Toyoura sand included conchoidal fractures, edge abrasions, fractured plates and other angularities (Helland, Huang, & Diffendal Jr., 1997). These characteristics create bonding and frictional surfaces for cementitious material and can partially explain the 33.5-43.7° friction angle of the Toyoura sand.

Silica flour displayed angular to sub-angular grains with a plate-like structure (Figure 4.2a & b). The plate-like structure is a by-product of the manufacturing process of the silica flour, rather than natural weathering processes. At 100x magnification the relative size of silica flour became apparent,

and at 30,000x optical zoom, the minutia of the particles (many smaller than 56.6 nm) could be seen. The silica flour fills the voids between the Toyoura sand particles and, up to 35-42% silica flour content, increases the soil maximum density as seen in Figure 3.2 of Section 3.3. Surface features of the silica flour included angular and rounded outlines, step features, edge abrasions, and micro-abrasions (Helland, Huang, & Diffendal Jr., 1997).

The PVA fibres vary in diameter from 110-120 μm, with striation widths of 5 μm to less than 1 μm along the 12 mm length (Figure 4.3a & b). These micro-striations have small filaments protruding from them; likely a result of the extrusion process used in their fabrication. These striations and filaments give the fibres a surface roughness, and with the existing angularity of the Toyoura sand, an ideal medium for cementitious bonding (Toutanji et al., 2010; Al-Attar, 2013). It has been shown in the literature that the addition of fibres up to a concentration of 2% by mass can improve sample strength and rigidity, but above this threshold they tend to increase soil porosity and negate the strength increase (Gray & Refeai, 1986). The positive effects of fibre addition below this threshold can be further augmented via the addition of cement. These concepts will be discussed further in the forthcoming sections.

Cement hydration bonds the granular particles to each other and the PVA fibres, supplementing the existing mechanical bonds and improving the undrained shear strength of the sample as mentioned above. Because Portland cement can take several months to fully hydrate, the three day curing period used for these tests leaves some granular cement visible (shown in the CT scans in Section 4.3.1). It is also likely that the outer portions of the cement grains began to hydrate first based on the metastable barrier hypothesis (Bullard et al., 2010; Jennings & Pratt, 1979), which delays the hydration of the interior and prevents uniform distribution. The mechanical bonds created by the expansion of the OPC between the sand grains can be seen in Figure 4.4.

Figure 4.4-4.7 show the combinations of silica flour, cement, fibre and Toyoura sand. Progressively zooming in on the cementitious bond between the soil grains and fibres shows how each component potentially interacts. Figure 4.5 shows a broken cement bond between the fibre and soil caused by extraction of the sample for SEM scanning. This figure is representative of the soil after failure of the mechanical and chemical bonds. Figure 4.6 clearly shows cement hydration products such as Ettringite needles (Sasanian & Newson, 2013). It also illustrates the cement coating the PVA fibres during hydration and the bonding of the silt particles to individual fibres. Finally, Figure 4.7 supports the hypothesis that the cement coats the PVA fibres and fills the striations, further improving the strength of the bonds.

The microstructural views of Toyoura sand with and without silt and stabilizers provides further understanding of the behaviour seen on a macro scale. From the surface texture of individual constituents, to the interaction between the multiple additives, the SEM scans show how the fibres and cement may strengthen a silty sand by bonding the constituents together, creating rougher particles and enhancing interlocking. The addition of these stabilizers decreases the compressibility of soil and improves resistance to dynamic loading and static shearing, as evidenced by this interlocking.

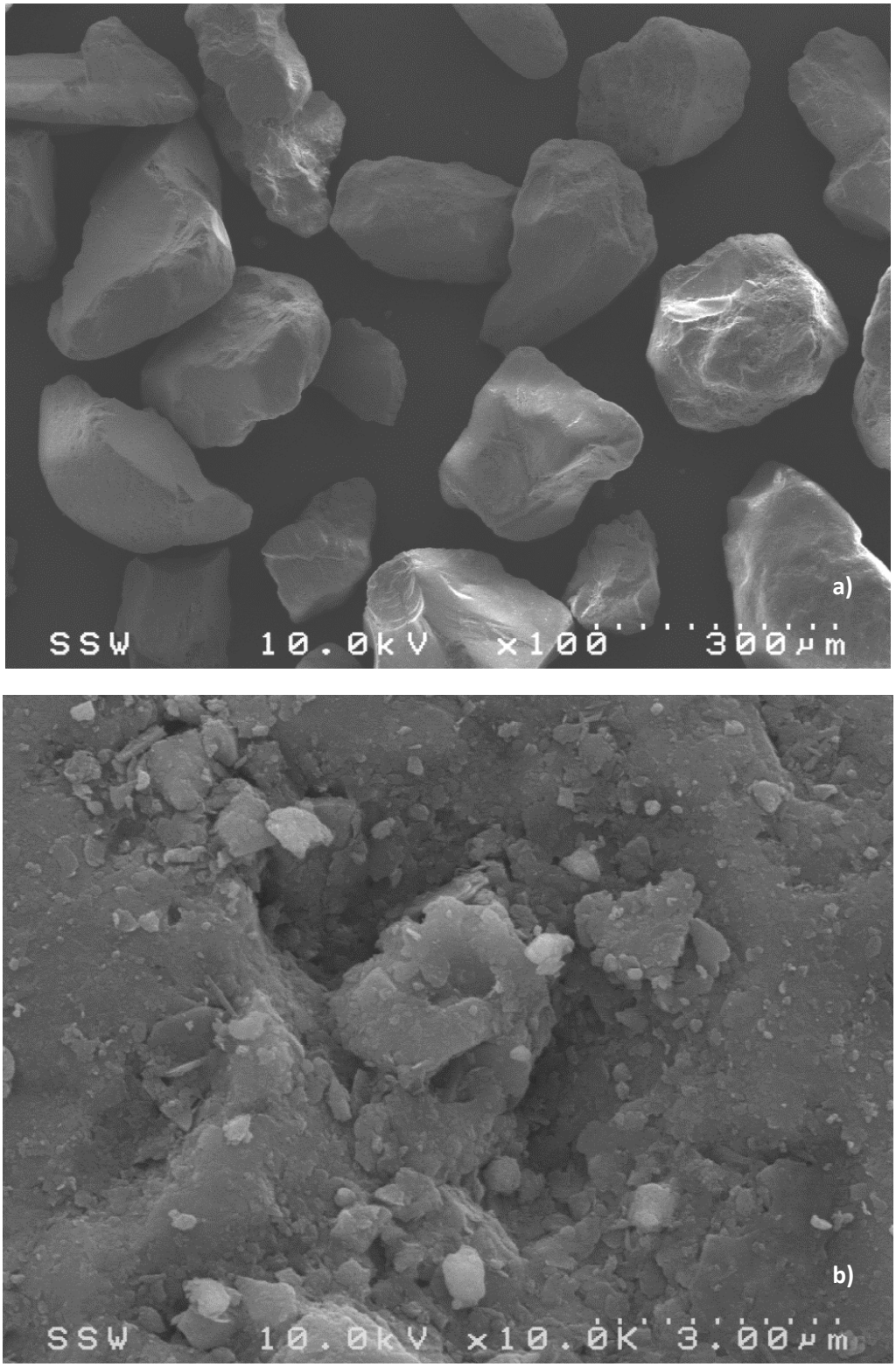

Figure 4.1. Toyoura sand at a) 100x optical zoom; b) 10,000x optical zoom

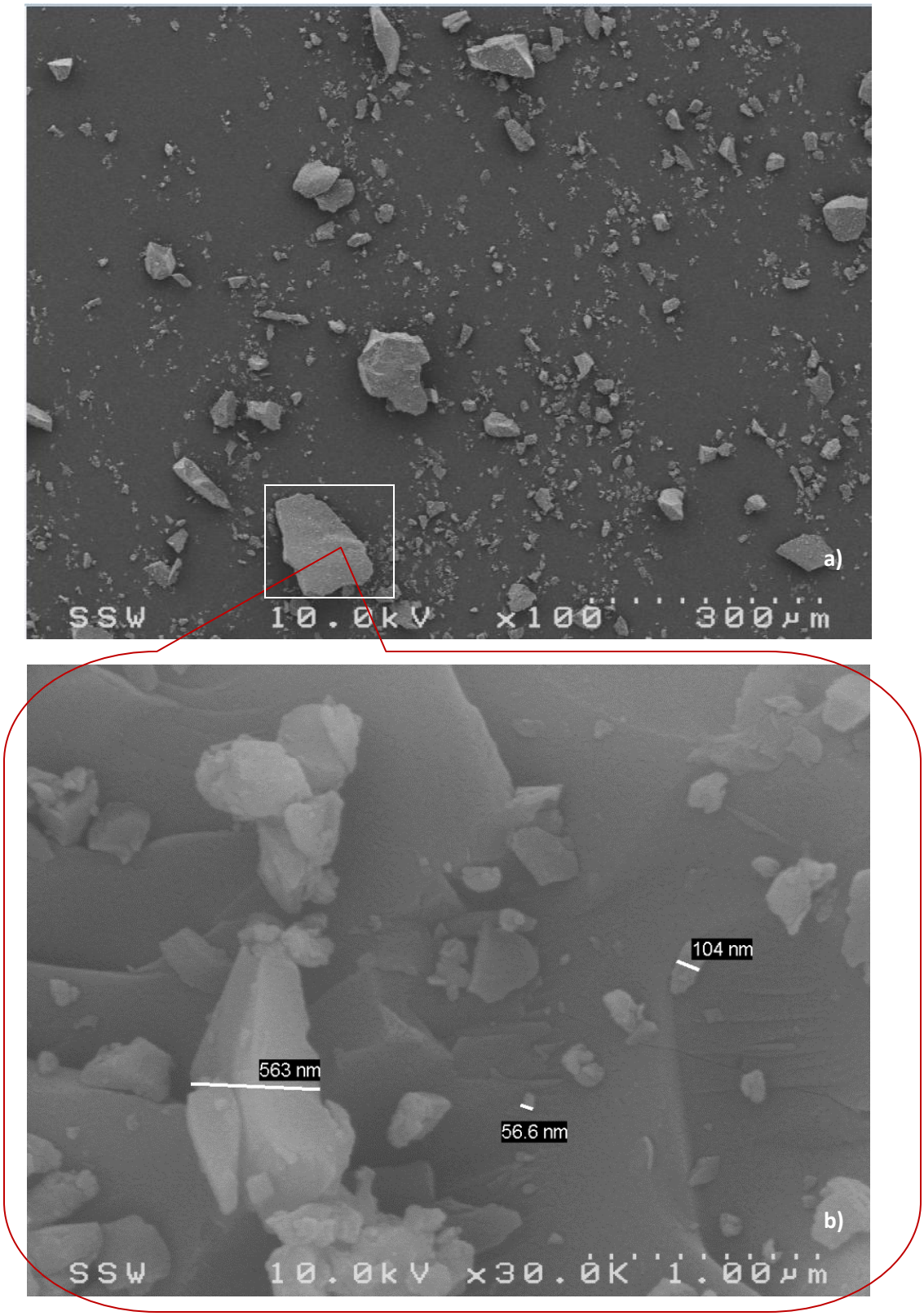

Figure 4.2. Silica flour a) 100x optical zoom; b) 30,000x optical zoom of silica flour particle in 1a)

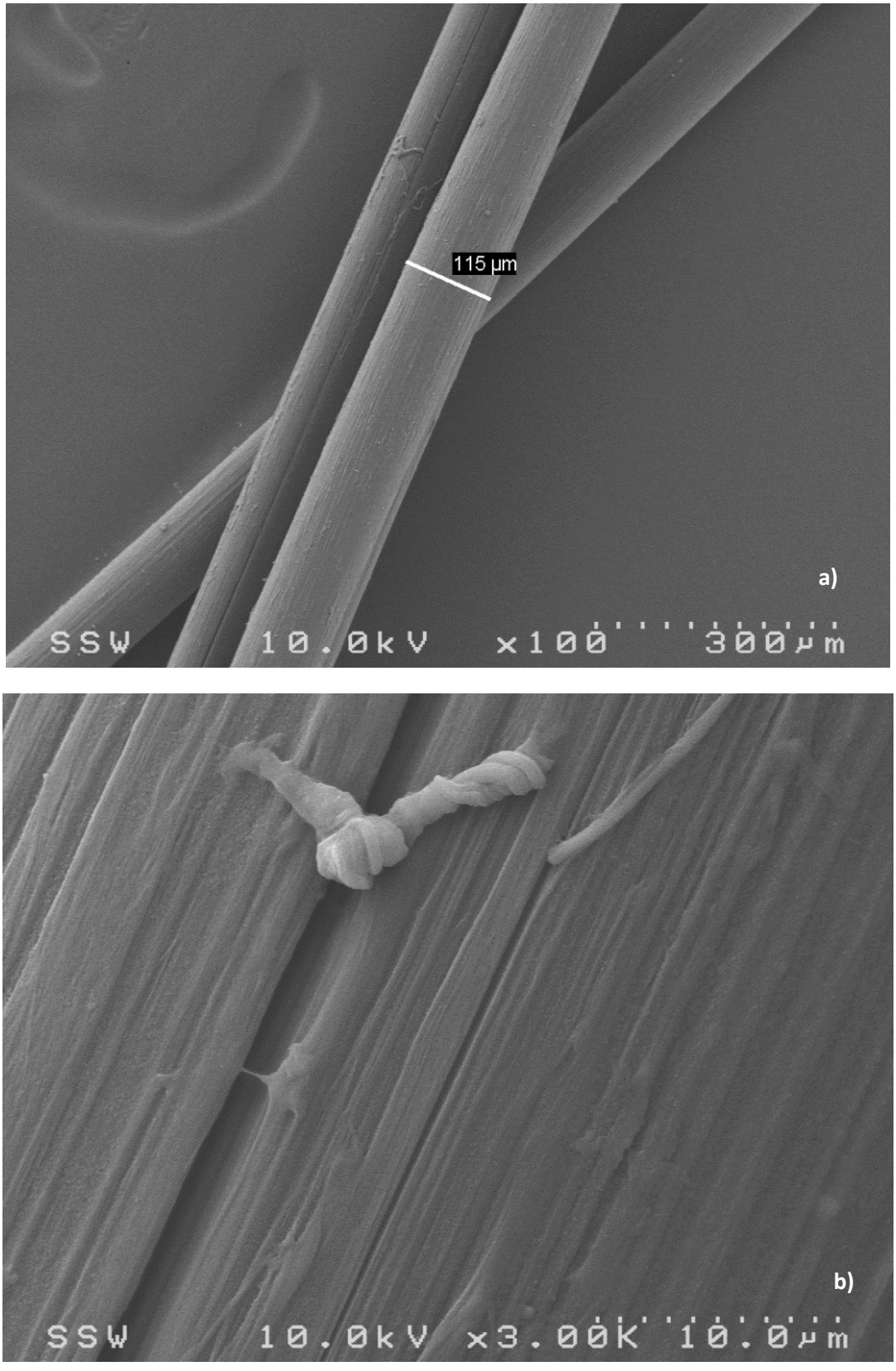

Figure 4.3. PVA fibre a) 100x optical zoom; b) 3000x optical zoom

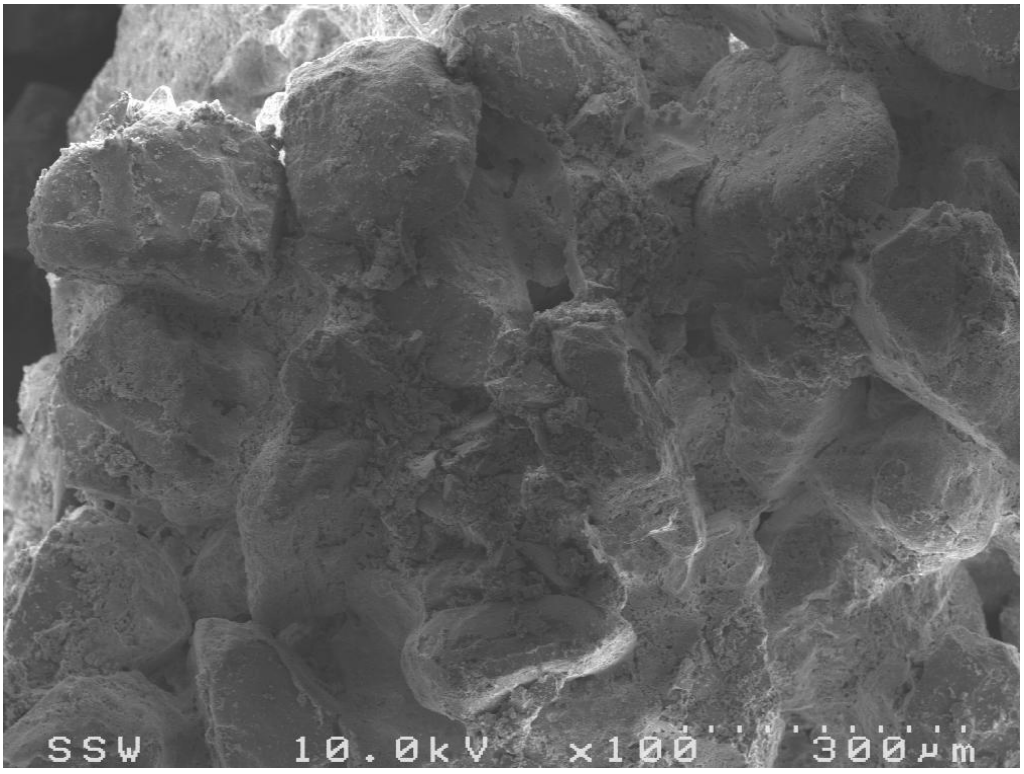

Figure 4.4. Cemented Toyoura sand 100x optical zoom

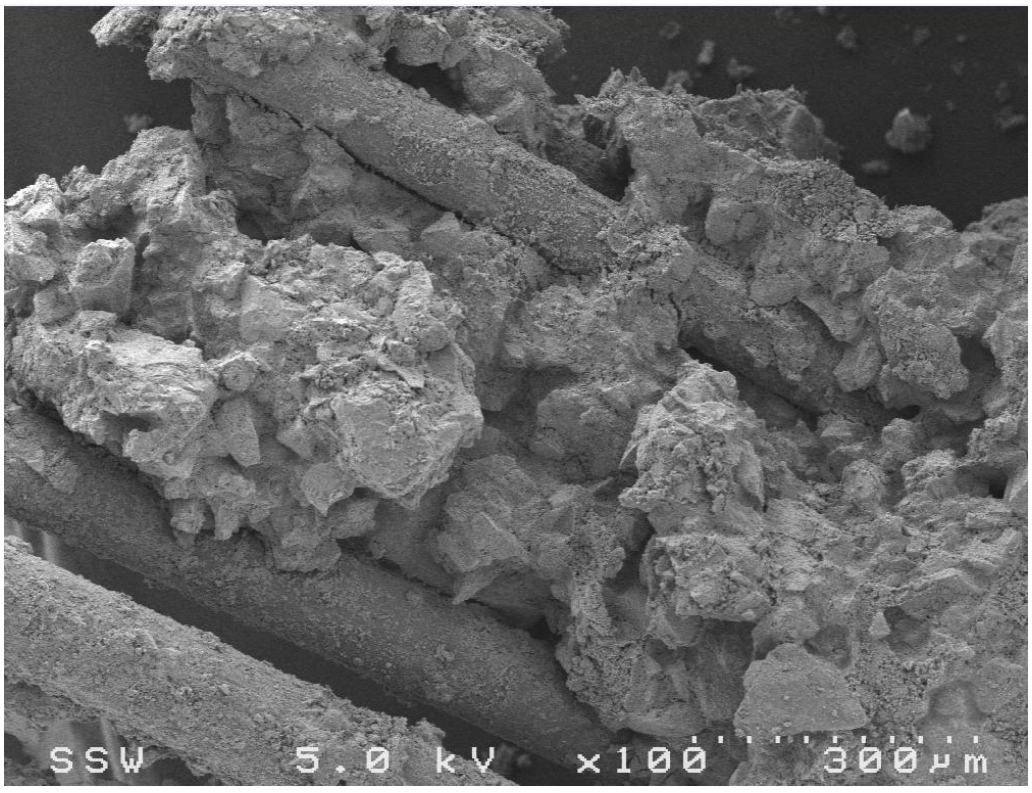

Figure 4.5. Cemented Toyoura sand with PVA fibres and silica flour 100x optical zoom

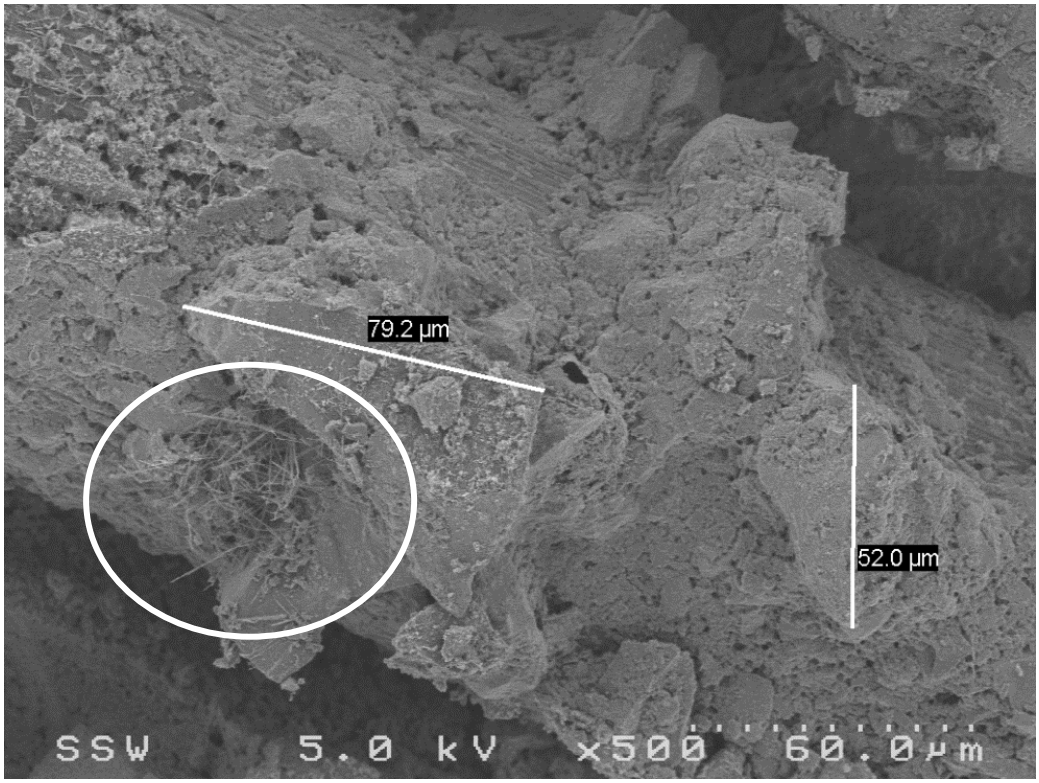

Figure 4.6. Ettringite and cement bonding of Toyoura Sand with silica flour and PVA fibres 500x optical zoom

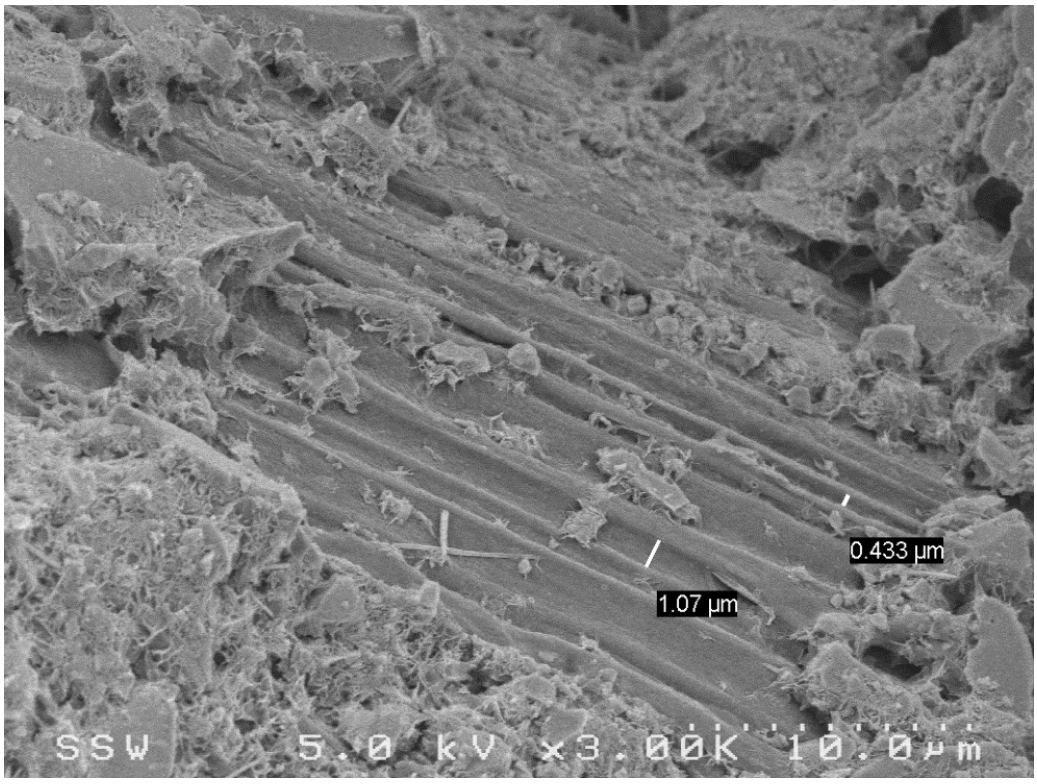

Figure 4.7. Striations along cement-bonded PVA fibre 3000x optical zoom

4.3. Computerized Tomography & Mercury Intrusion Porosimetry

Through computerized tomography (CT) scans, the isotropy and homogeneity of several samples of Toyoura sand with and without silica flour and stabilizers was visualized. Mercury intrusion porosimetry (MIP) testing was conducted in parallel to the SEM and CT scans' qualitative soil structure analysis to further quantify the pore structure dimensions and volumes. Each of these tests helped to develop a greater understanding of the skeletal and pore structure of Toyoura sand, silica flour, and their stabilized forms.

4.3.1. Computerized Tomography Imaging

CT imaging was conducted to confirm the isotropy and homogeneity of samples constructed using the moist tamping method. For all of the CT images, the brighter the pixels are (i.e. the greater the Hounsfield unit grayscale value), the higher the relative density and mineralogy of the constituent (Mah, Reeves, & McDavid, 2010). Representative cross sections of each sample are illustrated in Figure 4.8-4.14 . Consistent bulk density was found for all of the tested cylindrical triaxial samples throughout the X, Y and Z cross sections (an example of which is shown in Figure 4.8), though often the interfaces between tamped layers were slightly less dense than the layers themselves. Samples with silica flour, cement, and fibre were the most visually representative due to the high variation in the gray scales of each constituent. For clean Toyoura sand, the voxel resolution of 50 μm is not accurate enough spatially to distinguish individual particles, though the bright pixels in Figure 4.8 may represent mineral constituents (i.e. magnetite). Overall, there are a few minor densified zones (circled as an example in Figure 4.8) which are likely to be due to the moist tamping method of sample preparation (Ladd, 1978).

Due to the use of the moist tamping method, the PVA fibres tend to randomly orient themselves with a slight preferential horizontal orientation as shown in Figure 4.9, Figure 4.13, and Figure 4.14 and

corroborated by (Ibraim et al., 2013). Quantitatively, there are approximately 4,600-36,000 fibres in any given bender element or cyclic triaxial sample (varying from 0.25% by mass to 2% by mass), and more in each Rowe cell sample (see Appendix A for a sample calculation). Therefore, in each layer there is an average of 23-183 fibres per cm^3 for bender element and cyclic triaxial samples. Many of these fibres are clustered together in group strands of about 5-30 fibres, making them visible to the CT scanner, while the individual strands are too thin to detect. The fibres represent 0.4-2.3% of the sample volume at 0.25-2% by mass.

The addition of the silica flour to the Toyoura sand creates local pockets of densified material as seen in Figure 4.10. During the sample preparation process, the silica flour and sand tend to exhibit clumping after moisture is added. This apparent adhesion is likely to be the cause of the dense regions, as the Toyoura sand and the silica flour have fairly similar specific gravities (2.647 for the sand versus 2.641 for the silica flour) and do not appear to contrast much in the CT images.

The CT images also indicate the dispersion of the cementitious materials and the location and orientation of the PVA fibres (Figure 4.12-4.14). The cement appears to initially hydrate locally in nodules rather than homogeneously distribute throughout the sample, likely due to the low initial cement concentration of 2% and the inability to completely hydrate during the three day curing time. Quantitatively, at 2% content by mass, the hydrated cement represents between 1.68-2.12% of the sample volume depending on the density, shown in the cross sections in Figure 4.11-4.14.

When all of the additives are combined in the soil sample, the result is a well dispersed silica flour/sand mixture with clear nodules of cement (shown in white in Figure 4.14). The fibres are, again, randomly oriented with a slight horizontal preference as visualized in 3D imagery. The CT scans do not, however, show any signs of the cement coating the PVA fibres as referenced in Section 4.2.

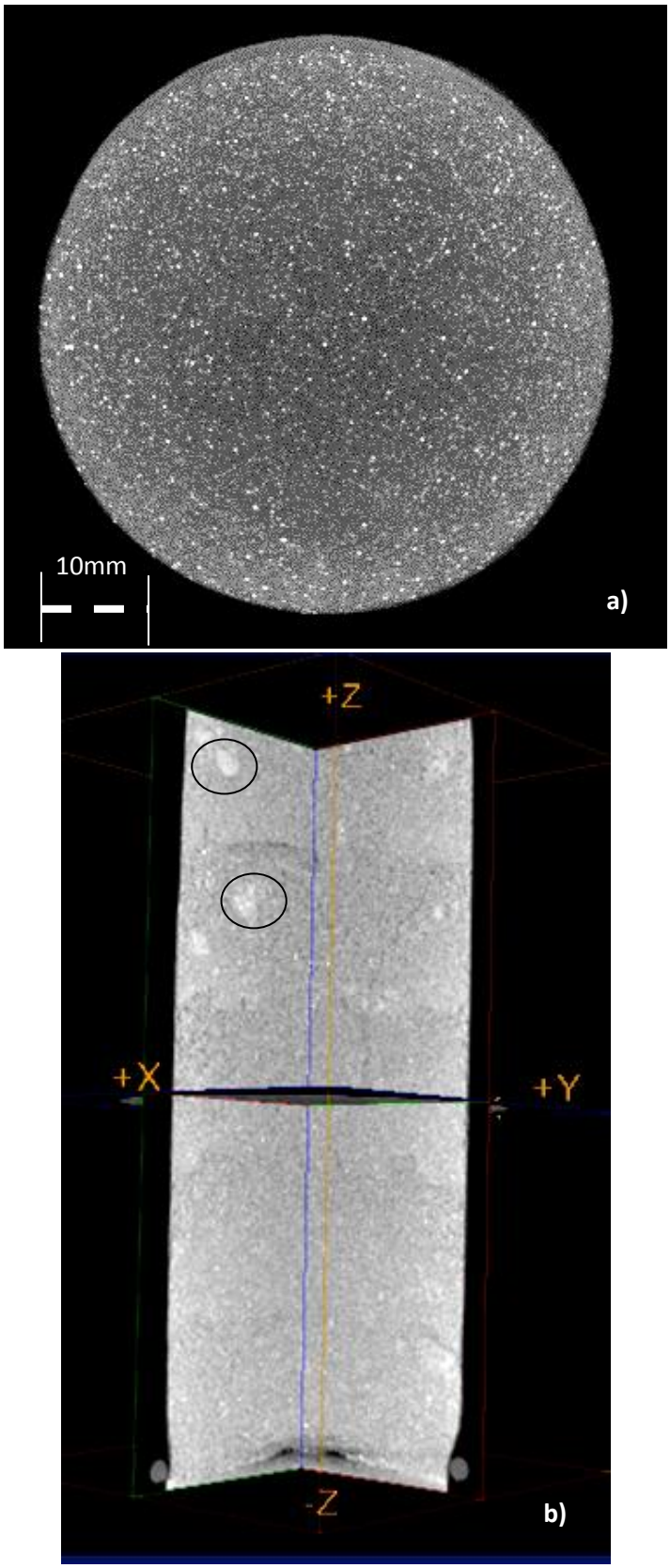

Figure 4.8. MicroCT image of Toyoura sand a) Z axis; b) X, Y, and Z planes with highlighted densified zones

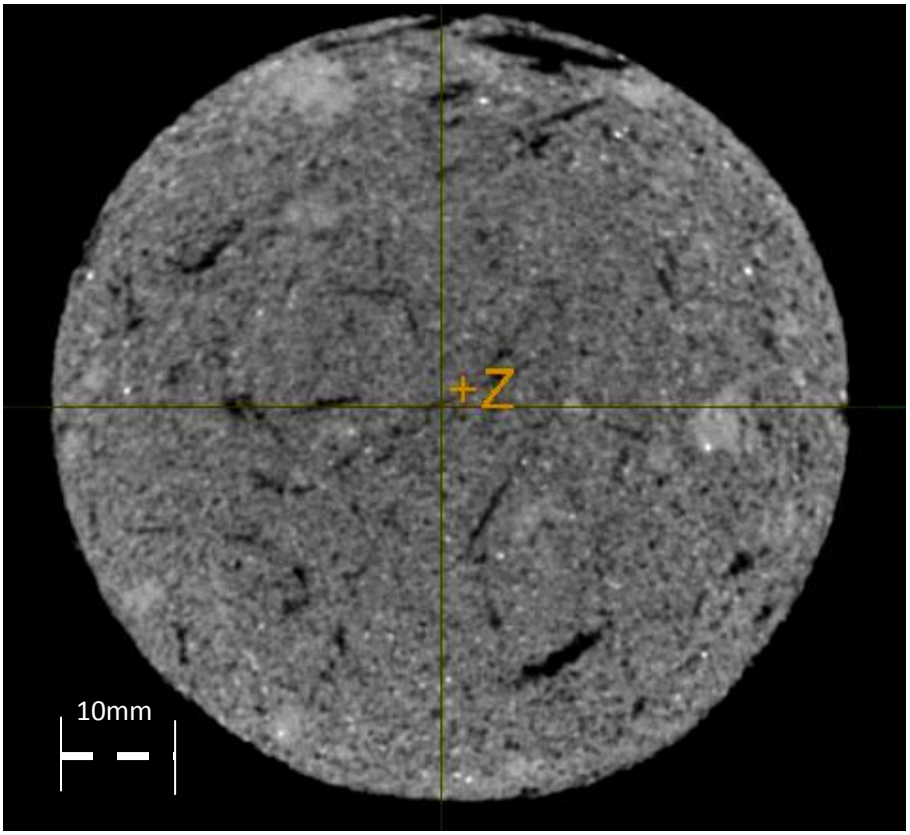

Figure 4.9. MicroCT Image of Toyoura sand with 1% fibre

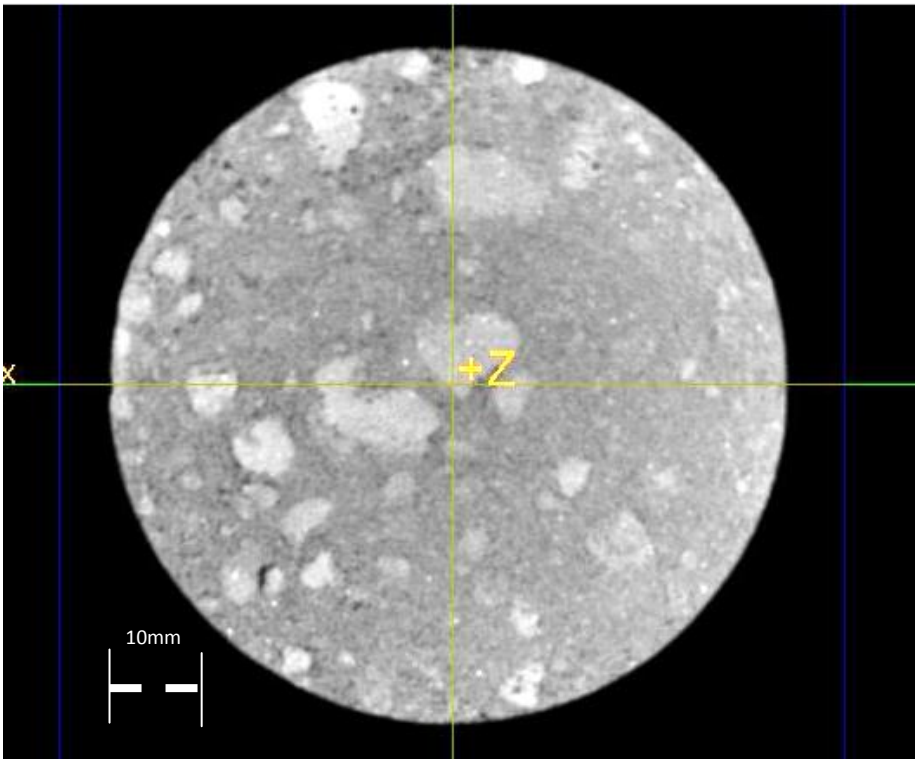

Figure 4.10. MicroCT image of Toyoura sand with 42% silica flour

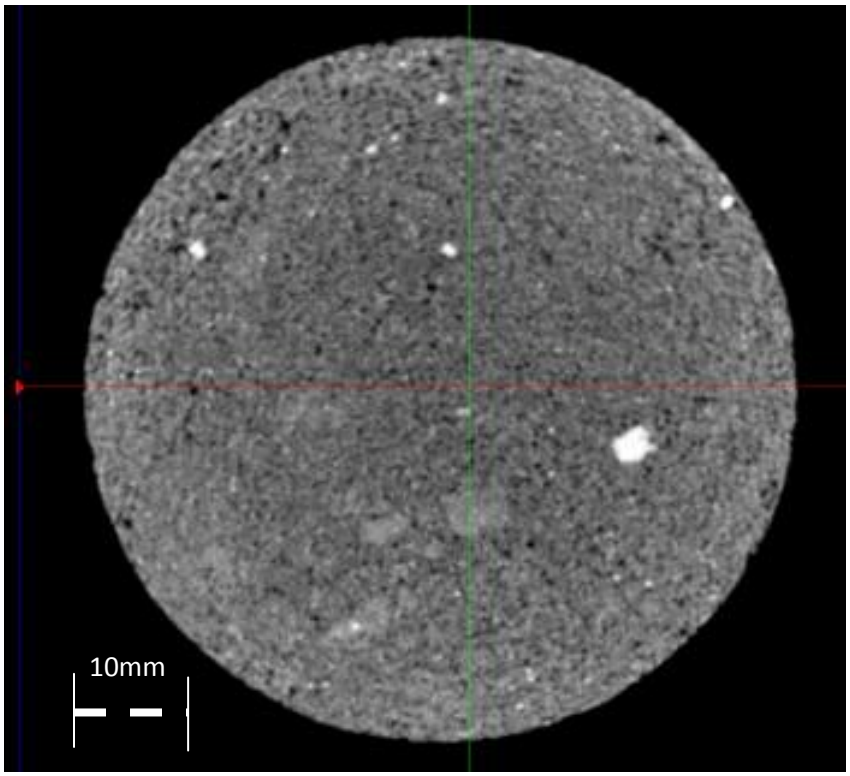

Figure 4.11. MicroCT image of Toyoura sand with 2% cement after three days hydration

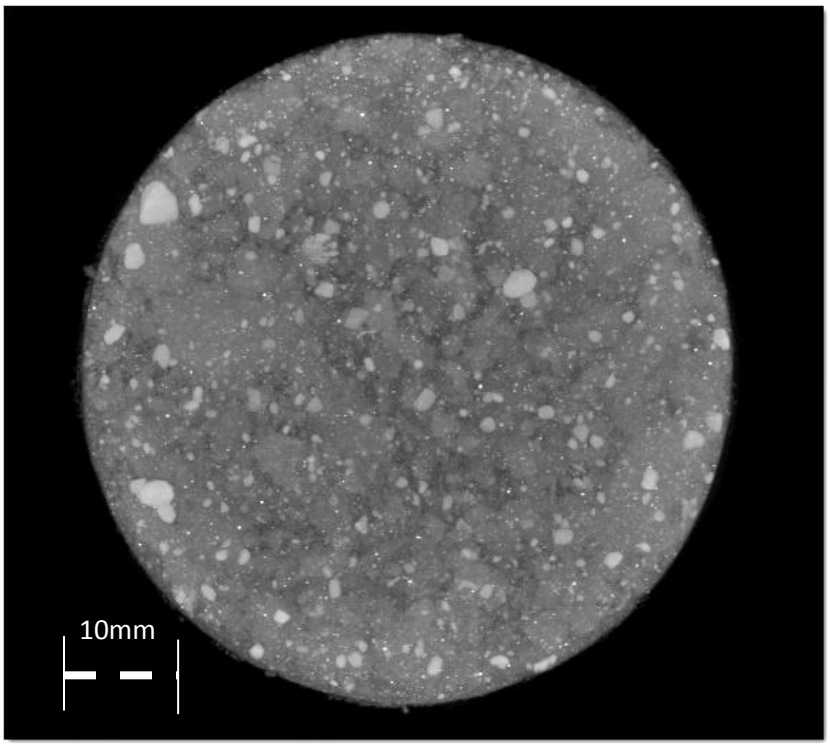

Figure 4.12. MicroCT image of Toyoura sand with 42% silica flour, 2% cement after one week hydration

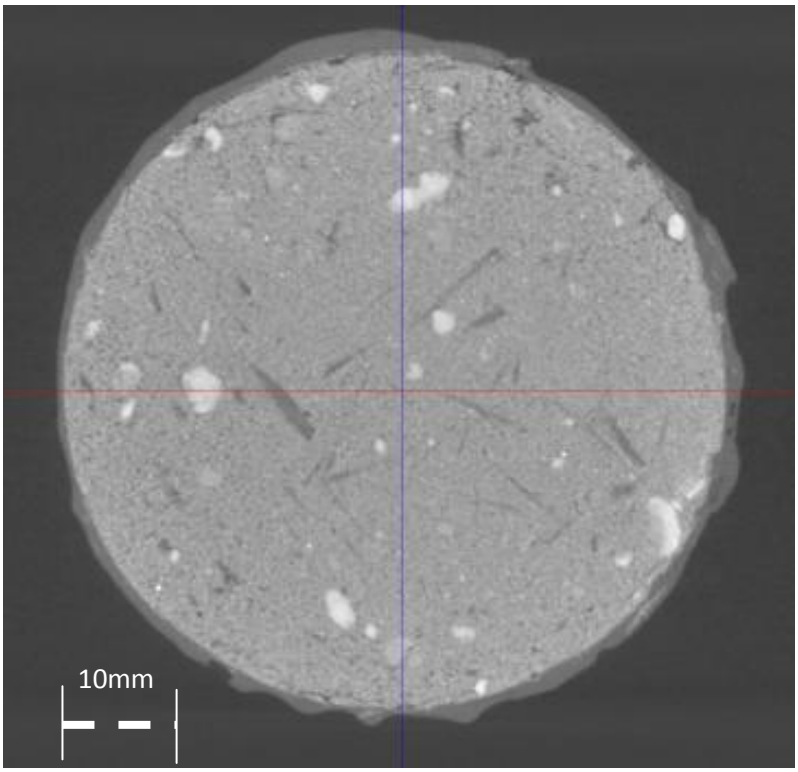

Figure 4.13. MicroCT image of Toyoura sand with 2% cement, 1% fibre after one week hydration

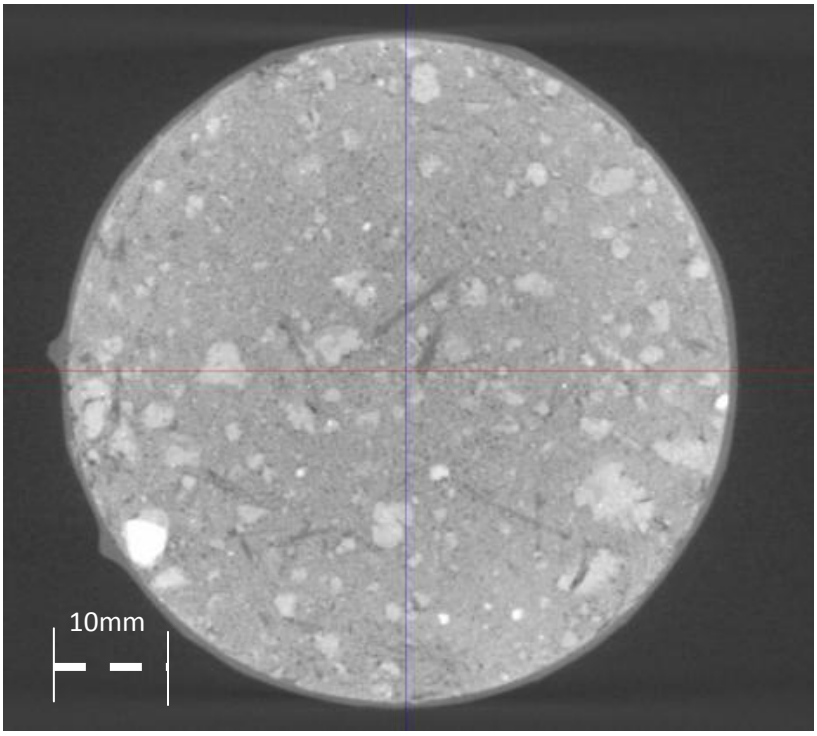

Figure 4.14. MicroCT image of Toyoura sand with 42% silica flour, 2% cement, 1% fibre after one week hydration

4.3.2. Mercury Intrusion Porosimetry

Mercury intrusion porosimetry has become a common way to determine the pore volume and pore size distribution of materials. The theory behind MIP testing, as described in Section 2.10 is based on the surface tension of mercury and the applied pressure required to infiltrate the mercury into progressively smaller pores. Knowledge of the pore size distribution allows for explanation of the change in permeability and microstructure of a sample when dosed with cement, PVA fibres, and silica flour. Testing was also performed to determine how the implementation of stabilizing additives affects the 'P_{50}' and 'P_{10}' values (representing the 50% and 10% finer pore size). Due to the potential sources of error in this test, most samples were tested in triplicate and compared to results from other test methods to validate the findings.

From Figure 4.15a it is clear that Toyoura sand has generally larger pore diameters, but a smaller overall volume of voids than the silica flour sample based on the initial sample mass found in Table 4.1. When all constituents (silt, cement, and PVA fibres) are added to Toyoura sand, a notable reduction in total intrusion volume (mL/g) is apparent, and the pore diameters reduce significantly as seen in the log differential intrusion graph in Figure 4.15b. A lower cumulative intrusion suggests a reduction in porosity of cemented samples as is expected from the cement hydration process. The process of mercury intrusion increased the bulk density of the loose soil (Table 4.1 column 5) from 0% (loose state) to 65.6% relative density for Toyoura sand, and from 0% (loose state) to 42.6% relative density for the silica flour.

When the cement content was varied from 0-4%, the trend generally indicated an increase in microporosity and a tendency toward more uniform pore sizes with an increase in cement content, consistent with the results of (Neri, 2013). This microporosity is the leading cause of decreased permeability within cemented samples. Regardless of cementation, the peak pore diameter sits

between 60-80 μm as seen in Figure 4.16b and the average pore diameter 'P_{50}' decreases by 15 μm. Notably, the 'P_{10}' value decreases dramatically with increasing cement content, from 39 μm to 1.53 μm helping to explain the reduction in permeability determined from Rowe cell testing in Section 4.4.2.

In these cemented samples, seven types of pores can exist: entrapped air, entrained air (more common for concrete), capillary pores, gel pores in cement paste, cross-linked pores, through-pores, and the interface transition zone between particles and cement (Cho, 2012). Many of these pores are completely filled with mercury during testing, though entrapped air (inaccessible from the specimen surface), through-pores (pores that run right through the sample) and the inkbottle effect (a small opening leading to a much larger internal pore) are commonly acknowledged as inherent errors with respect to cumulative intrusion and pore diameter results in soils (Sasanian & Newson, 2013).

When fibre was added to Toyoura sand at 0-2% by mass, the trend shows a decreasing intrusion level with an increase in fibre content (Figure 4.17). This is primarily due to the impermeable fibres filling the void space of the sample. Based on the log differential intrusion graph 0-0.5% fibre content shifts the curve left, to a larger peak pore size. From 1-2% fibre content a shift toward uniformly smaller pore diameters occurs, explaining the low permeability of the sample. There was also a 30 μm shift in the median pore diameter 'P_{50}' from 0-2% fibre. Generally, the addition of fibres tends to minimally alter the pore size distribution, though the permeability appears to reduce slightly with increased fibre content (Figure 4.19).

The most interesting trend is the addition of silica flour (10.5-42% content by mass; the upper percentages found in Tokyo Bay) to cemented samples as shown in Figure 4.18. It is well known that the permeability of a soil is largely dependent on the particle shape, porosity, particle size distribution, and pore size distribution (Krumbein & Monk, 1942; Shepherd, 1989; Marshall, 1958), and the introduction of a poorly graded, very fine silt produces obvious effects. Both the peak pore diameter and the void

volume steadily decreased with increasing silica flour content due to this changing sample gradation. The peak pore diameter of silty samples dropped from 65 μm to 3 μm, with a notable increase in microporosity (indicated by the spike in the log differential curve and the elongated tail of the pore size distribution in Figure 4.18b). The reason for this trend is that many of the larger pores between sand particles are filled with silica flour and cementitious materials, reducing the average pore diameter and decreasing the overall intrusion volume (Barden, McGown, & Collins, 1973). The progressively more uniform log differential intrusion graph explains the large decrease in permeability caused by an increase in silica flour content as determined by Rowe cell testing in Section 0.

In terms of the sample tortuosity (τ), all of the additives cause a notable increase as seen in Figure 4.19. Most distinctive is the jump in tortuosity of silty samples from τ=2.320 with 0% silt content, to τ=4.175 with 42% silt. The cementation of the Toyoura sand and the addition of the silt alter the pore size distribution, porosity, and soil structure, which accounts for this increase in tortuosity (Ghassemi & Pak, 2010). These values are slightly higher than those determined by Reed, Briggs, & Lavoie (2002) who found a tortuosity of 2.2 for uniform porous media. With respect to permeability, a decrease was seen when higher concentrations of silt and fibre were added to Toyoura sand. Calculated permeability values from the MIP testing were of the same order of magnitude (10^{-5}-10^{-7} m/s) as expected for fine grained and silty sands though lower than the values calculated from permeameter and Rowe cell testing (Lambe & Whitman, 1969; Spangler & Handy, 1982; McCarthy, 1998; Day, 2006).

Increasing the silt and fibre content lead to a reduction in permeability, again, due to the increase in microporosity and volume of impermeable elements. The cement, on the other hand, caused an unexpected increase in permeability; further testing should be performed to determine the cause of this phenomenon.

Porosity was calculated using the void volume and total volume of the specimen (Equation 4.1):

$$\boldsymbol{n = \frac{V_{voids}}{V_0}} \quad \textbf{[4.1]}$$

where n is the porosity, V_{voids} is the void volume, and V_0 is the total specimen volume.

Porosity from the MIP testing was reasonable for sands and silty sands (Lambe & Whitman, 1969). Permeability was calculated after intrusion using the Katz-Thompson equation (Equation 3.4), relating permeability to the threshold pressure (the pressure at which mercury finds a path spanning the sample) (Webb & DeSousa, 2010).

Table 4.1. Mercury intrusion porosimetry testing regimen and basic properties

Description	Sample Mass (g)	Penetrometer Volume (mL)	Cumulative Intrusion Volume (mL/g)	Bulk Density*** (g/mL)	Porosity (%)	Permeability $x10^{-5}$ (m/s)	Tortuosity
100% Sand	1.00	6.131	0.2632	1.539	39.296	7.495	2.876
100% SF**	1.19	6.131	0.3075	1.196	35.802	0.533	2.508
2% C	3.42	7.442	0.249	1.585	38.988	4.304	2.320
3% C	0.69	6.131	0.1890	1.747	31.654	4.541	2.957
4% C	1.05	6.131	0.2036	2.862	57.490	7.798	3.202
2% C, 0.5% F	1.40	16.131	0.1993	1.063	21.176	3.183	2.980
2% C, 1% F	0.63	6.131	0.1487	1.852	26.035	3.272	3.045
2% C, 2% F	1.42	16.131	0.1447	1.639	23.715	2.101	3.253
2% C, 10.5% SF	2.65	16.131	0.2273	1.245	28.295	3.503	3.135
2% C, 21% SF	3.54	16.131	0.2206	1.352	29.830	2.872	3.429
2% C, 42% SF	2.12	16.131	0.2169	1.205	26.122	0.630	4.175
2% C, 1% F, 42% SF	1.21	6.131	0.2189	2.093	45.064	1.542	3.987

Notes: * P_{60}, P_{50}, P_{30}, and P_{10} represent pore diameter in Figure 4.15-Figure 4.18

** C=Cement, F=Fibre, SF=Silica flour percentages by mass, with the remaining percentage being Toyoura sand

*** Bulk density, porosity, and tortuosity are calculated after complete intrusion and are not necessarily indicative of values at 60% relative density

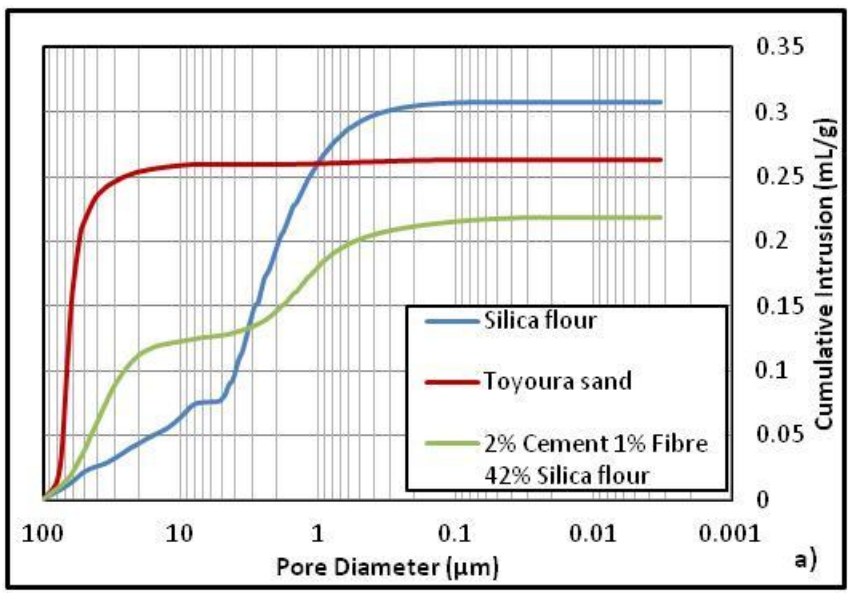

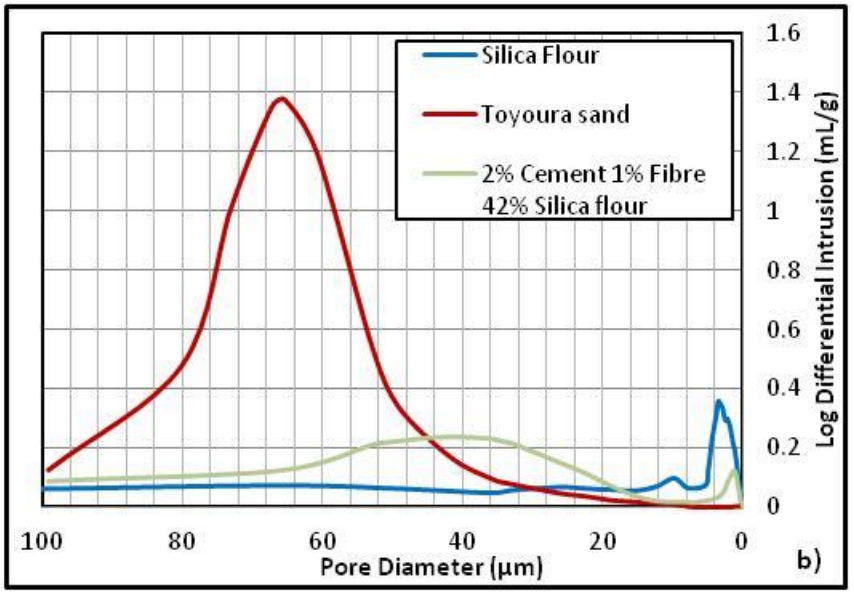

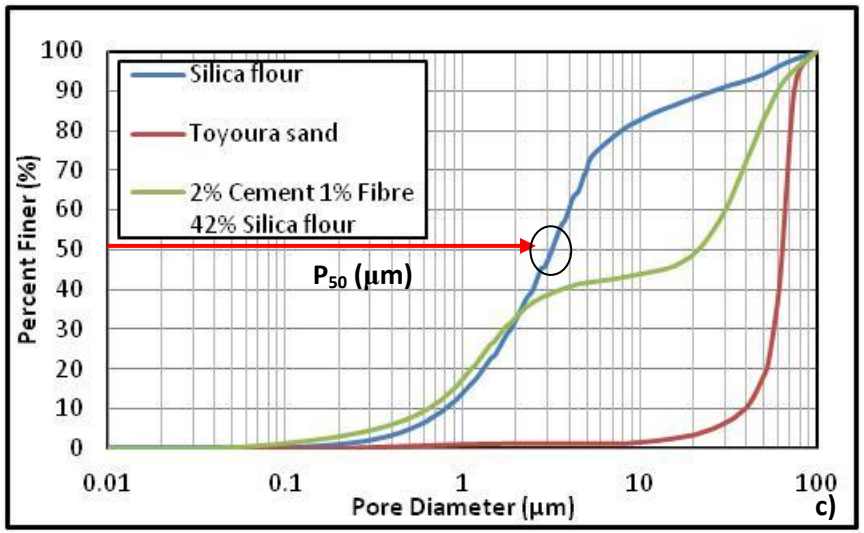

	Silica Flour	Toyoura Sand	42%SF, 2%C, 1%F
P_{60} (µm)	3.42	65.96	30.33
P_{50} (µm)	2.73	63.48	21.27
P_{30} (µm)	1.69	56.66	1.704
P_{10} (µm)	0.77	38.67	0.635

Figure 4.15. MIP for silica flour, Toyoura sand, and Toyoura sand with 42% silica flour, 2% cement, and 1% fibre a) cumulative intrusion, b) log differential intrusion and c) pore size distribution

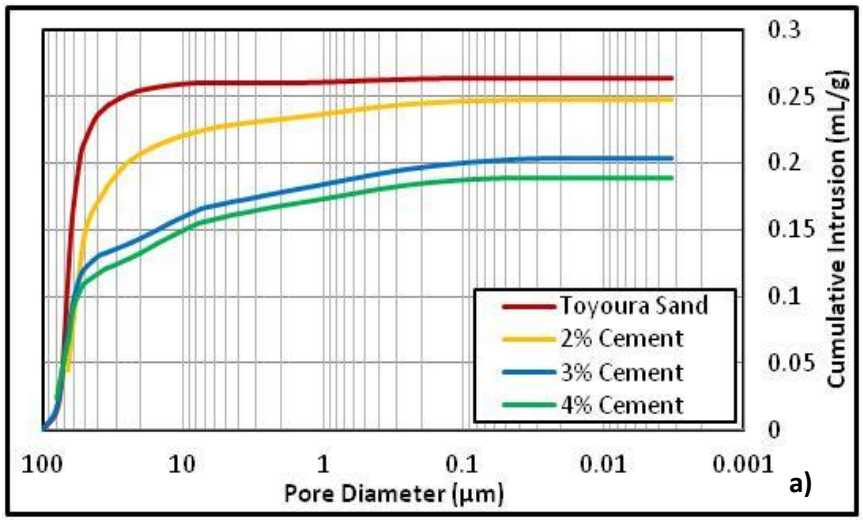

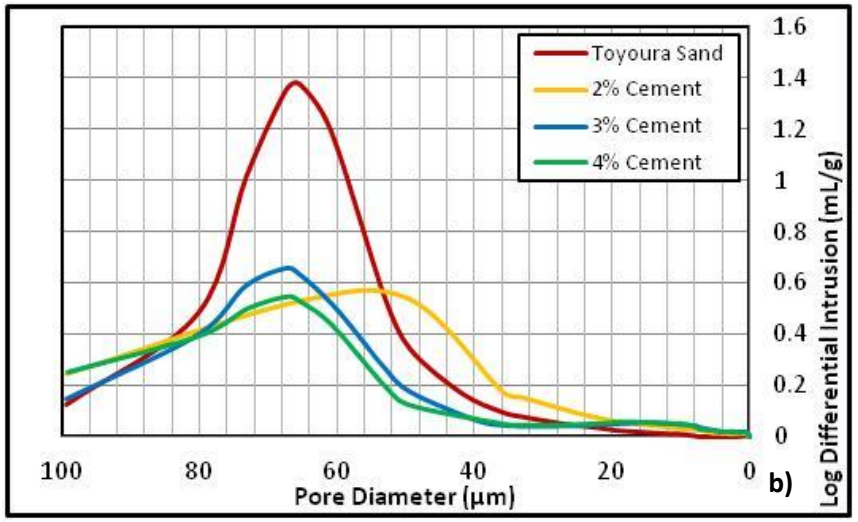

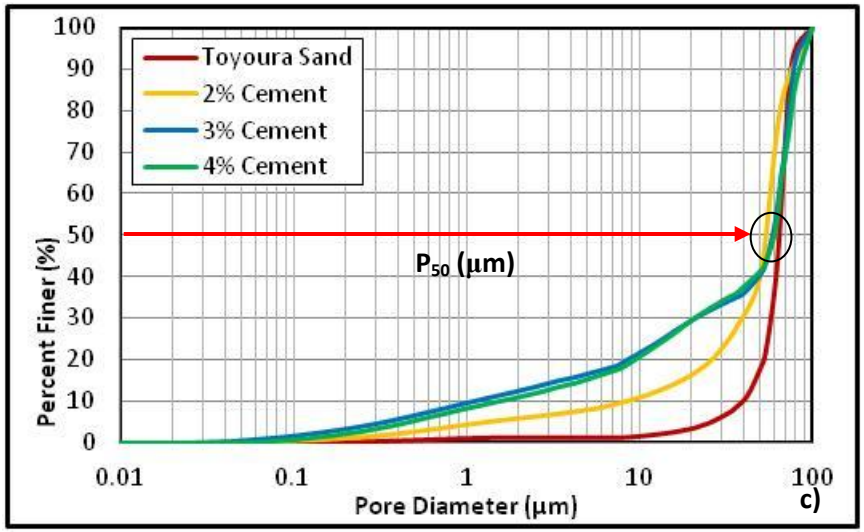

	1% Cement	2% Cement	3% Cement	4% Cement
P_{60} (µm)	65.96	57.18	63.39	64.02
P_{50} (µm)	63.48	53.29	58.11	59.27
P_{30} (µm)	56.66	38.33	20.8	20.51
P_{10} (µm)	38.67	8.20	1.09	1.53

Figure 4.16. MIP for Toyoura sand with 0-4% cement
a) cumulative intrusion, b) log differential intrusion, and c) pore size distribution

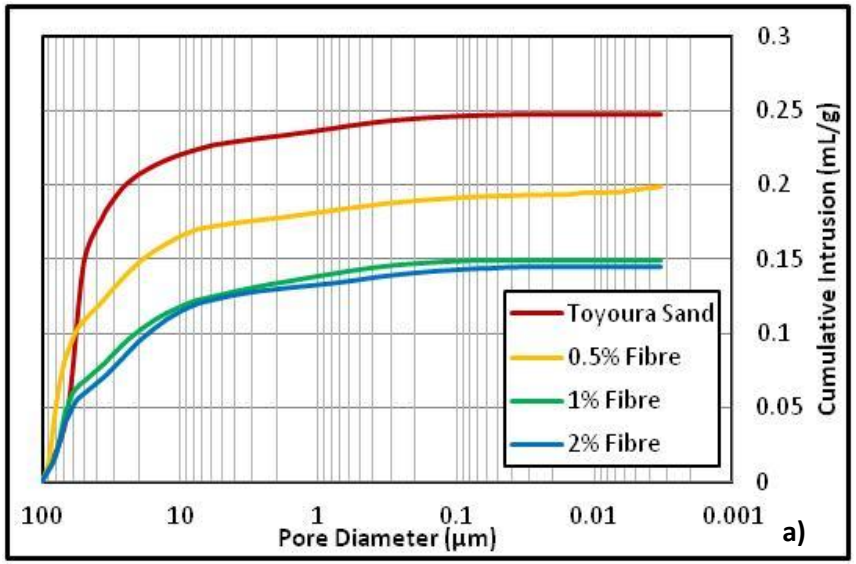

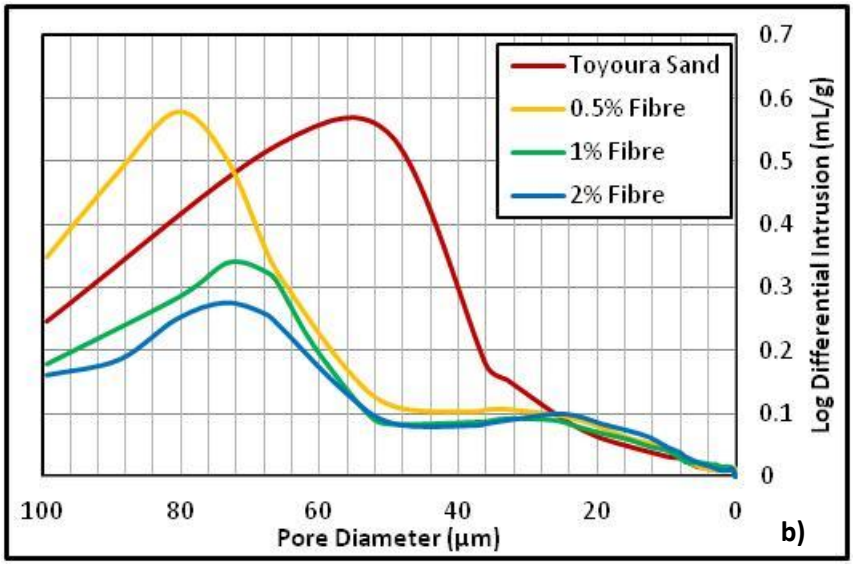

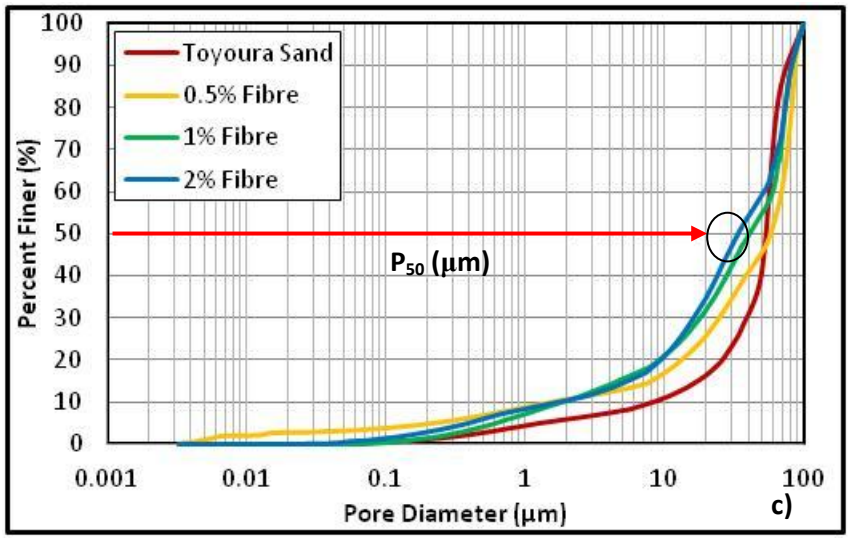

	0% Fibre	0.5% Fibre	1% Fibre	2% Fibre
P_{60} (µm)	57.18	68.81	64.97	51.19
P_{50} (µm)	53.29	57.48	58.89	33.62
P_{30} (µm)	38.33	24.57	22.38	16.16
P_{10} (µm)	8.20	1.51	1.3	1.74

Figure 4.17. MIP for Toyoura sand with 0-2% fibre
a) cumulative intrusion, b) log differential intrusion, and c) pore size distribution

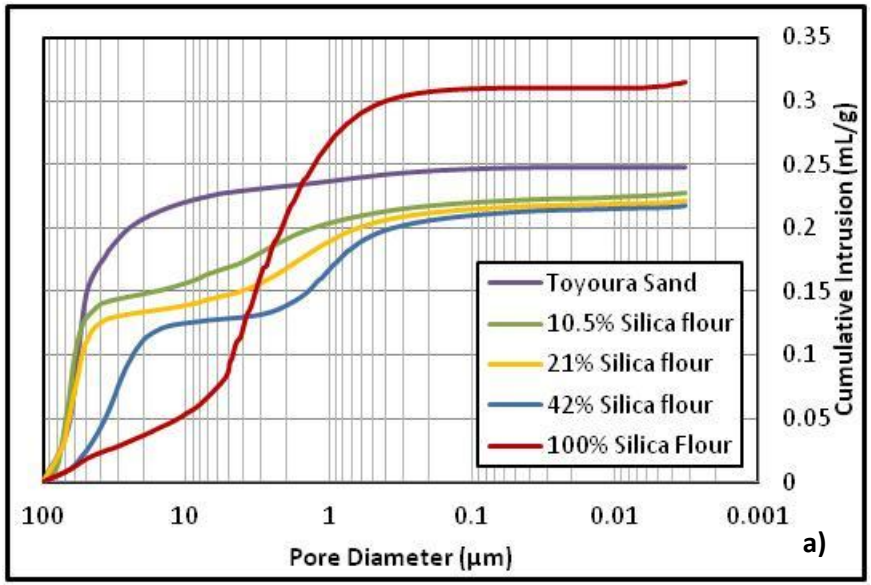

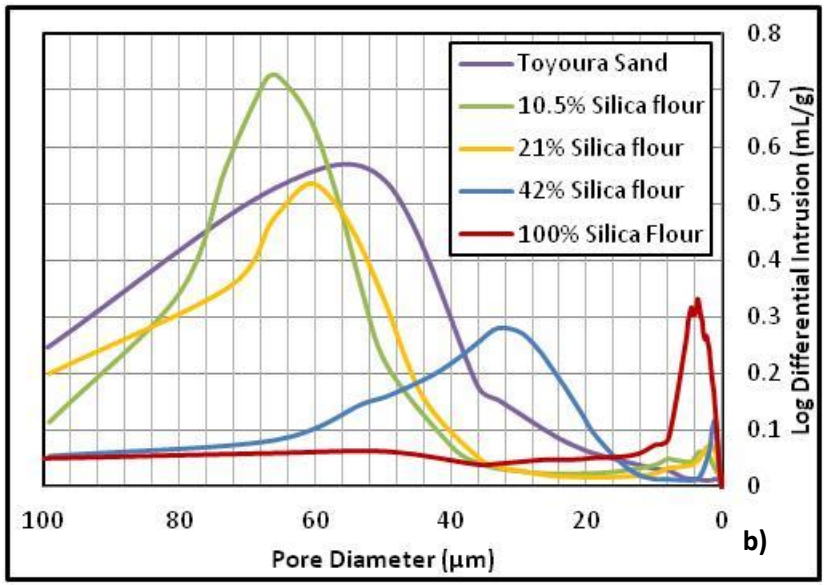

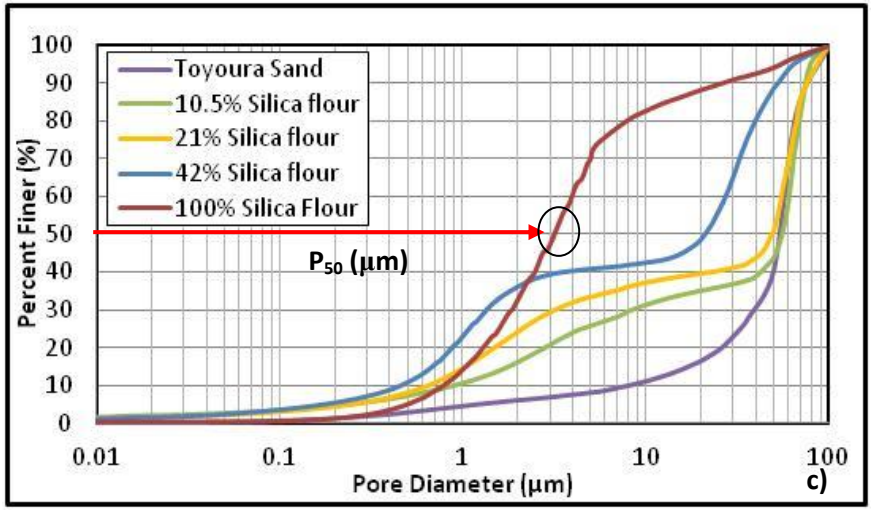

	0% Silt	10.5% Silt	21% Silt	42% Silt	100% Silt
P_{60} (µm)	57.18	61.16	55.43	27.43	3.42
P_{50} (µm)	53.29	55.85	48.99	21.17	2.73
P_{30} (µm)	38.33	8.6	3.25	1.37	1.69
P_{10} (µm)	8.20	0.92	0.66	0.469	0.77

Figure 4.18. MIP for Toyoura sand with 0-42% silica flour, 2% cement
a) cumulative intrusion, b) log differential intrusion, and c) pore size distribution

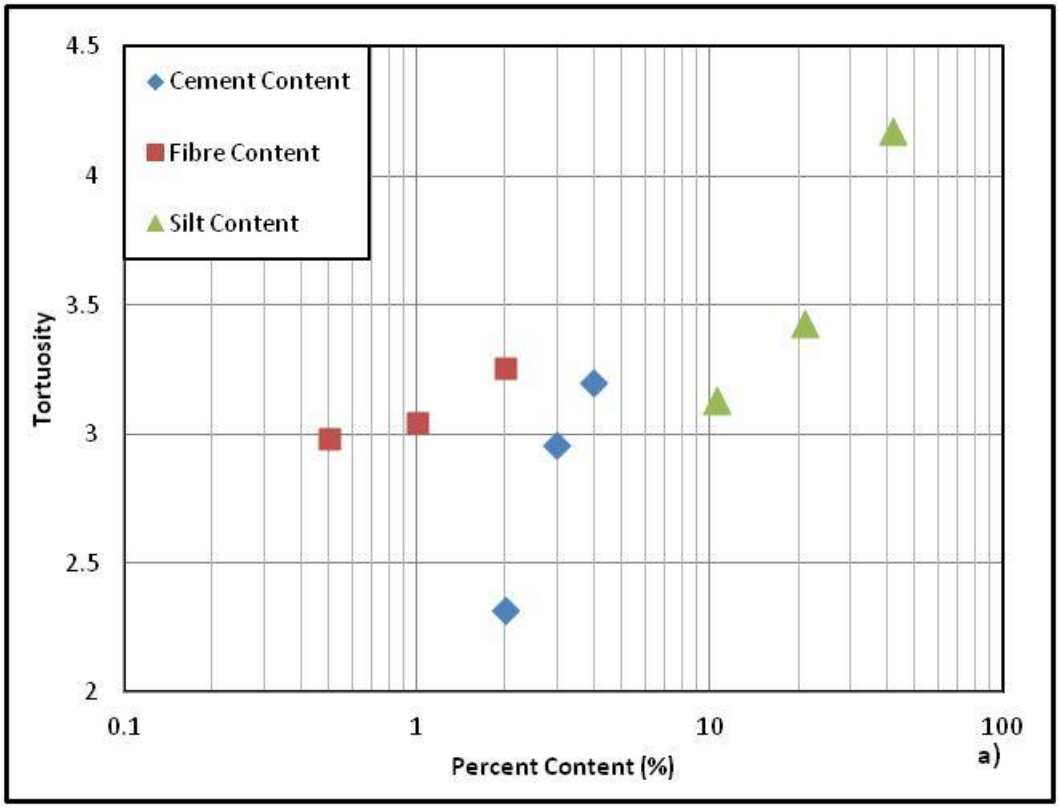

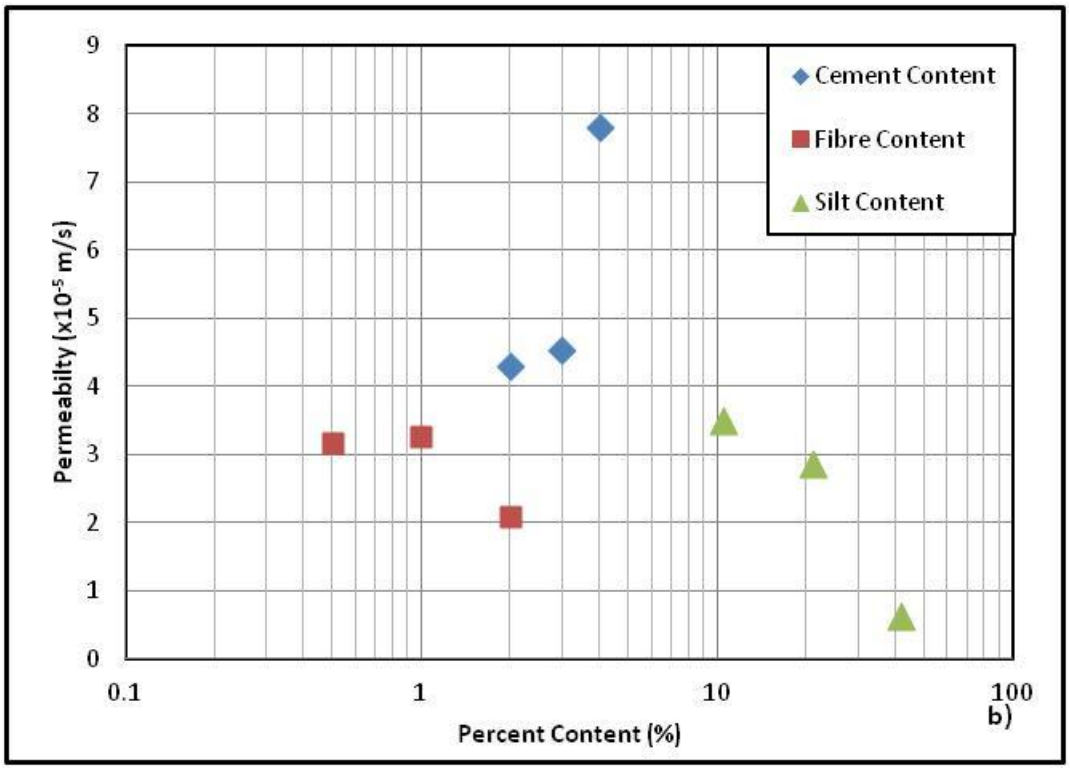

Figure 4.19. MIP a) Tortuosity: b) permeability: vs. percent content of cement, fibre, and silt

4.4. Compression and Flow Parameters

The determination of soil compressibility and flow parameters is common in engineering practice. Results from one dimensional compression tests shed light on how soils will behave on site under vertical loading (e.g. shallow foundations, roadways etc.) and can be used to determine permeability, elastic stiffness, K_0 values, and approximate total elastic and plastic settlement of a structure (Newson, 2013). The purpose of the one dimensional consolidation testing via Rowe cell and oedometer in this thesis was to investigate the permeability at different overburden stresses, characterize the settlement and compression behaviour, and explain the connection between the microstructure and the macro behaviour of Toyoura sand with silica flour, OPC, and PVA fibre additives.

4.4.1. Oedometer

Five oedometer tests were performed on Toyoura sand with silt content ranging from 0-100% by mass to provide preliminary test data to help plan the testing program and to provide validation for later results from the Rowe cell. Stress increments from 10-1600 kPa were applied and settlement was measured to determine the sample compressibility, constrained modulus, and permeability. Although tests were run for 24 hours per stress increment, more than 90% of the consolidation of the Toyoura sand samples was obtained in well under 2 hours (Terzaghi & Peck, 1948). Due to the better consistency of the oedometer data compared to the Rowe cell, only this data was used to fit functions for the compression behaviour described in this section.

Pestana & Whittle (1995) modelled the behavior of naturally deposited cohesionless soils in one dimensional compression. Data from the oedometer was fitted to this model due to its ease of use, its applicability to small and large applied stresses, and its inclusion of elastic and plastic deformations. This model has been fitted to Toyoura sand in the past for various densities; however, this previous testing was at stresses of 1-50 MPa and the stress state came much closer to the limiting compression curve (LCC) than the tests in this thesis. The governing equations for the model are shown below:

$$\ln\left(\frac{e}{e_0}\right) = -\left(e_0^{\left(\frac{1}{\rho_c}\right)}\right)\beta\left(\frac{\sigma'_{v0}}{P_a}\right) - \frac{3}{2C_b}\left(\frac{\sigma'_{v0}}{P_a}\right)^{\frac{2}{3}} \quad \textbf{[4.2]}$$

$$\beta = \frac{\rho_c\theta_0}{\sigma_{vr}'/P_a} - \frac{3}{2C_b}\left(\frac{\sigma_{v0}'}{P_a}\right)^{\frac{2}{3}} \quad \textbf{[4.3]}$$

Where e is the void ratio, e_0 is the initial void ratio, ρ_c is the slope of the NCL in log e-log σ_v' space, β is a dimensionless material constant, C_b is a constant (set at 850 for all modelled cases), σ_{v0}' is the vertical effective stress, P_a is atmospheric pressure (taken to be 100 kPa), θ_0 is the elasto-plastic

transition point (0.2-0.7 for most sands), and σ'_{vr} is a reference pressure where the void ratio equals unity.

The initial void ratio at 60% relative density decreased from 0.741 for Toyoura sand, to 0.695 for 50% silica flour, after which it increased again to 1.190 for 100% silica flour based on the relative density results in Figure 3.2. Based on this trend in void ratio, it was not unexpected that the soil compressibility increased as the silt content increased. This was indicated by the slope of the normal consolidation line in the log e-log σ' plot in Figure 4.20, in which the slope was near horizontal for Toyoura sand ($m=-3.03x10^{-5}$) but clearly steepened for 100% silica flour ($m=-1.6x10^{-4}$). What was also interesting to note was the development of plastic strains in the silty sand samples and very little elastic rebound. From the swelling lines in Figure 4.20a it is obvious that applied strain becomes significantly more plastic than elastic. This indicates that the silt addition will not only weaken the soil, but will exhibit permanent deformation after experiencing static or dynamic loads.

The constrained modulus followed the same trend as that found in the Rowe cell testing, reducing until 50% silica flour content from nearly 60 MPa for the Toyoura sand to 6.4 MPa for 50% silica flour, then back up to 13.4 MPa for 100% silica flour at σ_v'=1,600 kPa (Figure 4.20b). Since the stress intervals were identical for all tests, this decrease in one dimensional stiffness was caused by the higher strains experienced by the soil. These M_0 values are somewhat higher than those found from the Rowe cell, and may be caused by the drainage conditions (vertical two way drainage through a sand porous disc for the oedometer, versus vertical one way drainage to the center of the base through a sintered bronze porous disc for the Rowe cell) or the sample size (50 mm diameter oedometer versus 100 mm diameter Rowe cell).

Again it was noted that the sample of 100% silica flour collapsed upon initial saturation. This collapse of the soil structure was caused by a local shear failure between particles, specifically the

diminishing of the silt-silt and silt-sand bonds usually seen in granular (primarily silty) soils that have a metastable, open structure that fails during the flow of water (Barden, McGown, & Collins, 1973).

The permeability of the Toyoura sand at 1,600 kPa effective stress linearly dropped with the addition of the silica flour, from 8.7×10^{-6} m/s for the Toyoura sand, to 2.89×10^{-8} m/s for 100% silica flour as seen in Figure 4.20c, matching fairly closely with the values found empirically from the Rowe cell tests in Section 4.4.2.

Calibrating the Pestana and Whittle model to the oedometer results using nonlinear regression indicated that the model is quite accurate for the Toyoura sand; however it loses its robustness when the silica flour is added. The coefficient of determination (R^2) value steadily decreases with increasing silt content (Figure 4.20d). The equation representing the best fit line consists of two main parameters: the leading coefficient representing initial void ratio and the y-intercept of the model, and the exponent representing the curvature of the exponential best fit line. This curvature exponent generally increased with additional silt content.

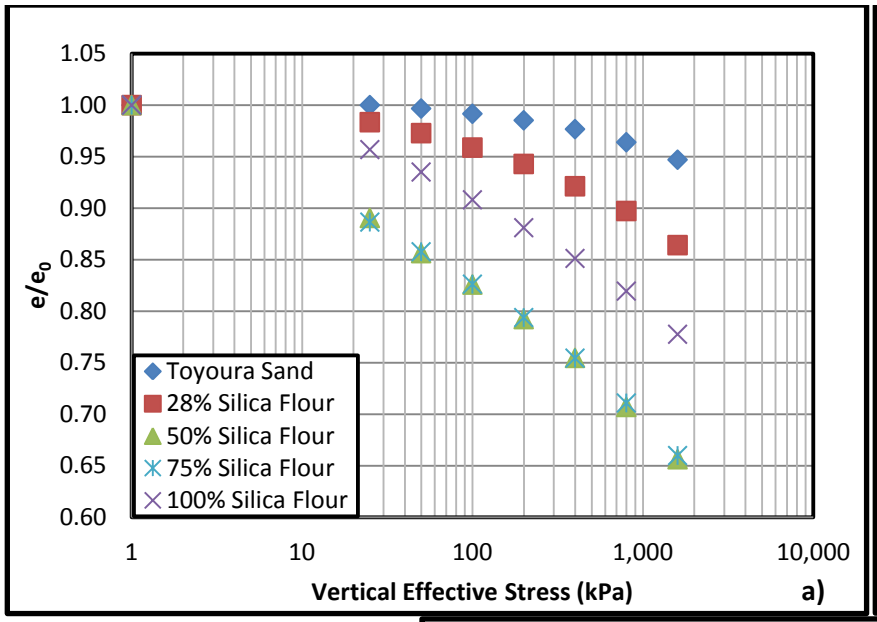
1.05
1.00
0.95
0.90
0.85
0.80
0.75
0.70
0.65
0.60
e/e0
1
10
100
1,000
10,000
Vertical Effective Stress (kPa)
a)
Toyoura Sand
28% Silica Flour
50% Silica Flour
75% Silica Flour
100% Silica Flour

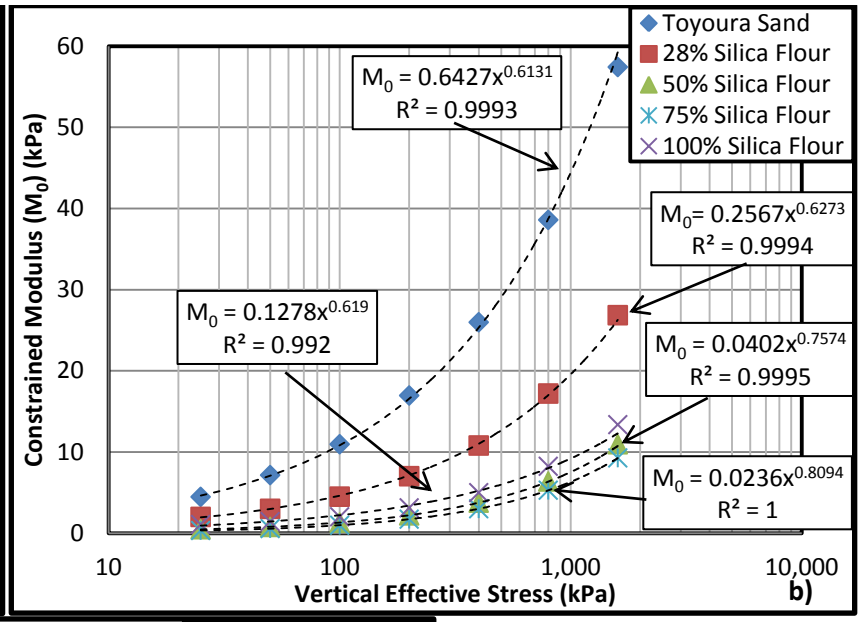
60
50
40
30
20
10
0
Constrained Modulus (M0) (kPa)
M0 = 0.6427x0.6131
R² = 0.9993
M0= 0.2567x0.6273
R² = 0.9994
M0 = 0.1278x0.619
R² = 0.992
M0 = 0.0402x0.7574
R² = 0.9995
M0 = 0.0236x0.8094
R² = 1
10
100
1,000
10,000
Vertical Effective Stress (kPa)
b)
Toyoura Sand
28% Silica Flour
50% Silica Flour
75% Silica Flour
100% Silica Flour

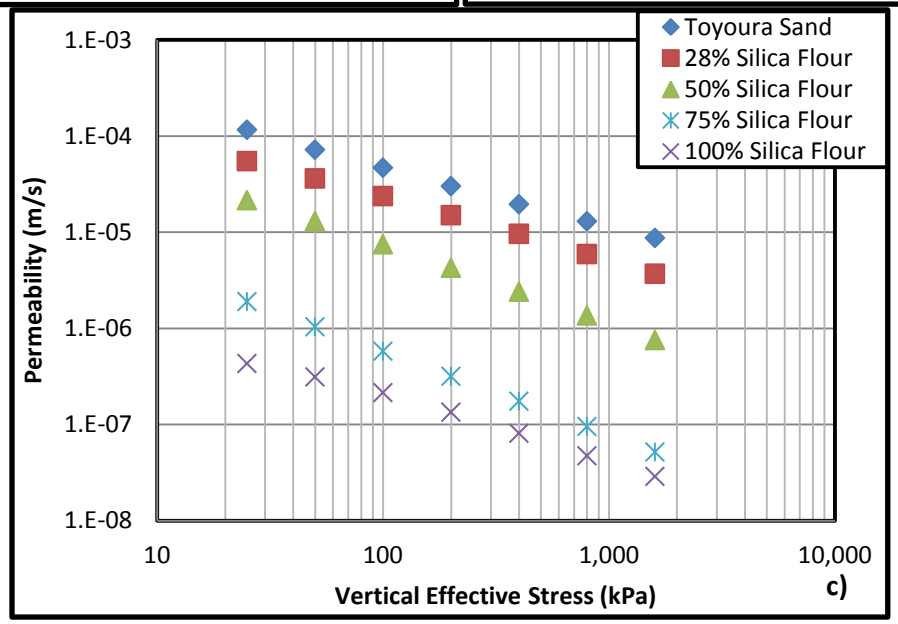
1.E-03
1.E-04
1.E-05
1.E-06
1.E-07
1.E-08
Permeability (m/s)
10
100
1,000
10,000
Vertical Effective Stress (kPa)
c)
Toyoura Sand
28% Silica Flour
50% Silica Flour
75% Silica Flour
100% Silica Flour

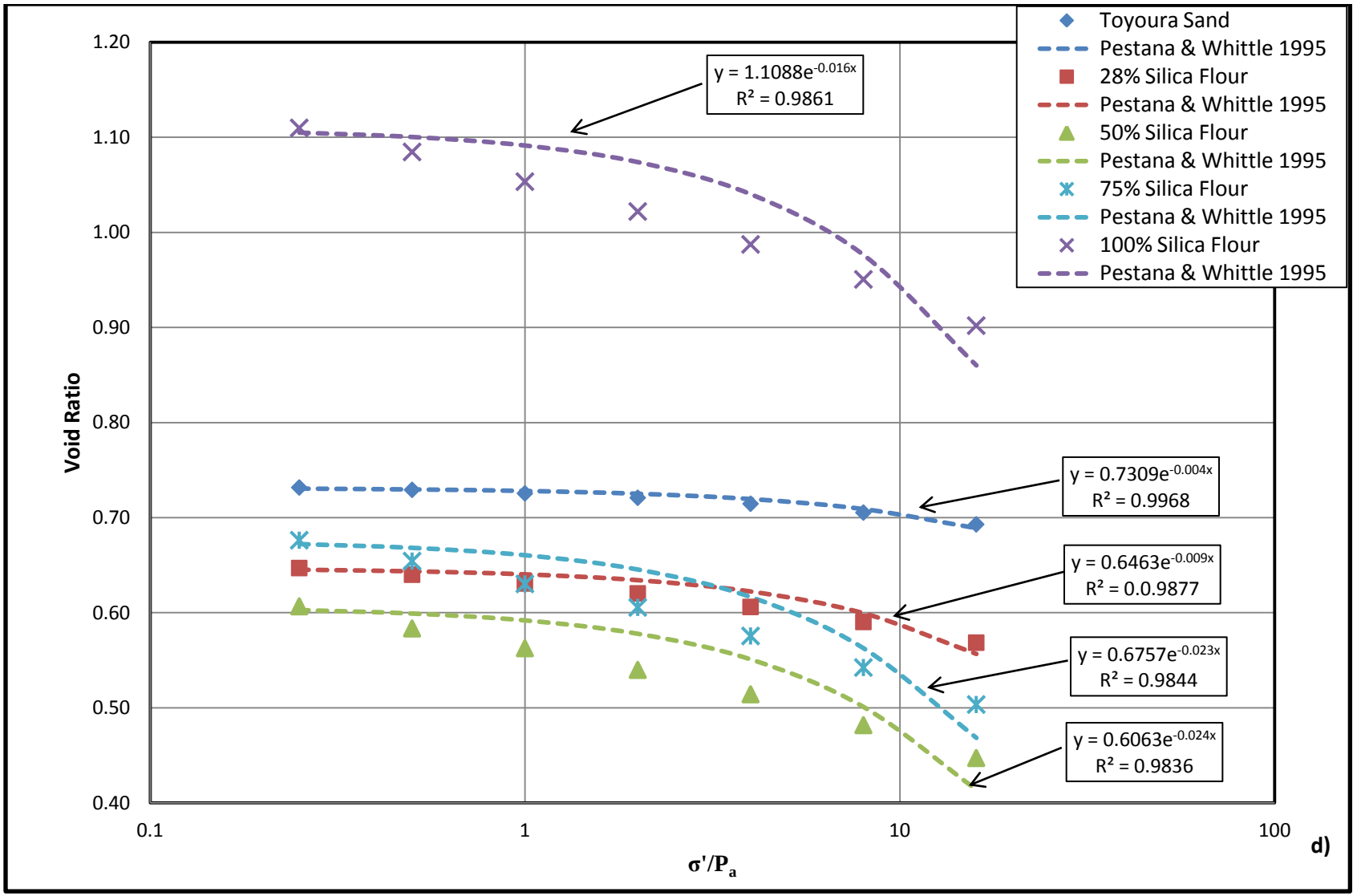

Figure 4.20. Oedometer results for 0-100% silica flour a) e/e_0 vs. vertical effective stress; b) constrained modulus vs. vertical effective stress; c) permeability vs. vertical effective stress; d) Pestana & Whittle (1995) model fitting

There are some discrepancies between the previous modelling for Toyoura sand (Pestana & Whittle, 1995) using these relationships and the empirical data in this thesis. These are likely a result of the authors using the following:

- Rounded Toyoura sand rather than angular;
- Stresses up to 50 MPa that approach or surpass the LCC of the Toyoura sand;
- Hydrostatic compression rather than one dimensional in the oedometer;
- Pure Toyoura sand rather than silty sand.

Due to the inapplicability of these functions to the stabilized soils tested in the Rowe cell further modelling was not attempted.

4.4.2. Rowe Cell

At low stresses, compressibility and collapse rate of granular soils is dominated by elastic deformation of the soil structure caused by particle rearrangement. At very high stresses (approximately 20-40 MPa) Toyoura sand reaches the limiting compression curve (LCC), when the void ratio reaches a minimum and particle crushing begins, though this stress range is beyond the scope of this thesis. It should be noted, however, that 'pseudo-particles' (groups of particles and cement bonds) will begin to crush at much lower pressures.

Many factors affect the compression behaviour of cohesionless soils and the location of the LCC (Pestana & Whittle, 1995):

- Initial density, void ratio, and soil fabric
- Cementation of the sample
- Mineralogy of the soil
- Particle shape, size, angularity, and gradation
- Boundary conditions
- Time dependent creep behaviour
- Interstitial fluids

In one dimensional consolidation tests such as the Rowe cell, elastic and plastic deformations occur upon loading, with a tendency toward plastic deformation due to changes in the coefficient of lateral earth pressure, K_0, which is caused by the boundary conditions induced by the confinement (Liu & Znidarcic, 1991). Plots of void ratio versus vertical effective stress, constrained modulus versus vertical effective stress, and permeability versus vertical effective stress from the Rowe cell tests are shown in Figure 4.21-Figure 4.26. These have been grouped to show the effects of fibre, cement, silica flour alone and various combinations of the additives on the behaviour of the soils.

A model for the constrained modulus (M_0) based on a power curve that takes into account two fitting parameters, c_1 and m (Equation 4.2) is also shown on these figures with a dashed line.

$$\frac{M_0}{P_a} = c_1 \left(\frac{\sigma_v'}{P_a}\right)^m \quad \textbf{[4.4]}$$

Where M_0 is the constrained modulus, P_a is atmospheric pressure (100 kPa), σ_v' is the vertical effective stress, c_1 is the ratio of constrained modulus/P_a at σ_v'/P_a=1 and m is a fitting exponent.

Two lines have been plotted to represent upper and lower bound values for the data set. In all cases, the power curve fit has an R^2 value of greater than 0.900, indicating that the data is well represented by the calculated power curve model.

4.4.2.1. Rowe cell tests on Toyoura sand with 0-2% PVA fibre

The following graphs summarize the void ratio, constrained modulus, and permeability changes with vertical pressure for the Toyoura sand with various fibre contents ranging from 0-2% by mass. The trends suggest that the increasing fibre content improves the one dimensional strength and permeability of the Toyoura sand, and that high fibre concentrations can cause rapid and large settlements with increasing vertical pressure.

The initial void ratio of the Toyoura sand with various fibre contents was assumed to have stayed approximately constant at around e_0=0.751. When the vertical effective stress was increased, the fibre concentrations of 1-2% tended to exhibit faster reduction in void ratio than at concentrations of 0-0.5%. This is likely due to the increasing number of collapsible fibre clusters commonly found in the Toyoura sand with high fibre concentrations. These clusters allow large settlements to occur when they collapse. When used in high concentrations, the fibres have been proven to occasionally have negative effects (Gray & Maher, 1989).

In this study, the pure Toyoura sand was found to have a maximum constrained modulus M_0=27 MPa at a vertical effective stress of 1,000 kPa; much lower than the E_{sec} determined from the cyclic triaxial testing (E_{sec}=135 MPa at CSR=0.20). This discrepancy is likely due to the one dimensional nature of the static compression in the Rowe cell versus the three dimensional dynamic loading in the cyclic triaxial tests, though further testing should be performed to verify this theory. The permeability of Toyoura sand has been documented to be $2x10^{-4}$ m/s at 50% relative density (Majarjan & Takahashi, 2013). Data from Rowe cell tests suggested that the permeability of clean Toyoura sand decreased almost linearly in log k vs. log σ_v' space (from $1.15x10^{-4}$ m/s at 100 kPa to $1.94x10^{-6}$ m/s at 1000 kPa) using Equation 3.7.

The addition of 0.25-0.5% PVA fibres caused a notable increase in M_0, but above 1% content by mass there was a slight reduction in 1-D soil stiffness (Figure 4.21). This limiting percentage of fibre varies based on the soil type, shearing mode, and sample preparation technique as corroborated by many authors (Michalowski & Cermak, 1994; Ibraim & Fourmont, 2006; Gray & Refeai, 1986). This suggests that replacement of sand grains with flexible and moderately compressible fibres can have negative effects on the soil stiffness above a certain concentration, though 1% by mass is low compared to some authors' findings. The addition of fibres hardly altered the permeability of the Toyoura sand at all, with a change in permeability at 1,000 kPa from 1.94×10^{-6} for pure Toyoura sand to 2.44×10^{-6} m/s at a 1% fibre concentration, similar to results from MIP testing in Section 4.3.2.

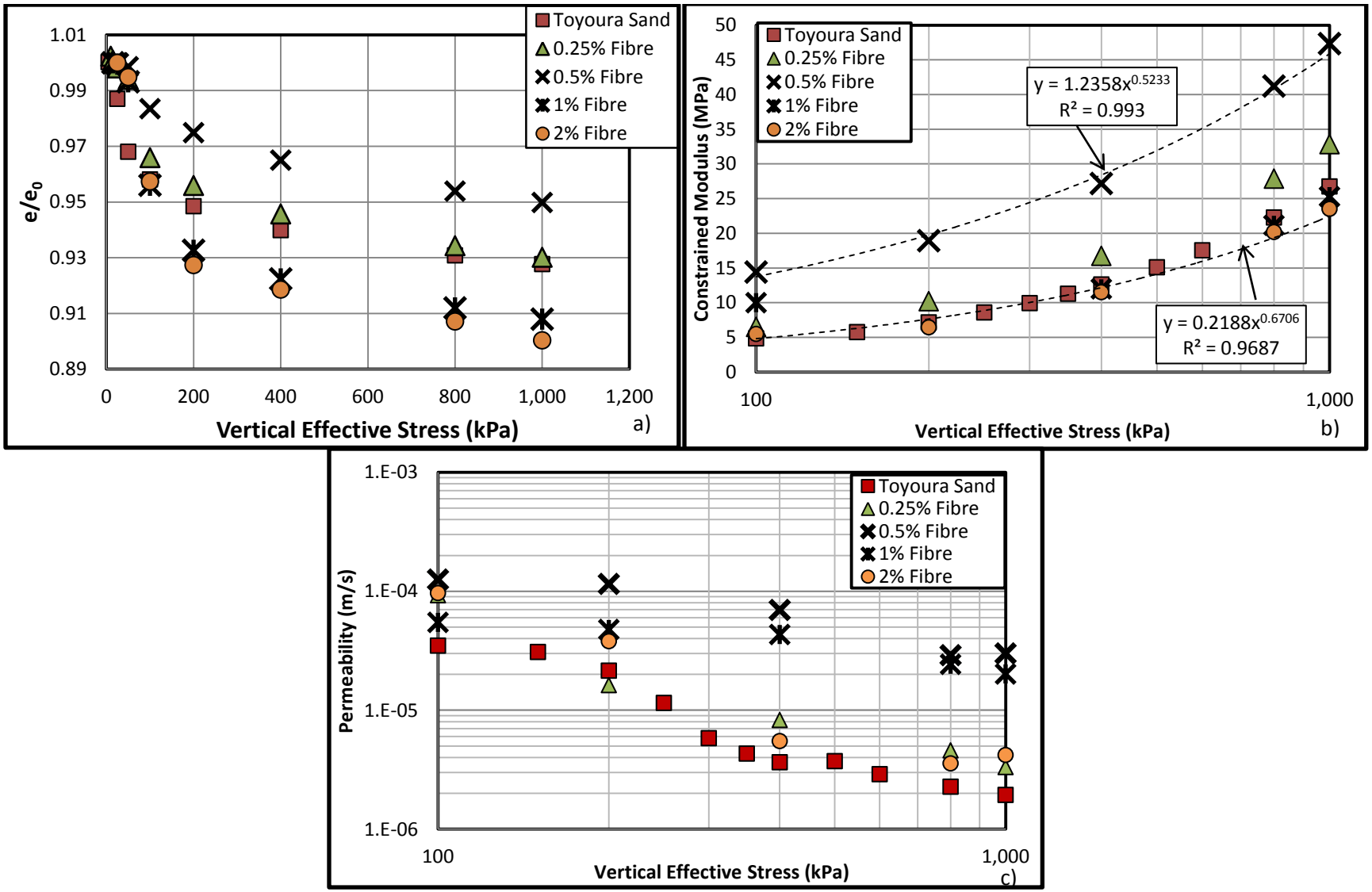

Figure 4.21. Rowe cell tests on Toyoura sand with 0-2% fibre, D_r=60% a) normalized void ratio vs. vertical effective stress; b) constrained modulus vs. vertical effective stress; c) permeability vs. vertical effective stress

4.4.2.2. Rowe cell tests on Toyoura sand with 0-4% Cement

The following graphs summarize the void ratio, constrained modulus, and permeability changes with vertical stress for the various cement contents ranging from 0-4% by mass. The trends suggest that the increasing cement content did not markedly improve the one dimensional strength or stiffness of the Toyoura sand. The soil permeability was decreased slightly versus the pure Toyoura sand, though the rate of decreasing permeability was slowed by the addition of the cement.

There was minimal change in the void ratio of the Toyoura sand regardless of the cement concentration, as shown in Figure 4.21a. This is likely due to the short curing time preventing significant strength gain, and thus maintaining roughly the same mechanical strength between particles as the unstabilized Toyoura sand thereby not decreasing the compressibility. Given a longer curing period, the compressibility would likely decrease due to the filling of the voids with the fine cement particles and hydrated cement products (Bullard, et al., 2010).

Cement addition from 2-4% did not have a dramatic effect on the one dimensional stiffness (constrained modulus) of the Toyoura sand. All three of the samples tended to exhibit the same consolidation behaviour and a minimal increase in constrained modulus as seen in Figure 4.22a-c.

It is important to note that the permeability of cemented sands and silty sands is not well documented in the literature, with some sources citing a general decrease in permeability of approximately one to two orders of magnitude over a 7-28 day curing period (Ingles & Metcalf, 1973; Miura, Tokunaga, Kitazume, & Hirota, 2004). Based on these findings, for this thesis the initial permeability of cemented sands and cemented, silty sands was assumed to decrease by exactly one order of magnitude when compared to the corresponding unstabilized mixture.

As mentioned in the MIP discussion (Section 4.3.2) the initial drop in permeability of the cemented sand when compared to the pure Toyoura sand is primarily due to the increasing microporosity. What is interesting to note about the cemented Toyoura sand is the existence of a yield point on the permeability curve. For many of the tests, including the cemented sands, a yield point at 100 kPa was noted, where it was assumed that one of two things occurred: either the microstructure began to collapse and the cemented bonds began to break, the mechanical friction of the Rowe cell apparatus was limiting sample compression until an applied stress of 100 kPa, or a combination of the two. For the 4% cement addition this inflection point was at 200 kPa, suggesting the higher yield stress of this stabilized soil may actually be the cause of the inflection point (Figure 4.22).

As expected, the sample of the Toyoura sand with 4% cement exhibited a significantly smaller reduction in permeability and void ratio than the pure Toyoura sand due to its skeletal stiffness and the filling of the voids with the fine cement particles (Figure 4.22a-c).

With respect to the constrained modulus, the power curve model tended to deviate slightly due to the aforementioned yield point of the cemented sample. Minimal strength gain was seen in the cemented samples, once again due primarily to the short curing time. The slight strength gain seen in the sample with 4% cement was likely due to the filling of the voids with fine cement powder and partially hydrated cement products.

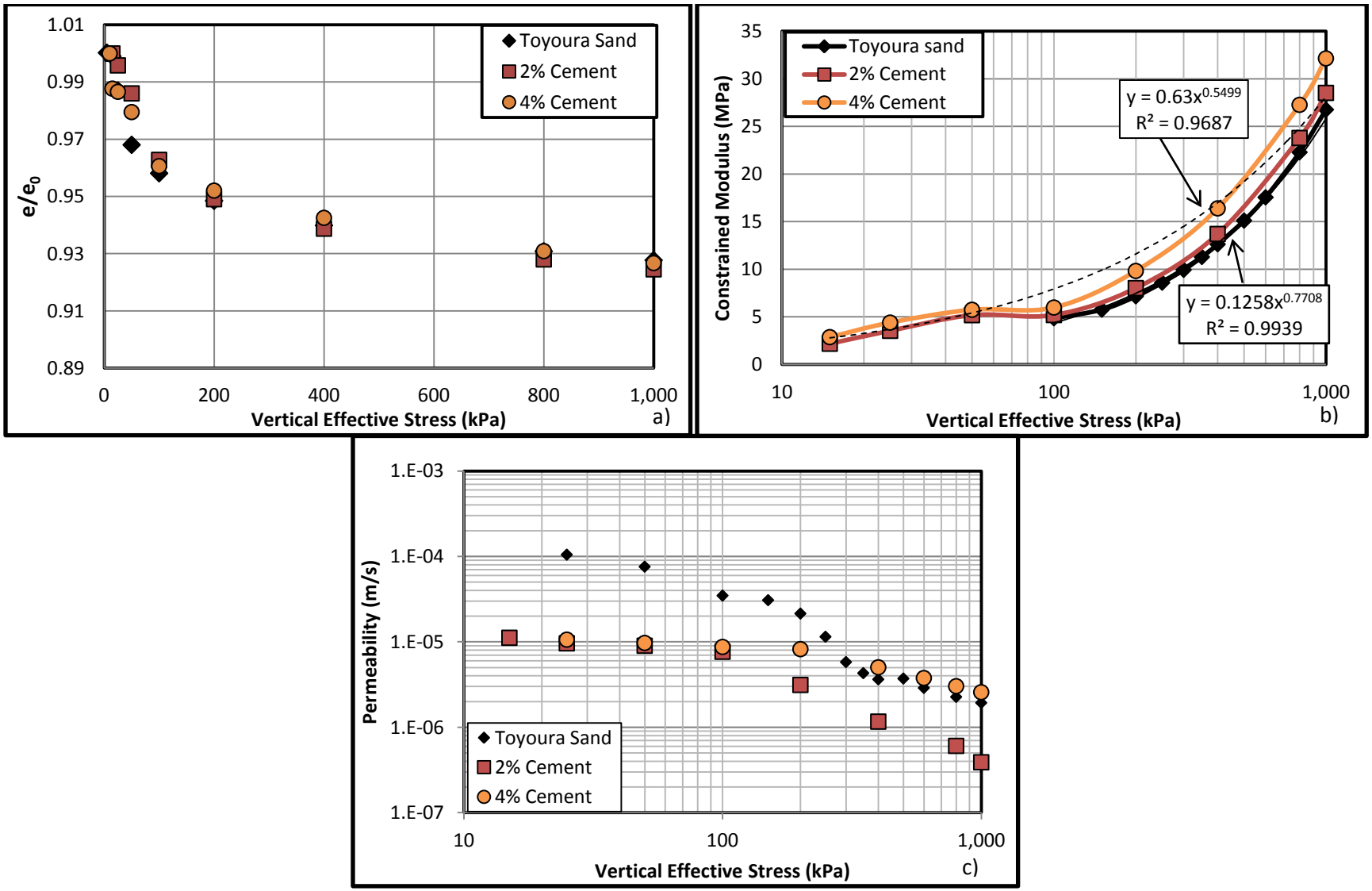

Figure 4.22. Rowe cell tests on Toyoura sand with 0-4% cement, D_r=60% a) Normalized void ratio vs. vertical effective stress; b) constrained modulus vs. vertical effective stress; c) permeability vs. vertical effective stress

4.4.2.3. Rowe cell tests on Toyoura sand with 0-100% silica flour

The following graphs summarize the void ratio, constrained modulus, and permeability results for the various silt contents ranging from 0-100% by mass in increments representative of the in-situ conditions in the Tokyo Bay region. The trends suggest that the increasing silt content increased the sample compressibility, and consequently decreased the constrained modulus. The sample permeability was also seen to decrease with the increasing silt.

The silica flour addition seen in Figure 4.24 indicated a similar trend in sample stiffness as the bender element testing in Section 4.6, with a decrease in constrained modulus from 0-35% silica flour, and then a very slight increase from 35-100%. This relationship between silt content and constrained modulus is not well documented in the literature but matched the void ratio and permeability trends determined in the oedometer tests and the stiffness determined in the bender element tests (Sections 4.4.2.5 & 4.6) discussed later in this thesis.

The silica flour also decreased the initial permeability by three orders of magnitude from 1.05×10^{-4} m/s for Toyoura sand to 4.3×10^{-7} m/s for 100% silica flour, which matches data documented by several sources: (Carter & Bentley, 1991; Leonards 1962; Dysli & Steiner, 2011; West, 1995; and Day, 2006). Since permeability is related to the size, gradation, and compaction of the granular media, as well as the pore size distribution of each sample, this trend was unsurprising.

The collapse rate of silty sand is governed by several properties: soil saturation, applied stress, and mechanical and chemical bonds within the soil (Barden, McGown, & Collins, 1973). In the case of saturated, unstabilized Toyoura sand, the mechanical bonds between the soil grains provide the resistance to collapse. The addition of the silica flour creates a fine silt bond with the sand grains, transferring much of the mechanical shear strength into capillary forces between the particles instead.

The wetting behaviour of the non-plastic silica flour lubricates the existing intergranular bonds allowing particles to slide over each other, thereby reducing the effective stress required to cause collapse (Barden, McGown, & Collins, 1973).

The concentration of silt at which this collapse mechanism initiates is related to the skeletal void ratio of the soil. Based on skeletal void ratio calculations in Equation 4.3, at a silt content of between 21-28% silica flour the Toyoura sand particles on average are no longer in contact as shown in Figure 4.23. The silty sand exists in a state that it could not achieve without the presence of the fines (-#200 sieve, <0.075mm) and is thus primarily supported by the silt matrix which now dominates soil behaviour during shearing (Carraro, Bandini, & Salgado, 2003). The weakness of the silt matrix is evident throughout all tests within this thesis, and the clear transition point around 28-42% silt addition for many tests can be partially explained by this structural phenomenon.

$$e_{sk} = \frac{1+e}{1-\frac{M_{fines}}{M_{total}}} - 1 \qquad \textbf{[4.5]}$$

Where e_{sk} is the skeletal void ratio, e is the current void ratio, M_{fines} is the mass of soil passing through the #200 sieve (0.075mm), and M_{total} is the total mass of solids in the sample.

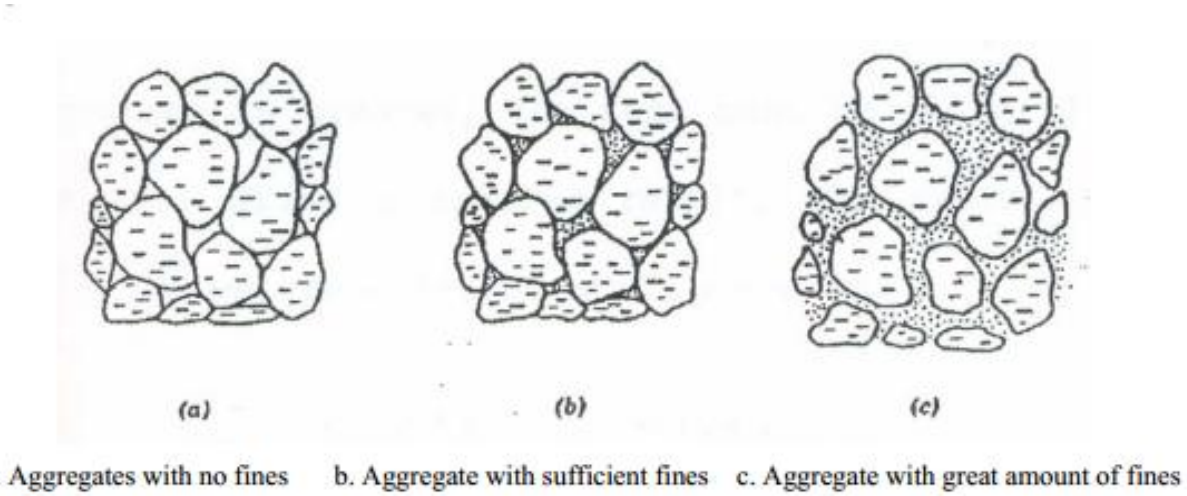

Figure 4.23. Granular aggregate behaviour with various fines contents (Yoder & Witczak, 1975)

Samples of 100% silica flour best illustrate the severe collapse of soil structure caused by wetting, with a drop in void ratio of 0.310 (from 1.076 to 0.766) during the saturation stage (σ_v'=10 kPa). This structural collapse was also observed in undocked bender element tests, where samples of 100% silica flour were seen to settle several millimeters (though this collapse was mitigated using extension top caps in cyclic triaxial testing). The aforementioned lubricating effect appeared to exist in samples of Toyoura sand that contained silica flour above 28%, as evidenced by a significant drop in void ratio at 50-100 kPa as seen in Figure 4.24. Most noticeably, samples with greater than 28% silica flour experienced decreases in void ratio significantly higher than samples with less than 28% silica flour. This agrees with findings from cyclic triaxial tests performed in this thesis, and data from the literature that indicate a 30-50% silica flour content exhibits very little liquefaction resistance (Belkhatir et al. 2012; Polito & Martin II, 2001; Amini & Qi, 2000).

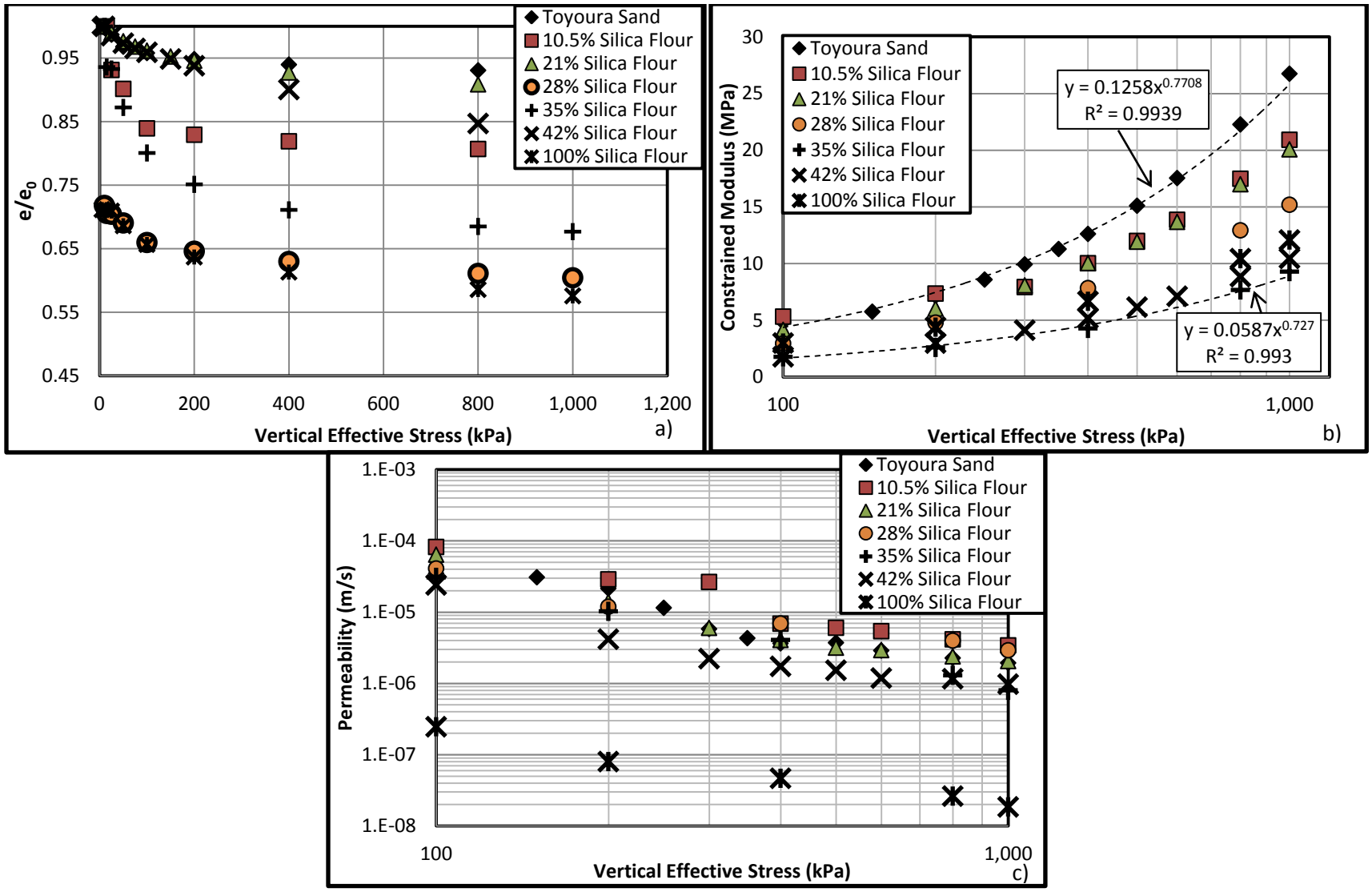

Figure 4.24. Rowe cell tests on Toyoura sand with 0-100% silica flour, D_r=60% a) normalized void ratio vs. vertical effective stress; b) constrained modulus vs. vertical effective stress; c) permeability vs. vertical effective stress

4.4.2.4. Rowe cell tests on Toyoura sand with 0-100% silica flour & 1% PVA fibre

The above graphs summarize the void ratio, constrained modulus, and permeability changes with vertical pressure for the various silt contents ranging from 0-100% by mass with 1% fibre stabilizer. The trends suggest that the increasing silt content increased the sample compressibility, and consequently decreased the constrained modulus in much the same manner as the unstabilized samples. The sample permeability was also seen to decrease with the increasing silt.

The void ratios of the fibre stabilized silty sands tended to follow the same trend as the unstabilized silty sand, though the overall consolidation of each sample was slightly reduced (Figure 4.25a). This suggests that the addition of both silt and PVA fibres helps to slightly reduce sample compressibility. The addition of PVA fibres to the silty sand maintained the same trend in constrained modulus as the unstabilized mixture. Figure 4.25b shows how the addition of fibres tended to improve the constrained modulus of the silty sands, converging the values toward that of the Toyoura sand with 1% fibre.

There were some notable differences in soil behaviour when 1% PVA fibre was added, however. For example, 100% silica flour had the lowest M_0 when fibres were included, whereas without the fibre addition, 35% silica flour was the weakest mixture. This has been noted as a fairly clear transition, right around the point where the shear stresses are transferred into the silt matrix rather than the sand particles. The fibres act as addition mechanical bonds, keeping the shear stresses on the soil structure rather than the silt matrix. Also, the rate at which the constrained modulus increased was quite different, starting with virtually no change and then increasing dramatically at around 100 kPa compared to the smooth curve of the unstabilized silty sand. This suggested a potentially similar yielding point as the cemented Toyoura sand.

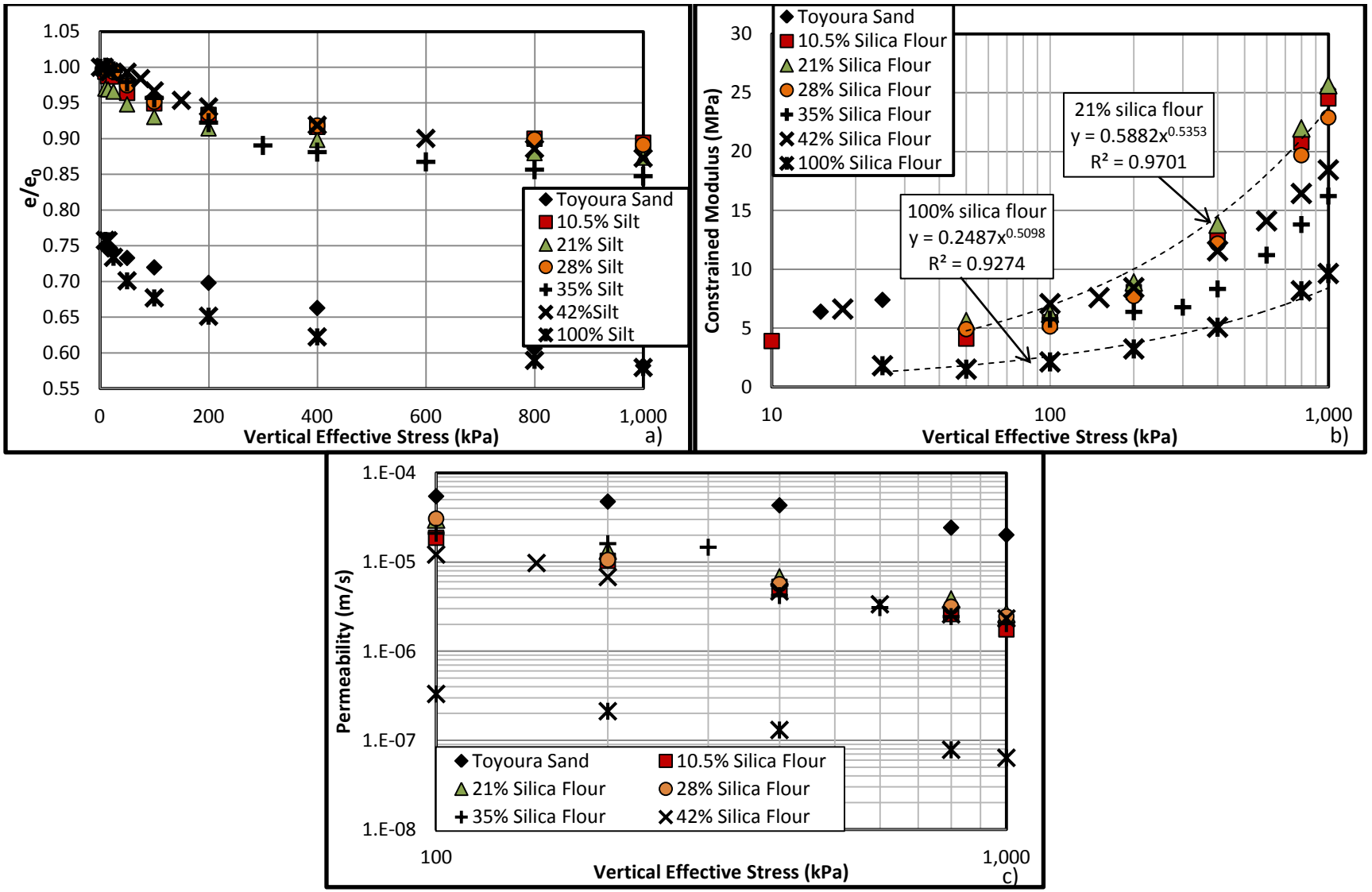

Figure 4.25. Rowe cell tests on Toyoura sand with 0-100% silica flour and 1% fibre, D_r=60% a) normalized void ratio vs. vertical effective stress; b) constrained modulus vs. vertical effective stress; c) permeability vs. vertical effective stress

4.4.2.5. Rowe cell tests on Toyoura sand with 0-100% silica flour, 2% cement, & 1% PVA fibre

The following graphs summarize the void ratio, constrained modulus, and permeability results for the various silt contents ranging from 0-100% with 2% cement and 1% fibre stabilizer. The trends suggest that the increasing silt content increased the sample compressibility, and consequently decreased the constrained modulus in much the same manner as the unstabilized samples. The sample permeability was also seen to decrease with the increasing silt.

The addition of the cement to the silty sand with PVA fibres followed the same trend in void ratio reduction as the unstabilized samples. Once again, the short curing time did not allow the samples to fully mobilize the strength and stiffness gained via the addition of cementitious material. This led to the cemented samples being slightly less compressible than the uncemented samples.

When both PVA fibres and OPC were mixed with silty Toyoura sand, the results were essentially the same as above but with some slight discrepancy for 35% and 42% silt contents (Figure 4.26a-c). These variations from the pattern are likely due to the heterogeneousness of the cemented, fibrous, silty samples as will also be discussed further in bender element testing in Section 4.6. As per earlier in this section, the addition of OPC did not improve the constrained modulus very much due to the short curing time. The permeability of the stabilized silty sand did reduce significantly, as witnessed in MIP testing (Section 4.3.2), and followed the same trend as the unstabilized silty Toyoura sand. As was seen in the cemented Toyoura sand, there was a definitive inflection point in the permeability curves at 100 kPa for the cemented, silty sand with fibres.

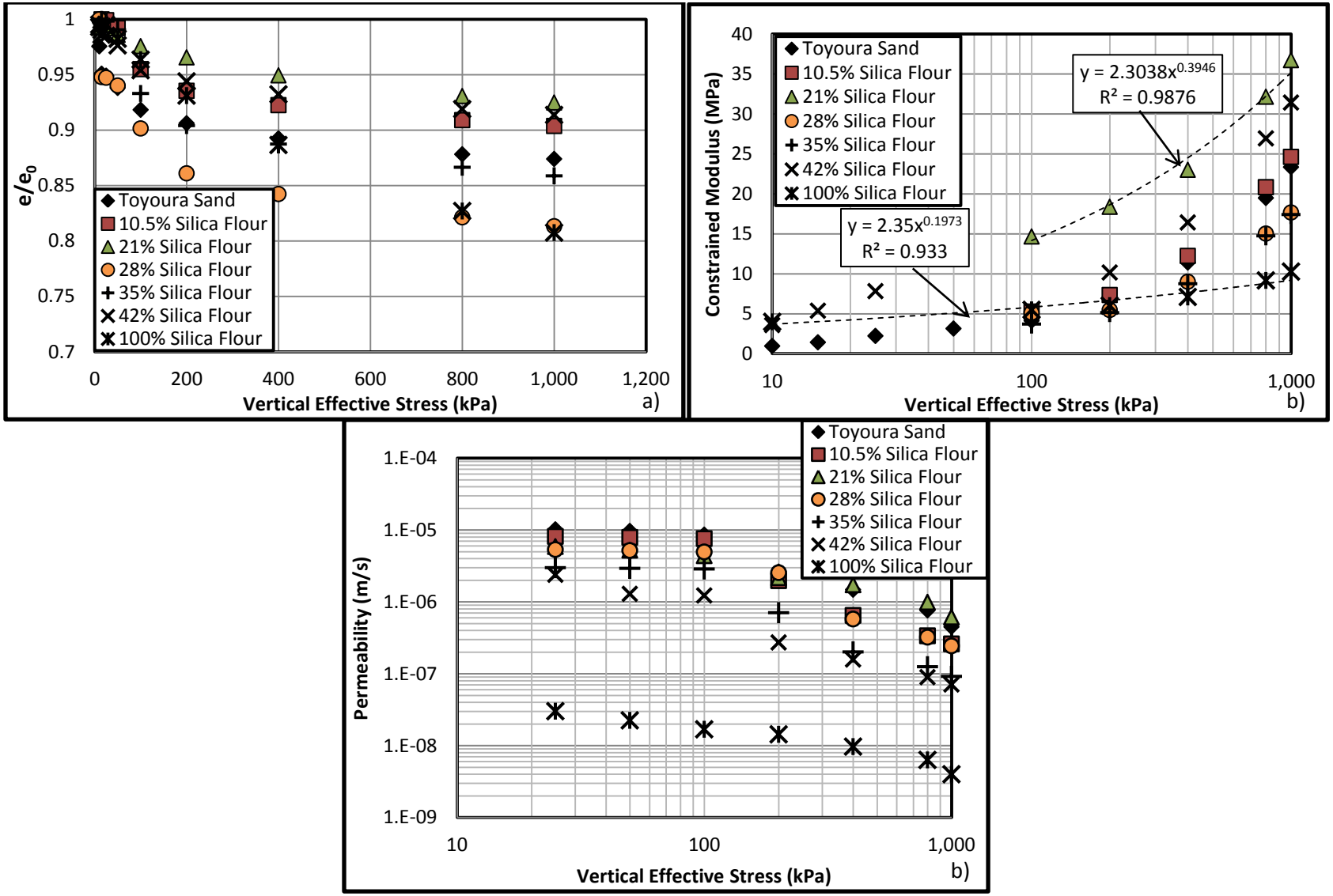

Figure 4.26. Rowe cell tests on Toyoura sand with 0-100% silica flour, 2% cement, 1% fibre, D_r=60% a) normalized void ratio vs. vertical effective stress; b) constrained modulus vs. vertical effective stress; c) permeability vs. vertical effective stress

4.5. Direct Shear

Direct shear tests were performed to determine the stress-strain response during plane strain shearing, and the peak (φ') and critical state internal friction angle (φ_{cs}'), and the dilation angle (ϕ) of the Toyoura sand and the silica flour. Each test was performed at a density of roughly 1.40 g/cm^3, and normal stresses ranging from 25 kPa to 300 kPa.

For the silica flour ϕ_{pk}'=40.8°, ϕ_{cs}'=33.4°, and φ_{pk}≈6.4°. For Toyoura sand ϕ_{pk}'=34.3°, ϕ_{cs}'=33.2°, and φ_{pk}≈1.1°. The friction angle results for the Toyoura sand match well with the findings of Nakamichi & Sato (2013), and the peak and critical state friction angles of the silica flour are within the ranges for inorganic silts suggested by Terzaghi & Peck (1948) and Ojha & Trivedi (2013). The dilation angle was calculated two ways: $\varphi = \phi'_{pk} - \phi'_{cs}$, and ϕ≈maximum slope of vertical vs. horizontal displacement (Bolton, 1986; Simoni & Houlsby, 2006). Several tests on silica flour were found to have had a defective LVDT (tests b, d, and e), but the shear stress data was valid and results were used to calculate the aforementioned parameters. The direct shear data can be found in Appendix B.

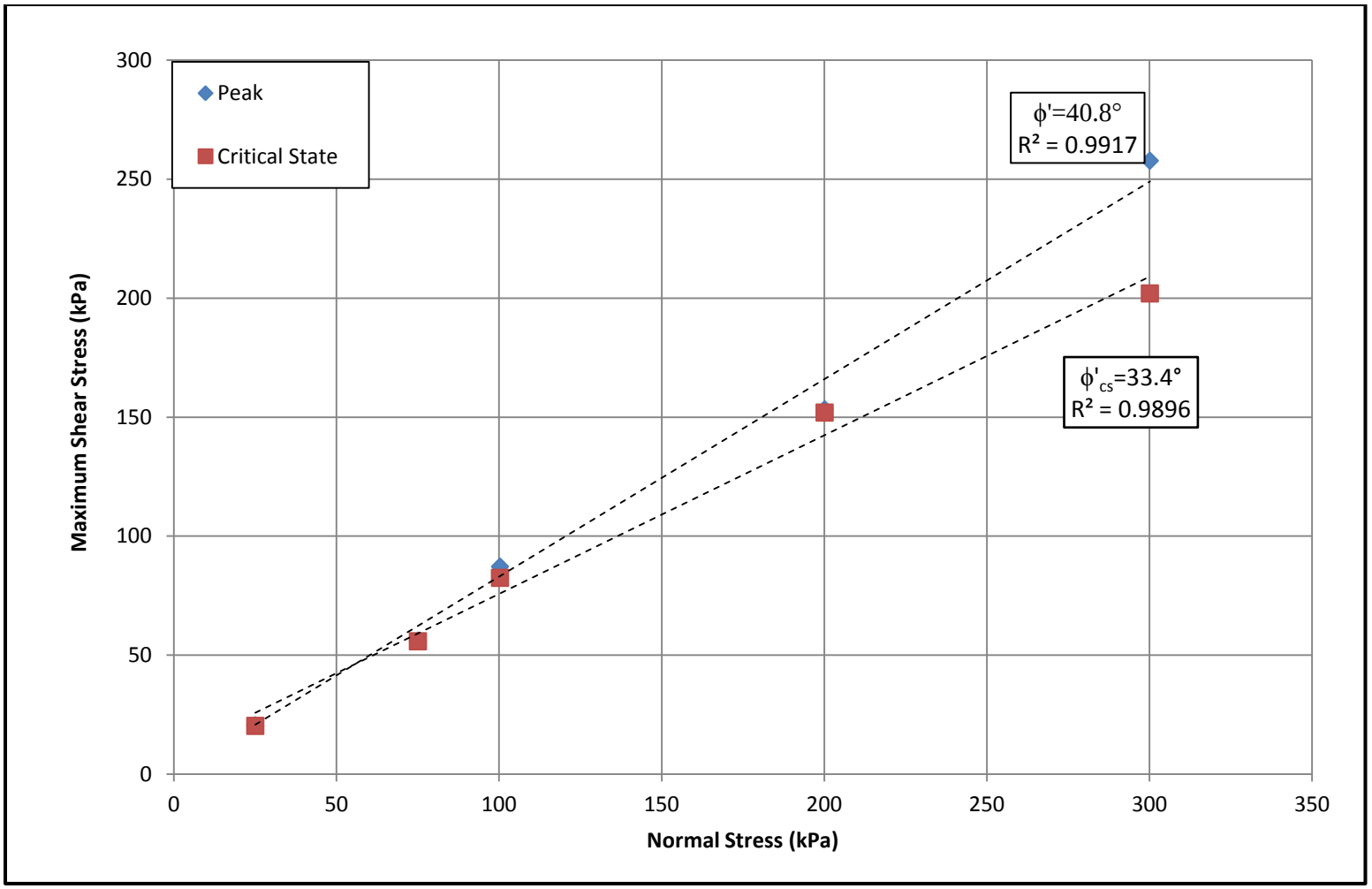

Figure 4.27. Internal friction angle of dense silica flour

Silica Flour: Shear rate: 0.182mm/min, Density of silt: 1.43g/cm^3, Dr= 100%, Void ratio: 0.849

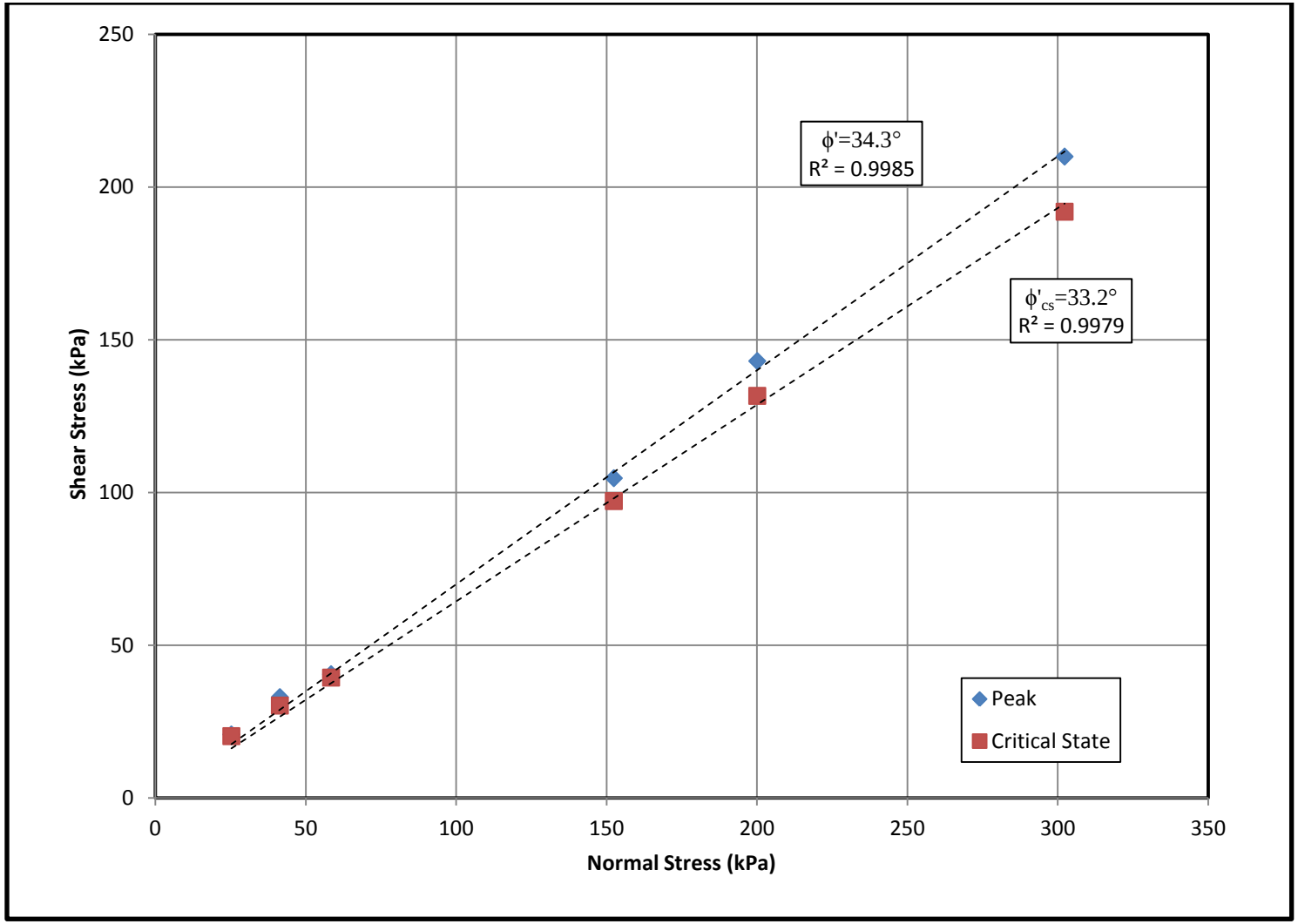

Figure 4.28. Internal friction angle of loose Toyoura sand

Toyoura Sand: Shear rate: 0.182mm/min, Density of sand: 1.40g/cm^3, Dr=20%, Void ratio: 0.889-0.892

4.6. Bender Element

4.6.1. Shear and P-wave Velocity Measurements

The small strain stiffness (G_{max}) of a soil sample is directly related to external forces such as confining stress, strain amplitude, and number of loading cycles, as well as internal characteristics such as density, void ratio, and shear wave velocity. Measurement of shear wave propagation has become one of the most common and versatile methods for assessing this parameter (Cha et al., 2014; Kramer, 2013) since its introduction by Shirley and Hampton (1978). The small strain shear modulus of a soil is instrumental in determining the soil behaviour during dynamic and vibratory loads, such as earthquakes. Knowing the small strain effects of cement and PVA fibre additions as stabilizers is useful in the design of earth structures that need to withstand such loading conditions.

Using piezoelectric bender elements, the P-wave (V_p) and shear wave velocity (V_s) were determined for 19 samples of Toyoura sand with silt, fibre, and cement additives. Both velocities were calculated from the response signal using a peak-to-peak relationship or cross-correlation techniques in the time domain performed by the bender element analysis tool (BEAT) software provided by GDS Instruments. The sample density and shear wave velocity were used to calculate the small strain shear modulus of the sample at effectives stresses ranging from 10-400 kPa using Equation 4.6:

$$G_{max} = \rho V_s^2 \qquad \textbf{[4.6]}$$

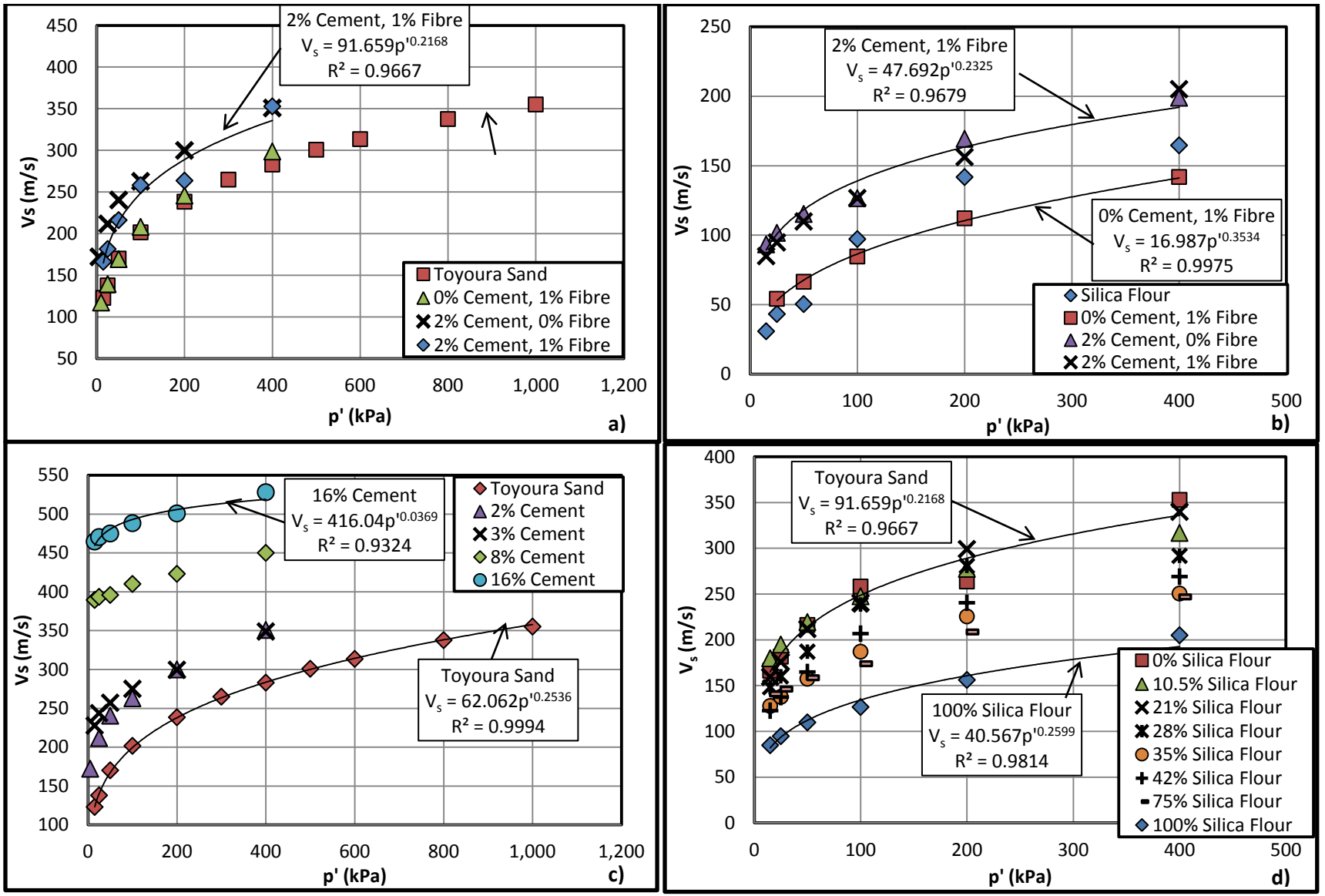

Figure 4.29. Bender element: shear wave velocity vs. effective stress at D_r=60% for a) Toyoura sand with and without stabilizers; b) silica flour with and without stabilizers; c) Toyoura sand with 0-16% cement; d) 0-100% silica flour, 2% cement, 1% fibre;

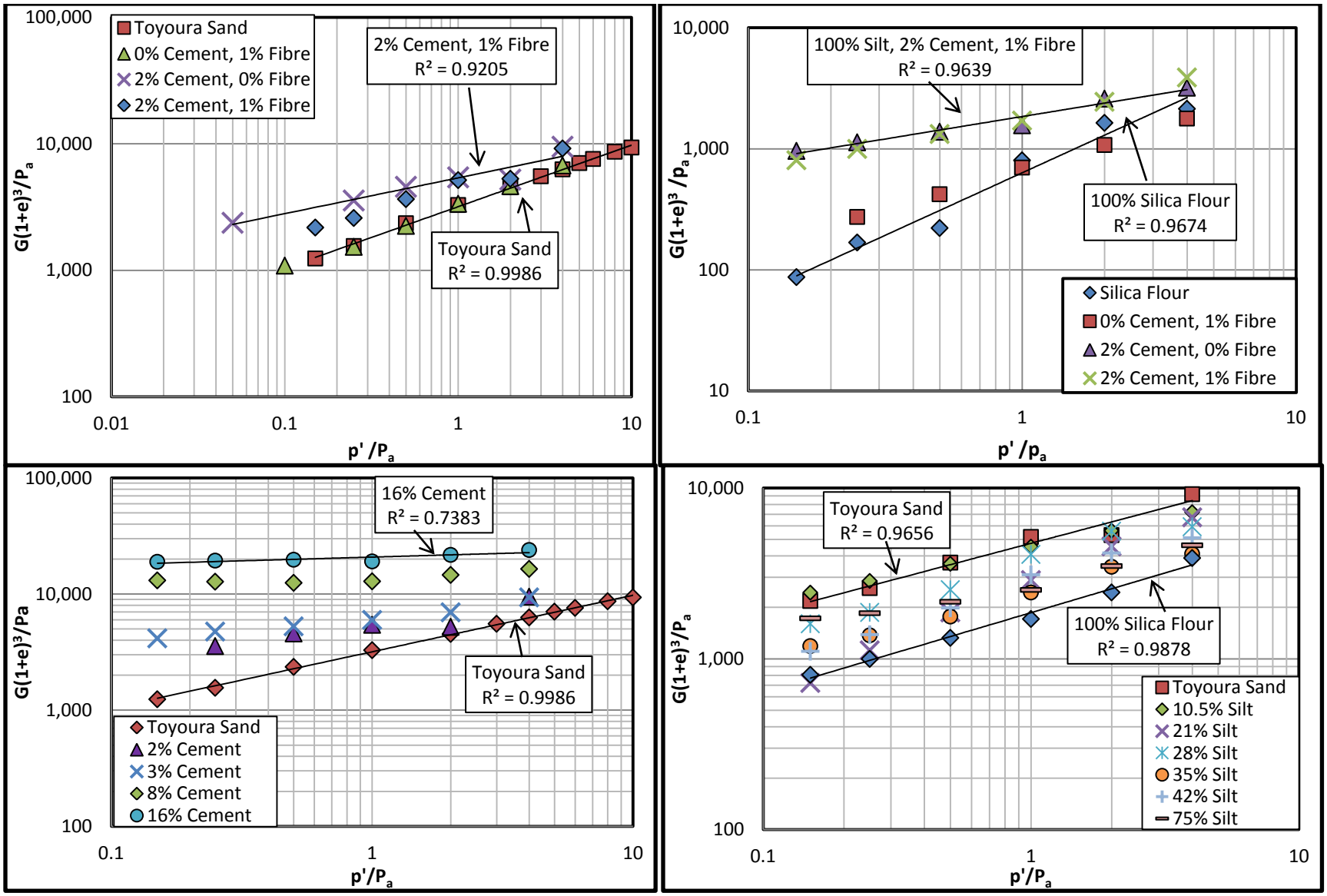

Figure 4.30. Bender element: normalized shear modulus vs. normalized confining stress at D_r=60% for a) Toyoura sand with and without stabilizers; b) silica flour with and without stabilizers; c) Toyoura sand with 0-16% cement; d) 0-100% silica flour, 2% cement, 1% fibre

The shear modulus was normalized using the void ratio function $G_{max}(1+e)^3/P_a$ according to Oztoprak & Bolton (2013) and plotted as log $G_{max}(1+e)^3/P_a$ vs. log p'/P_a.

The shear wave velocity of Toyoura sand ranged from V_s=117 m/s to V_s=355 m/s at mean effective stresses ranging from 10-1000 kPa (Figure 4.29a), matching closely with the findings of Whitlow (2001) and Youn, Choo, & Kim (2008). The clean Toyoura sand has a moderate compressibility compared to other sands (Figure 4.31) denoted by α=62.06 and validated by the 1D compression tests using the Rowe cell (Section 4.4.2). The sensitivity of the skeletal shear stiffness to changes in stress (β=0.254) is also moderate, and suggests particle angularity and particle contact yield during stress changes (Cha et al., 2014). Toyoura sand was found to have a shear modulus ranging linearly (in normalized log G–log p' space) from 22 MPa to 200 MPa at confining stresses of 15-1,000 kPa matching closely with the findings of Lanzo & D'Elia (2003) and Builes, Garcia & Riveros (2007).

When stabilized with the PVA fibres, the shear wave velocity of the Toyoura sand was virtually unaffected (Figure 4.29a). A very minimal increase over unstabilized sand was seen at higher effective stress values. This confirms that the addition of fibres alone does not dramatically change a soil's behaviour during very small strain loading conditions (Consoli, Bassani, & Festugato, 2010). The shear modulus was consequently minimally affected by the PVA fibres, decreasing slightly at lower confining pressures, consistent with the findings of (Heineck, Coop, & Consoli, 2005). There was also no significant change in the α or β values for the Toyoura sand with 1% fibre, suggesting that in triaxial compression a 1% fibre concentration does not improve or lessen the stiffness of Toyoura sand.

For the case of the Toyoura sand with 2% cement and 1% fibre content, the fibres no longer control the skeletal stiffness. Instead, the cementitious bonding dominates by interlocking the fibres and the sand grains (as seen in Figure 4.5 in Section 4.2) and creating a less compressible specimen (Salahuddin, Marri, & Kumar, 2013). Though the change in these α and β values was small, due mostly to

the relatively short curing time of 3 days, it is clear that the addition of OPC both strengthened and stiffened the Toyoura sand (Table 4.2).

High percentages of cement additive clearly affected the Toyoura sand regardless of the curing time, stiffening the sample significantly and raising the shear wave velocity from 117 m/s to 528 m/s and the shear modulus from 123 MPa to 428 MPa (at σ_c'=400 kPa) in samples with 0% and 16% cement content respectively (Figure 4.29c & Figure 4.30c). The hydrated cement bonds markedly improved the ability of the soil to withstand high confining stresses and dynamic small strains, reducing volumetric strain even at confining stresses as high as 400 kPa. As modelled by (Cha et al. 2014) in Figure 4.31 Figure 4.32, the alpha value increases to nearly 500 and the beta value drops well below 0.1 at high cement contents. This model was matched exceptionally well at 4-16% cement content. At concentrations of 1-3% cement, however, the data did not quite reach β=0.1 as seen in Table 4.2.

With 2% cement and 1% PVA fibre, the percentage addition of the silica flour was inversely proportional to the shear wave velocity, decreasing it from 350 m/s to 200 m/s at 0-100% silica flour (σ_c'=400 kPa) (Figure 4.29d). Once again, the compressibility of the sample was seen to decrease until a limiting concentration of silica flour (somewhere between 28-42% silica flour), after which it increased very slightly. This trend was also noted with a much clearer threshold in Rowe cell and oedometer tests (Sections 0 & 4.4.2.5) and in the literature: (Belkhatir et al. 2012; Polito & Martin II, 2001; Amini & Qi, 2000). It has also been shown that the silty sands exhibited greater compressibility at low confining pressures, explaining the large settlements seen during saturation in both Rowe cell and bender element tests.

In contrast to the Toyoura sand, un-stabilized silica flour is a weak, collapsible soil with a low shear wave velocity and shear modulus, and a high compressibility (V_s=31-165 m/s at G_{max}=1.5-40 MPa, α=7.23, β=0.54) similar to the values associated with a soft clay. Stabilization of this soil has pronounced

effects: the addition of 1% fibre slightly decreases the shear wave velocity and increases soil compressibility, whereas the addition of 2% cement has the opposite effect, increasing the shear wave velocity and decreasing the compressibility. Addition of both stabilizers (OPC and PVA fibres) is clearly the most effective, increasing the stiffness and internal friction angles as will also be discussed in Section 4.6.2.

To summarize, the normalized small strain shear modulus (G) of the Toyoura sand exhibited an increasing linear trend in normalized log G–log p' space, and was highly influenced by the addition of cement and silt, with PVA fibre having a negligible effect at a concentration of 1% by mass. The cement dramatically improved the sample stiffness and lowered compressibility, while the silt addition initially stiffened the soil as gradation improved, but appeared to lower the stiffness after a threshold concentration of 35-42%. This trend could also be seen in one dimensional compression (Rowe cell) and triaxial analysis regardless of cementation or fibre addition. Overall, in terms of small strain response, the addition of both cement and PVA fibres to silty Toyoura sand was the most effective amendment. This is due to the cement bonding the soil particles and fibres together into aggregated units. These larger units resist static and dynamic shearing more effectively than the individual components. When silt is added to this mixture the gradation of the soil is improved, thus the void space is reduced and the cement hydrates to fill more of the voids and bond more particles together.

The shear wave velocity was also plotted against mean effective stress and the data was fitted with a power curve (Equation 4.6) (Cha et al., 2014).

$$V_s = \alpha(p')^{\beta_0} \quad \textbf{[4.7]}$$

$$\alpha = 13.5C_c^{-0.63} \quad \textbf{[4.8]}$$

$$\beta_0 = 0.17 log C_c + 0.43 \quad \textbf{[4.9]}$$

$$\beta_0 = 0.73 - 0.27 log \alpha \quad \textbf{[4.10]}$$

where the factor (α) represents the shear wave velocity at a mean effective stress of p'=1 kPa (Equation 4.7), the exponent (β_0) is related to the sensitivity of the sample to changes in stress (Equation 4.8), and C_c is the sample compressibility. This power relationship between V_s and p' includes effects of contact behaviour and fabric change of the sample during consolidation.

Table 4.2. Bender element testing regimen with fitting parameters α and β_0 from power fit curve of Vs (m/s) vs. p', and β_0* from Cha et al. (2014)

Specimen	α	β_0	β_0*
Toyoura Sand	62.06	0.254	0.246
Toyoura Sand, 1% Fibre	62.78	0.258	0.245
Toyoura Sand, 1% Cement	104.96	0.202	0.184
Toyoura Sand, 2% Cement	133.94	0.146	0.156
Toyoura Sand, 2% Cement, 1% Fibre	91.66	0.217	0.200
Toyoura Sand, 3% Cement	162.25	0.121	0.133
Toyoura Sand, 4% Cement	143.07	0.173	0.148
Toyoura Sand, 8% Cement	337.69	0.052	0.047
Toyoura Sand, 16% Cement	416.04	0.0369	0.023
100% Silica Flour	7.23	0.539	0.498
100% Silica Flour, 1% Fibre	16.99	0.353	0.398
100% Silica Flour, 2% Cement	47.69	0.233	0.277
10.5% Silica Flour, 2% Cement, 1% Fibre	112.29	0.172	0.176
21% Silica Flour, 2% Cement, 1% Fibre	83.36	0.236	0.211
28% Silica Flour, 2% Cement, 1% Fibre	79.24	0.228	0.217
35% Silica Flour, 2% Cement, 1% Fibre	69.66	0.216	0.232
42% Silica Flour, 2% Cement, 1% Fibre	62.56	0.250	0.245
75% Silica Flour, 2% Cement, 1% Fibre	84.33	0.171	0.210
100% Silica Flour, 2% Cement, 1% Fibre	40.57	0.260	0.296

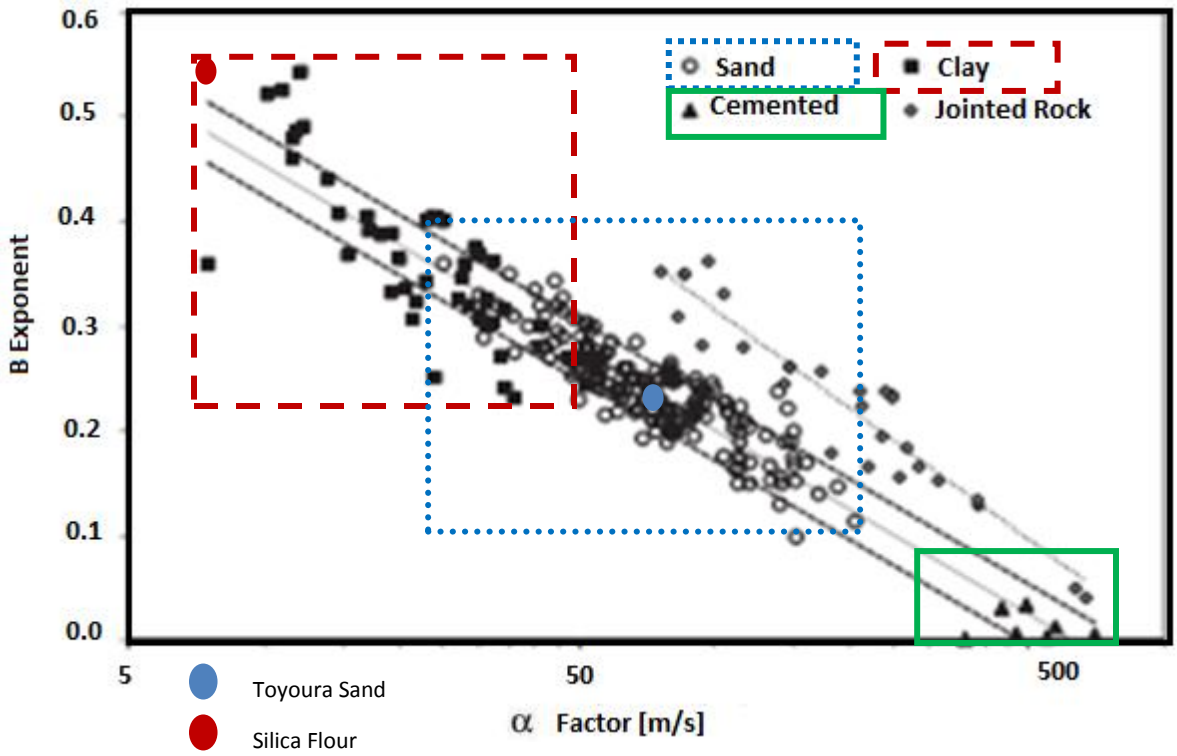

Figure 4.31. β exponent and α factor from power curve fitting of shear wave velocity (Cha et al. 2014)

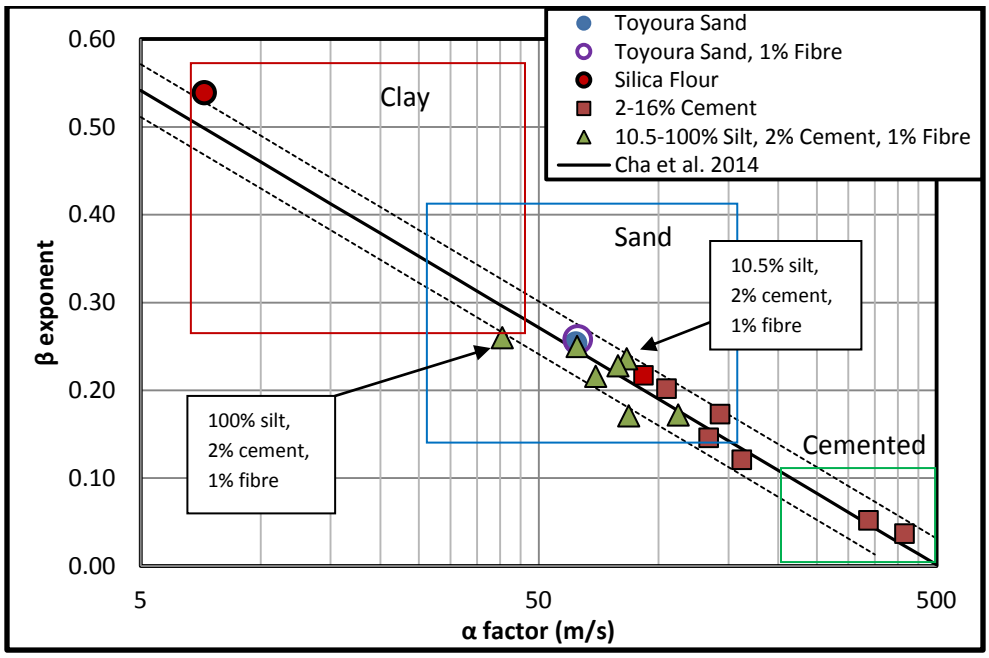

Figure 4.32. β exponent and α coefficient from experimental results for shear wave velocity

Dashed lines represent standard error of ±0.03 from (Cha et al. 2014)

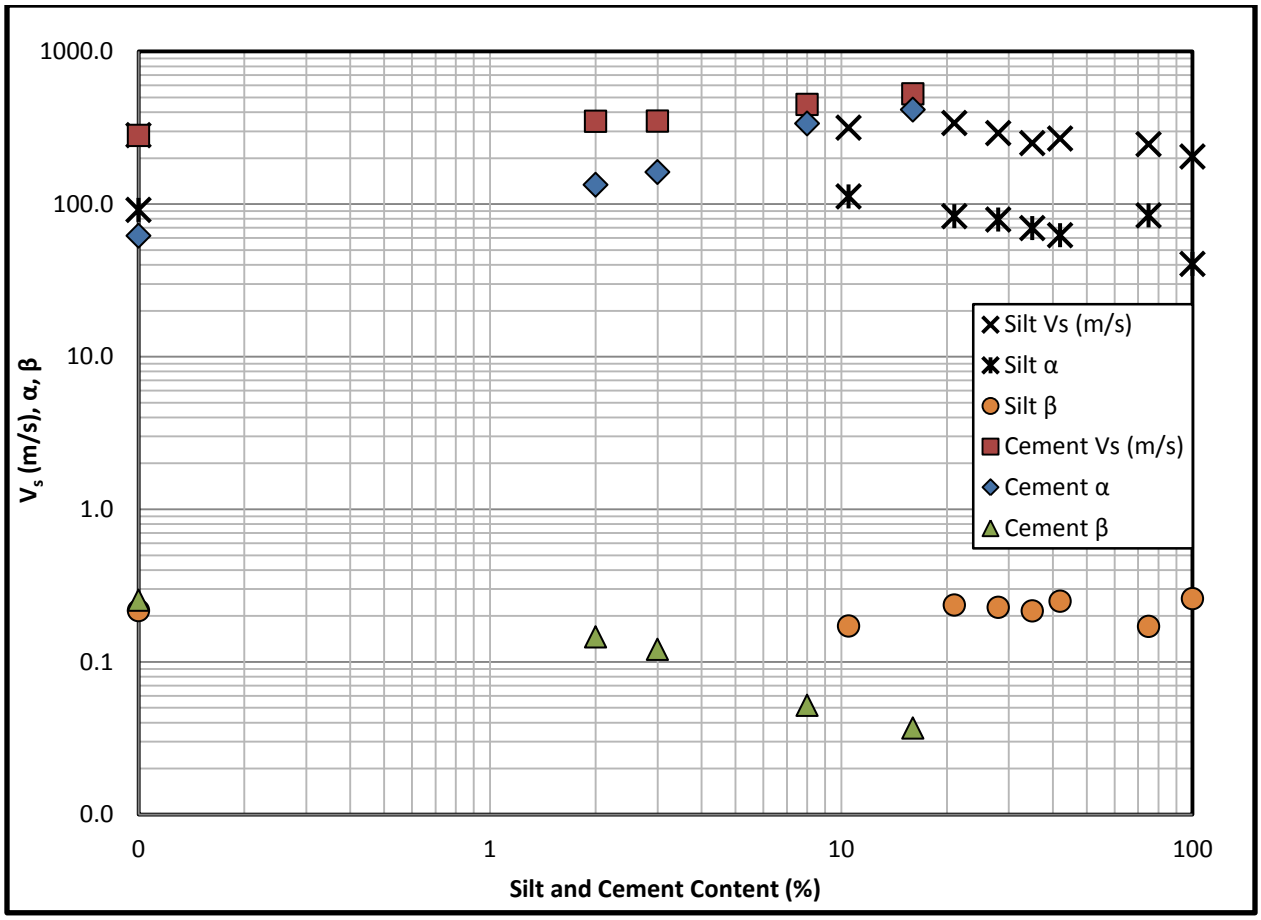

Figure 4.33. Vs (m/s), α, and β values at 400 kPa versus silica flour content (%) and cement content (%)

4.6.2. Consolidated Undrained Shearing

Consolidated undrained triaxial tests were used to determine the strength and stress-strain relationships for the soil samples in Table 4.2 following the bender element testing in Section 4.6.1. Tests were conducted to plot a strength envelope, and explain the large strain behaviour of stabilized silty sand. After consolidation to an effective stress of 400 kPa, the soil samples were monotonically sheared at a rate of 0.06 mm/min (Head, 1986). Plots of deviator stress (q) vs. axial strain (ε_a), excess pore water pressure (r_u) vs. axial strain (ε_a), and deviator stress (q) vs. Cambridge effective stress (p') were created for comparative purposes, and results were interpreted based on the microstructure seen in Sections 4.2 and 4.3, and the trends seen in the Rowe cell and cyclic triaxial testing.

The slope of the critical state line was determined directly from the aforementioned q vs. p' plots, and the critical state friction angle was calculated using Equation 4.11:

$$\phi_{cs}{}' = sin^{-1}\left(\frac{3M}{6+M}\right) \quad \textbf{[4.11]}$$

Where ϕ'_{cs} is the critical state friction angle and M is the slope of the critical state line (Wood, 1990).

4.6.2.1. Monotonic Shearing of Stabilized Toyoura Sand

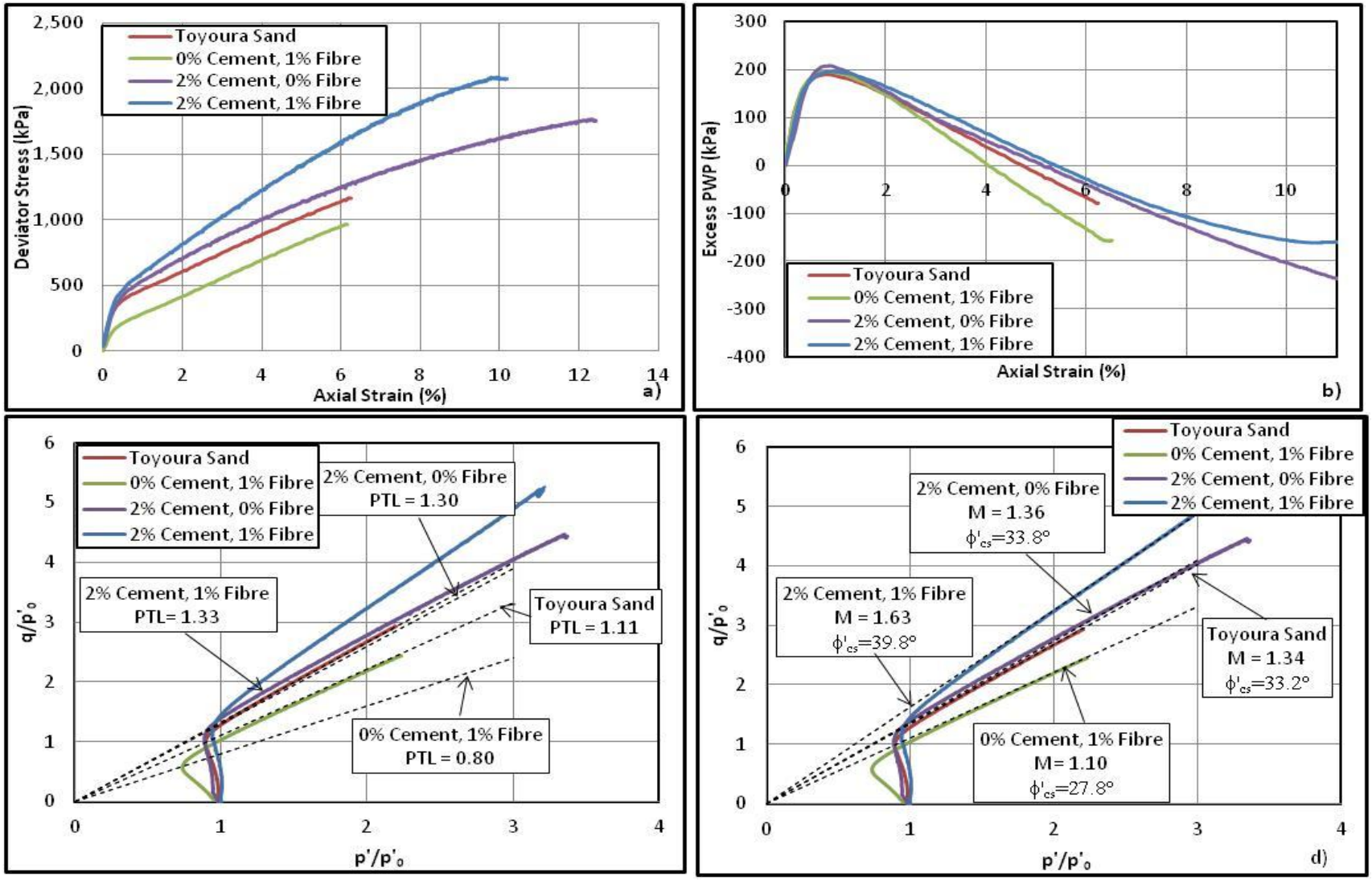

Figure 4.34. Monotonic shearing of stabilized Toyoura sand D_r=60%, p_0'=400kPa a) q vs. axial strain; b) excess pore water pressure vs. axial strain; c) phase transformation line (PTL); d) critical state line (CSL)

The critical state line of Toyoura sand was found to have a slope of M=1.34 matching very closely with results from (Yang, Li, & Yang, 2008) as seen in Figure 4.34d, and a phase transformation line (PTL) slope of PTL=1.11. During shearing, excess pore pressure rose to nearly 200 kPa at around 1% axial strain and the peak deviator stress (q) was 1,160 kPa at just over 6% axial strain, thus the peak undrained shear strength (q/2) was c_u=580 kPa, consistent with the values found by Ling & Yang (2006).

When stabilized with 1% PVA fibre, 2% cement, or a combination of the two, the Toyoura sand exhibited the same general trend in excess pore pressure generation and deviator stress increase. Positive pore pressure reached nearly 200 kPa indicating contraction of the sample, followed by a near linear decrease into negative pore pressures, indicating dilation (Figure 4.34b). The peak deviator stress decreased slightly from 1,160 kPa to 970 kPa (c_u=485 kPa) when 1% fibre was added, though the addition of 2% cement increased it to 1,760 kPa (c_u=880 kPa) and the combination of both additives produced the strongest sample, with a peak undrained shear strength of 1,050 kPa (Figure 4.34a) suggesting that the two stabilizers work better together than individually (Nakamichi & Sato, 2013).

The addition of fibres to the Toyoura sand increased the compressibility and reduced the initial yield surface of the sand as shown in Figure 4.34c-d, reducing the PTL and the M value to 0.8 and 1.1 respectively. This corresponded well with Rowe cell axial strain results from Section 4.4.2 and suggested a reduction in small strain shear modulus caused by replacement of sand grains with a flexible and low compressibility fibre. Any clumps of fibres within each sample can leave open and compressible voids allowing additional compaction, and it has been theorized that fibres in compression can actually have negative effects on sand caused by this increased sample porosity (Michalowski & Cermak, 1994; Ibraim & Fourmont, 2006; Gray & Refeai, 1986).

4.6.2.2. Monotonic Shearing of Toyoura Sand with 0-16% Cement

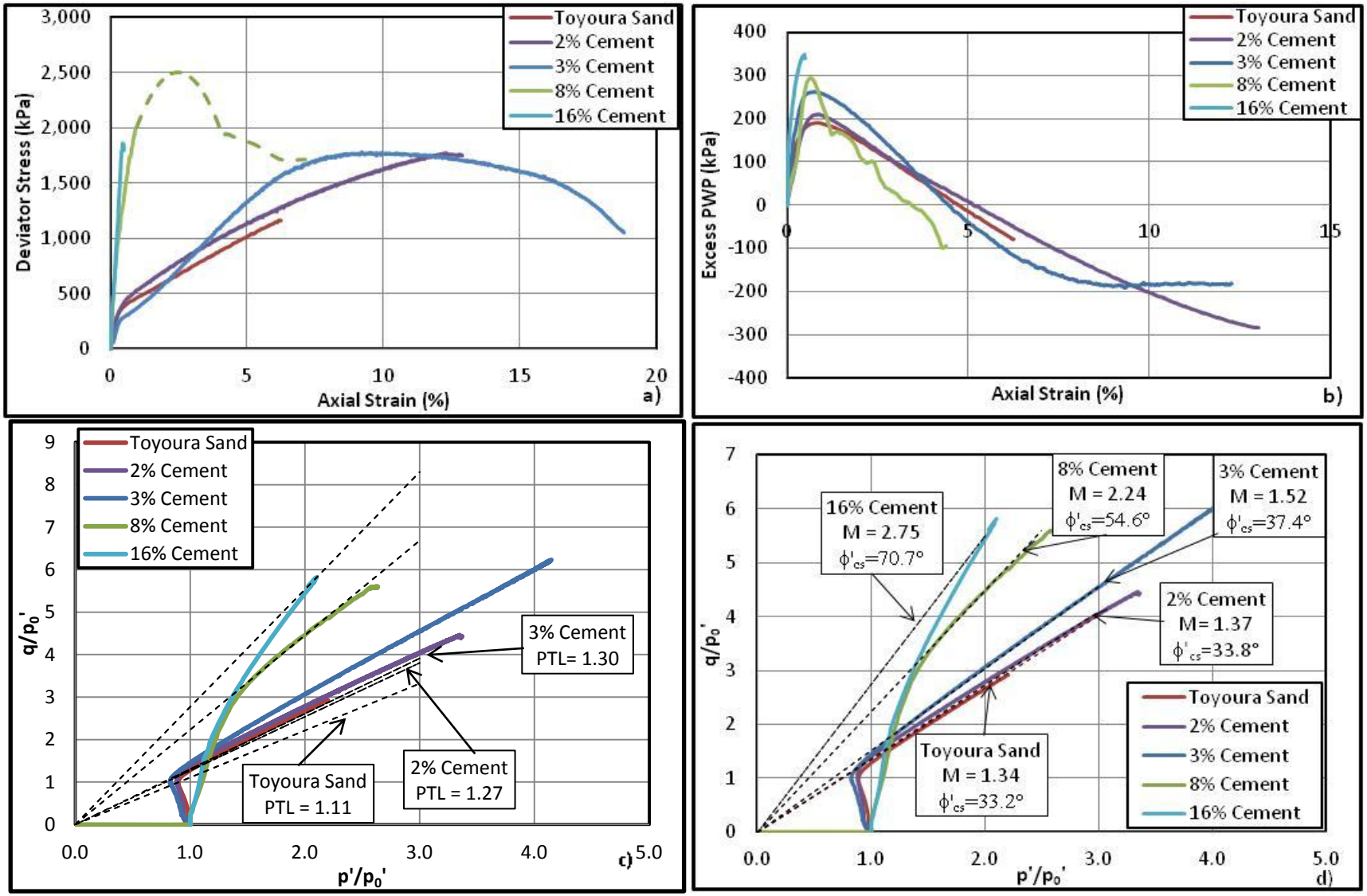

Figure 4.35. Monotonic shearing of 0-16% Cement at D_r=60%, p_0'=400kPa a) q vs. axial strain; b) excess pore water pressure vs. axial strain; c) phase transformation line (PTL); d) critical state line (CSL); *NOTE: Dashed line in a) is an estimation of the peak strength for 8% cement*

OPC addition, in contrast to the addition of fibres, increases the M value of the Toyoura sand significantly, from M=1.34 for Toyoura sand, to M=2.75 for 16% cement (Figure 4.35c-d). Toyoura sand with cement concentrations of 3% or less develop excess pore water pressures of 200-275 kPa quite rapidly, with a gradual decline into negative excess pore water pressure at high strains. Concentrations above 3% tend to rapidly develop excess pore water pressures up to 300-350 kPa and then more steeply decline into negative excess pore water pressure as seen in Figure 4.35a. In all cases the samples reach the peak excess pore water pressure after the phase transition point at the minimum p' value. The bond strength of the cemented soil structure requires significantly higher stresses to be broken despite the build-up of excess pore pressures being very high at low strains. This makes it far less susceptible to liquefaction than the un-stabilized Toyoura sand (Nakamichi & Sato, 2013). Though the yield stress of the Toyoura sand with high concentrations of cement is far higher than the clean sand, it experiences a more brittle shear failure at a steeper friction angle as shown in Figure 4.36.

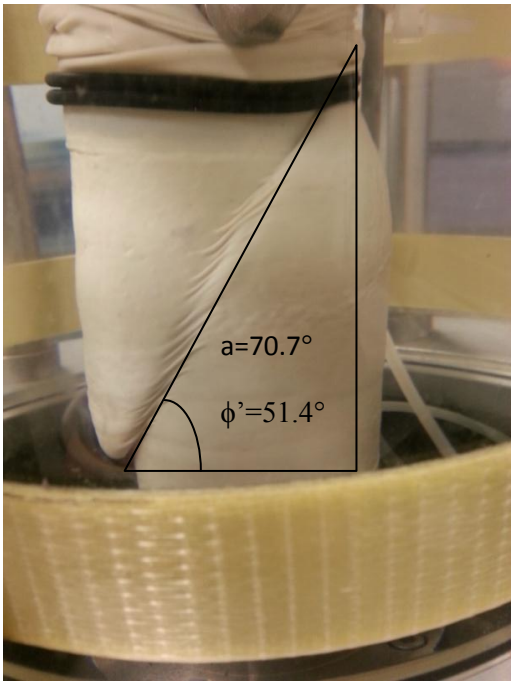

Figure 4.36. Consolidated undrained shear failure of Toyoura sand with 16% cement (σ'_c=400kPa, ϕ'=51.4°)

4.6.2.3. Monotonic Shearing of Stabilized Silica Flour

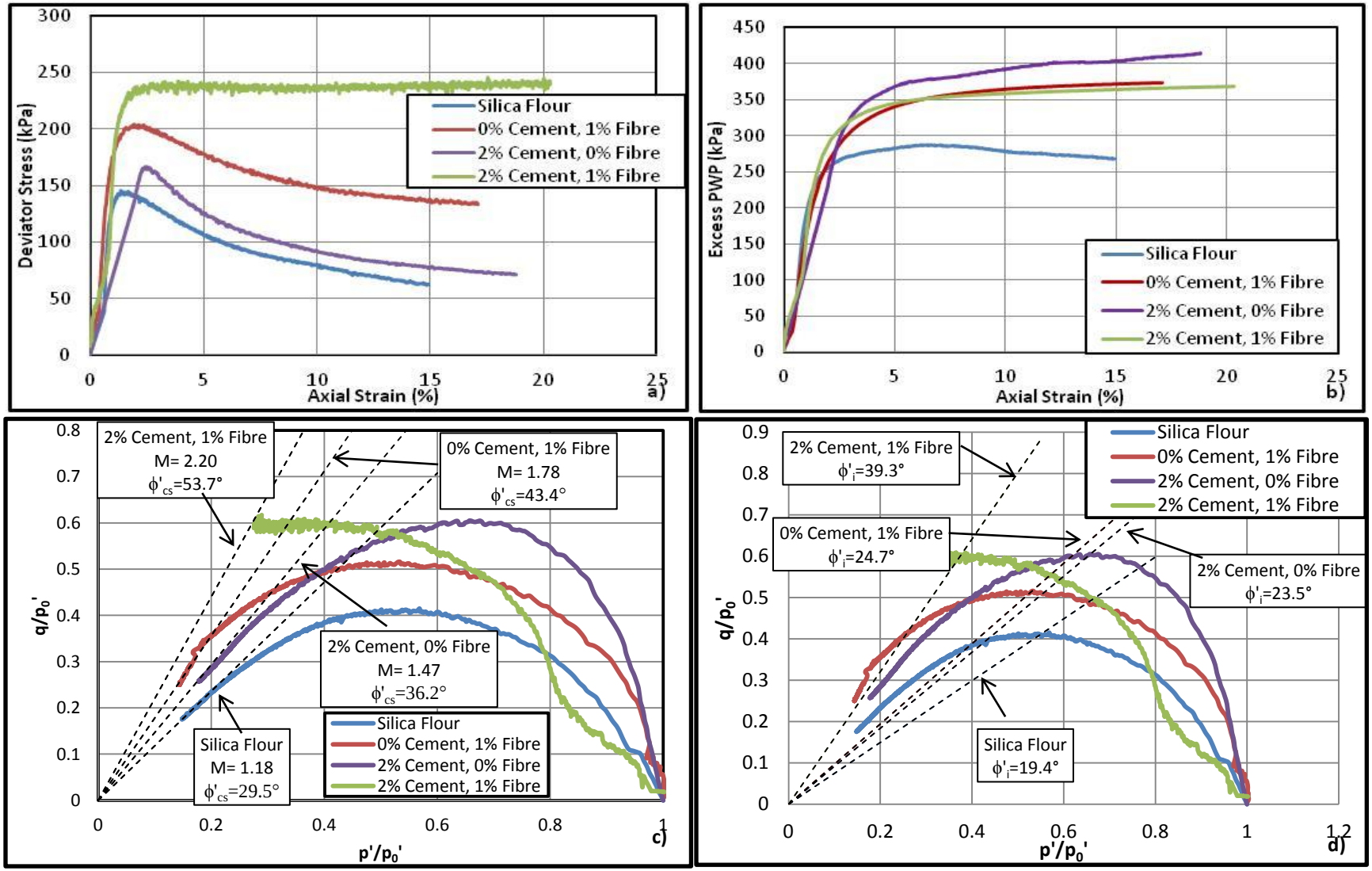

Figure 4.37. Monotonic shearing of stabilized silica flour at D_r=60%, p_0'=400kPa a) q vs. axial strain; b) excess pore water pressure vs. axial strain; c) critical state line (CSL); d) instability line

The silica flour, as expected, is significantly weaker than the Toyoura sand in undrained shearing, reaching a peak deviator stress of just 140 kPa and a residual strength of q_{res}=60 kPa as shown in Figure 4.37b, similar to Fraser River silt (Sanin, 2010). The addition of fibre stabilized the soil significantly to a q_{peak}=200 kPa and q_{res}=135 kPa by reducing the occurrence of shearing planes and enhancing frictional resistance in the soil matrix (Michalowski & Cermak, 1994; Collins, 2011). The collapsible nature of the silt negates any major increase in porosity caused by fibrous inclusions (as seen in Toyoura sand) by filling these voids. This stabilization was also noted in the Rowe cell tests (Section 0).

Likely due to the high initial void ratio and the short duration of curing, the addition of 2% cement to the silica flour had only moderate effects, raising the peak deviator stress to 170 kPa and the residual value to just above that of un-stabilized silica flour. Once again, the addition of both cement and PVA fibres had the largest effect, with a 100 kPa increase in peak stress over un-stabilized silica flour. In all cases, excess pore water pressure rapidly increased to between 275-410 kPa, indicating constant sample contraction during shearing Figure 4.37a.

Clearly silica flour is a soft soil with minimal shear strength when saturated, as indicated by the yield surfaces of clean and stabilized samples of silica flour in Figure 4.37c. In all four cases shown, strain softening is noted after shear failure. It has been shown that when sands are mixed with non-plastic silts unstable and compressible soil structures are formed allowing for considerable volumetric strain upon initial collapse (Yamamuro & Lade, 1998). This also helps to explain the strain softening phenomenon. The slope of the critical state line of silica flour gets progressively steeper with the addition of cement and fibre, ranging from 1.18 for silica flour to 2.2 for silica flour with 2% cement, 1% fibre (Figure 4.37c). This same trend is seen in the instability line, with the instability angle (ϕ'_i) increasing from 19.4° to 39.3° for the same mixtures (Figure 4.37d).

4.6.2.4. Monotonic Shearing of 0-100% Silica Flour with 2% Cement, 1% Fibre

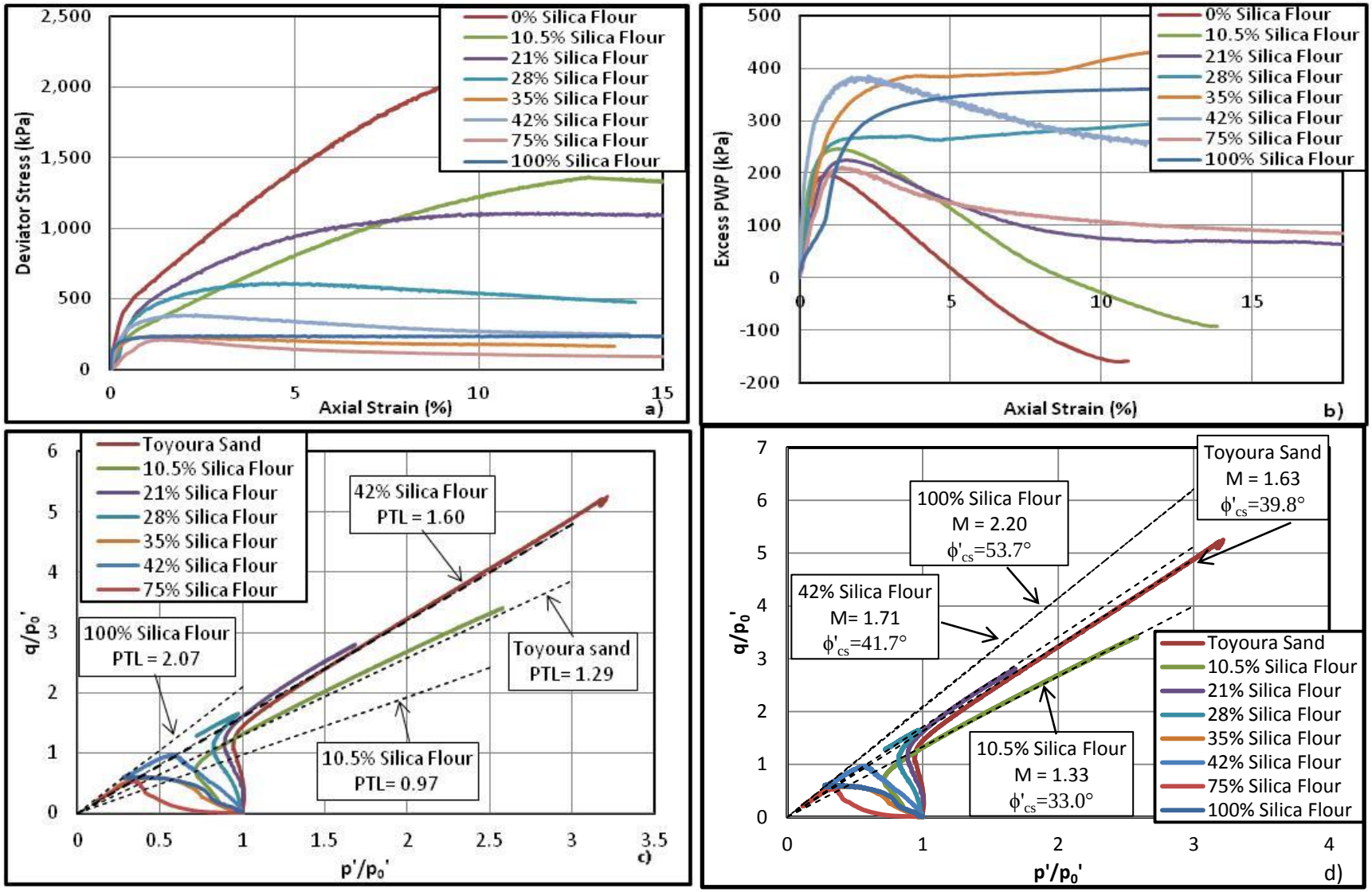

Figure 4.38. Monotonic shearing of 0-100% silica flour, 2% cement, 1% fibre D_r=60%, p_0'=400kPa a) q vs. axial strain; b) excess pore water pressure vs. axial strain; c) phase transformation line (PTL); d) critical state line (CSL)

Due to time constraints all samples with the different silica flour concentrations were stabilized with both OPC and PVA fibres. Concentrations of the silica flour ranged from 0-100%, converging on the range 0-42% found in Tokyo Bay. This had effects consistent with the trends seen in un-stabilized silty sands (similar to Rowe cell results in Section 4.4.2 and cyclic triaxial results in Section 4.7), with the peak deviator stress consistently decreasing, but the build-up of excess pore pressure reaching a maximum at around 35% silica flour concentration by mass as seen in Figure 4.38a-b. The most interesting trend to note when the silica flour content increases is the change in the yield behaviour. The addition of 0-28% silica flour exhibits strain hardening behaviour at a relative density of 60%, but 28% silica flour addition marks the transition point from strain hardening to strain softening; above 28% silica flour exhibits a purely strain softening response (Cubrinovski & Rees, 2008).

Silty sands exist in a “meta-stable” state, therefore an initial collapse of the soil allows sand particles to regain contact and increase dilation later in the shearing stage as opposed to the contraction normally seen. This could explain the behavioural shift of the silty sand mixtures seen in this section (Terzaghi, 1986).

4.7. Cyclic Triaxial Testing

For this thesis a series of 45 cyclic triaxial tests were performed (Table 3.7 in Section 3.8) to determine the effectiveness of PVA fibres and OPC as stabilization materials for preventing liquefaction of silty sands. Toyoura sand was mixed with 0-42% silica flour to simulate the in-situ conditions of Tokyo Bay described in Table 2.1 (Section 2.7), and tested with various fibre and cement combinations (ranging from 0-2% and 0-3% respectively). Benchmark tests of 100% silica flour with and without stabilizing additives were also performed to establish an upper bound for the behaviour of the silty sand. All tests were performed at a B value greater than 0.95 and a relative density of 60%.

The liquefaction potential of a soil can be determined via many laboratory tests including cyclic direct simple shear, cyclic torsional shear, and cyclic triaxial testing, all of which are relatively large strain tests used to simulate in-situ dynamic load events. The cyclic triaxial test is, however, the most common test to evaluate this phenomenon (Ladd, 1977; Polito, 1999).

When stress reversal occurs during cyclic loading (i.e. τ_{static}-τ_{cyclic}<0), and the steady state strength is not exceeded, the soil sample experiences compressional and extensional loading. This cyclic behavior is characterized by an increasing rate of excess pore water pressure build-up, and eventual tracking along the positive and negative drained failure envelope (Kramer, 2013). Based on a cyclic stress approach (Seed & Lee, 1966) or cyclic strain approach (Dobry et al., 1982), the onset of this cyclic mobility can be defined as the point at which the pore pressure ratio (Equation 1.1.) reaches unity, or the number of cycles to required reach a certain axial strain. This onset was defined as the number of cycles to reach 2% double amplitude axial strain for all samples at a certain cyclic stress ratio (CSR) (El Mohtar, 2009).

To validate the cyclic triaxial results, and to compare and contrast the effects of the silt, cement, and fibre addition, the excess pore water pressure generation was modelled using Equation 4.11 below (Seed, Martin, & Lysmer, 1975):

$$\mathbf{r_u = \frac{1}{2} + \frac{1}{\pi} \sin^{-1}\left(2\left(\frac{N}{N_L}\right)^{\frac{1}{\beta_1}} - 1\right)} \quad \textbf{[4.11]}$$

Where r_u is the pore water pressure ratio, N is the current cycle, N_L is the number of cycles to liquefaction and β_1 is a fitting exponent.

This section discusses the results of all of the cyclic triaxial tests listed in Table 3.7. Specifically these relate to tests on 100% silica flour, 42% silica, 0-100% silica flour with 1% fibre, 42% silica flour with 1% fibre, Toyoura sand with 2% cement, and 0-100% silica flour with 2% cement and 1% fibre. Please note that the data for stabilized pure silt can be found in Appendix C. Of particular importance in this section are the phase transformation lines (PTL) (determined from the deviator stress vs. Cambridge effective stress plots), the changes in axial and shear strain, the changes in excess pore water pressure, and the cyclic stress ratio (CSR) required to cause liquefaction.

4.7.1. Toyoura Sand

4.7.1.1. Pure Toyoura Sand, Various CSR

Toyoura sand was evaluated for liquefaction resistance at cyclic stress ratios (CSR=σ_1-σ_3/2σ_3) of between 0.200-0.243 and a relative density of 60% (ρ=1.49g/cm^3) as shown in Table 4.3. Compared to results from Fukuoka University (Nakamichi & Sato, 2013), and Toki et al. (1986), a slightly higher liquefaction resistance was found for the Toyoura sand (approximately 9 to 10% higher) as seen in Figure 4.41c. In all cases the Toyoura sand failed in a cyclic mobility deformation pattern that is often observed for a medium dense sand (Sze & Yang, 2014).

Table 4.3. Cyclic triaxial tests for pure Toyoura sand with various CSRs

Sample	CSR
Pure Toyoura Sand	0.200, 0.217, 0.233, 0.243

The critical state line was determined to have an approximate slope of CSL=1.34-1.4 in compression and extension (Figure 4.39a-c). This value did not change with relative density or CSR (Lade & Ibsen, 1997), though the slope was found to be slightly higher in cyclic shearing than in monotonic shearing.

Plots of deviator stress (q) vs. Cambridge effective stress (p') and deviator stress (q) vs. axial strain (ε_a) indicated that an increase in cyclic stress ratio will cause a sample to fail in fewer cycles, though always tracking along the critical state line in what will henceforth be referred to as the "butterfly" pattern (i.e. the transition point from stable soil behaviour to the onset of cyclic mobility), after Rahman, Baki, & Lo (2014).

These tests were performed at B=1.0, indicating 100% saturation. With increasing CSR the excess pore water pressure build-up in Figure 4.41a increased more rapidly, indicating that as the load amplitude increased the intergranular drainage between cycles decreased, causing failure to occur in

fewer cycles. This followed the curve predicted in the model proposed by Seed et al. (1975) very closely (Figure 4.41a). Damping was also seen to increase from 1% to nearly 9% with increasing CSR due to higher energy dissipation (Kramer, 2013). Regardless of the CSR, at the onset of cyclic mobility the plastic strain accumulation began to increase at a much faster rate, gradually tapering off at a maximum post failure axial strain around 22% as shown in Figure 4.41b. The secant shear modulus of the Toyoura sand (G_{sec}) was found to be an average of 36 MPa, which, as expected, was smaller than the G_{max} of 62 MPa found in the bender element testing at lower strain levels.

Based on Youd & Idriss (2001) the equivalent magnitude 7.5 earthquake is the CSR required to cause 5% double amplitude axial strain in 15 uniform cycles, which is CSR=0.235 for Toyoura sand. For an equivalent magnitude 9.0 earthquake (e.g. the Great East Japan Earthquake) they also suggest a failure criteria of roughly 34 cycles to reach 5% double amplitude axial strain; for Toyoura sand this is CSR=0.219 based on Figure 4.41c.

This process was repeated for the seven samples that were tested at four different CSR values (shown in Appendix C): Toyoura sand, silica flour, 2% cement, 2% cement & 1% fibre, 42% silica flour, 42% silica flour & 1% fibre, 48.5% silica flour & 2% cement & 1% fibre.

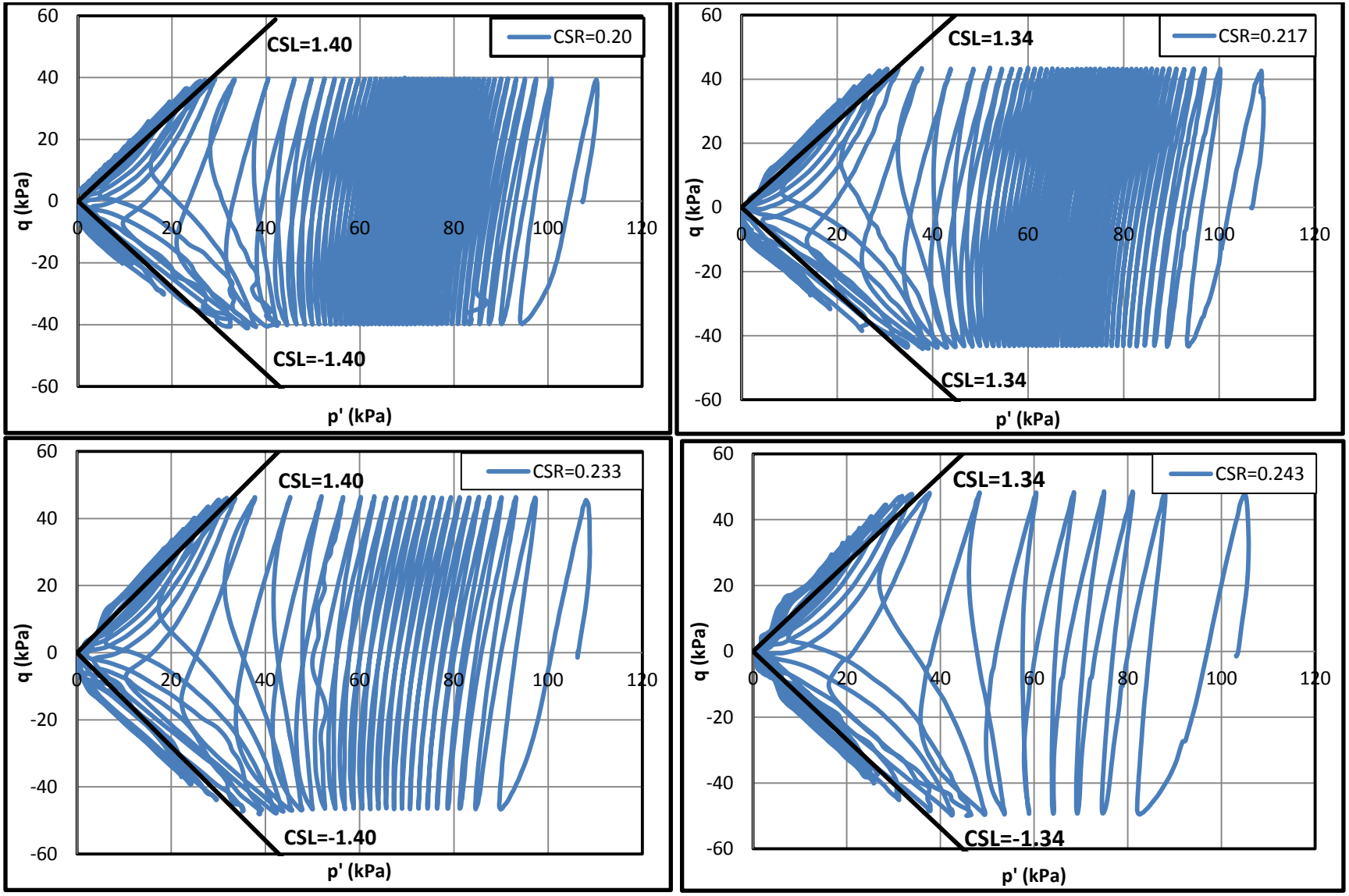

Figure 4.39. Deviator stress vs. Cambridge effective stress for Toyoura sand at D_r=60%, σ_c'=100kPa a) CSR=0.200; b) CSR=0.217; c) CSR=0.233; d) CSR=0.243

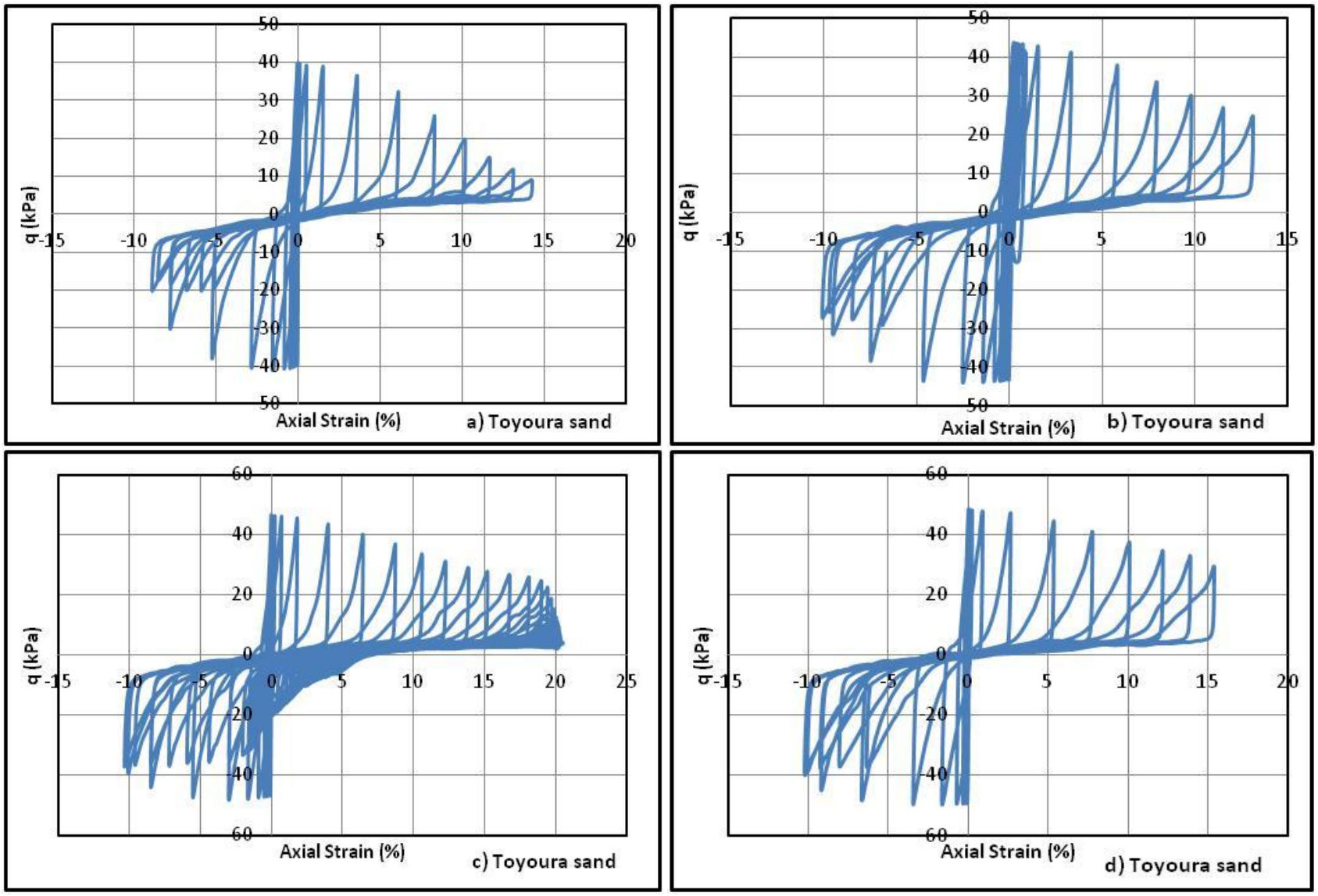

Figure 4.40. q vs. ε_a (%) for Toyoura sand at D_r=60%, σ_c'=100kPa a) CSR=0.200; b) CSR=0.217; c) CSR=0.233; d) CSR=0.243

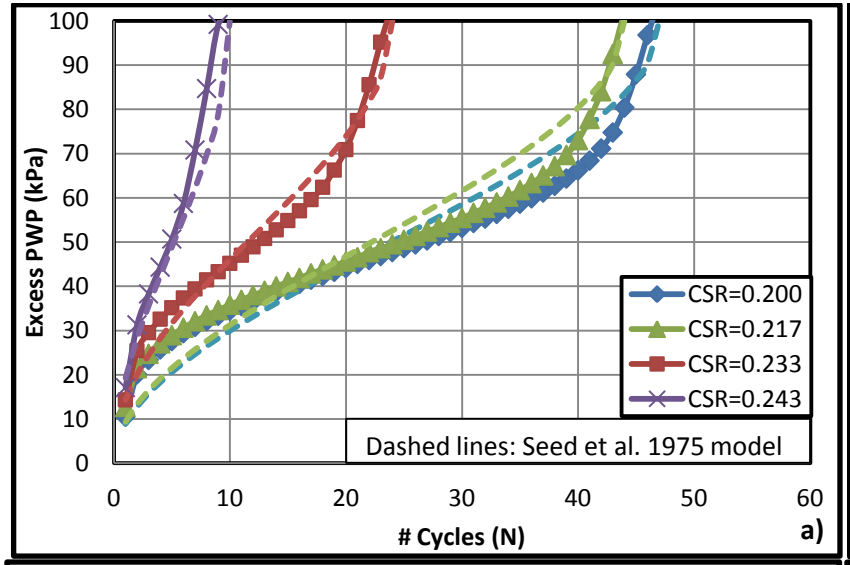
Excess PWP (kPa)
# Cycles (N)
CSR=0.200
CSR=0.217
CSR=0.233
CSR=0.243
Dashed lines: Seed et al. 1975 model
a)

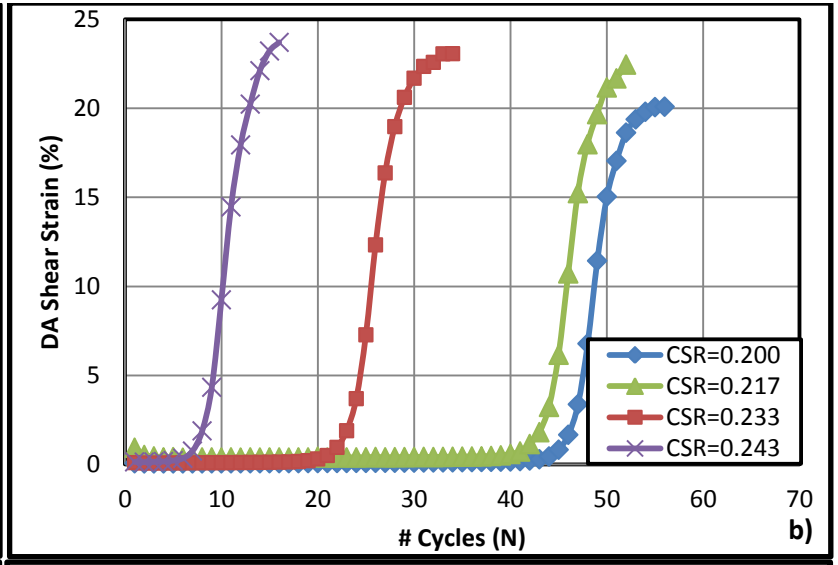
DA Shear Strain (%)
# Cycles (N)
CSR=0.200
CSR=0.217
CSR=0.233
CSR=0.243
b)

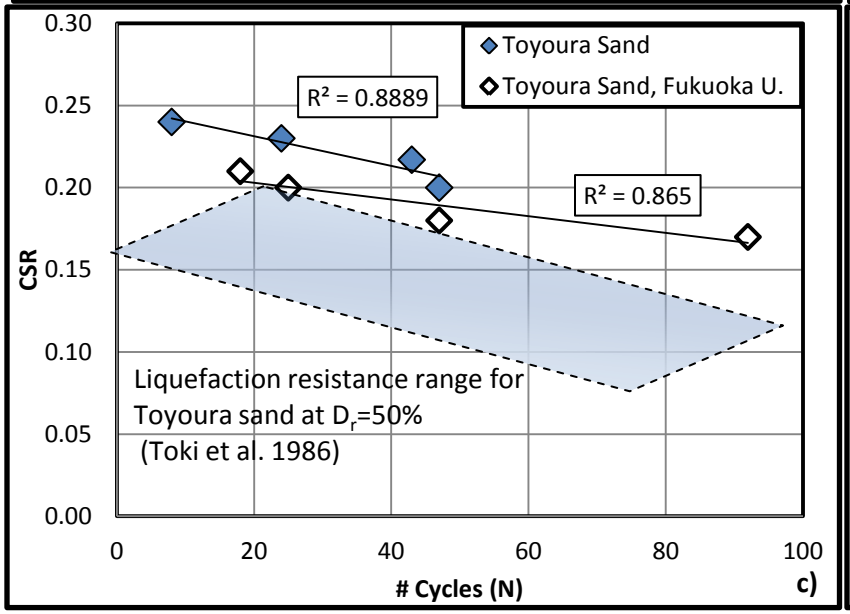
CSR
Cycles (N)
Toyoura Sand
Toyoura Sand, Fukuoka U.
R² = 0.8889
R² = 0.865
Liquefaction resistance range for
Toyoura sand at Dr=50%
(Toki et al. 1986)
c)

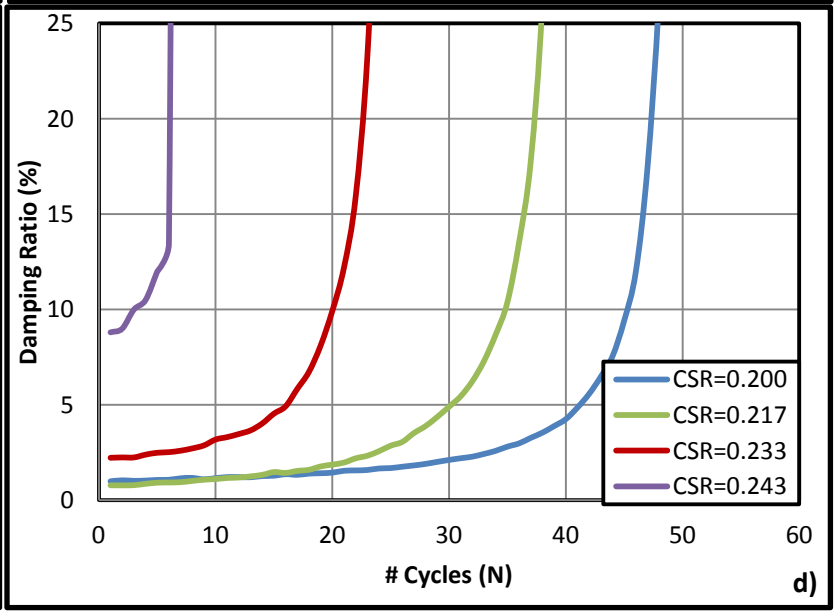
Damping Ratio (%)
# Cycles (N)
CSR=0.200
CSR=0.217
CSR=0.233
CSR=0.243
d)

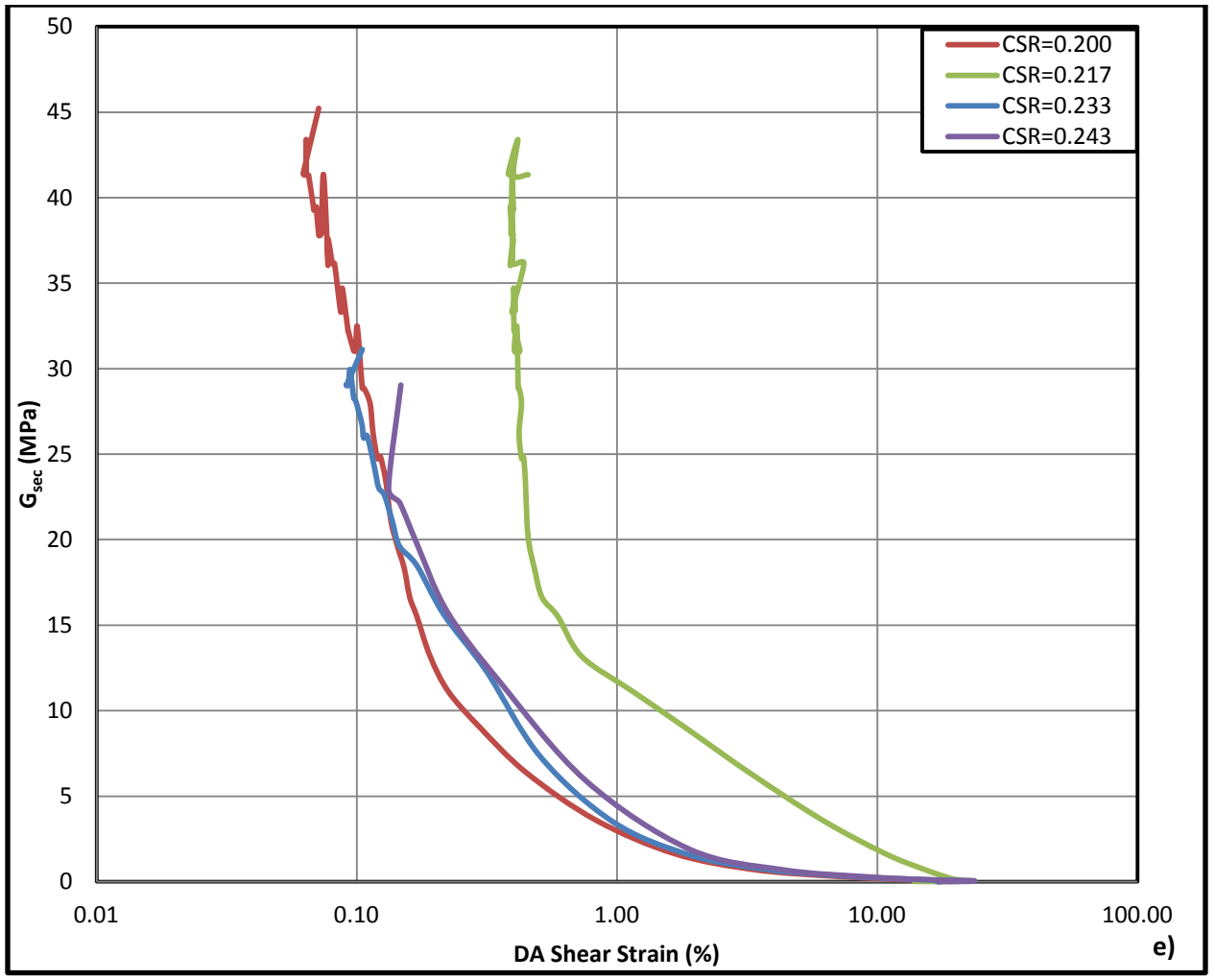

Figure 4.41. For Toyoura sand at D_r=60%, σ_c'=100kPa a) excess pore pressure vs. N; b) double amplitude shear strain vs. N; c) liquefaction resistance curve; d) damping ratio vs. N; e) G_{sec} vs. DA shear strain

4.7.2. Particle Size Distribution

The following section contains cyclic triaxial results from the tests outlined in Table 4.4. These tests were performed to determine the effect of the various silt concentrations found in the Tokyo Bay region of Japan on the liquefaction resistance of the Toyoura sand.

Table 4.4. Cyclic Triaxial Tests for Various Particle Size Distributions

Sample	CSR
42% Silt	0.07, 0.08, 0.09, 0.10
Pure Silt	0.07, 0.09, 0.10, 0.16
0-28% Silt	0.20
35-100% Silt	0.10

4.7.2.1. 42% Silt, Various CSR

To get a general idea of the overall liquefaction behavior of a silty soil, the peak concentration found in Tokyo Bay (42% by mass) was tested four times at various CSR values ranging from 0.07-0.10. In all cases, the slope of the CSL was between 1.10-1.20 (Figure 4.42).

These tests were performed at B values of 0.95-1.0. In terms of excess pore water pressure build-up, the rate changed based on the double amplitude shear strain. When the strain began to increase due to the onset of liquefaction, the slope of the excess pore water pressure curve began to steepen (Figure 4.44a). After full cyclic mobility of the silty sand, plastic shear strains reached between 6.5-7.8% in about 4 cycles, all of which showed clear signs of necking during their final few cycles Figure 4.44b).

Damping of the 42% silica flour mixture was constant at about 1% and the secant shear modulus was an average of 16 MPa (Figure 4.44d).

The liquefaction resistance of sand (CSR vs. number of cycles) does not follow a perfectly linear curve as shown in Figure 4.44c and corroborated by Tatsuoka, et al. (1986). This holds true for silty sands as well (Cubrinovski & Rees, 2008; Xenaki & Athanasopolous, 2003). It has been assumed that this non-linear trend will be seen for all concentrations of silt between 42-100%, which is how equivalent earthquake magnitudes have been calculated (as per the example for Toyoura sand at the start of this section). Thus, the equivalent magnitude 7.5 earthquake (5% DA strain in 15 cycles) is at CSR=0.110, and the equivalent magnitude 9.0 earthquake at 34 cycles to failure is at CSR=0.090.

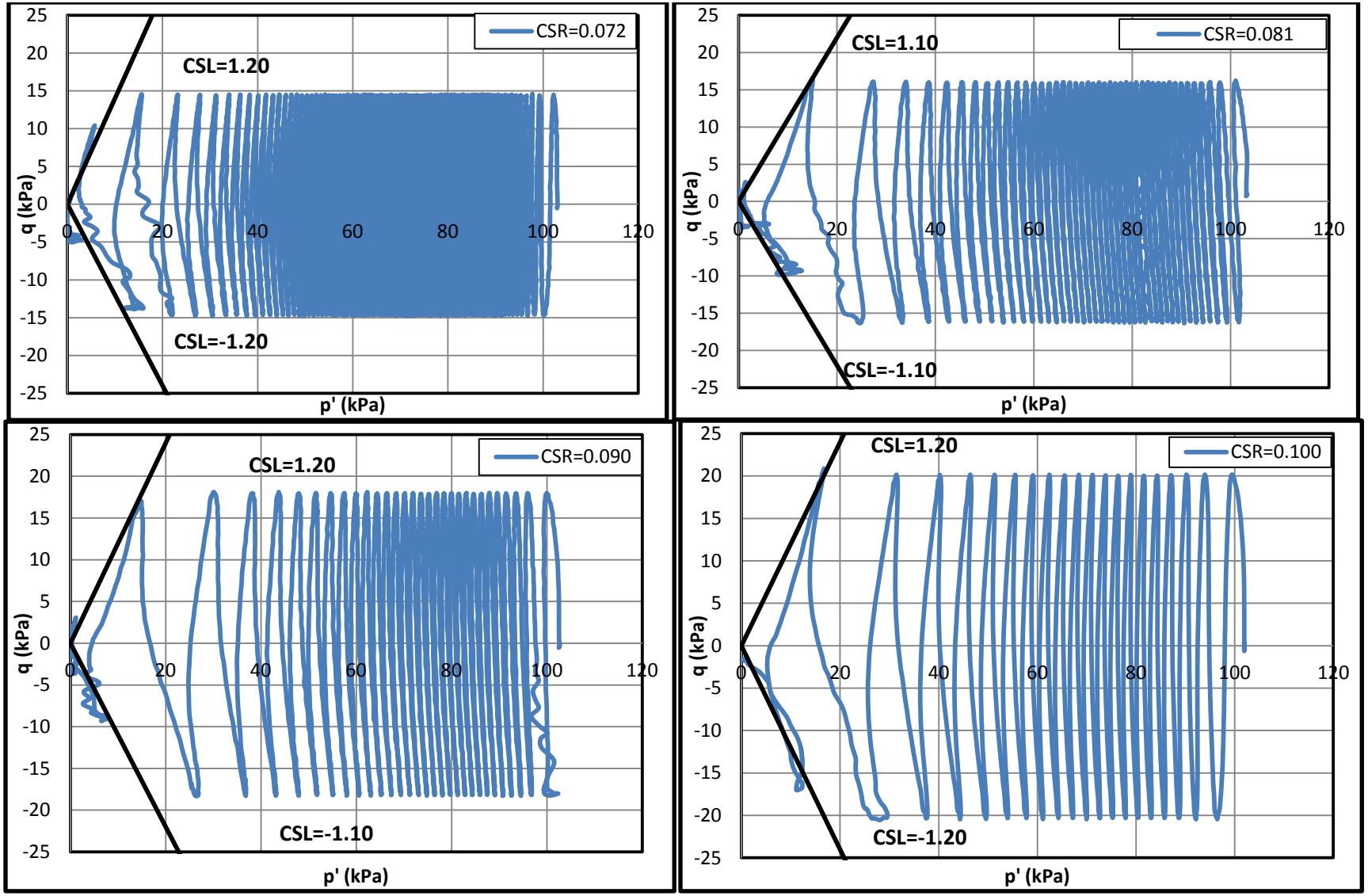

Figure 4.42. Deviator stress vs. Cambridge effective stress for Toyoura sand with 42% silica flour at Dr=60%, σ_c'=100kPa a) CSR=0.072; b) CSR=0.081; c) CSR=0.090; d) CSR=0.100

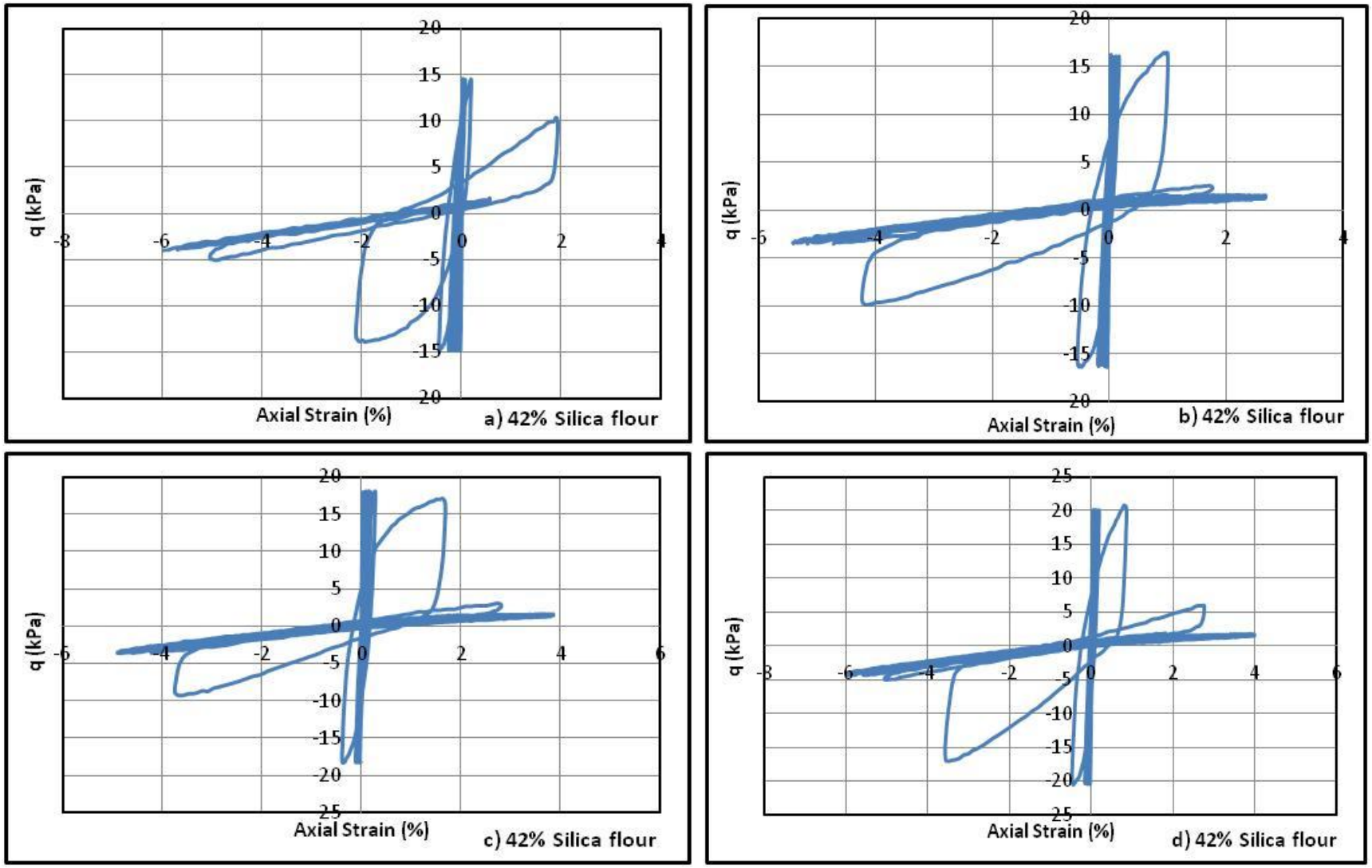

Figure 4.43. q vs. ε_a (%) for Toyoura sand with 42% silica flour at Dr=60%, σ_c'=100kPa a) CSR=0.072; b) CSR=0.081; c) CSR=0.090; d) CSR=0.101

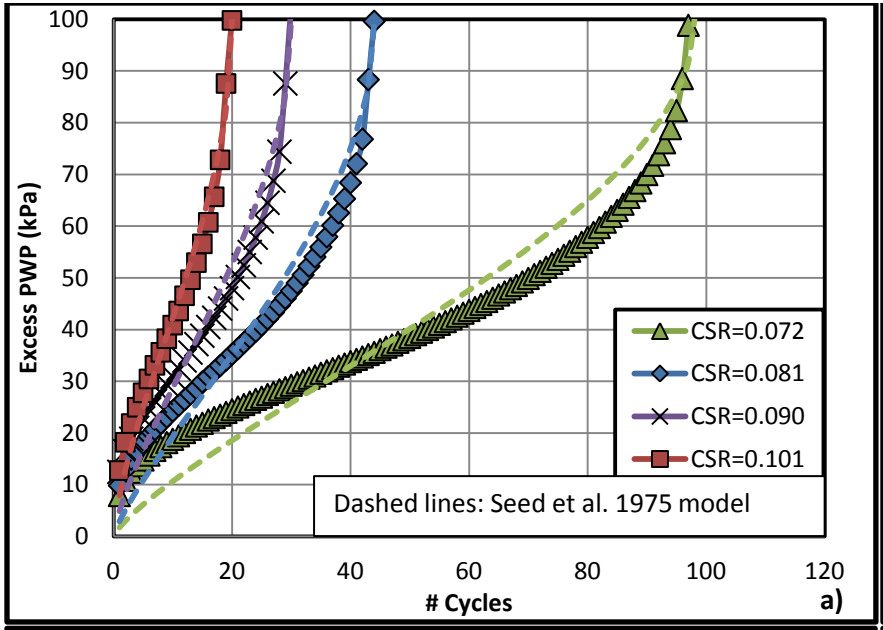
Excess PWP (kPa)
# Cycles
CSR=0.072
CSR=0.081
CSR=0.090
CSR=0.101
Dashed lines: Seed et al. 1975 model
a)

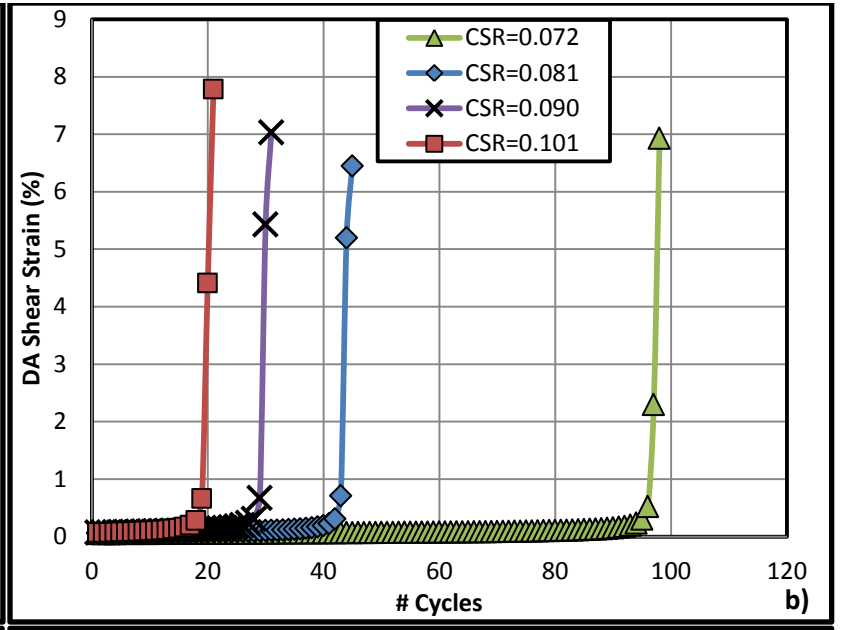
DA Shear Strain (%)
# Cycles
CSR=0.072
CSR=0.081
CSR=0.090
CSR=0.101
b)

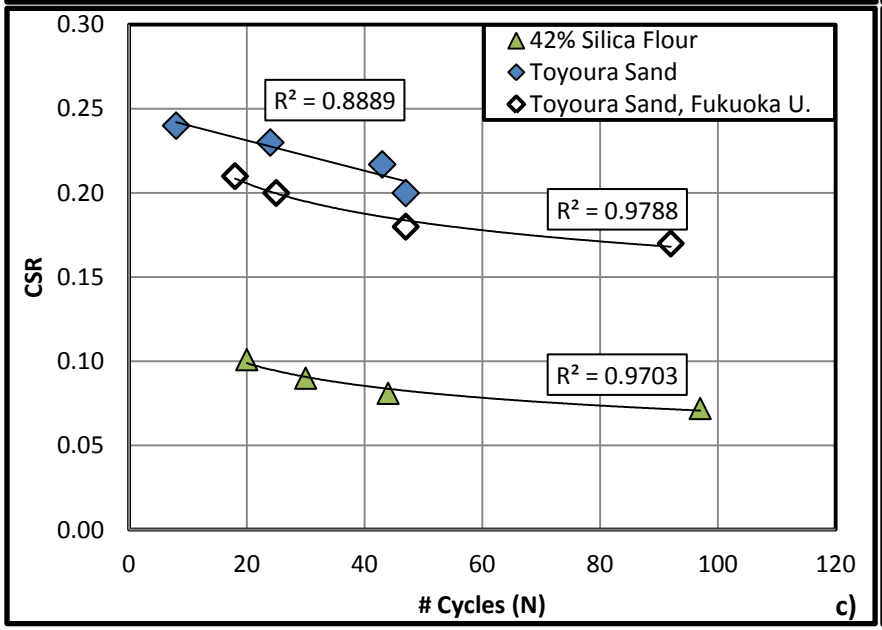
CSR
Cycles (N)
42% Silica Flour
Toyoura Sand
Toyoura Sand, Fukuoka U.
R² = 0.8889
R² = 0.9788
R² = 0.9703
c)

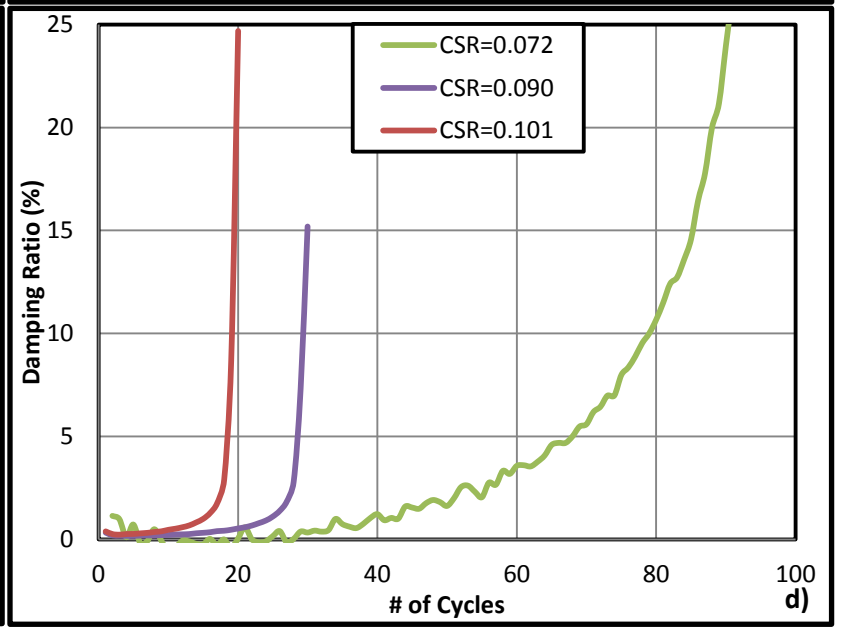
Damping Ratio (%)
# of Cycles
CSR=0.072
CSR=0.090
CSR=0.101
d)

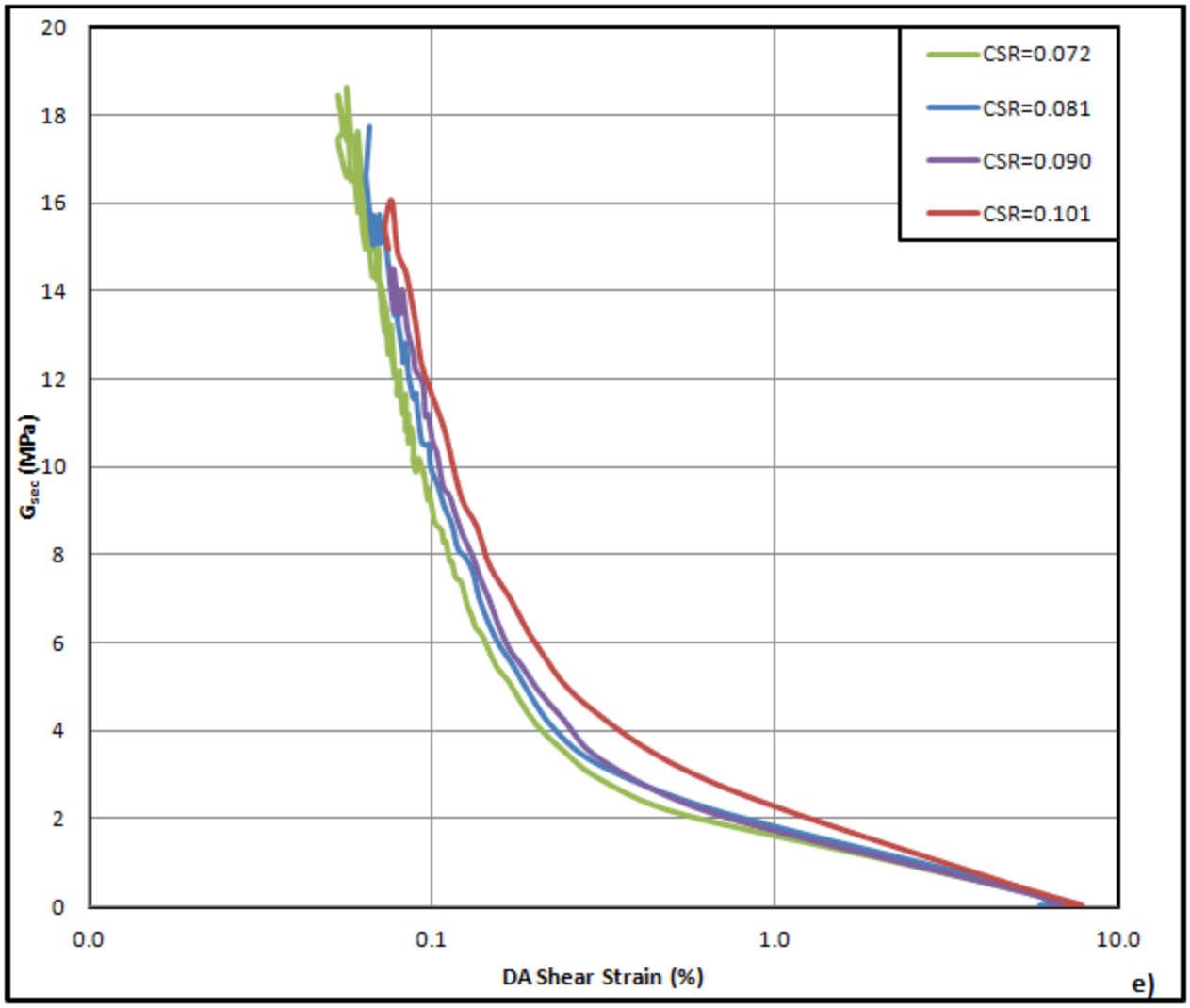

Figure 4.44. For Toyoura sand with 42% silica flour at Dr=60%, σ_c'=100kPa a) excess pore pressure vs. N; b) DA shear strain vs. N; c) liquefaction resistance curve; d) damping ratio vs. N; e) G_{sec} vs. DA shear strain

4.7.2.2. Pure Silt, Various CSR

Silica flour was evaluated for cyclic liquefaction resistance at cyclic stress ratios (CSR) of between 0.074-0.16 and a relative density of 60% (ρ_{dry}=1.28g/cm^3). The critical state line was determined to have an approximate slope of between 0.65-0.70 in compression and 0.5-0.65 in extension (Figure 4.45). These tests were performed at a B value of 0.95-1.0. With increasing CSR the pore pressure build-up increased further, always following an elongated 'S' shape with a large initial increase followed by a predominantly linear steep section and eventually tapering off at r_u=100 kPa (Figure 4.47a). Damping stayed consistent at around 5% regardless of increasing CSR values (Figure 4.47d).

The maximum post failure shear strain sat around 3%, and it is interesting to note that at lower CSR values the build-up to maximum plastic strain takes significantly more cycles than at higher CSRs (Figure 4.47b). At a CSR of 0.090 and 0.100 there is a clear and very large jump in double amplitude shear strain during the last three cycles. This is an indicator that necking had occurred in the sample due to particle settlement (Saxena, Reddy, & Avramidis, 1988).

The secant shear modulus of the silica flour (G_{sec}) was found to be an average of 9 MPa, which, as expected, sits lower than the G_{max} of 14 MPa found from bender element testing (Figure 4.47e).

The equivalent magnitude 7.5 earthquake for silica flour is approximately CSR=0.102, and a CSR of 0.087 causes failure in 34 cycles and would best simulate a magnitude 9.0 earthquake based on cyclic strength curve. Because the silica flour did not reach 5% shear strain during cycling, this value is an approximation.

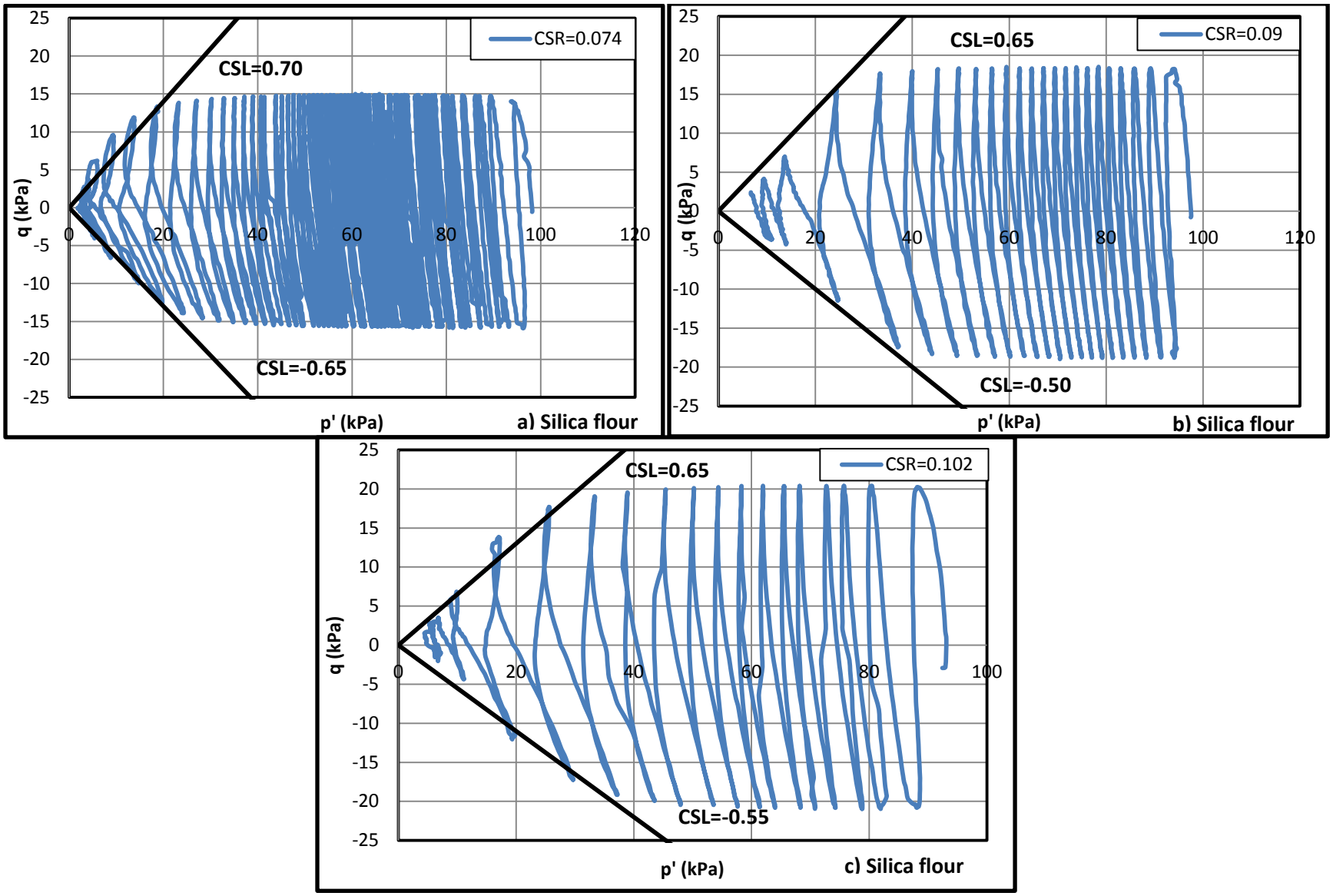

Figure 4.45. Deviator stress vs. Cambridge effective stress for 100% silica flour at Dr=60%, σ_c'=100kPa a) CSR=0.074; b) CSR=0.091; c) CSR=0.102;

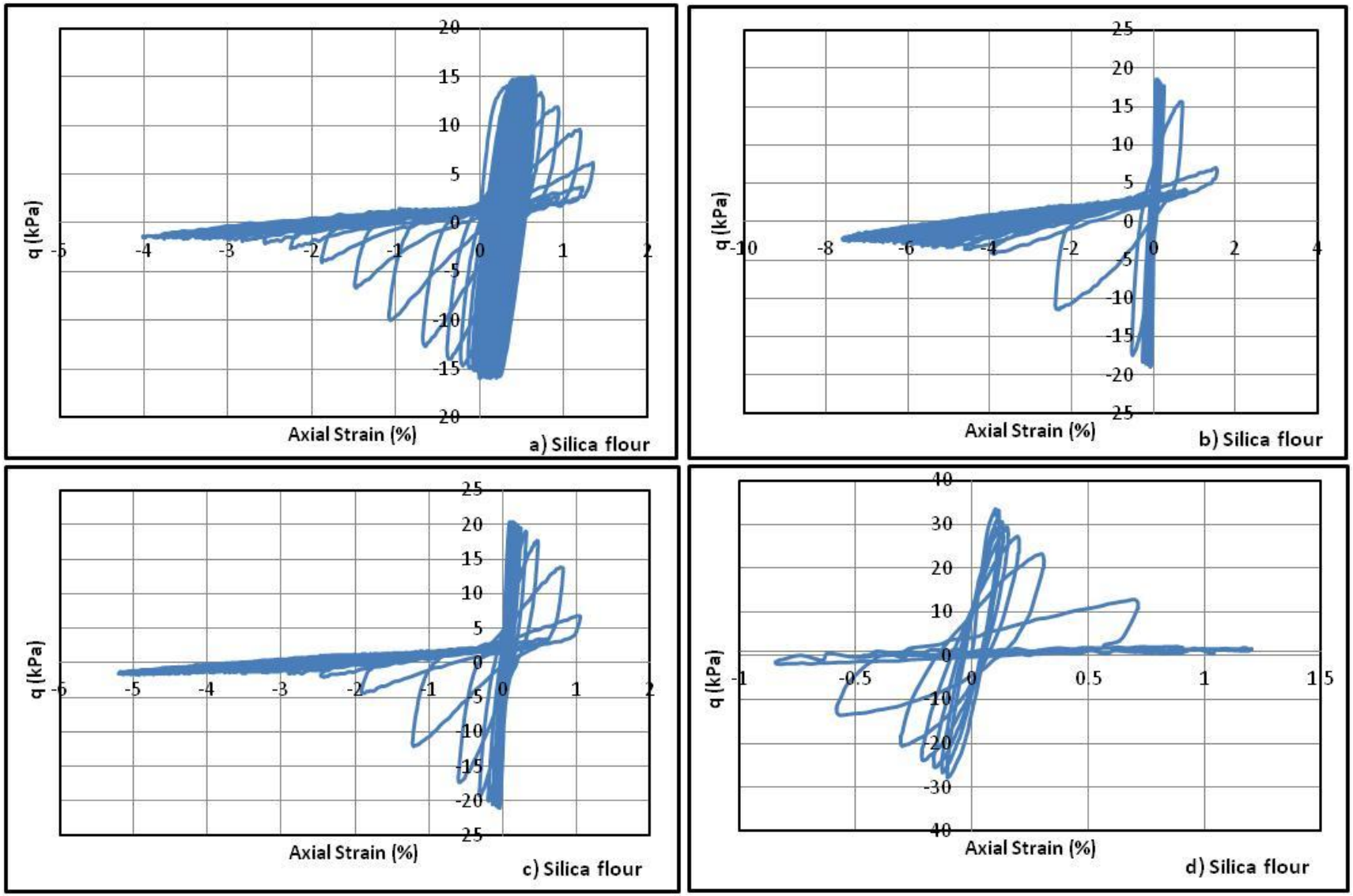

Figure 4.46. q vs. ε_a (%) for 100% silica flour at D_r=60%, σ_c'=100kPa a) CSR=0.074; b) CSR=0.091; c) CSR=0.102; d) CSR=0.167

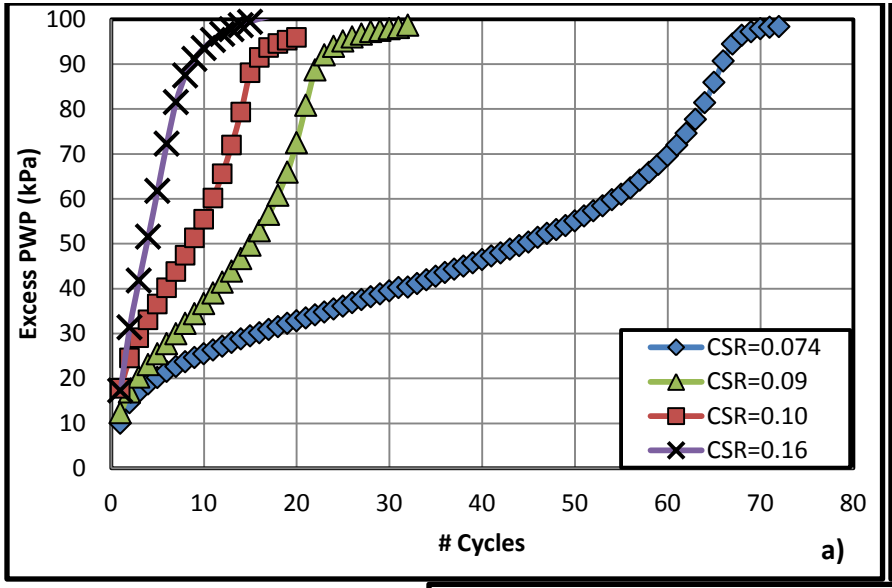
Excess PWP (kPa)
Cycles
a)
CSR=0.074
CSR=0.09
CSR=0.10
CSR=0.16

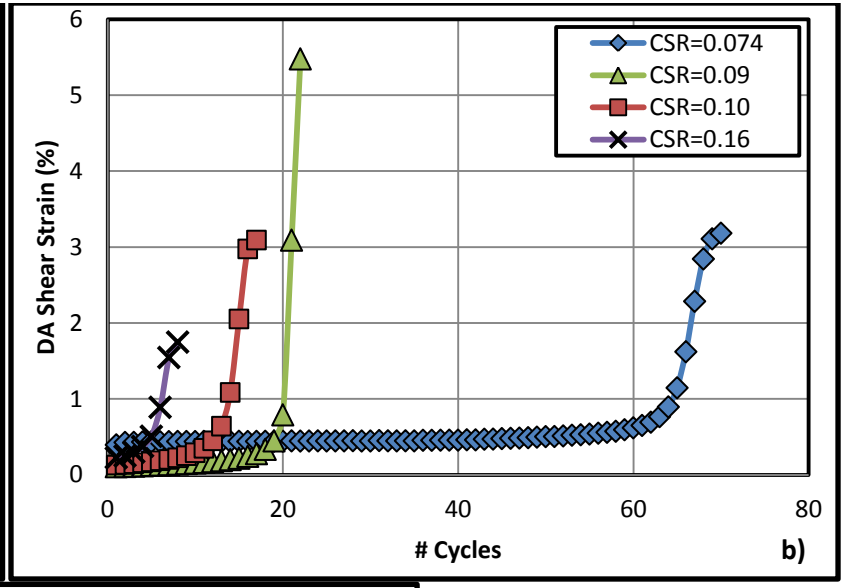
DA Shear Strain (%)
Cycles
b)
CSR=0.074
CSR=0.09
CSR=0.10
CSR=0.16

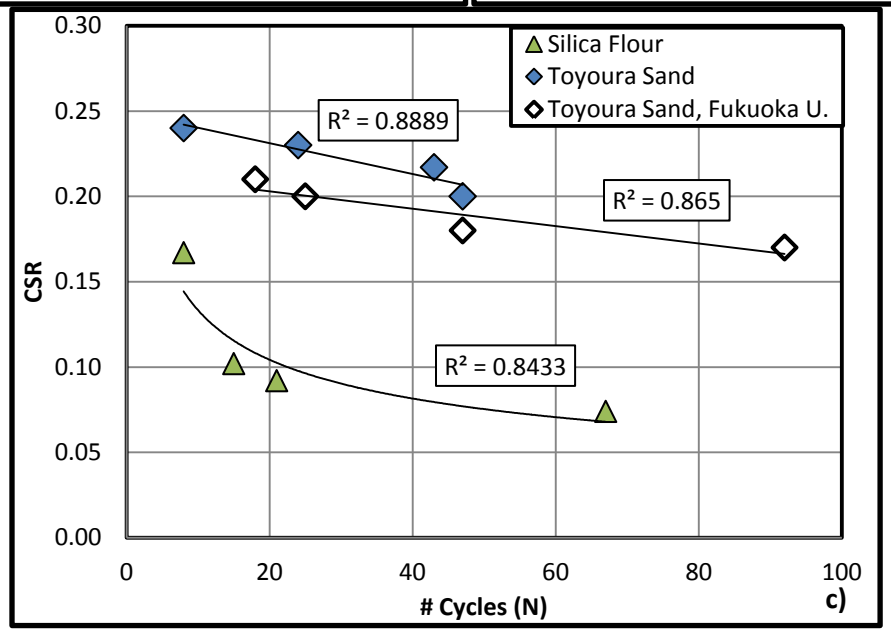
CSR
Cycles (N)
c)
Silica Flour
Toyoura Sand
Toyoura Sand, Fukuoka U.
R² = 0.8889
R² = 0.865
R² = 0.8433

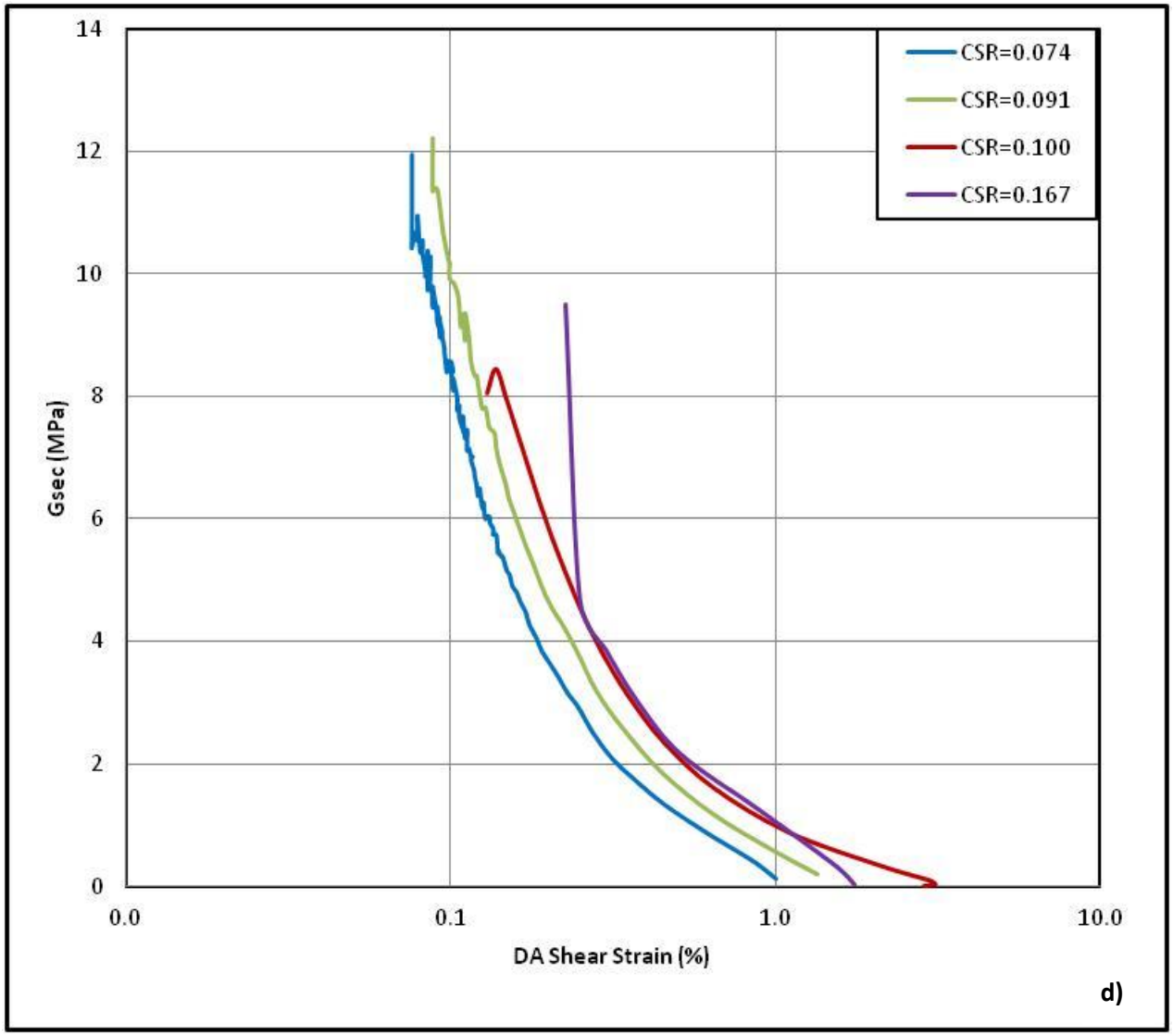

Figure 4.47. For 100% silica flour at Dr=60%, σ_c'=100kPa a) excess pore pressure vs. N; b) DA shear strain vs. N; c) liquefaction resistance curve; d) G_{sec} vs. DA shear strain

4.7.2.3. Varying Silt (%), Same CSR

Toyoura sand was evaluated for cyclic liquefaction resistance at silica flour contents ranging from 0-100% with the primary focus on 0-42% as per Tokyo Bay in-situ conditions (60% relative density: ρ_{dry}=1.28 g/cm^3 for 100% silica flour to 1.586 g/cm^3 for 35% silica flour). The first aspect to note is that liquefaction resistance decreased with increasing silt content (Cubrinovski & Rees, 2008; Yamamuro & Lade, 1998; Thevanayagam, 1998). This is because high silt content retards the speed of drainage, distorts the granular structure, and causes looser samples to collapse more readily (Sitharam, GovindaRaju, & Srinivasa Murthy, 2004).

At 0% and 10.5% silica flour the Toyoura sand failed in 46 and 25 cycles respectively at a CSR of 0.20. Above 10.5% silica flour, the Toyoura sand failed in 1 cycle at a CSR of 0.20, thus it was brought down to 0.10 to better show the liquefaction resistance (Figure 4.48). What is interesting to note is that the trend seen in Rowe cell testing in Section 4.4.2 was not seen in cyclic triaxial testing. There was no noticeable threshold at 28-42% silt content; instead the strength of the silty sand continuously decline. This conflicts slightly with the findings of (Law & Ling, 1992), which suggest that above 30% content, Little Jackfish silt offers higher liquefaction resistance than 30%, though their silt has a larger grain size and these tests were performed at a constant void ratio, meaning the higher concentrations of silt also had a much higher relative density.

The slope of the critical state line for the silty Toyoura sand was found to reduce steadily from CSL=1.40 for the Toyoura sand, to CSL=0.65 for 100% silica flour (Figure 4.48). With increasing CSR the pore pressure build-up got steeper, always following an elongated 'S' shape with a large initial increase followed by a mostly linear steep section until r_u=100 kPa as seen in Figure 4.50a. Damping varied slightly from 1-3% but did not follow a discernible trend in terms of the silt content. The maximum post

failure shear strain decreased from 22% for the Toyoura sand to just over 3% for the silica flour as shown in Figure 4.50b, indicative of the fact that higher load amplitudes cause larger plastic strains.

The secant shear modulus of the Toyoura sand and the silica flour mixes (G_{sec}) was found to decrease from 45 MPa for the Toyoura sand to just less than 10 MPa for the silica flour in Figure 4.50e which matches closely with the findings of (Kezdi, 1974).

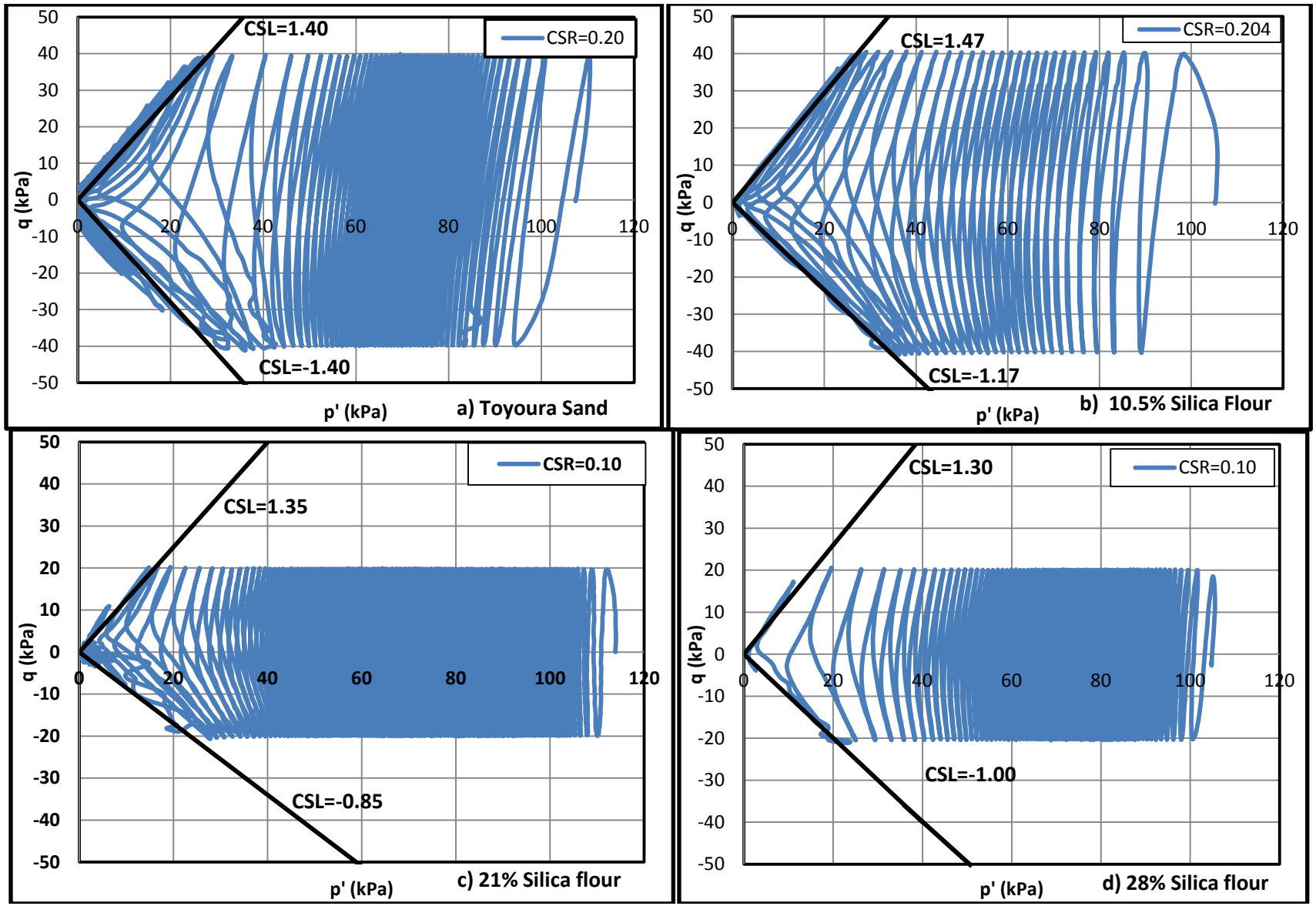
CSL=1.40
CSR=0.20
CSL=-1.40
q (kPa)
p' (kPa)
a) Toyoura Sand
CSL=1.47
CSR=0.204
CSL=-1.17
b) 10.5% Silica Flour
CSR=0.10
CSL=1.35
CSL=-0.85
c) 21% Silica flour
CSL=1.30
CSR=0.10
CSL=-1.00
d) 28% Silica flour

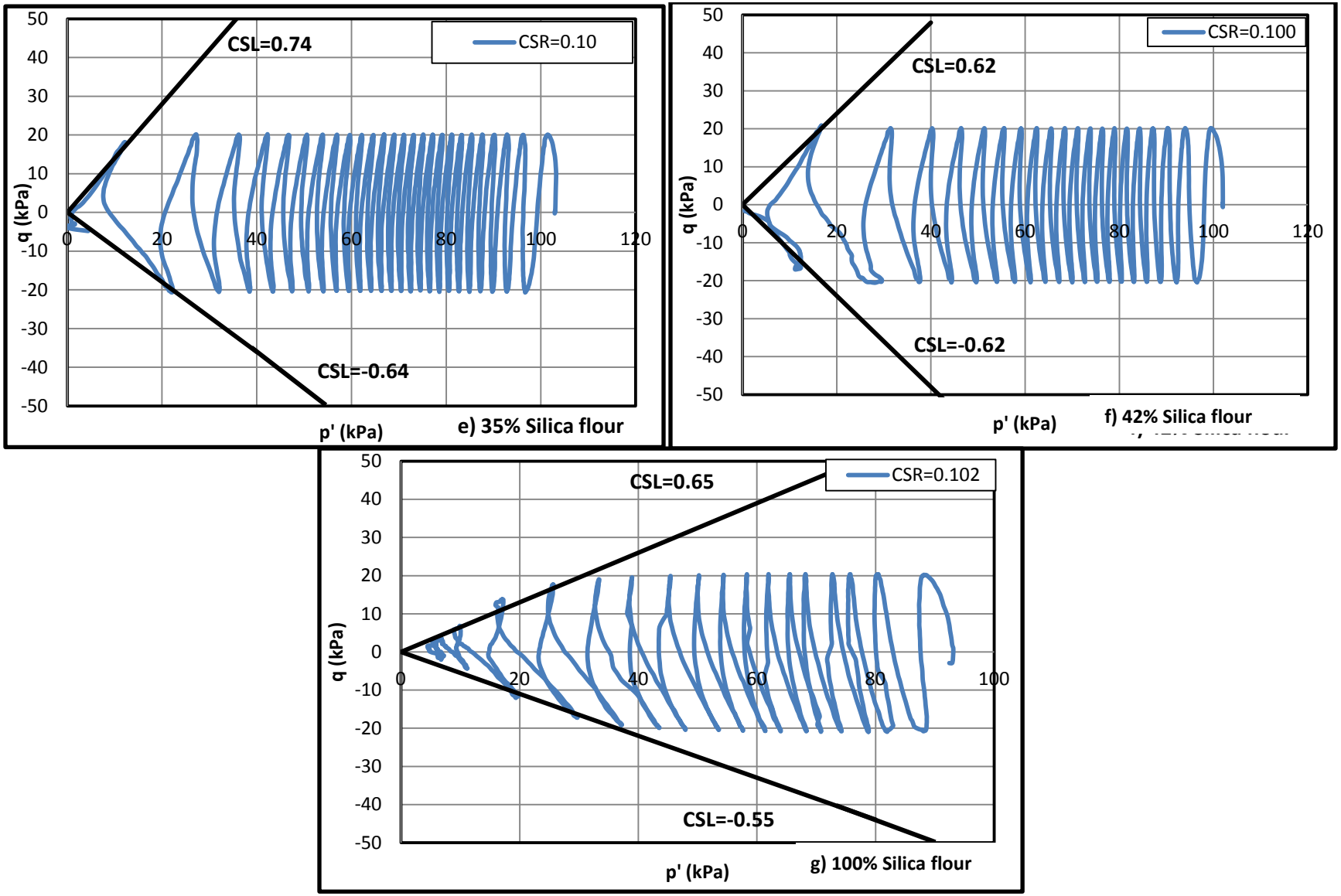

Figure 4.48. Deviator stress vs. Cambridge effective stress for Toyoura sand with 0-100% silica flour at D_r=60%, σ_c'=100kPa a) Toyoura sand, CSR=0.200; b) 10.5% silica flour, CSR=0.204; c) 21% silica flour, CSR=0.10; d) 28% silica flour, CSR=0.10; e) 35% silica flour, CSR=0.10; f) 42% silica flour, CSR=0.10; g) 100% silica flour, CSR=0.10

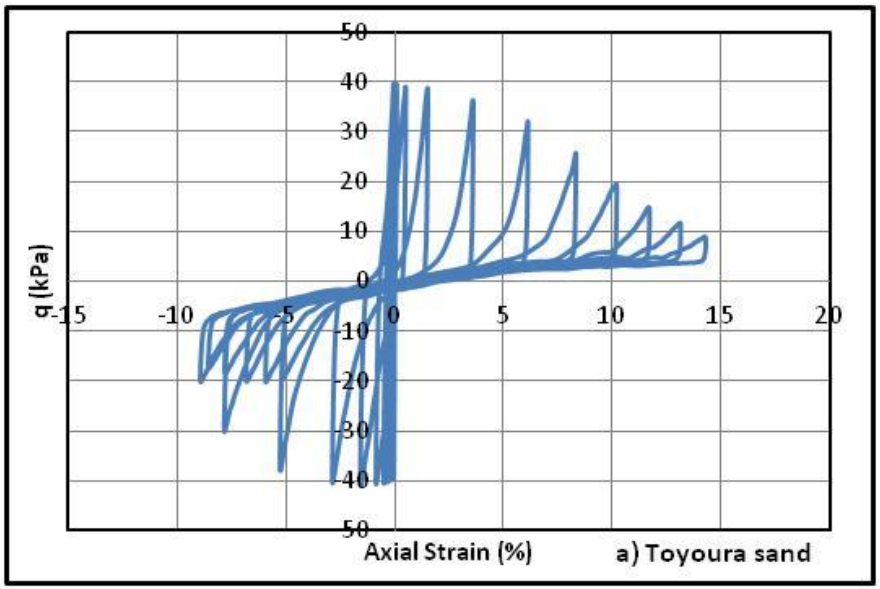
q (kPa)
Axial Strain (%)
a) Toyoura sand

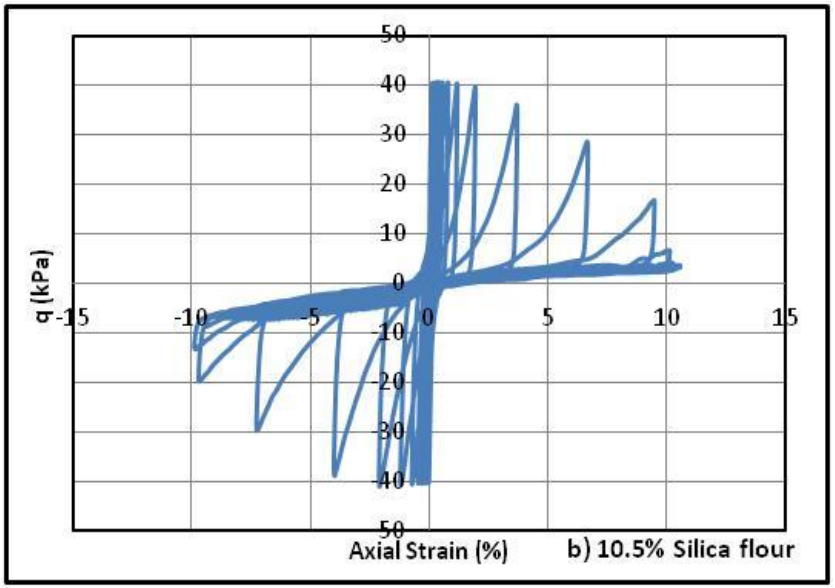
q (kPa)
Axial Strain (%)
b) 10.5% Silica flour

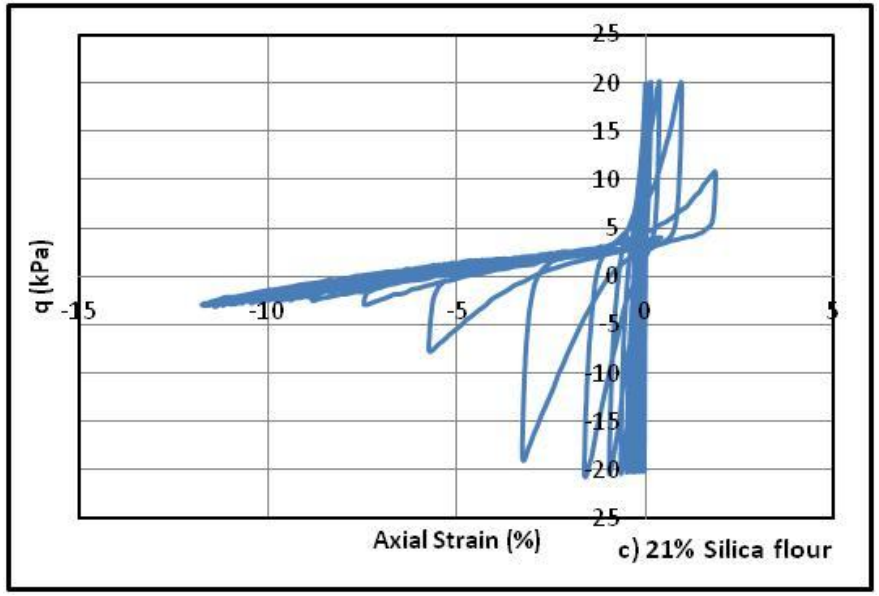
q (kPa)
Axial Strain (%)
c) 21% Silica flour

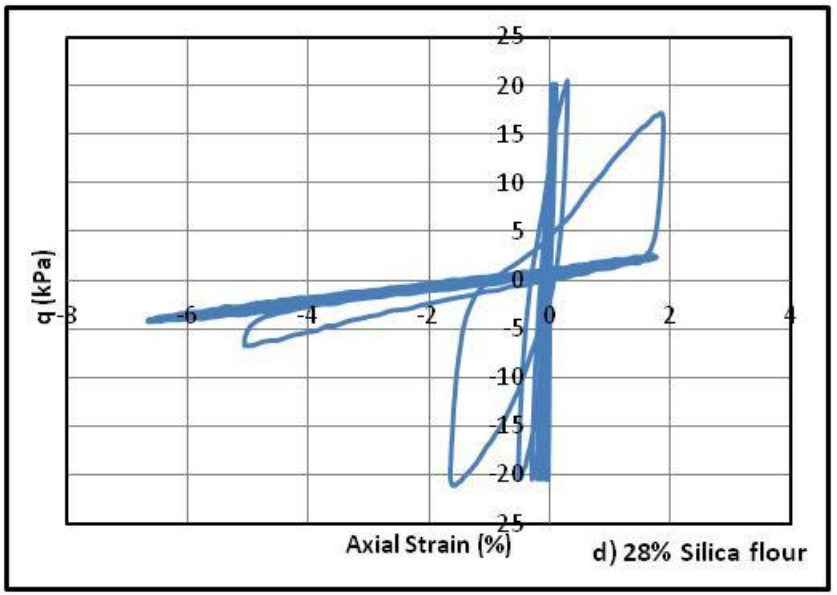
q (kPa)
Axial Strain (%)
d) 28% Silica flour

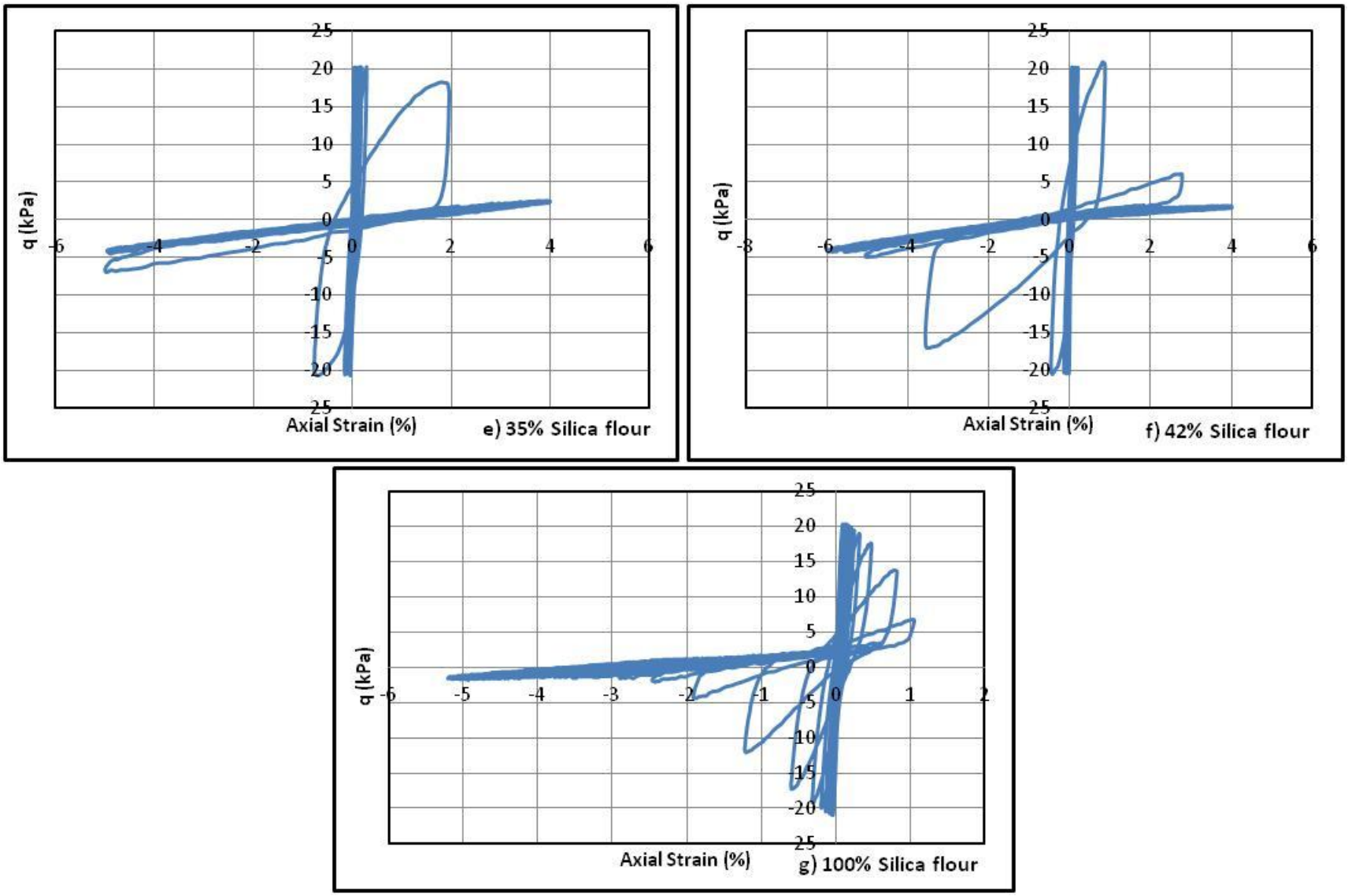

Figure 4.49. q vs. ε_a (%) for Toyoura sand with 0-100% silica flour at D_r=60%, σ_c'=100kPa a) Toyoura sand, CSR=0.200; b) 10.5% silica flour, CSR=0.204; c) 21% silica flour, CSR=0.10; d) 28% silica flour, CSR=0.10; e) 35% silica flour, CSR=0.10; f) 42% silica flour, CSR=0.10; g) 100% silica flour, CSR=0.10;

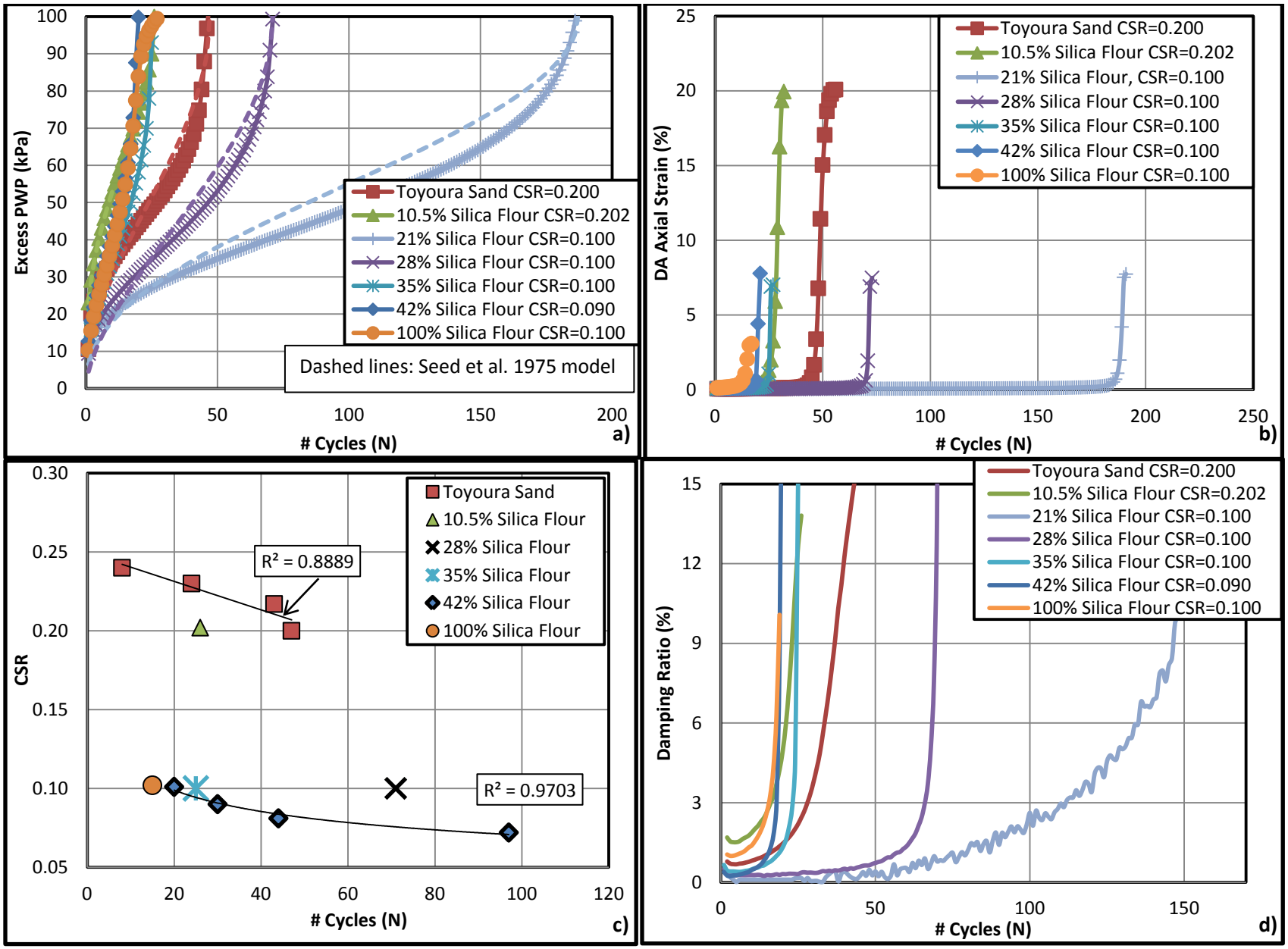
Excess PWP (kPa)
Cycles (N)
a)
Toyoura Sand CSR=0.200
10.5% Silica Flour CSR=0.202
21% Silica Flour CSR=0.100
28% Silica Flour CSR=0.100
35% Silica Flour CSR=0.100
42% Silica Flour CSR=0.090
100% Silica Flour CSR=0.100
Dashed lines: Seed et al. 1975 model
DA Axial Strain (%)
Cycles (N)
b)
Toyoura Sand CSR=0.200
10.5% Silica Flour CSR=0.202
21% Silica Flour, CSR=0.100
28% Silica Flour CSR=0.100
35% Silica Flour CSR=0.100
42% Silica Flour CSR=0.100
100% Silica Flour CSR=0.100
CSR
Cycles (N)
c)
Toyoura Sand
10.5% Silica Flour
28% Silica Flour
35% Silica Flour
42% Silica Flour
100% Silica Flour
R² = 0.8889
R² = 0.9703
Damping Ratio (%)
Cycles (N)
d)
Toyoura Sand CSR=0.200
10.5% Silica Flour CSR=0.202
21% Silica Flour CSR=0.100
28% Silica Flour CSR=0.100
35% Silica Flour CSR=0.100
42% Silica Flour CSR=0.090
100% Silica Flour CSR=0.100

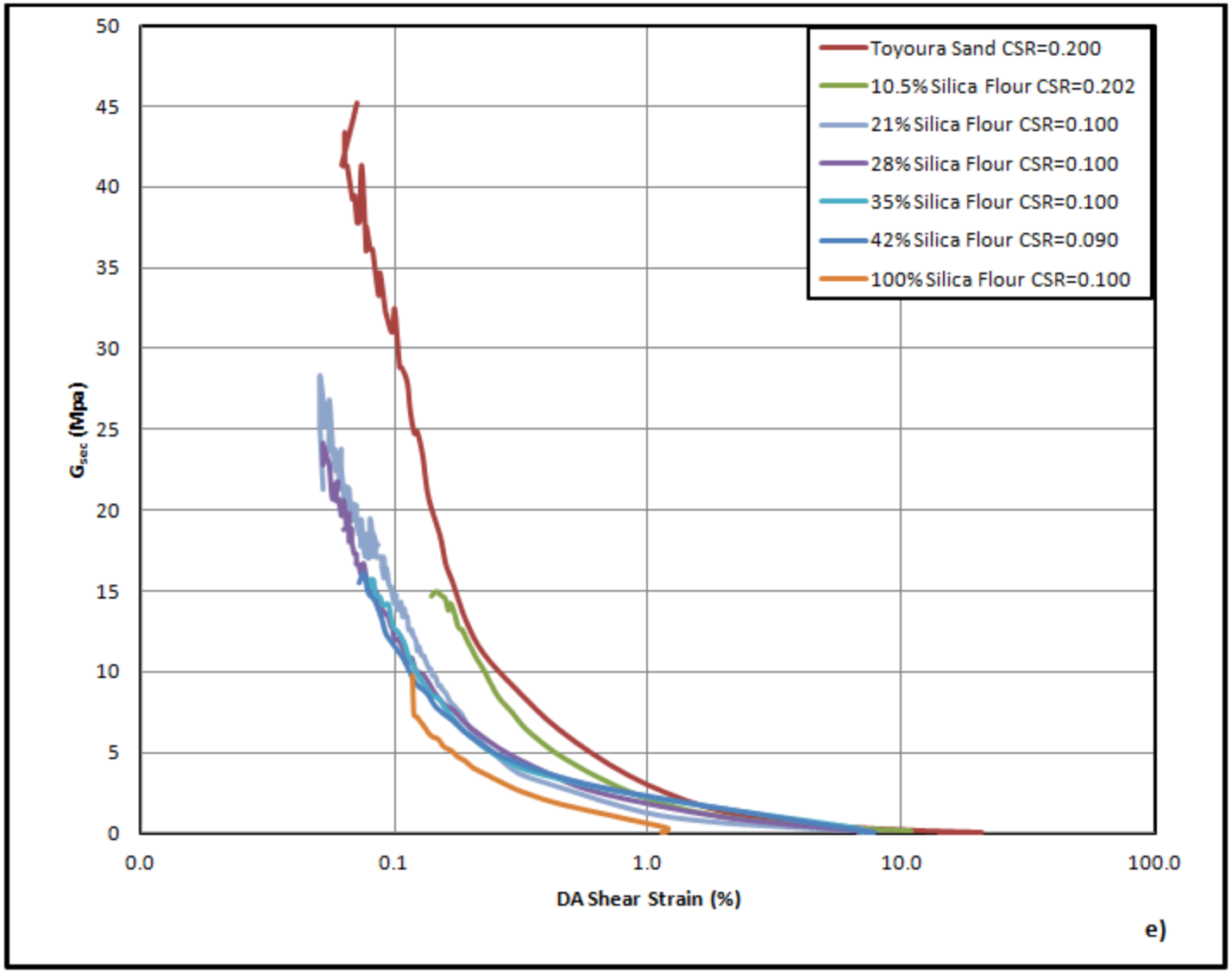

Figure 4.50. For Toyoura sand with 0-100% silica flour at D_r=60%, σ_c'=100kPa a) excess pore pressure vs. N; b) DA shear strain vs. N; c) liquefaction resistance curve; d) damping ratio vs. N; e) G_{sec} vs. DA shear strain

4.7.3. Silt & Fibre Content

The following section contains cyclic triaxial results from the tests outlined in Table 4.5. These tests were performed to determine the effect of PVA fibre addition on the silty Toyoura sand examined in Section 4.7.2.

Table 4.5. Cyclic Triaxial Tests for Various Silt and Fibre Concentrations

Sample	CSR
Varying Fibre	0.20
0-28% Silt, 1% Fibre	0.20
35-100% Silt, 1% Fibre	0.10
42% Silt, 1% Fibre	0.08, 0.09, 0.94, 0.11

4.7.3.1. Toyoura Sand & Fibre (%), Same CSR

To test the effectiveness of PVA fibres as a stabilizer against cyclic liquefaction, these were added to the Toyoura sand at percentages ranging from 0-2% by mass at 60% relative density. The Rowe cell results in 4.4.2 suggested that 0.5% fibre addition provided the best strength increase of any fibre content based on the constrained modulus values, whereas bender element testing suggested virtually no change in shear modulus when 1% fibre was added, although a fairly large improvement in the undrained shear strength occurred. Cyclic triaxial testing on the other hand suggested that 2% fibre addition was the most effective concentration against cyclic mobility as shown in Figure 4.53c. The fact that 0.5-1% fibre actually seemed to weaken the soil against liquefaction contradicts the findings of Nakamichi & Sato (2013), but can possibly be explained by the definition of the fibre concentration during sample preparation (i.e. for a 100 g sample of Toyoura sand with 2% fibre: either 100 g sand plus 2 g of fibre, or 98 g of sand plus 2 g of fibre), which alters the initial sample density and fabric.

These tests were performed at B=0.98-1.0. The CSL for the Toyoura sand samples with PVA fibres varied from 1.14-1.50 in extension and 1.40-1.90 in compression (Figure 4.51). In terms of excess

pore water pressure build-up, it was seen that the addition of 2% fibre followed the pore pressure generation of the Toyoura sand closely, as seen in Figure 4.53a. For all cyclic triaxial tests, the excess pore water pressure generation had two clear inflection points in a transformed sinusoidal curve; the first after about 2 cycles of loading where the slope of the curve began to flatten slightly, and the second at the onset of large plastic strain generation where the curve steepened again (Figure 4.53b). The excess pore water pressure model in Equation 4.11 accurately depicted this trend for the Toyoura sand stabilized with PVA fibres.

The double amplitude shear strain of the Toyoura sand with fibres reached between 16-21%. What is interesting to note is the rate at which the shear strain developed. For the Toyoura sand there were noticeable large increases after the onset of liquefaction. When stabilized with 1% and 2% fibre, this generation of plastic shear strain was significantly slower. The damping ratio again suggests that 2% fibre addition was the most effective concentration, which was confirmed by the improved secant shear modulus in Figure 4.53d-e.

It has been shown that the addition of randomly oriented fibres can increase the ductility and energy absorption, but may also cause shear strength anisotropy, if the failure plane is aligned with the preferential fibre orientation (Li, 2005). This could potentially explain why the lower fibre concentrations used in the cyclic triaxial testing appeared to weaken the Toyoura sand.

In relation to the Great East Japan Earthquake, it is proposed that the addition of 0.5-2% PVA fibre addition on its own is not an effective liquefaction countermeasure for the Tokyo Bay region if it is added as a replacement for the Toyoura sand as mentioned above. Further testing should be completed to better understand why this trend is counter to the improvement caused by fibre addition seen in the Rowe cell testing and monotonic shearing.

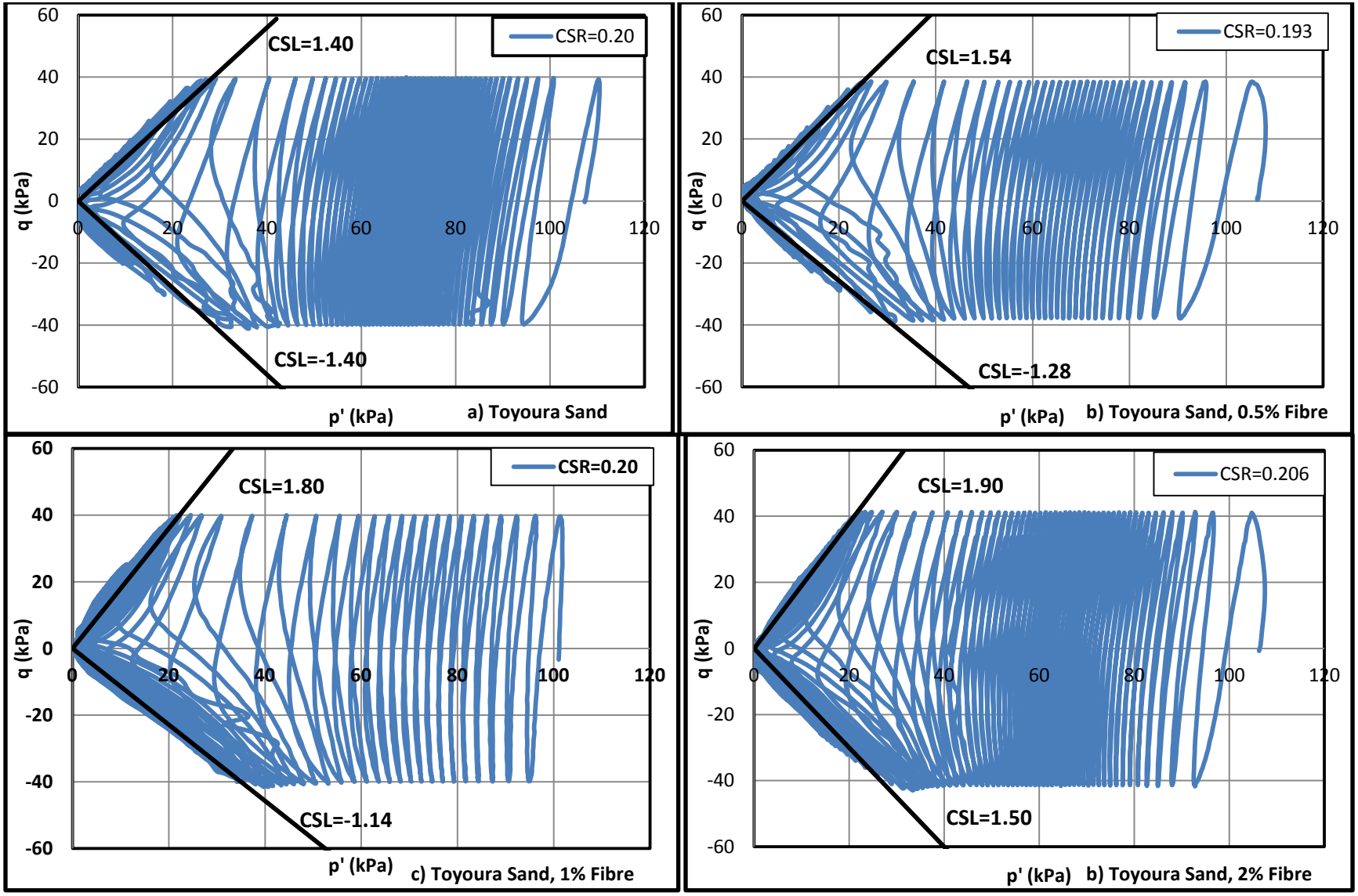

Figure 4.51. Deviator stress vs. Cambridge effective stress for Toyoura sand with 0-2% PVA fibre at D_r=60%, σ_c'=100kPa a) Toyoura sand, CSR=0.200; b) 0.5% fibre, CSR=0.193; c) 1% fibre, CSR=0.200; d) 2% fibre, CSR=0.206

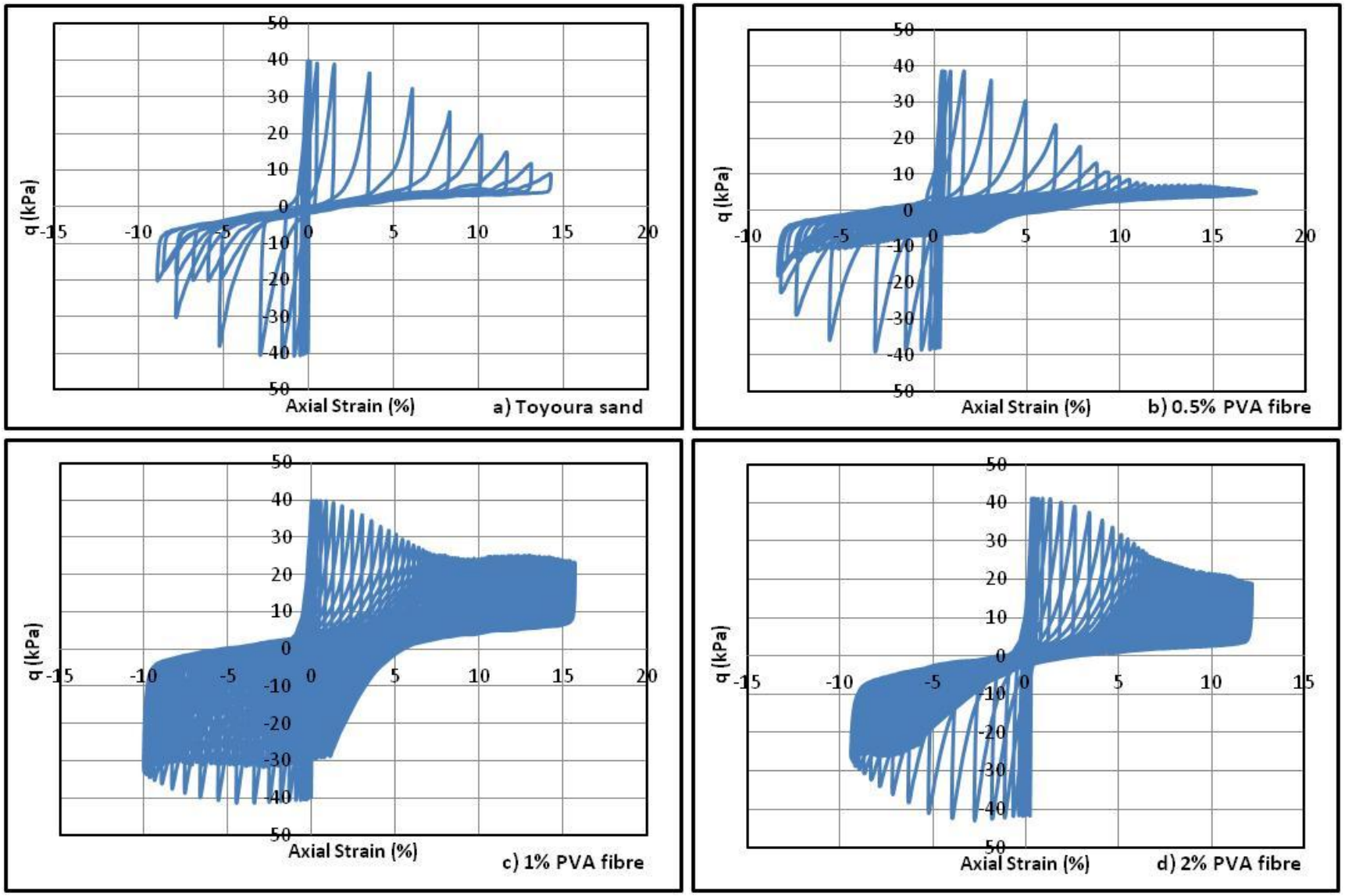

Figure 4.52. q vs. ε_a (%) for Toyoura sand with 0-2% PVA fibre at D_r=60%, σ_c'=100kPa a) Toyoura sand, CSR=0.200; b) 0.5% fibre, CSR=0.193; c) 1% fibre, CSR=0.175; d) 2% fibre, CSR=0.206

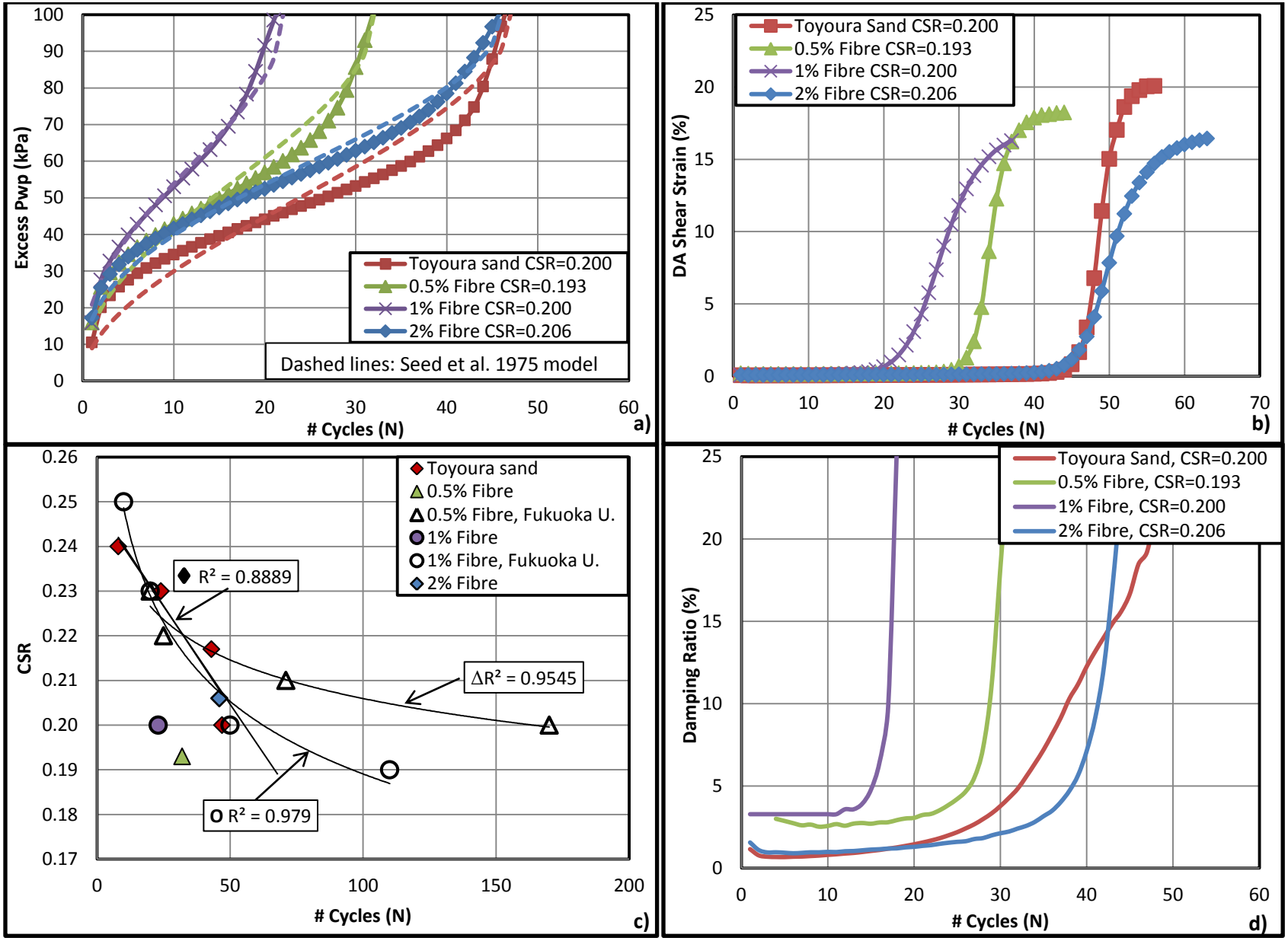
Excess Pwp (kPa)
Cycles (N)
Toyoura sand CSR=0.200
0.5% Fibre CSR=0.193
1% Fibre CSR=0.200
2% Fibre CSR=0.206
Dashed lines: Seed et al. 1975 model
a)
DA Shear Strain (%)
Toyoura Sand CSR=0.200
0.5% Fibre CSR=0.193
1% Fibre CSR=0.200
2% Fibre CSR=0.206
b)
CSR
Toyoura sand
0.5% Fibre
0.5% Fibre, Fukuoka U.
1% Fibre
1% Fibre, Fukuoka U.
2% Fibre
R² = 0.8889
ΔR² = 0.9545
O R² = 0.979
c)
Damping Ratio (%)
Toyoura Sand, CSR=0.200
0.5% Fibre, CSR=0.193
1% Fibre, CSR=0.200
2% Fibre, CSR=0.206
d)

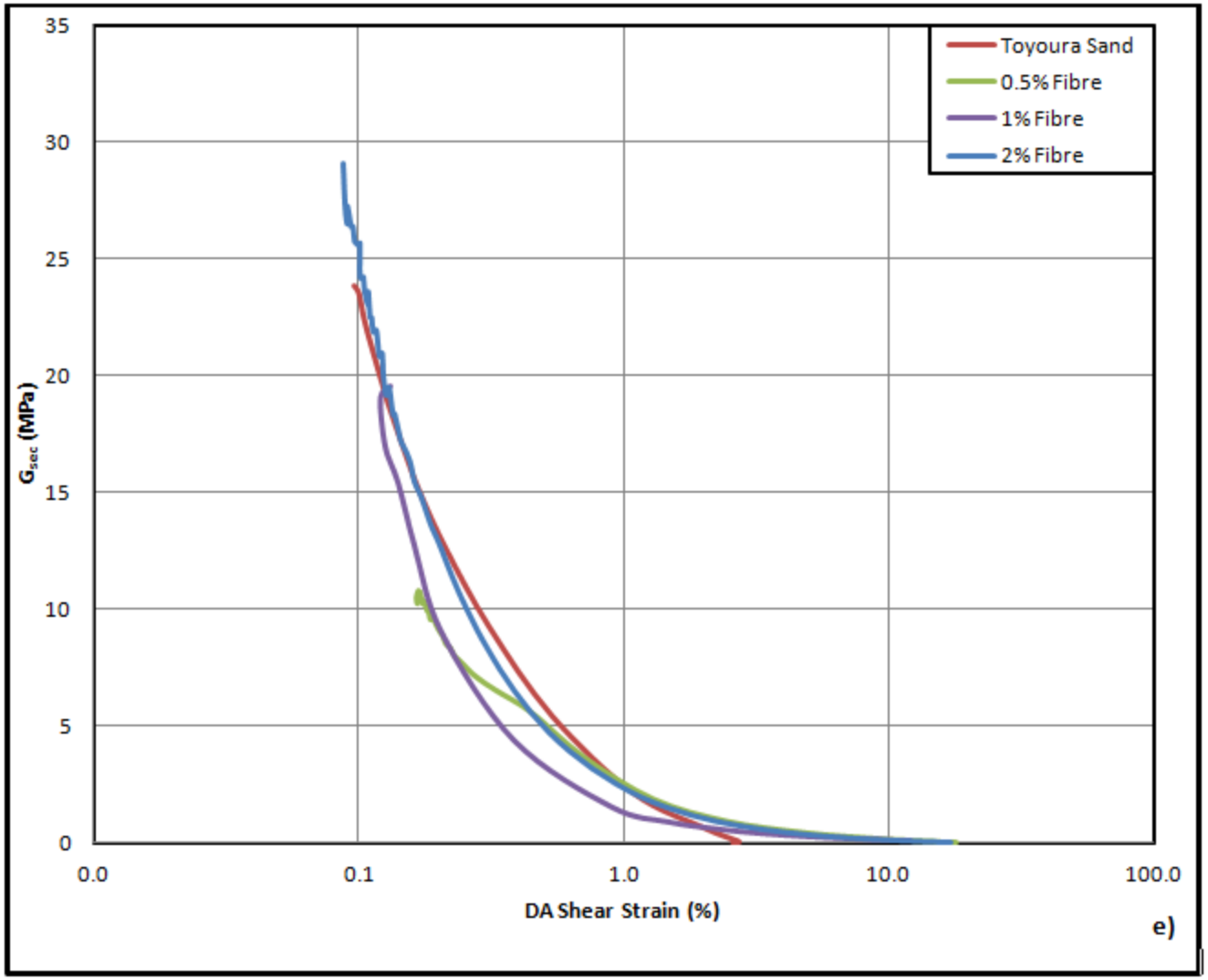

Figure 4.53. For 0-2% PVA fibre at D_r=60%, σ_c'=100kPa a) excess pore pressure vs. N; b) DA shear strain vs. N; c) liquefaction resistance curve; d) damping ratio vs. N; e) G_{sec} vs. DA shear strain

4.7.3.2. Varying Silt (%), 1% Fibre, Same CSR

Toyoura sand was also evaluated for cyclic liquefaction resistance with silica flour contents ranging from 0-100% and 1% PVA fibre addition, again with the primary focus on 0-42% as per Tokyo Bay in-situ conditions. Once again, the liquefaction resistance of the silty sand mixtures was seen to constantly reduce.

The slope of the critical state line for the silty Toyoura sand with 1% PVA fibre was found to have increased by 0.4 over the unstabilized silty sand (Figure 4.54). The increase in CSL indicates that the addition of PVA fibre inhibits the onset of cyclic mobility slightly for the silica flour, and to a greater extent for the silty Toyoura sand. Following the same trend as unstabilized silty sand, the CSL reduced steadily from CSL=1.80 for the Toyoura sand, to CSL=0.54 for 100% silica flour.

These samples were tested at B values of 0.96-0.98. Again, the excess pore water pressure curve always followed an elongated 'S' shape with a large initial increase followed by a mostly linear steep section until r_u=100 kPa. For 100% silt however, the excess pore water pressure curve hit 90 kPa and then saw a more gradual increase to 100 kPa (Figure 4.56a). Damping varied from 1-4% but again did not follow a discernible trend in terms of the silt content (Figure 4.56d). This is likely due to the changing CSR used in each test.

Interestingly, the maximum post failure shear strain was dramatically lower for the silty sand stabilized with fibres (Figure 4.56b). As mentioned earlier, the peak strain was nearly 22% for Toyoura sand, and about 5% for the silica flour. When fibres were added, these strains reduced to just 12% and 2% respectively. Since applied shear stresses in the silty Toyoura sand mobilize the tensile resistance of the fibres, the fibres begin to deform and direct their tensile resistance into a component normal to the

shear plane, thereby increasing the confining pressure along the failure surface and reducing shear strain (Gray & Refeai, 1986).

The secant shear modulus (G_{sec}) of the Toyoura sand and the silica flour mixes with 1% PVA fibre in Figure 4.56e was found to decrease from 45 MPa for the Toyoura sand to just less than 10 MPa for the silica flour which matches closely with the findings of (Kezdi, 1974). The calculated G_{sec} is directly proportional to the applied load amplitude. For future testing it is recommended that liquefaction resistance curves be plotted for each soil type and have at least two CSR values in common for comparative purposes.

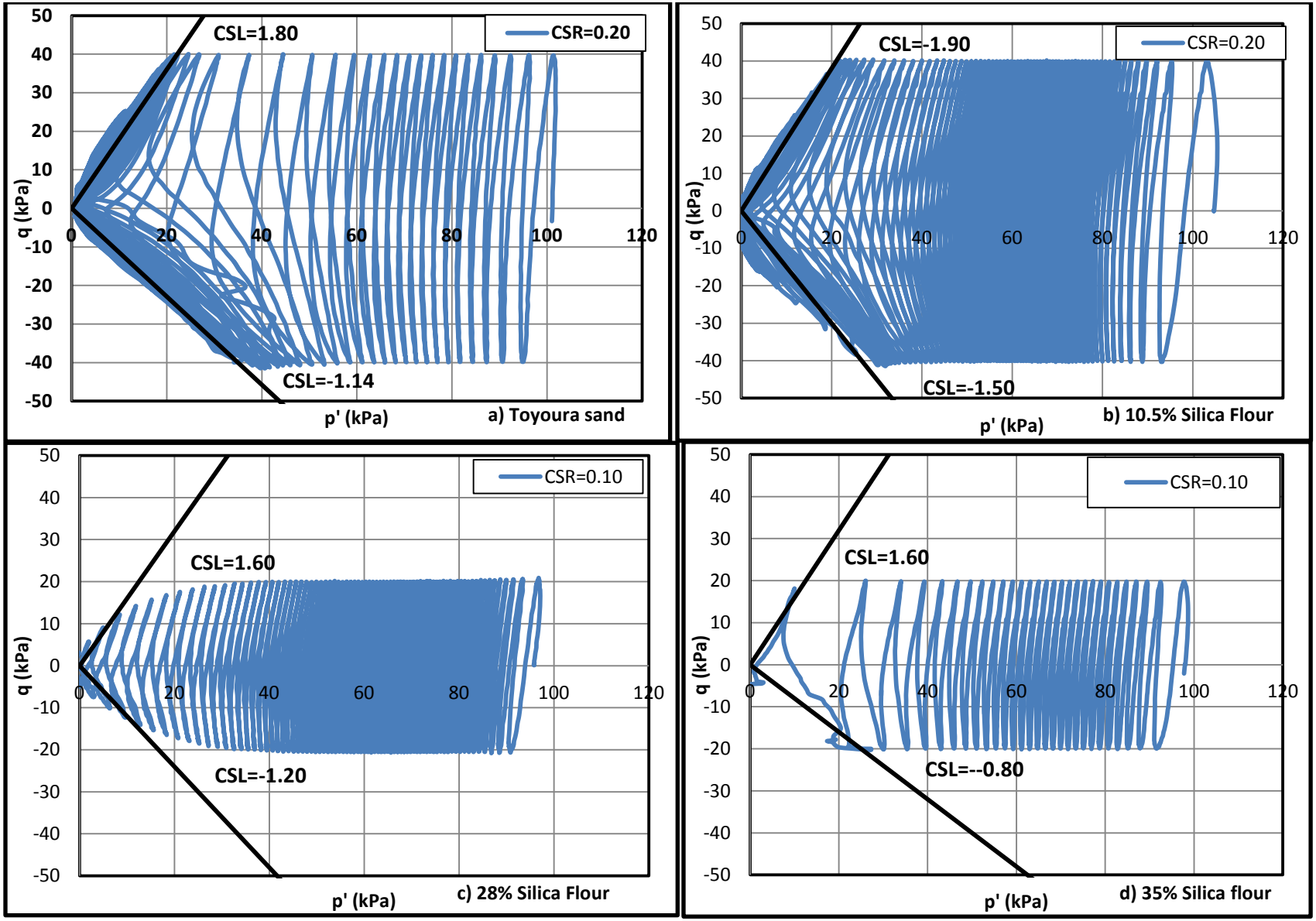
CSL=1.80
CSR=0.20
CSL=-1.14
q (kPa)
p' (kPa)
a) Toyoura sand
CSL=-1.90
CSR=0.20
CSL=-1.50
q (kPa)
p' (kPa)
b) 10.5% Silica Flour
CSL=1.60
CSR=0.10
CSL=-1.20
q (kPa)
p' (kPa)
c) 28% Silica Flour
CSL=1.60
CSR=0.10
CSL=--0.80
q (kPa)
p' (kPa)
d) 35% Silica flour

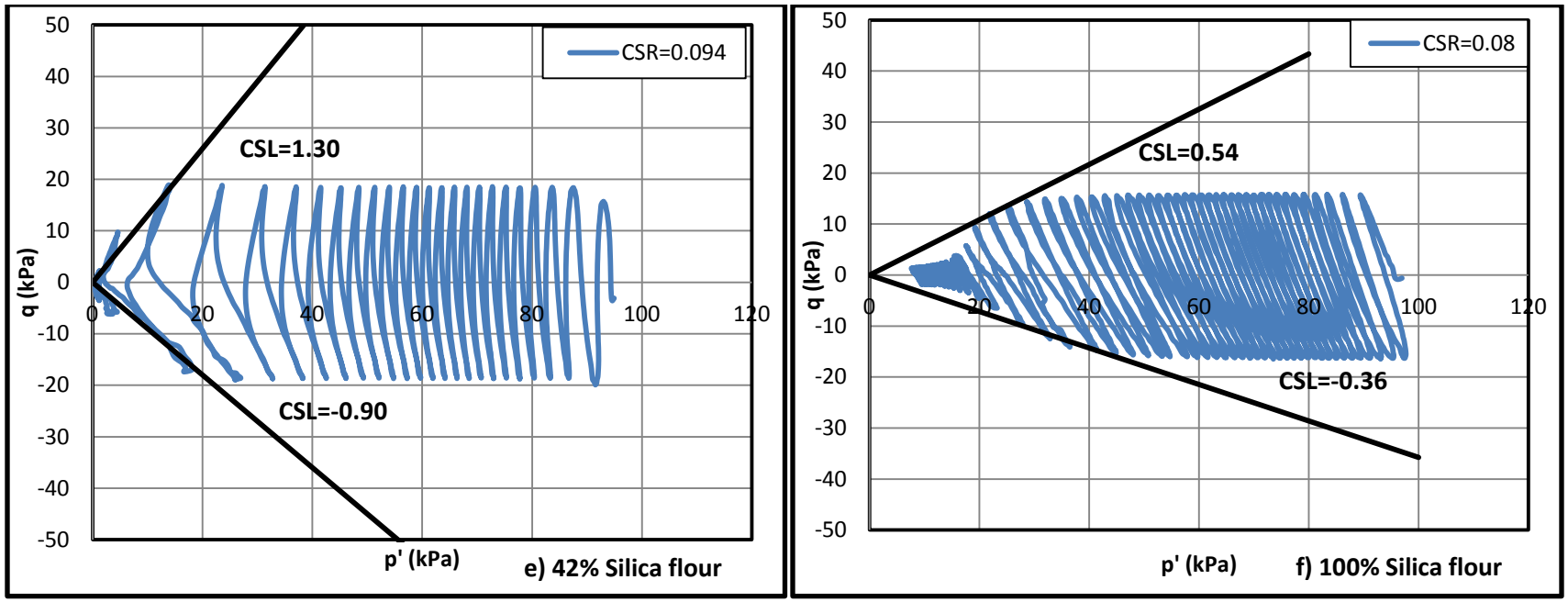

Figure 4.54. Deviator stress vs. Cambridge effective stress for Toyoura sand with 0-100% silica flour, 1% PVA fibre at Dr=60%, σc'=100kPa a) Toyoura sand, CSR=0.18; b) 10.5% silica flour, CSR=0.20; c) 28% silica flour, CSR=0.10; d) 35% silica flour, CSR=0.10; e) 42% silica flour, CSR=0.094; f) 100% silica flour, CSR=0.08

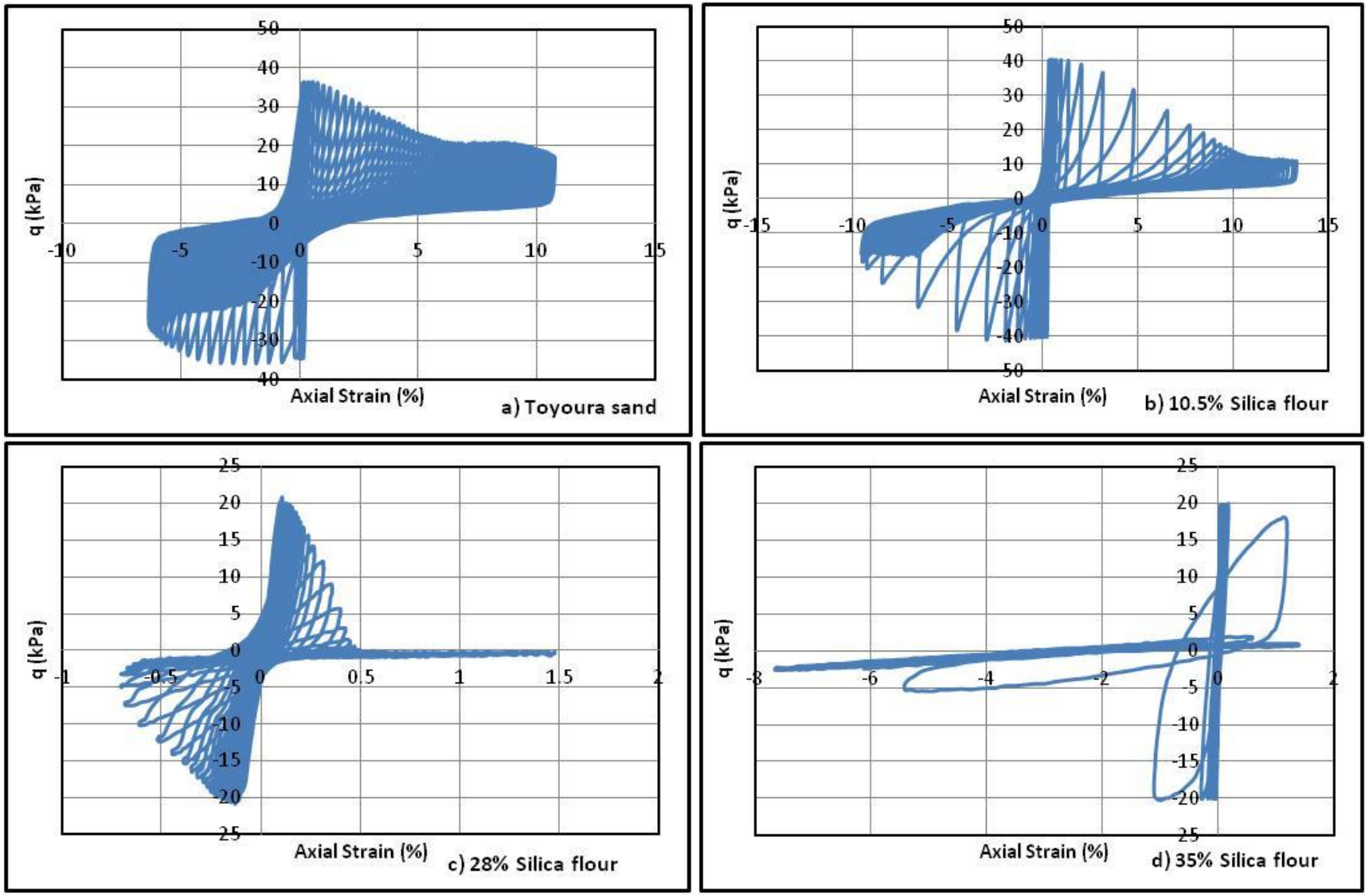
q (kPa)
Axial Strain (%)
a) Toyoura sand
b) 10.5% Silica flour
c) 28% Silica flour
d) 35% Silica flour

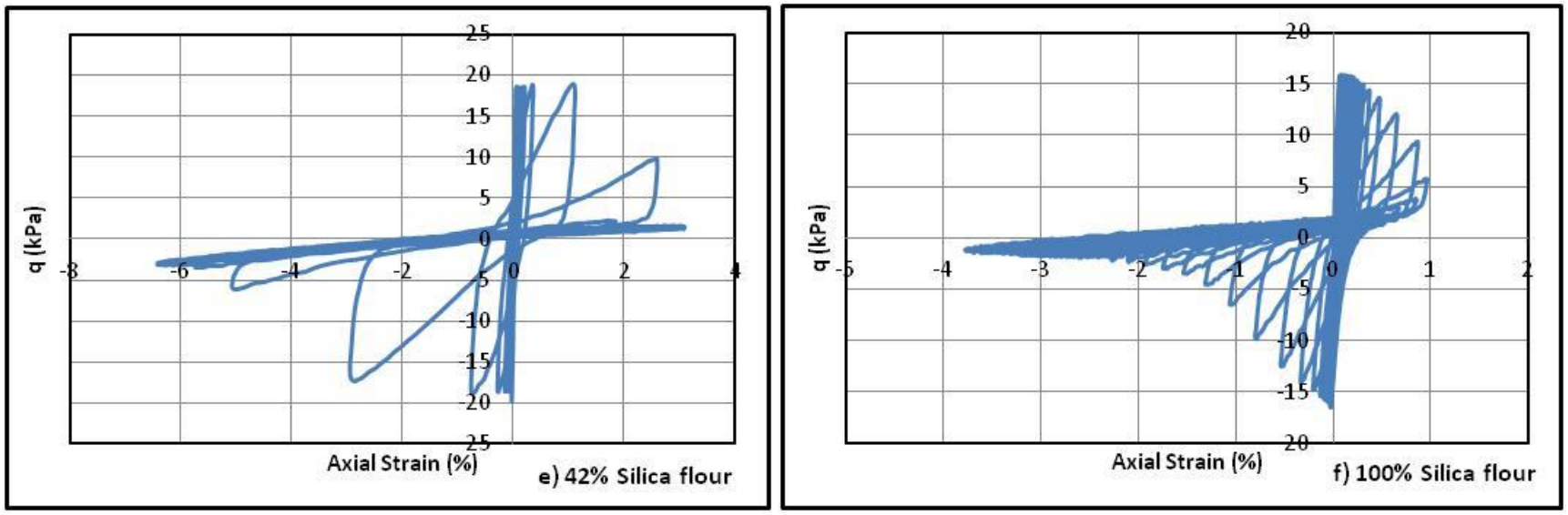

Figure 4.55. q vs. ε_a (%) for Toyoura sand with 0-100% silica flour, 1% fibre at D_r=60%, σ_c'=100kPa a) Toyoura sand, CSR=0.18; b) 10.5% silica flour, CSR=0.20; c) 28% silica flour, CSR=0.10; d) 35% silica flour, CSR=0.10; e) 42% silica flour, CSR=0.094; f) 100% silica flour, CSR=0.08

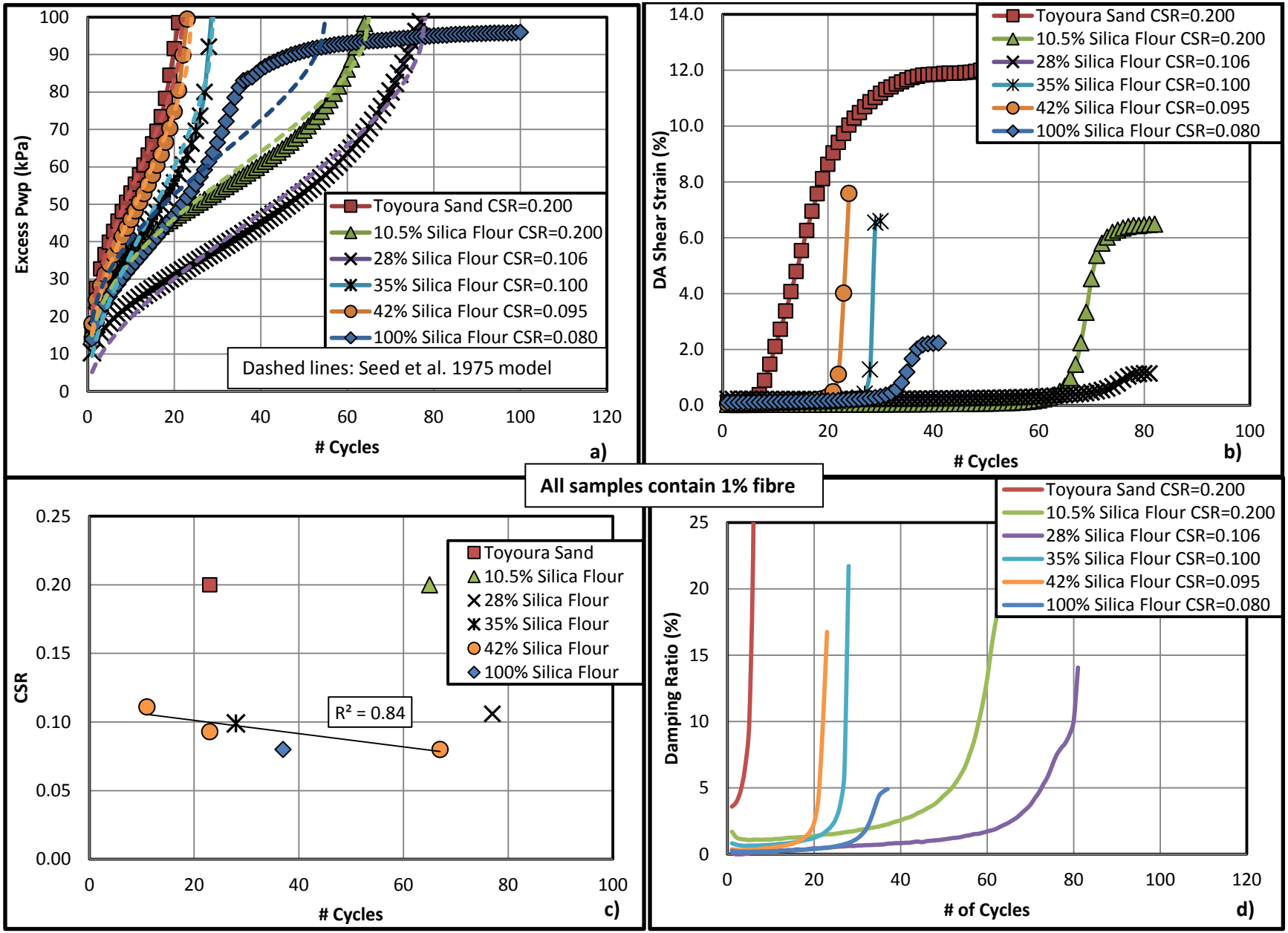
Excess Pwp (kPa)
Cycles
a)
Toyoura Sand CSR=0.200
10.5% Silica Flour CSR=0.200
28% Silica Flour CSR=0.106
35% Silica Flour CSR=0.100
42% Silica Flour CSR=0.095
100% Silica Flour CSR=0.080
Dashed lines: Seed et al. 1975 model
DA Shear Strain (%)
Cycles
b)
All samples contain 1% fibre
CSR
R² = 0.84
Toyoura Sand
10.5% Silica Flour
28% Silica Flour
35% Silica Flour
42% Silica Flour
100% Silica Flour
Cycles
c)
Damping Ratio (%)
# of Cycles
d)

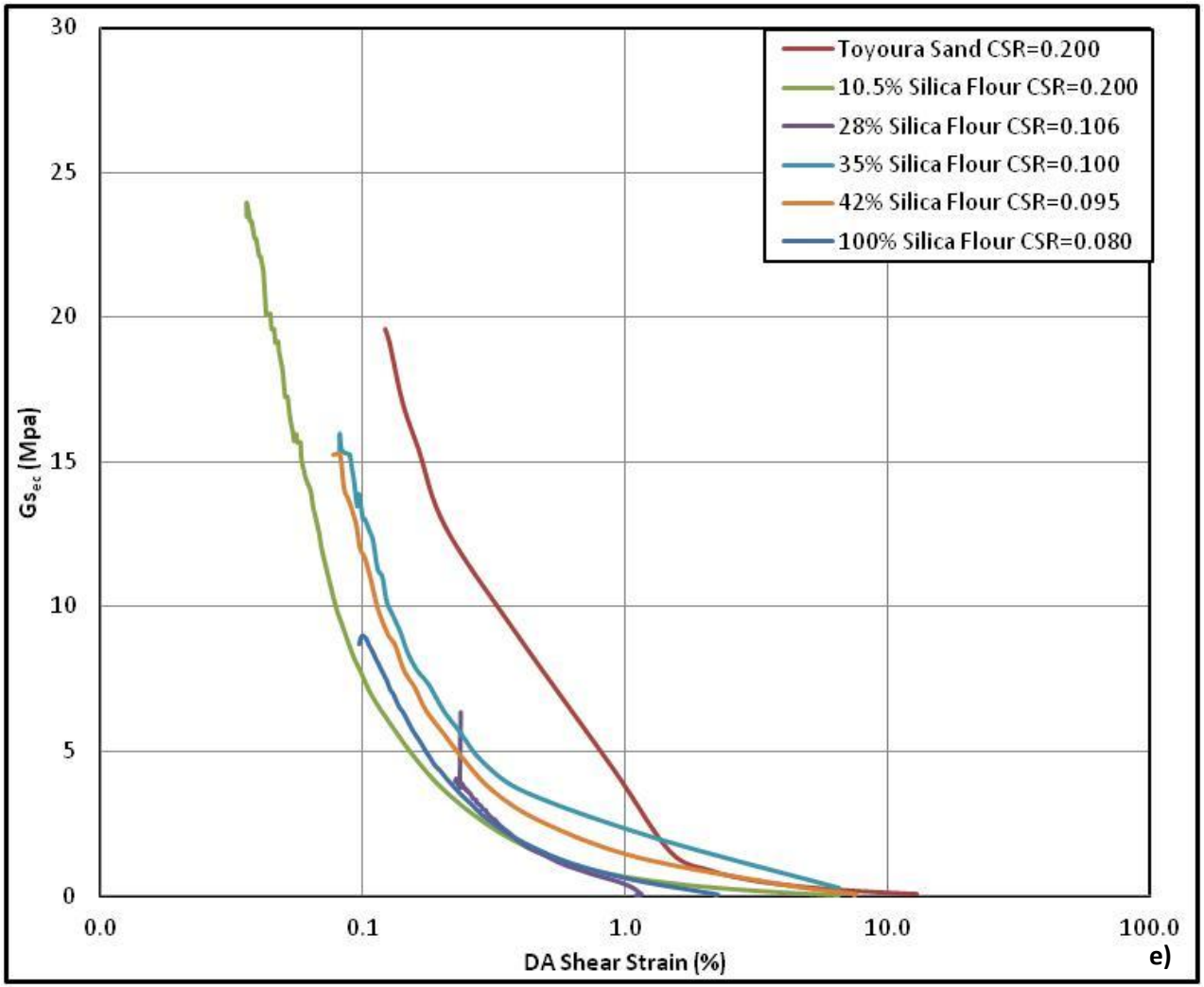

Figure 4.56. For Toyoura sand with 0-100% silica flour, 1% fibre at Dr=60%, σc'=100kPa a) excess pore pressure vs. N; b) DA shear strain vs. N; c) liquefaction resistance curve; d) damping ratio vs. N; e) GSec vs. DA shear strain

4.7.3.3. 42% Silt, 1% Fibre, Various CSR

To get a general idea of the overall liquefaction behavior of a silty soil with 1% PVA fibre, the peak concentration found in Tokyo Bay (42% by mass) was tested three times at varied CSR values ranging from 0.080-0.111. For the case of Toyoura sand with 42% silica flour and 1% fibre, the slope of the CSL was an average of 1.25 (with an outlying data point at CSR=0.09) in compression and 0.80 in extension (Figure 4.57). Clearly the randomly oriented fibres improved the cyclic strength of the silty Toyoura sand.

In terms of excess pore water pressure build-up, the trend was the same as for all silt contents (other than 100%), following an elongated 'S' (Figure 4.59a). After full liquefaction of the silty sand, plastic shear strains reached between 7-8.3% in about 3 cycles, slightly lower than for the silty Toyoura sand without fibres as mentioned in the description of Toyoura sand with 0-100% silica flour, 1% fibre (Figure 4.59b).

Damping of the 42% silica flour mixture with fibres decreased with CSR from 2% to just under 1%, and the secant shear modulus was an average of 15 MPa, which indicates that the fibres had virtually no effect on the sample stiffness (Figure 4.59d-e). This was also found in bender element testing in Section 4.6.

The equivalent magnitude 7.5 earthquake for the Toyoura sand with 42% silica flour and 1% PVA fibre is at CSR=0.104, a slightly lower value than for the unstabilized sample. The equivalent magnitude 9.0 earthquake at 34 cycles to failure is at CSR=0.095, which suggests that the overall slope of the liquefaction resistance curve is less steep for the fibrous sample than for the unstabilized sample and is thus less susceptible to liquefaction. When using the magnitude scaling factor, this value reduces to 0.064, significantly lower than the 34 cycle criteria.

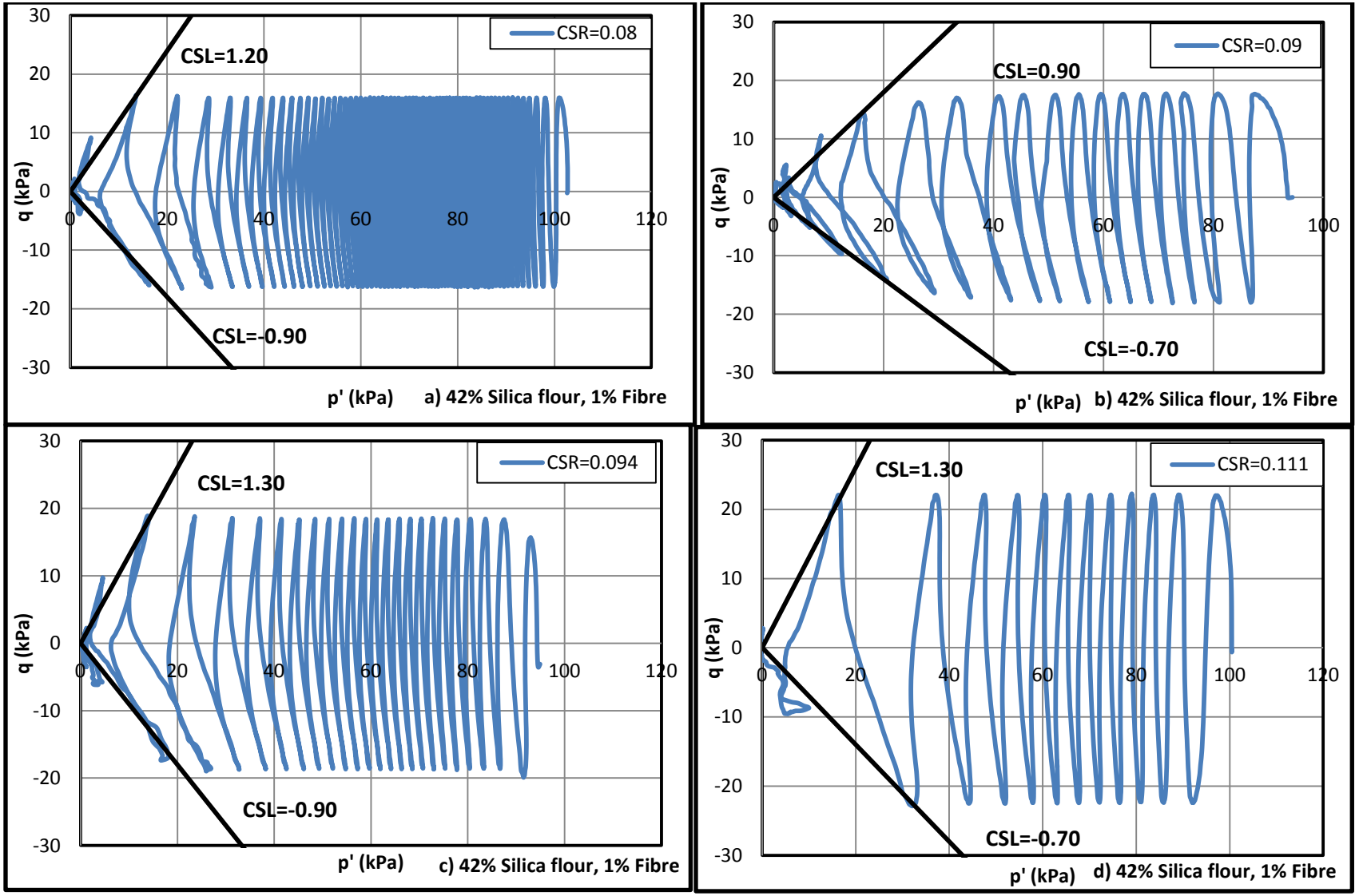

Figure 4.57. Deviator stress vs. Cambridge effective stress for Toyoura sand with 42% silica flour, 1% fibre at D_r=60%, σ_c'=100kPa a) CSR=0.080; b) CSR=0.090; c) CSR=0.094; d) CSR=0.111

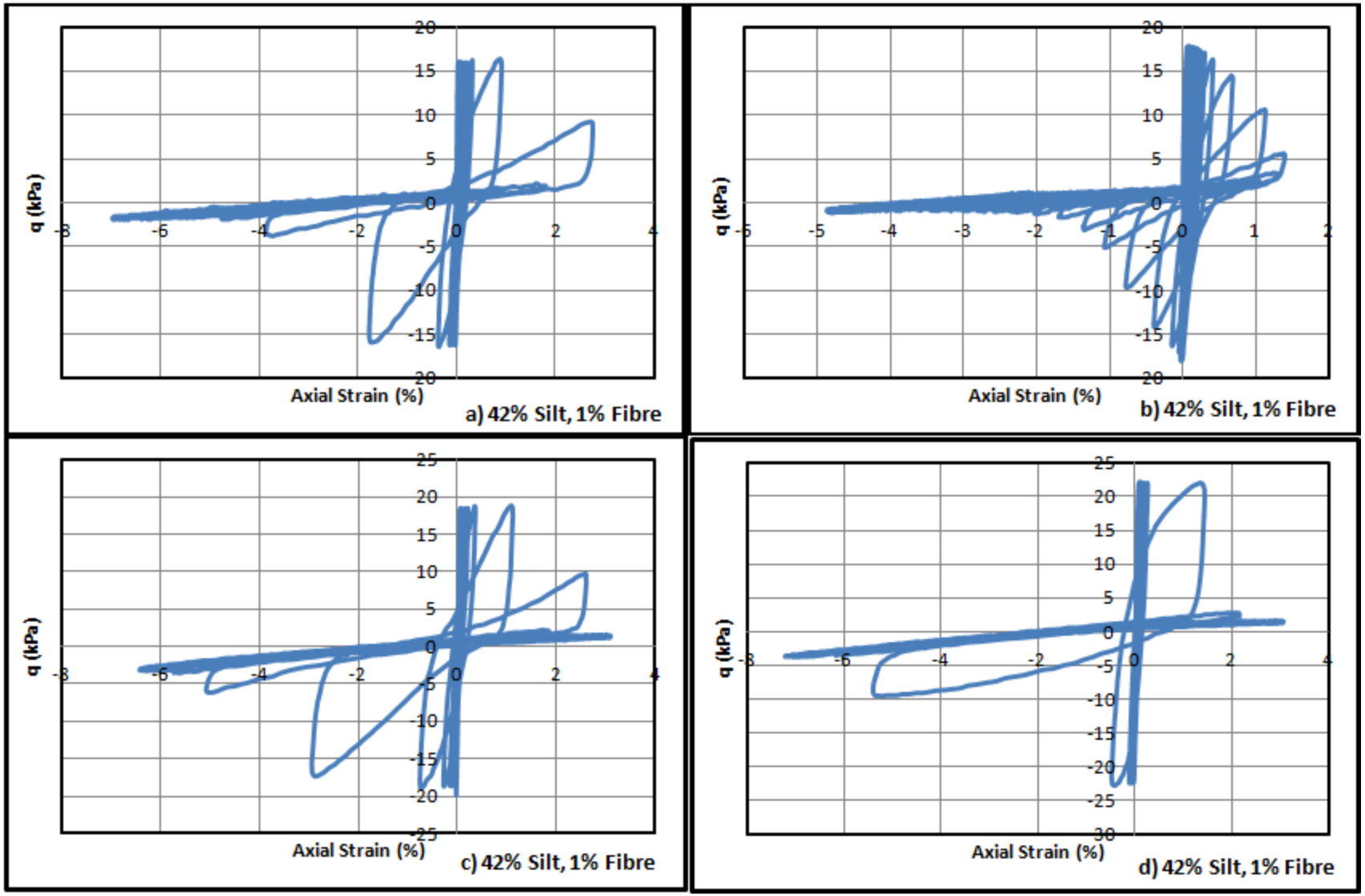

Figure 4.58. q vs. ε_a (%) for Toyoura sand with 42% silica flour, 1% fibre at D_r=60%, σ_c'=100kPa a) CSR=0.080; b) CSR=0.090; c) CSR=0.094; d) CSR=0.111

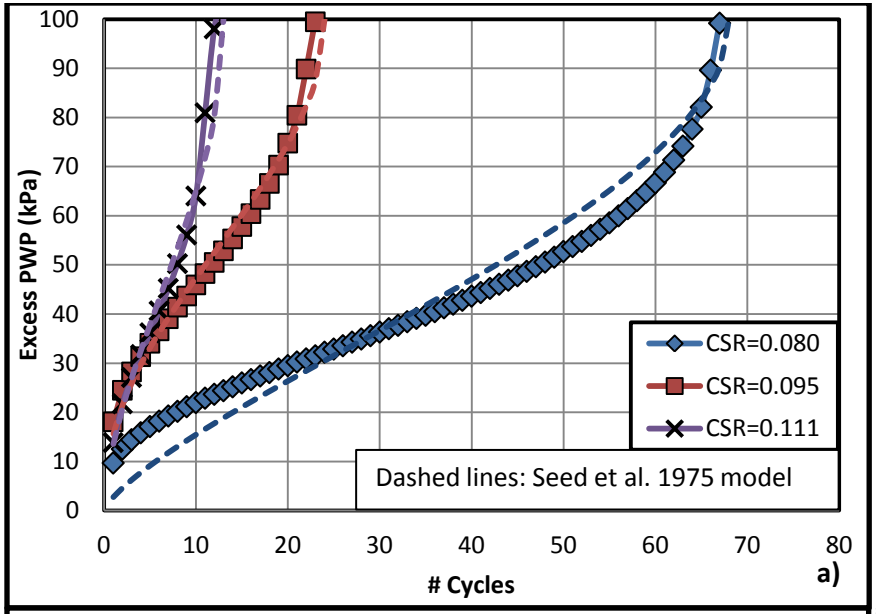
Excess PWP (kPa)
# Cycles
CSR=0.080
CSR=0.095
CSR=0.111
Dashed lines: Seed et al. 1975 model
a)

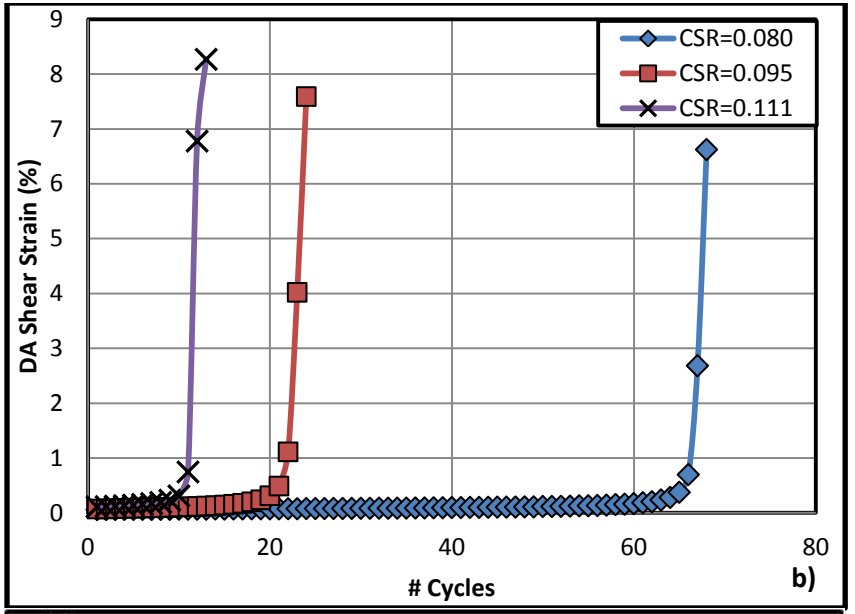
DA Shear Strain (%)
# Cycles
CSR=0.080
CSR=0.095
CSR=0.111
b)

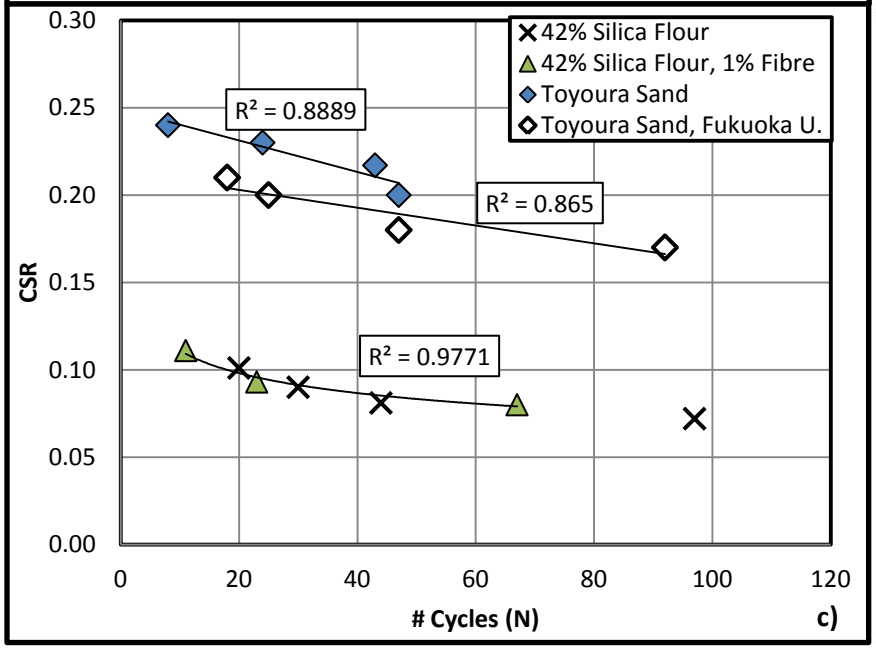
CSR
Cycles (N)
42% Silica Flour
42% Silica Flour, 1% Fibre
Toyoura Sand
Toyoura Sand, Fukuoka U.
R² = 0.8889
R² = 0.865
R² = 0.9771
c)

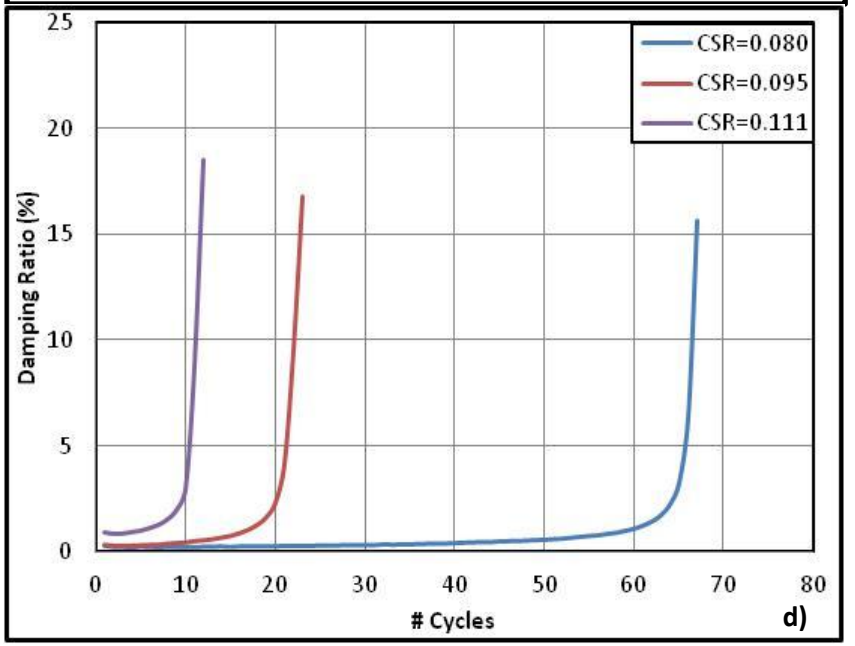
Damping Ratio (%)
# Cycles
CSR=0.080
CSR=0.095
CSR=0.111
d)

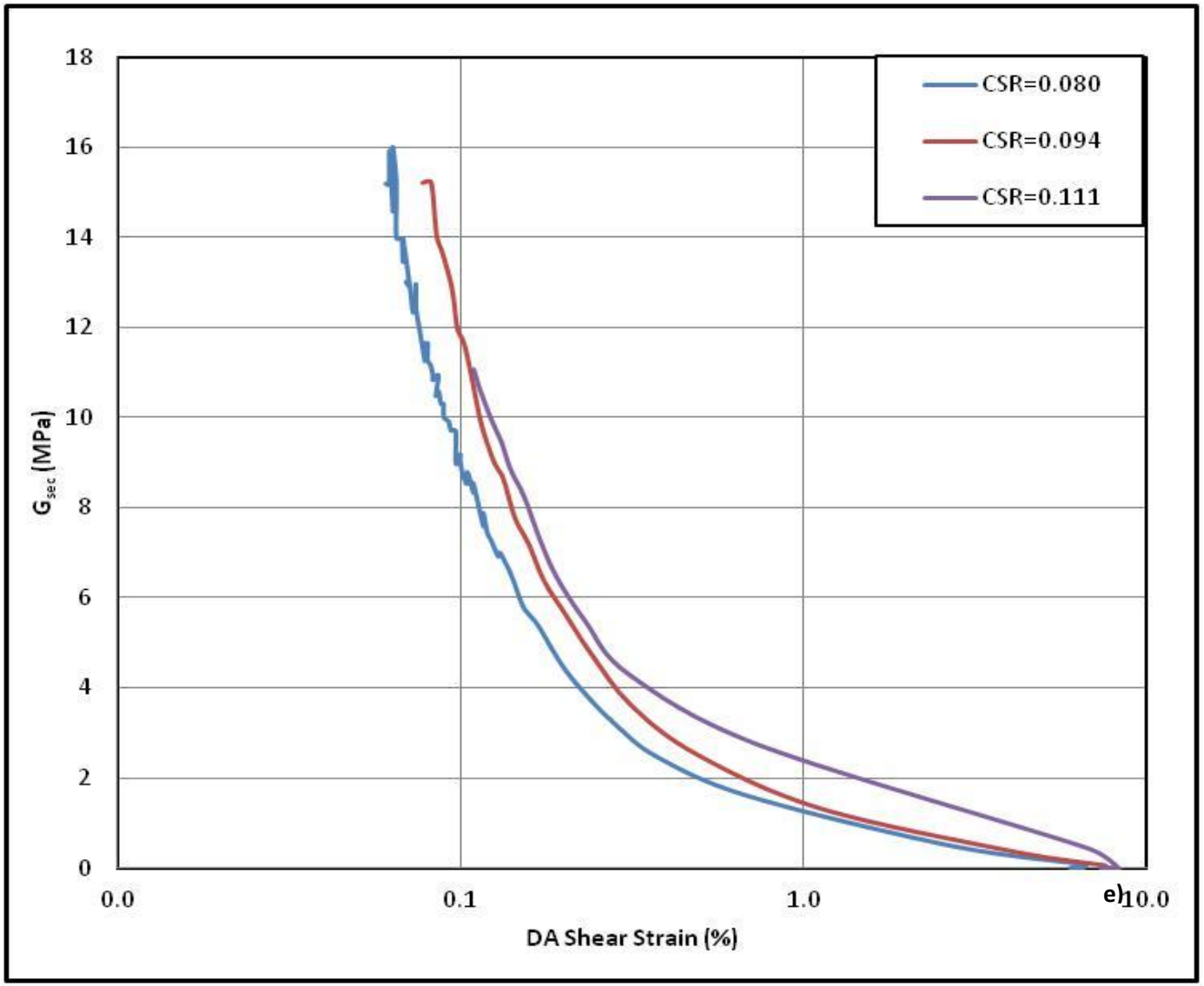

Figure 4.59. For Toyoura sand with 42% silica flour, 1% fibre at D_r=60%, σ_c'=100kPa; a) excess pore pressure vs. N; b) DA shear strain vs. N; c) normalized liquefaction resistance curves for 42% silica flour; d) damping ratio vs. N; e) G_{sec} vs. DA shear strain

4.7.4. Cement Content

The following section contains cyclic triaxial results from the tests outlined in Table 4.6. These tests were performed to determine the effect of various cement concentrations on the liquefaction resistance of Toyoura sand. Referring to previous work done by Fukuoka University (Nakamichi & Sato, 2013), a concentration of 2% cement was selected for closer examination at various CSRs.

Table 4.6. Cyclic Triaxial Tests for Various Cement Concentrations

Sample	CSR
Various Cement %	0.20, 0.31, 0.35
2% Cement	0.305, 0.314, 0.326, 0.335

4.7.4.1. Toyoura Sand, 0-3% Cement, Same CSR

The addition of 0-3% OPC to the Toyoura sand seemed to improve the shear strength, stiffness, and liquefaction resistance significantly, though with only a three day curing time the ultimate strength was only about 60% of a sample that had cured for seven days (Ingles & Metcalf, 1973). The CSL rose from 1.40 for the Toyoura sand, to 1.92 for 3% cement. It was also noted that the butterfly pattern in Figure 4.60a-c began at significantly higher effective stresses than for uncemented samples (35-40 kPa for 2-3% cement rather than 20-30 kPa for uncemented samples).

The cemented Toyoura sand also behaved differently in terms of excess pore water pressure build-up, though samples were tested at B values ranging from 0.95-0.96. Rather than the usual jumps in excess pore water pressure during the initial cycles and the cycles just before the onset of cyclic mobility, the Toyoura sand with 2-3% cement followed a path with no major pore water pressure increase immediately before liquefaction. This trend was inconsistent with the transformed sinusoidal curve proposed by Seed et al. (1975) (Figure 4.62a).

In terms of double amplitude shear strain, there is no evident trend in the maximum value though the striking thing to note is the rate at which the shear strains develop (Figure 4.62b). For the Toyoura sand the maximum shear strain developed within about 10 cycles after the onset of liquefaction. For the Toyoura sand with 2-3% cement, the shear strain development took 40-55 cycles after initial plastic strains began to develop. When compared to the Rowe cell results in Figure 4.22 for the Toyoura sand with varied cement content, the cyclic behaviour followed a similar trend to that of the constrained modulus. In both experiment sets an increase in cement content meant a stiffer sample that was able to withstand higher shear stresses. This trend was even more evident in bender element tests where cement contents of 16% were tested and exhibited significantly higher undrained shear strength than the uncemented soil.

The damping of the cemented Toyoura sand was seen to increase from 2% to about 4% with increasing cement content. This is because the wave propagation energy required to rearrange the particles of a weakly cemented soil, and thus propagate through the soil, is higher than that of clean sand (Saxena, Avramidis, & Reddy, 1988). This theory may also explain the apparent reduction in shear modulus seen in the cemented samples. This shear modulus reduction was also potentially due to the increased CSR, which can cause an apparent decrease in the initial shear modulus (Clough et al., 1989), though based on bender element testing in Section 4.6, the shear modulus should have a clear and definitive increase with increasing cement content.

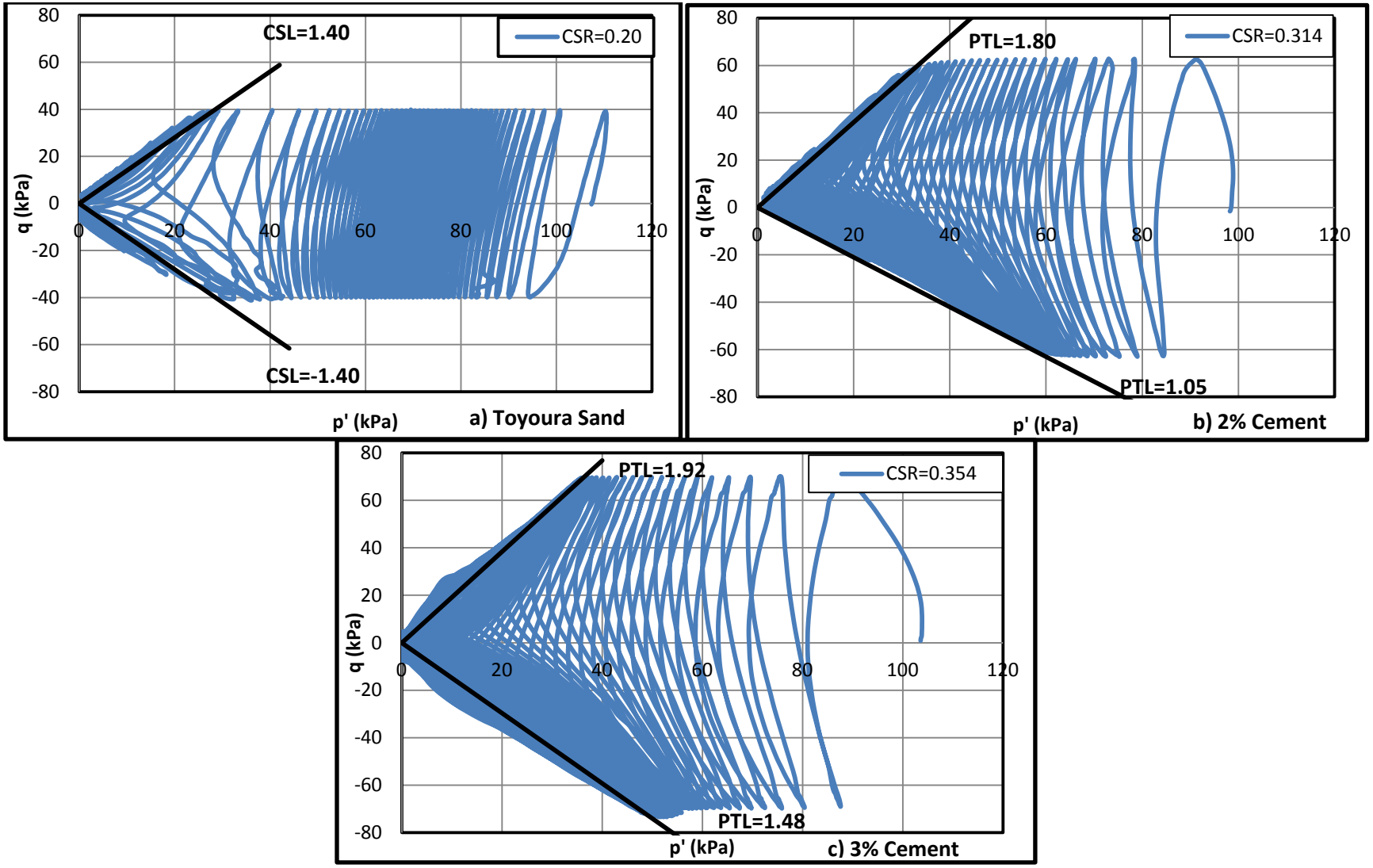

Figure 4.60. Deviator stress vs. Cambridge effective stress for Toyoura sand with 0-3% cement at D_r=60%, σ_c'=100kPa a) Toyoura sand, CSR=0.200; b) 2% cement, CSR=0.314; c) 3% Cement, CSR=0.354

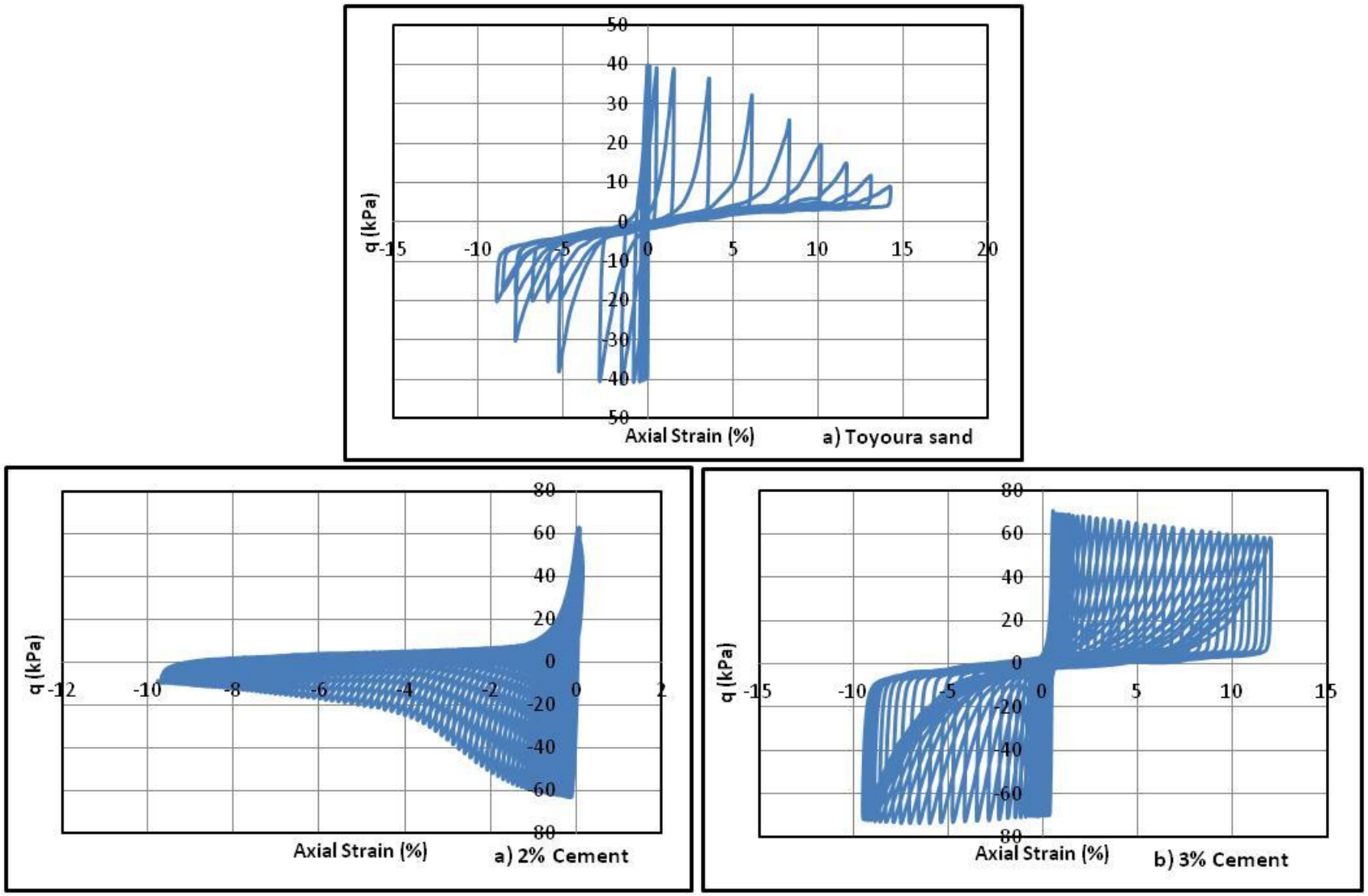

Figure 4.61. q vs. ε_a (%) for Toyoura sand with 0-3% cement at D_r=60%, σ_c'=100kPa a) Toyoura sand, CSR=0.200; b) 2% cement, CSR=0.314; c) 3% Cement, CSR=0.350

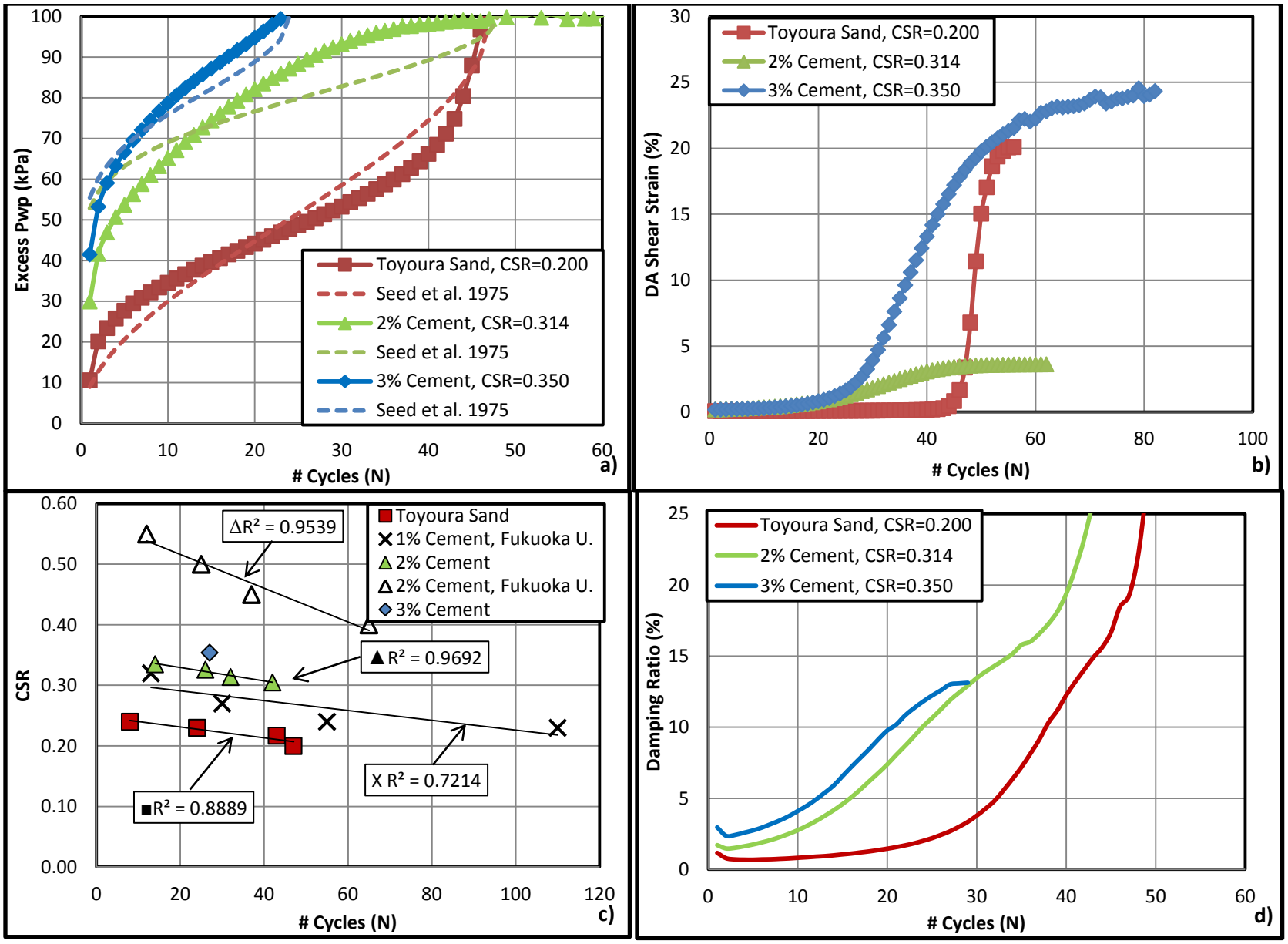
Excess Pwp (kPa)
Cycles (N)
a)
Toyoura Sand, CSR=0.200
Seed et al. 1975
2% Cement, CSR=0.314
Seed et al. 1975
3% Cement, CSR=0.350
Seed et al. 1975
DA Shear Strain (%)
Cycles (N)
b)
Toyoura Sand, CSR=0.200
2% Cement, CSR=0.314
3% Cement, CSR=0.350
CSR
Cycles (N)
c)
ΔR² = 0.9539
R² = 0.9692
X R² = 0.7214
■R² = 0.8889
Toyoura Sand
1% Cement, Fukuoka U.
2% Cement
2% Cement, Fukuoka U.
3% Cement
Damping Ratio (%)
Cycles (N)
d)
Toyoura Sand, CSR=0.200
2% Cement, CSR=0.314
3% Cement, CSR=0.350

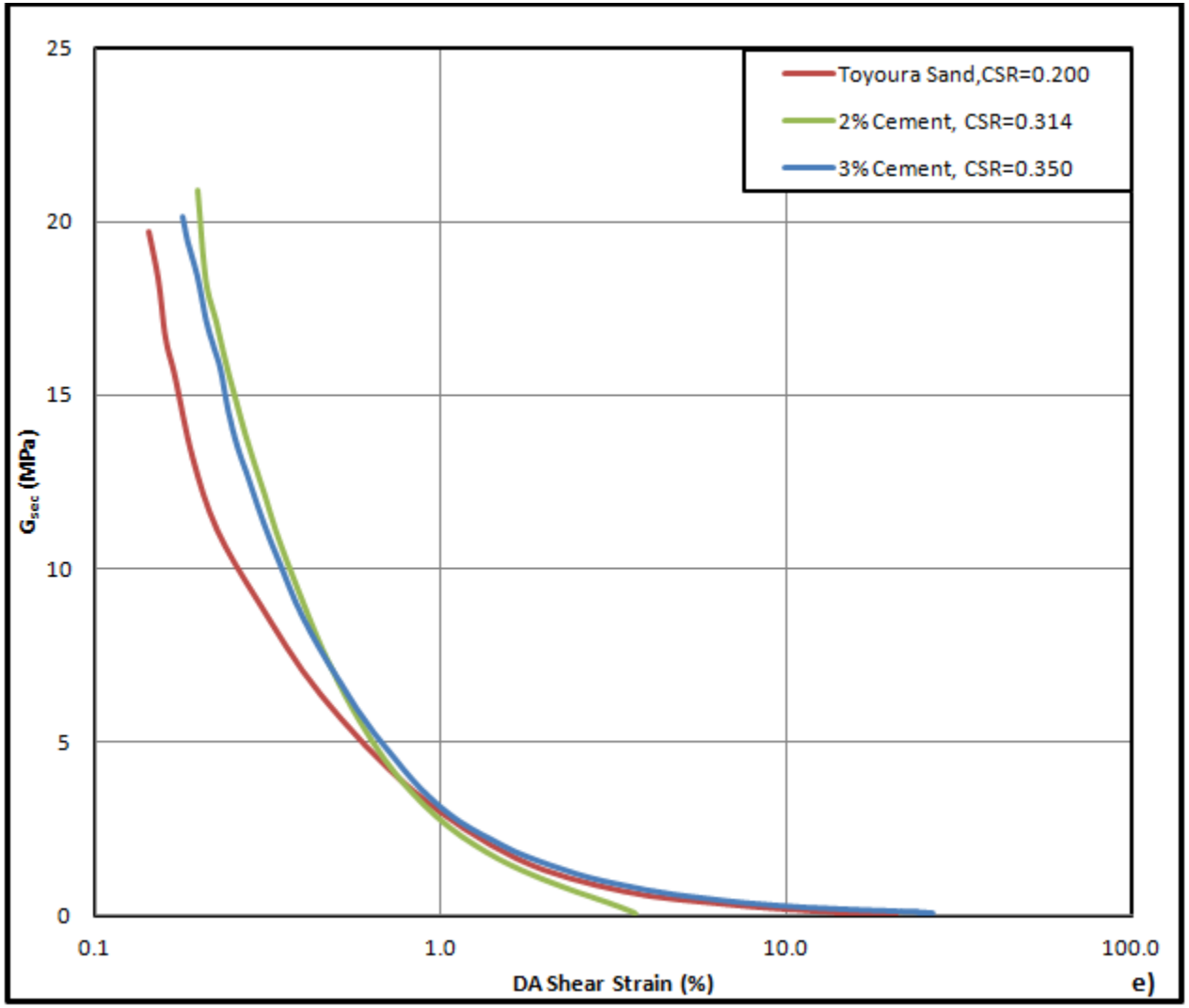

Figure 4.62. For Toyoura sand with 0-3% cement at D_r=60%, σ_c'=100kPa a) excess pore pressure vs. N; b) DA shear strain vs. N; c) liquefaction resistance curve; d) damping ratio vs. N; e) G_{sec} vs. DA shear strain

4.7.4.2. Toyoura sand, 2% Cement, Various CSR

For poorly graded sands it is common to add 2-4% OPC to achieve more suitable engineering properties (Ingles & Metcalf, 1973). In this thesis, the focus was primarily on the lower concentration of 2% for cyclic triaxial testing, though cement concentrations from 0-4% were tested on the Rowe Cell (Section 4.4.2) and bender element tests were performed on concentrations from 0-16% cement.

It can be seen that the CSL for the Toyoura sand with 2% OPC additive is an average of 1.80 (Figure 4.63). This is much higher than the CSL of 1.36 found from monotonic shearing (Figure 4.35 in Section 4.6.2), but the difference may be explained via the different loading mechanism and sample heterogeneousness (Neri, 2013). The onset of cyclic mobility appears to begin around 40 kPa effective stress, much higher than for the Toyoura sand or silty Toyoura sand samples.

When the deviator stress is plotted against the axial strain as shown in Figure 4.64, its clear that the sample is very weak in tension but very strong in compression, hence the large negative plastic strains accumulated (Saxena, Reddy, & Avramidis, 1988). This is clearly different than the behaviour of all of the uncemented samples that are approximately equal in compression and extension.

As mentioned above, the excess pore water pressure build-up for the cemented Toyoura sand follows a curved path that grows increasingly steeper with CSR (Figure 4.65a). The shear strain accumulation rate was also very gradual due to the high stiffness of the cemented sand (Figure 4.65b).

There was a very slight decrease in damping with increasing CSR (from 3% damping to 2%) and as expected there was no change in the secant shear modulus, which remained constant at 21 MPa (Figure 4.65d).

From the cyclic liquefaction resistance curve the equivalent magnitude 7.5 earthquake for the 2% cemented sand was at a CSR of 0.335, which decreased to 0.314 for the equivalent magnitude 9.0 Great East Japan Earthquake.

Relating these results to the visible microstructure of the cemented Toyoura sand in Section 4.2, it has been found that the stresses between cement and sand particles reach a maximum at the edges of the contact zones, and a minimum in the softer, though still load bearing and load distributing, center (Dvorkin & Yin, 1995). As the cement cures, these contact zones expand and thus provide additional strength. The three day curing period could explain the difference between the results gathered for this thesis and those gathered by Nakamichi & Sato, (2013) at Fukuoka university.

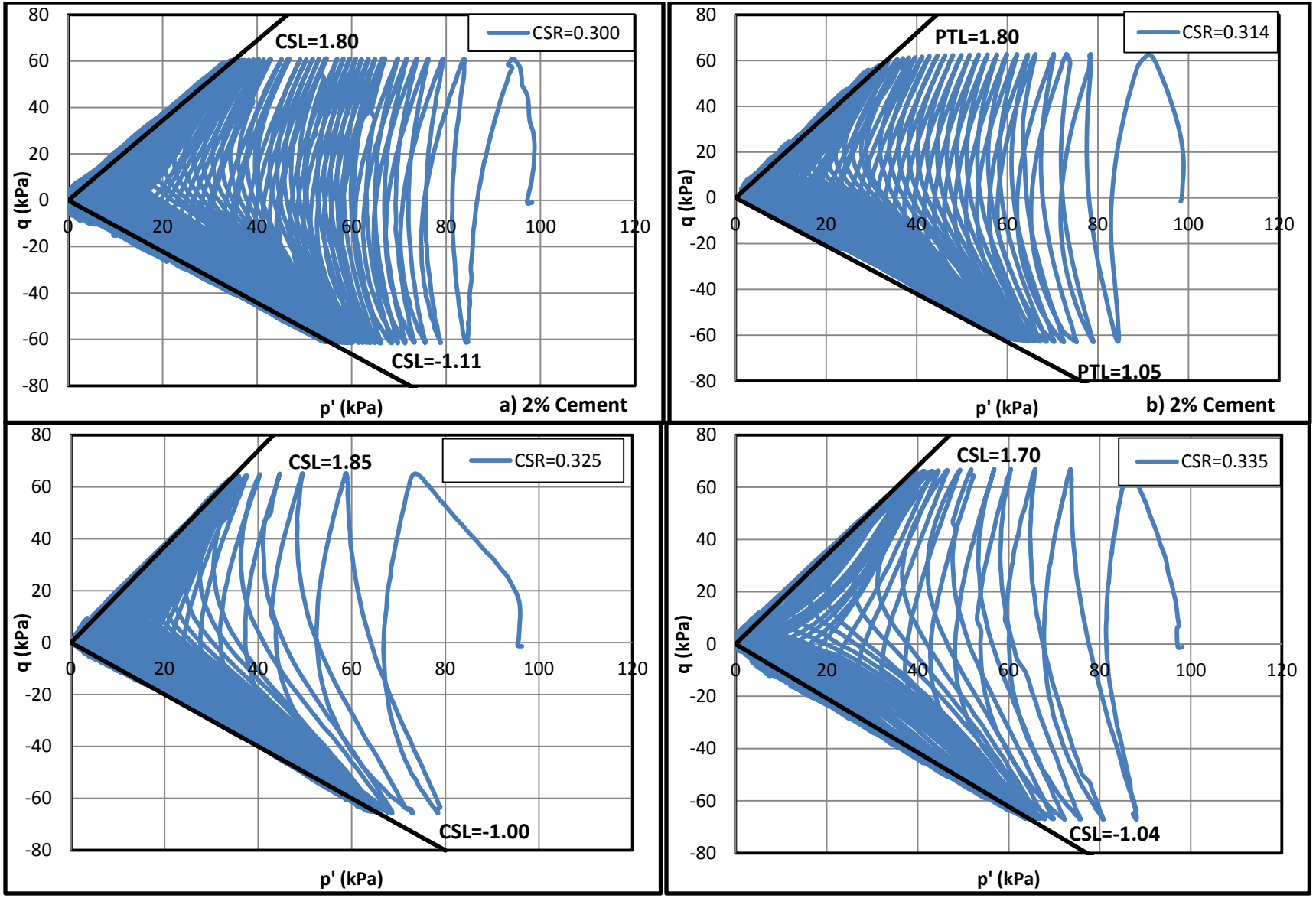

Figure 4.63. Deviator stress vs. Cambridge effective stress for Toyoura sand with 2% cement at D_r=60%, σ_c'=100kPa a) CSR=0.300; b) CSR=0.314; c) CSR=0.325; d) CSR=0.335

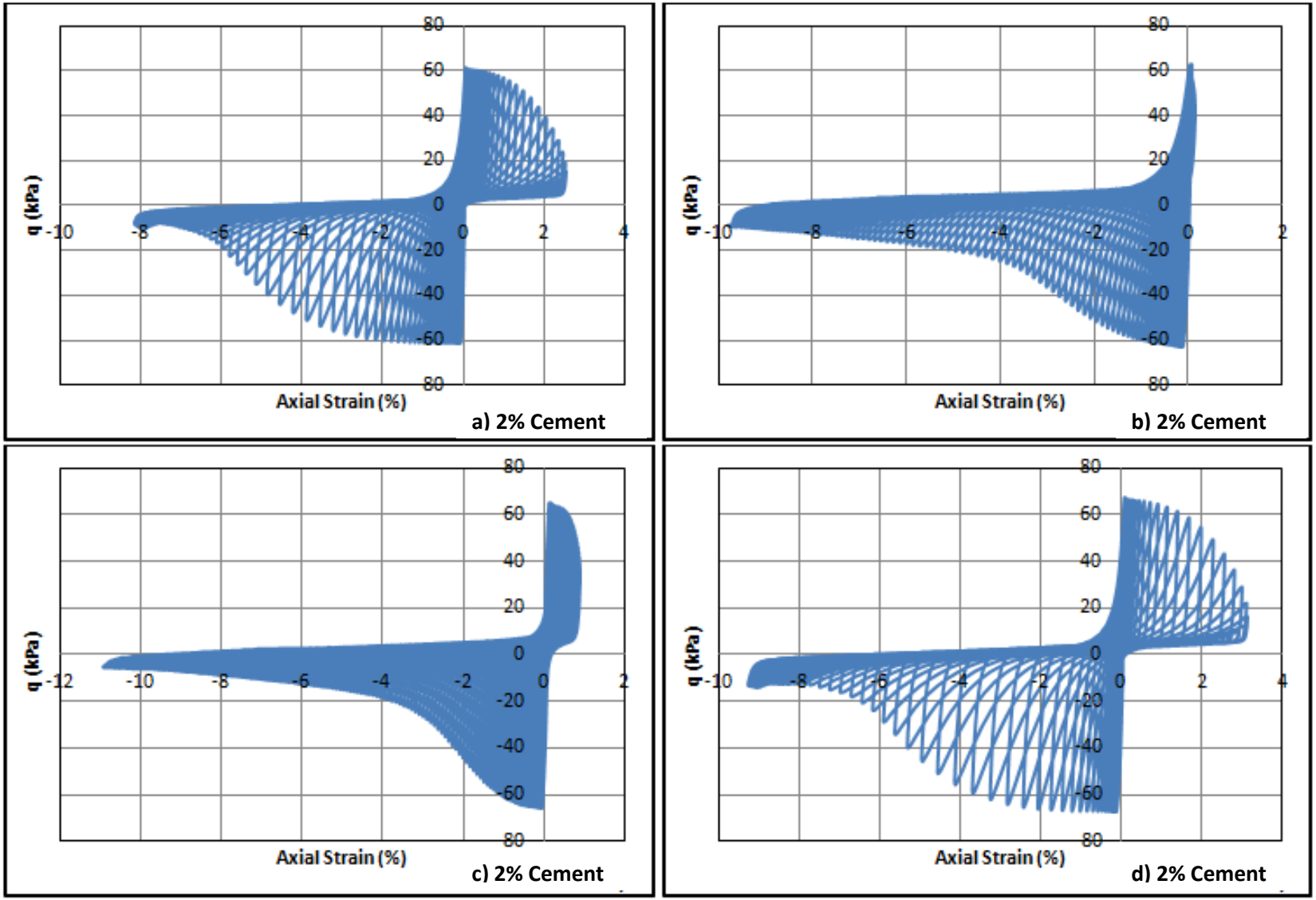

Figure 4.64. q vs. ε_a for Toyoura sand with 2% cement at D_r=60%, σ_c'=100kPa a) CSR=0.300; b) CSR=0.314; c) CSR=0.325; d) CSR=0.335

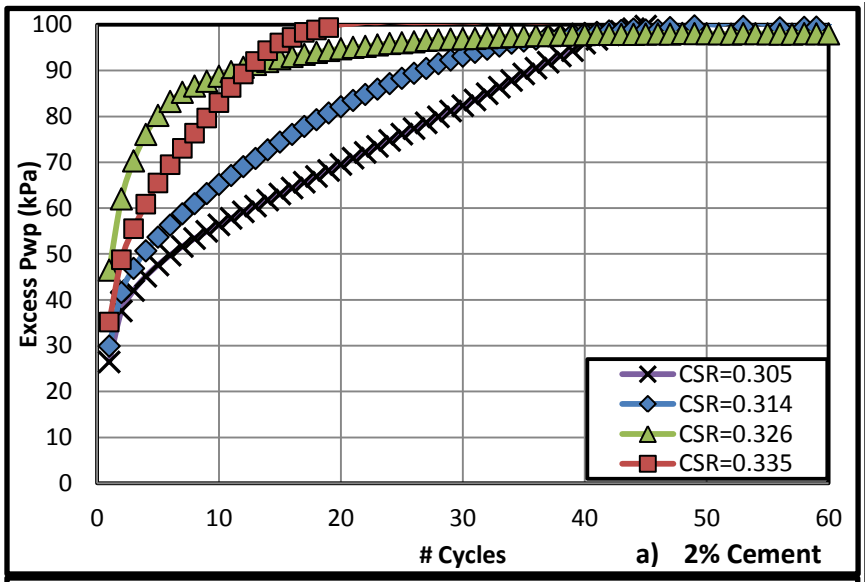
Excess Pwp (kPa)
Cycles
a) 2% Cement
CSR=0.305
CSR=0.314
CSR=0.326
CSR=0.335

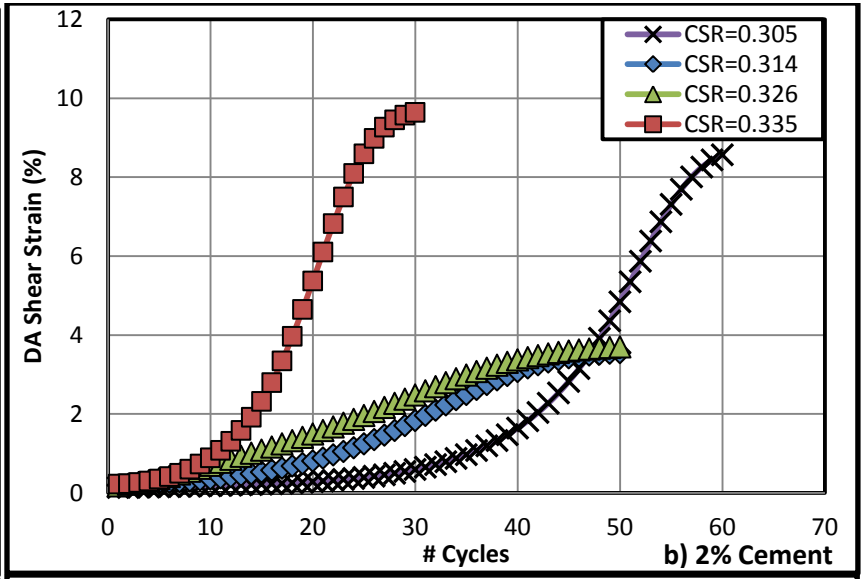
DA Shear Strain (%)
Cycles
b) 2% Cement
CSR=0.305
CSR=0.314
CSR=0.326
CSR=0.335

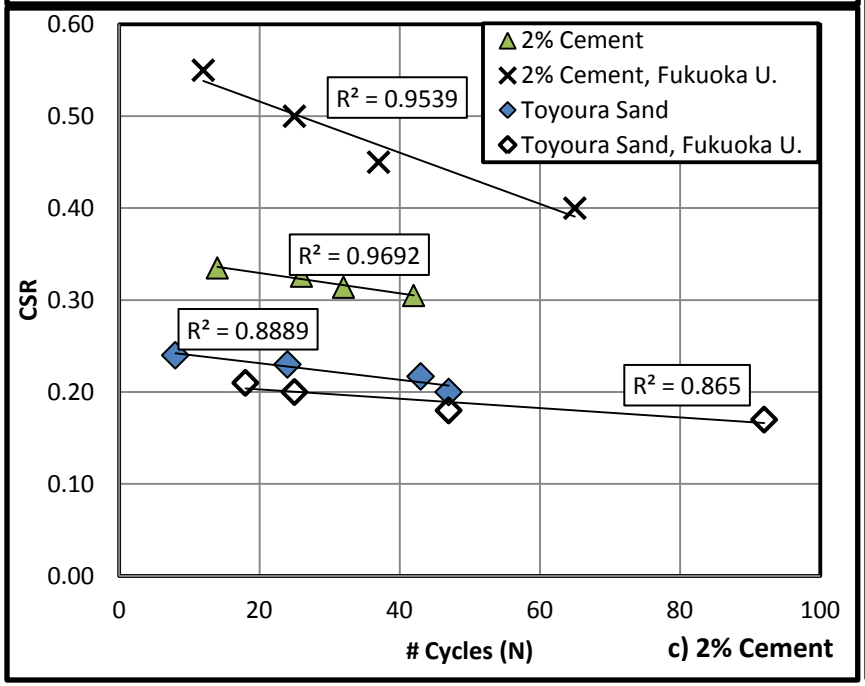
CSR
Cycles (N)
c) 2% Cement
2% Cement
2% Cement, Fukuoka U.
Toyoura Sand
Toyoura Sand, Fukuoka U.
R² = 0.9539
R² = 0.9692
R² = 0.8889
R² = 0.865

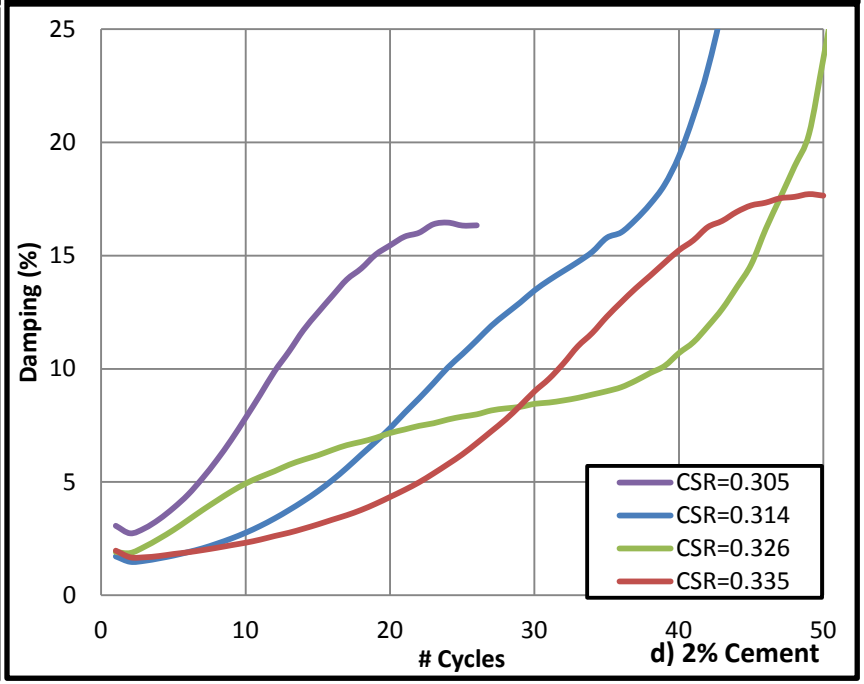
Damping (%)
Cycles
d) 2% Cement
CSR=0.305
CSR=0.314
CSR=0.326
CSR=0.335

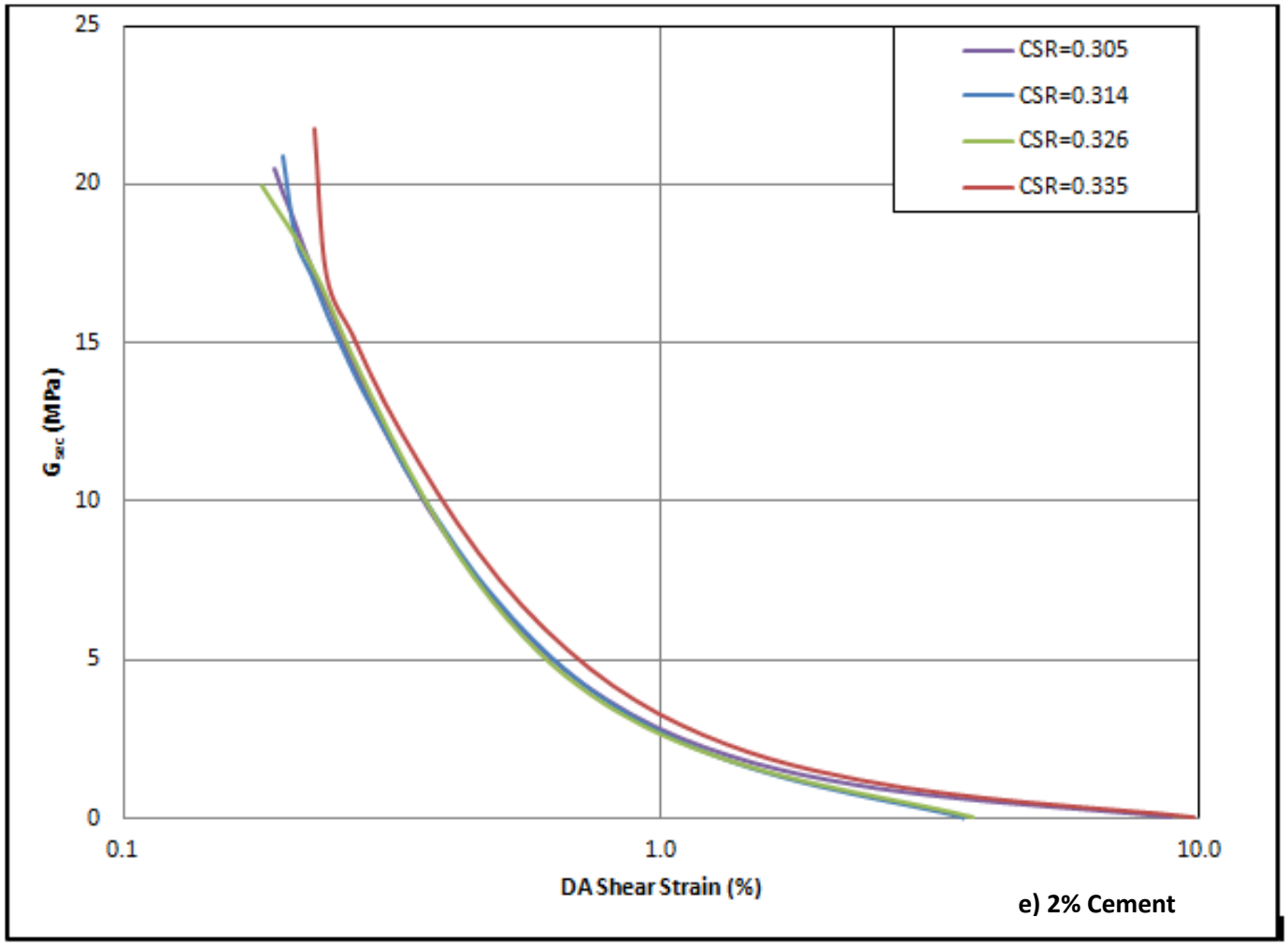

Figure 4.65. For Toyoura sand with 2% cement at D_r=60%, σ_c'=100kPa a) excess pore pressure vs. N; b) DA shear strain vs. N; c) liquefaction resistance curve; d) damping ratio vs. N; e) G_{sec} vs. DA shear strain

4.7.5. Fibre and Cement

The following section contains cyclic triaxial results from the tests outlined in Table 4.7. These tests were performed to determine the effect of cement and PVA fibre stabilizers on the liquefaction resistance of silty Toyoura sand. Silt concentrations were representative of concentrations found in the Tokyo Bay region of Japan. Referring to previous work done by Fukuoka University (Nakamichi & Sato, 2013) concentrations of 2% cement and 1% fibre were selected for closer examination at various CSRs. Please note that the data for 100% Silt, 0-2% Cement, 0-1% Fibre can be found in Appendix C.

Table 4.7. Cyclic Triaxial Tests for Various Silt Concentrations, 2% Cement, 1% Fibre

Sample	CSR
Toyoura Sand, 2% Cement, 1% Fibre	0.32, 0.34, 0.35
48.5% Silt, 2% Cement, 1% Fibre	0.16, 0.20, 0.22
Varying Silt, 2% Cement, 1% Fibre	0.175, 0.221, 0.323
100% Silt, 0-2% Cement, 0-1% Fibre	0.079, 0.100, 0.175, 0.175

4.7.5.1. Toyoura Sand, 2% Cement, 1% PVA Fibre, Various CSR

It was seen that for the cemented Toyoura sand with 1% fibres, there is an increase in the slope of the CSL over that of the purely cemented samples from 1.73 to an average of 2.25 (Figure 4.66). It is clear that the addition of PVA fibres to the cemented Toyoura sand greatly improves the liquefaction resistance, though it has been determined by other researchers that the strength gain effects of fibre inclusion increases asymptotically to a cement concentration of about 5% (Consoli, Vendruscolo, Fonini, & Dalla Rosa, 2009).

When the stress strain plots in Figure 4.67 are analyzed, it became apparent that the brittle failure seen in the Toyoura sand with 2% cement and no fibre is no longer present. Instead, a more

ductile failure can be seen (Consoli, Vendruscolo, Fonini, & Dalla Rosa, 2009), with the compression and extension strains being roughly equal at each CSR value.

To explain this strength gain and ductility, some researchers have examined the contact zones of the sand/cement bonds. The maximum stress transferred between sand grains and cement increases with radius of the contact zones and stiffness of the hydrated cement bonds, helping to explain why the fibres provide such improved strength in cemented sand (Dvorkin & Yin, 1995). The surrounding of the fibres by the hydrating cement creates larger linear contact zones and thus larger stiff regions around their periphery as mentioned in Section 4.2. The ductility is due to the tensile strength of the fibrous additives.

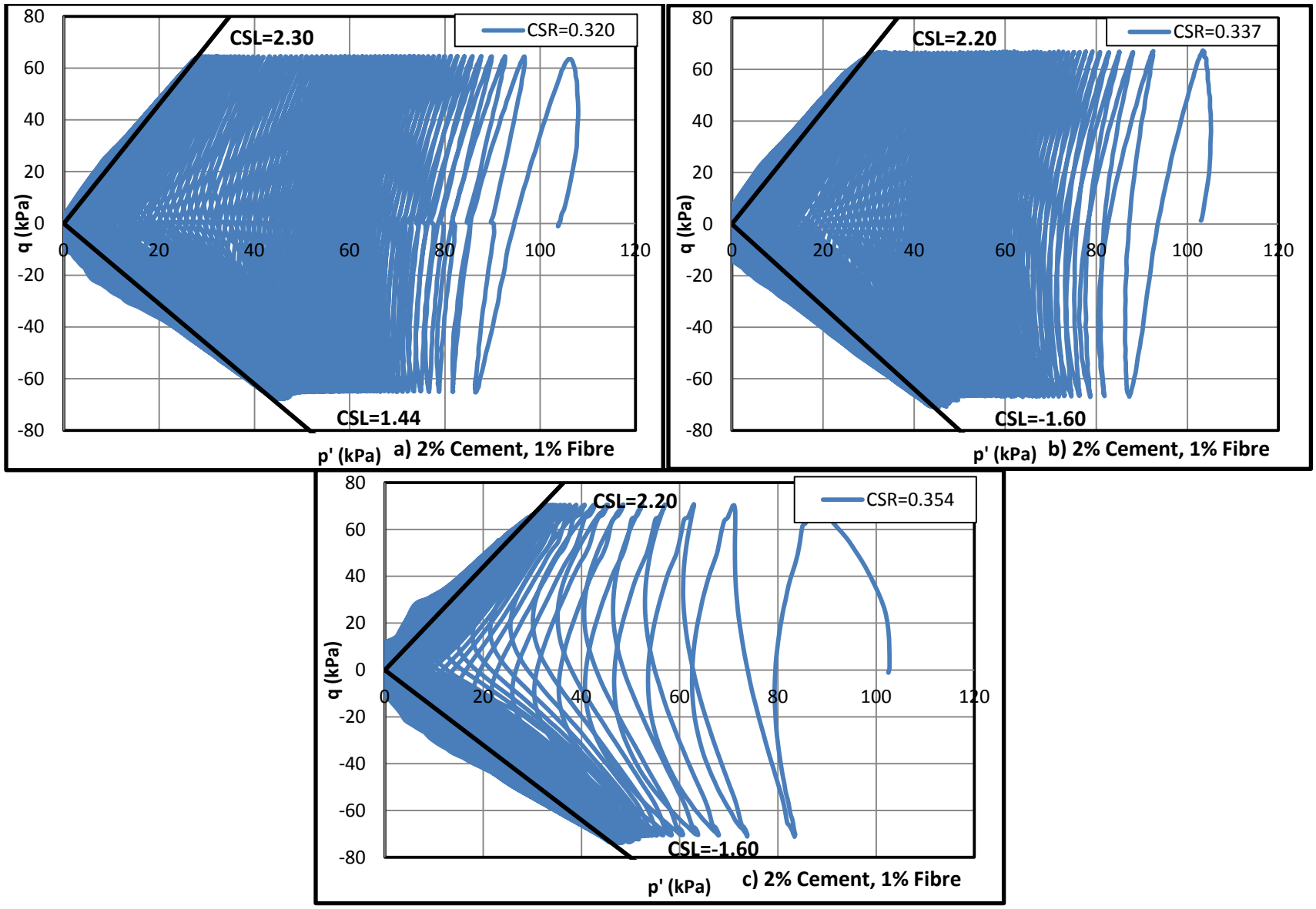

Figure 4.66. Deviator stress vs. Cambridge effective stress for Toyoura sand with 2% cement, 1% fibre at D_r=60%, σ_c'=100kPa a) CSR=0.320; b) CSR=0.337; c) CSR=0.354

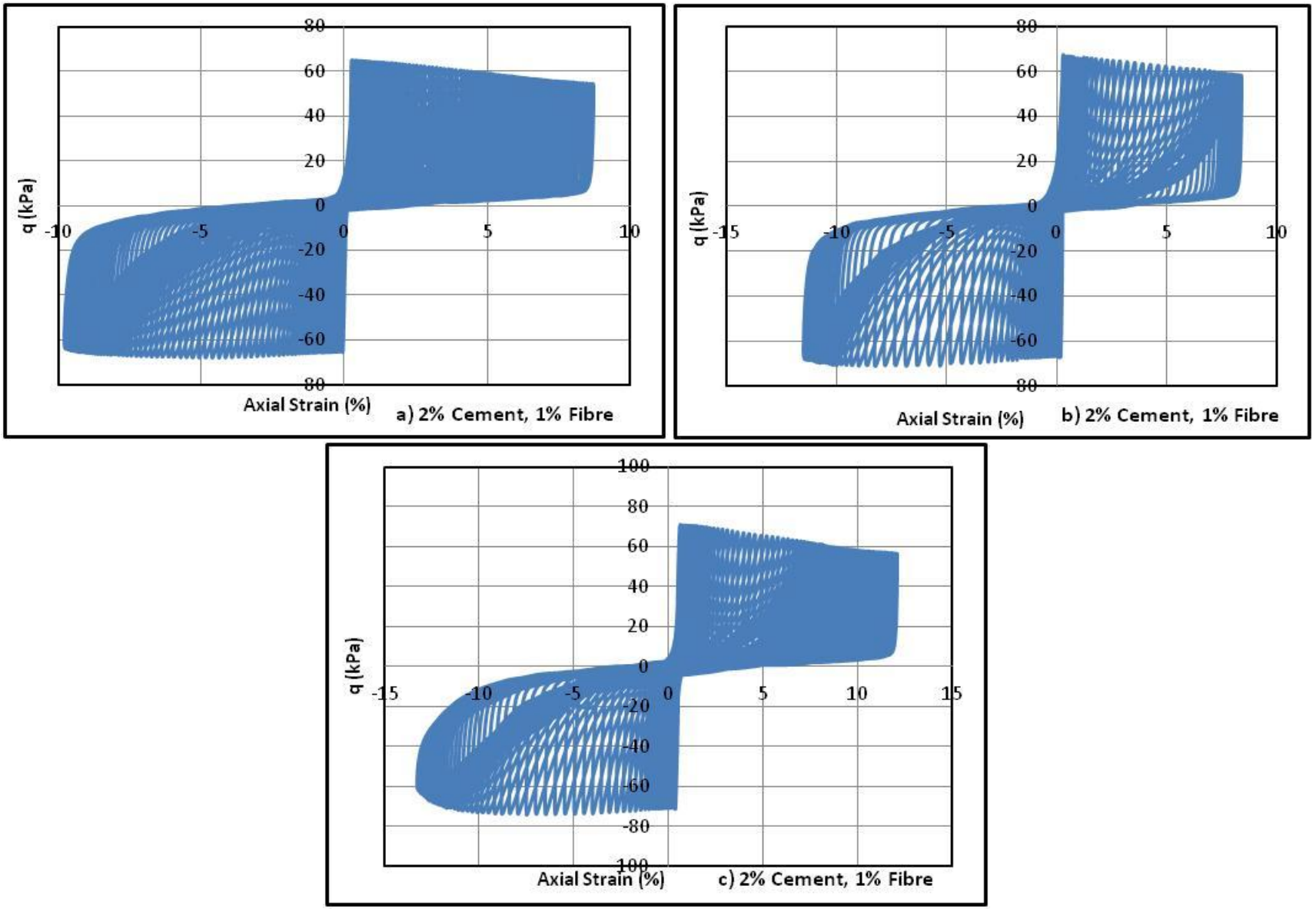

Figure 4.67. q vs. ε_a for Toyoura sand with 2% cement, 1% fibre at D_r=60%, σ_c'=100kPa a) CSR=0.320; b) CSR=0.337; c) CSR=0.354

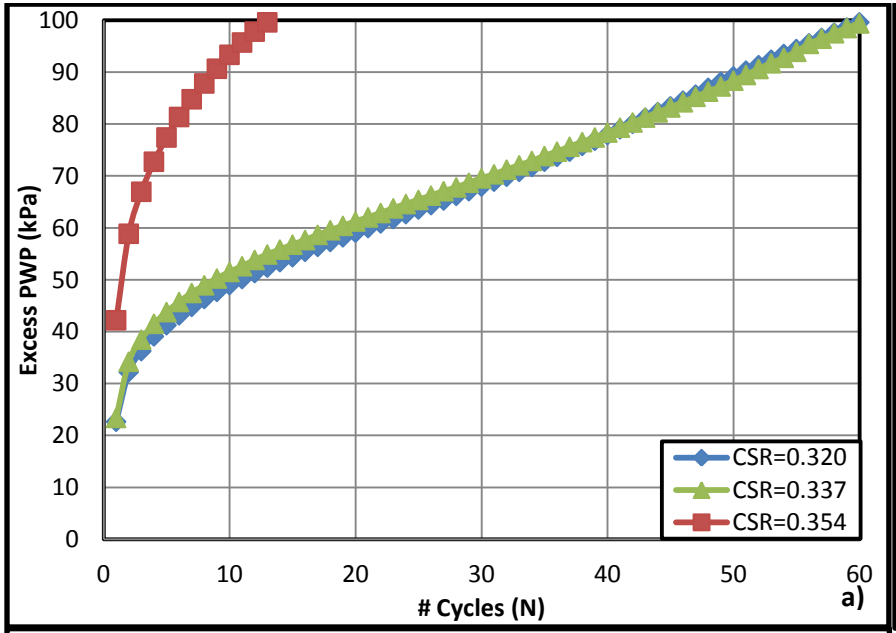
Excess PWP (kPa)
# Cycles (N)
CSR=0.320
CSR=0.337
CSR=0.354
a)

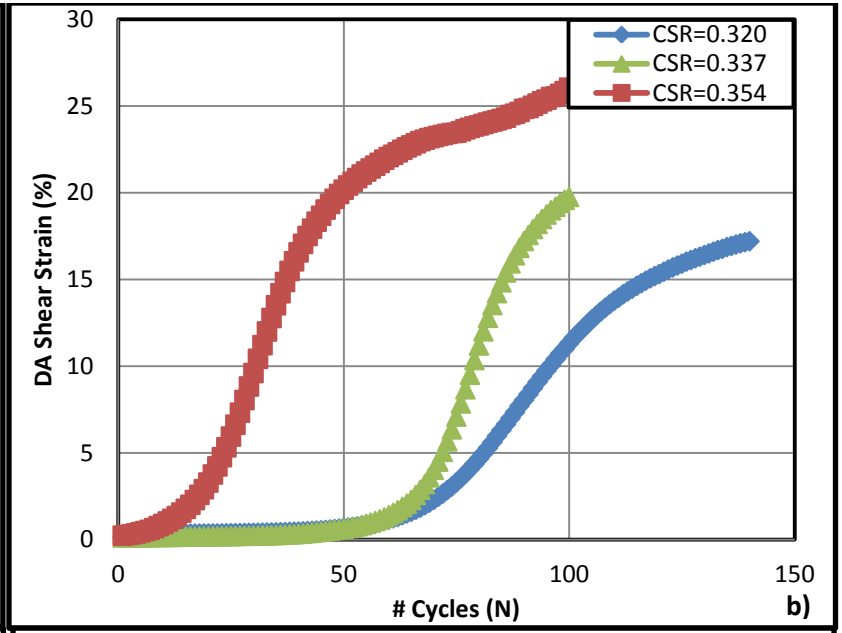
DA Shear Strain (%)
# Cycles (N)
CSR=0.320
CSR=0.337
CSR=0.354
b)

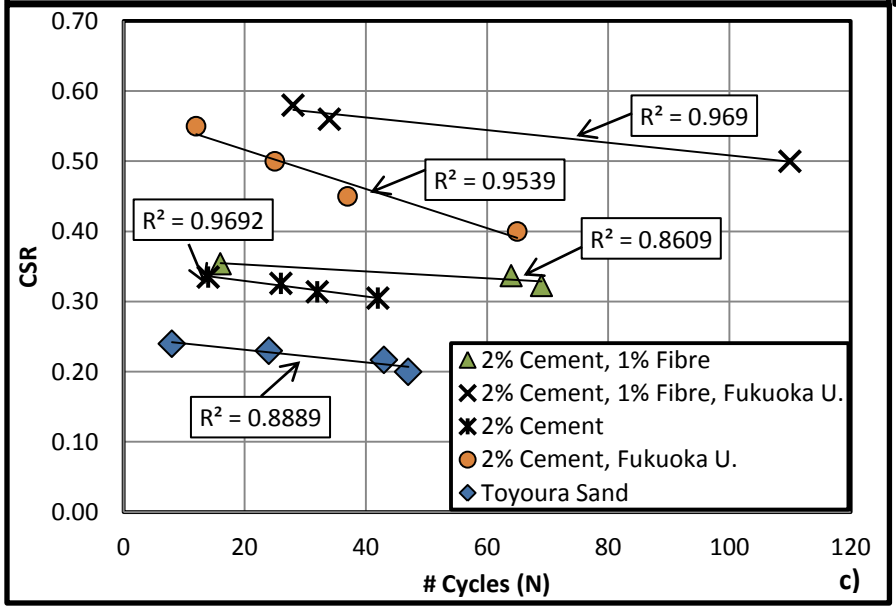
CSR
# Cycles (N)
R² = 0.969
R² = 0.9539
R² = 0.9692
R² = 0.8609
R² = 0.8889
2% Cement, 1% Fibre
2% Cement, 1% Fibre, Fukuoka U.
2% Cement
2% Cement, Fukuoka U.
Toyoura Sand
c)

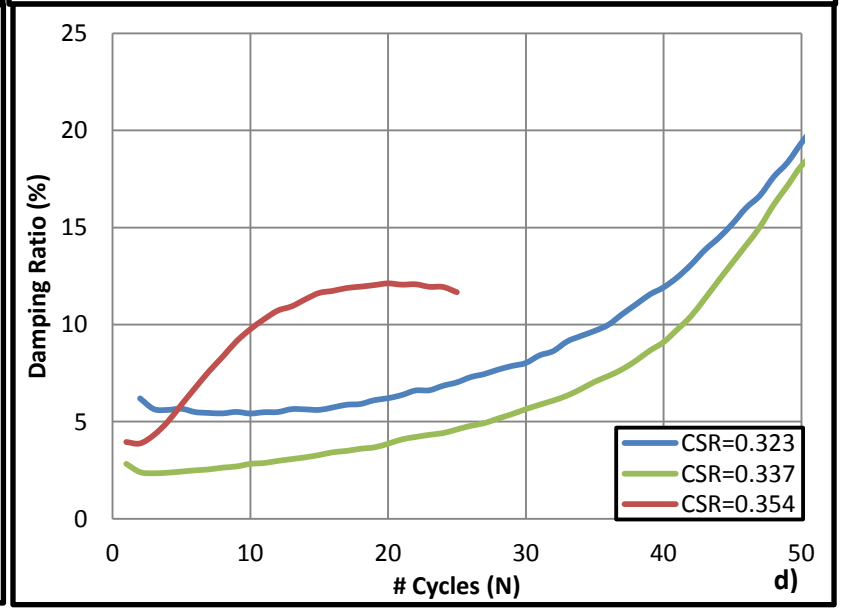
Damping Ratio (%)
# Cycles (N)
CSR=0.323
CSR=0.337
CSR=0.354
d)

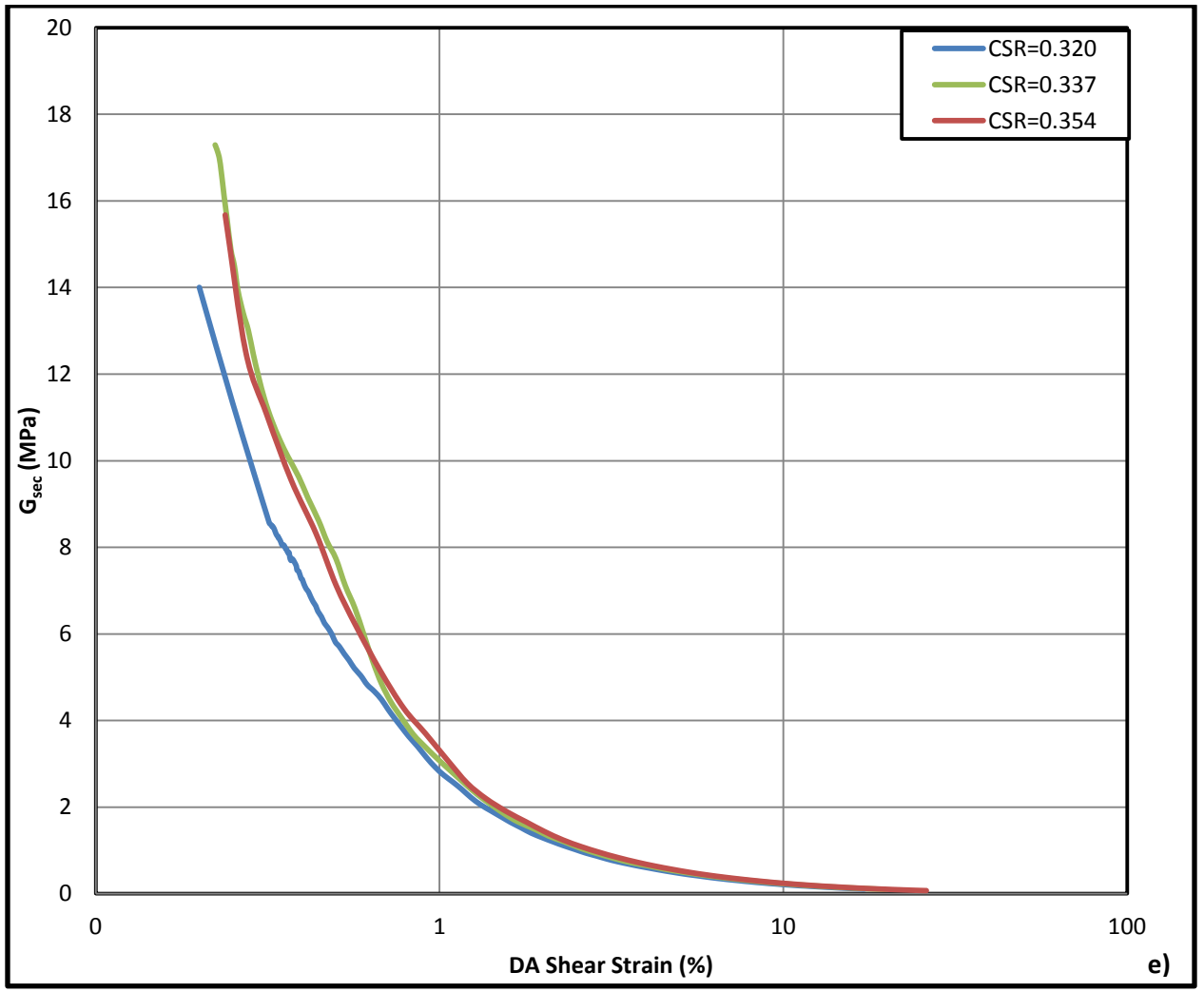

Figure 4.68. For Toyoura sand with 2% cement, 1% fibre at D_r=60%, σ_c'=100kPa a) excess pore pressure vs. N; b) DA shear strain vs. N; c) normalized liquefaction resistance curves for stabilized Toyoura sand; d) damping ratio vs. N; e) G_{sec} vs. DA shear strain

4.7.5.2. 48.5% Silt, 2% Cement, 1% Fibre, Various CSR

A series of three tests was performed on samples containing 48.5% Toyoura sand, 48.5% silica flour, 2% cement, and 1% fibre to gauge the liquefaction strength of a 50/50 silty Toyoura sand mix. The first thing to note is the increase in the slope of the CSL over the Toyoura sand with 42% silt and 0-1% fibre content. Adding the cement and fibres steepened the CSL from 0.59 for the Toyoura sand with 42% silica flour up to an average of 2.30 for the sample with both fibre and OPC (Figure 4.69).

The excess pore water pressure generation curve resembles a hybrid of the silty Toyoura sand and the Toyoura sand with 2% OPC, following a very flattened 'S' shape but still having noticeable inflection points (Figure 4.71a). This trend gives further credit to the superimposition theory discussed earlier.

It is interesting that the accumulation of plastic strains becomes more positive (compression) for these samples as the CSR increases. As shown by the large compressional strains (up to 17%) in Figure 4.70, specifically for the cyclic stress ratios greater than 0.200, the positive strain development is larger than the negative. This trend is actually seen in all fibrous samples, suggesting that although the PVA fibre addition improves liquefaction resistance and a more ductile failure during cyclic loading, it may actually decrease the compressional strength of the soil and allow larger plastic deformations (Ibraim & Fourmont, 2006).

The cyclic resistance curve for the stabilized sample of 48.5% silica flour in Figure 4.71c is much steeper and more linear than the fibrous or unstabilized versions. It is, however, notably stronger at high cyclic load amplitudes. As the CSR reduces, however, the soil behaviour tends to approach and become weaker than these unstabilized samples, suggesting that at these additive concentrations the mitigating effects are only significant for high stress loading.

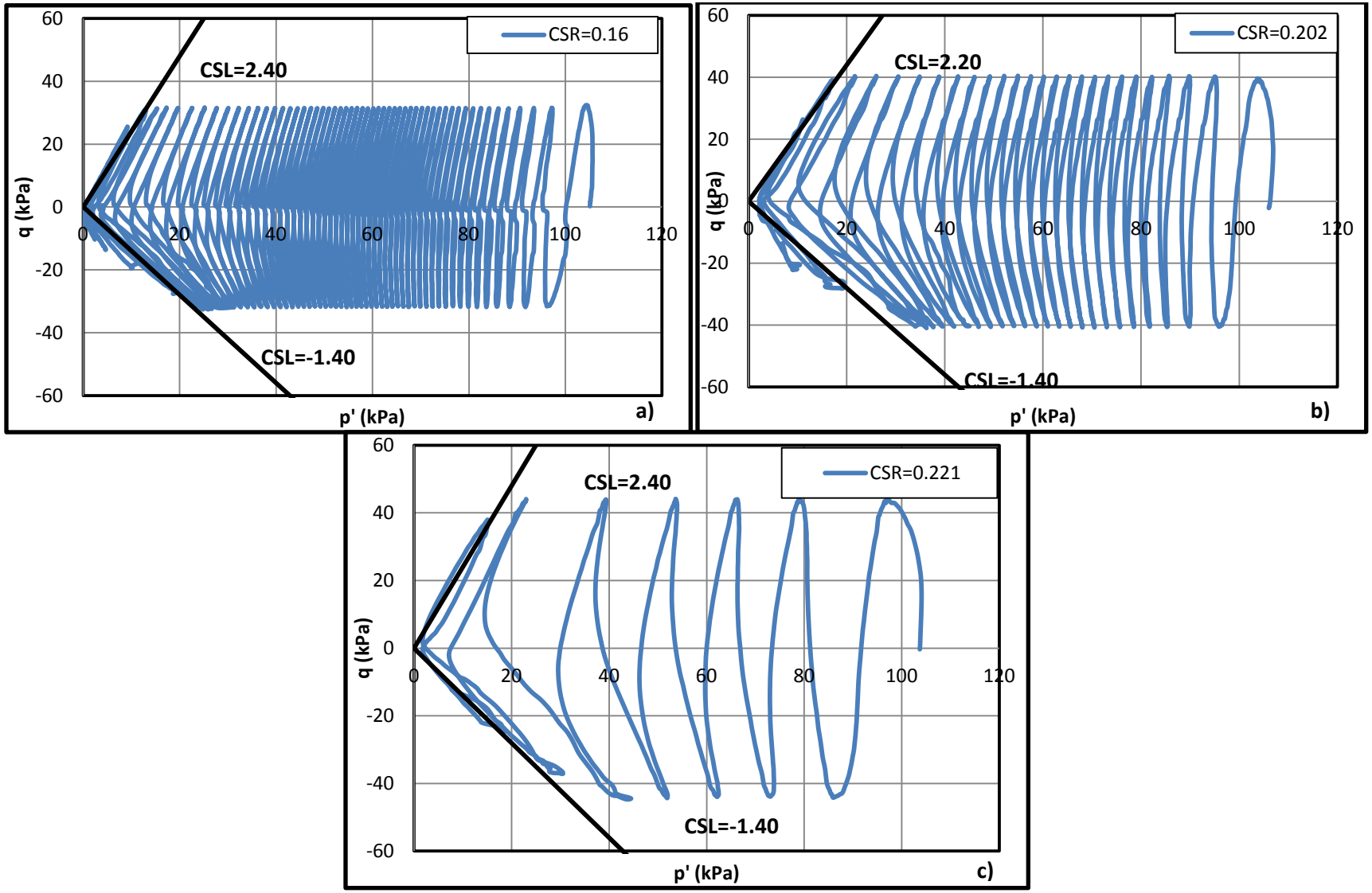

Figure 4.69. Deviator stress vs. Cambridge effective stress for Toyoura sand with 48.5% silica flour, 2% cement, 1% fibre at D_r=60%, σ_c'=100kPa a) CSR=0.160; b) CSR=0.202; c) CSR=0.221

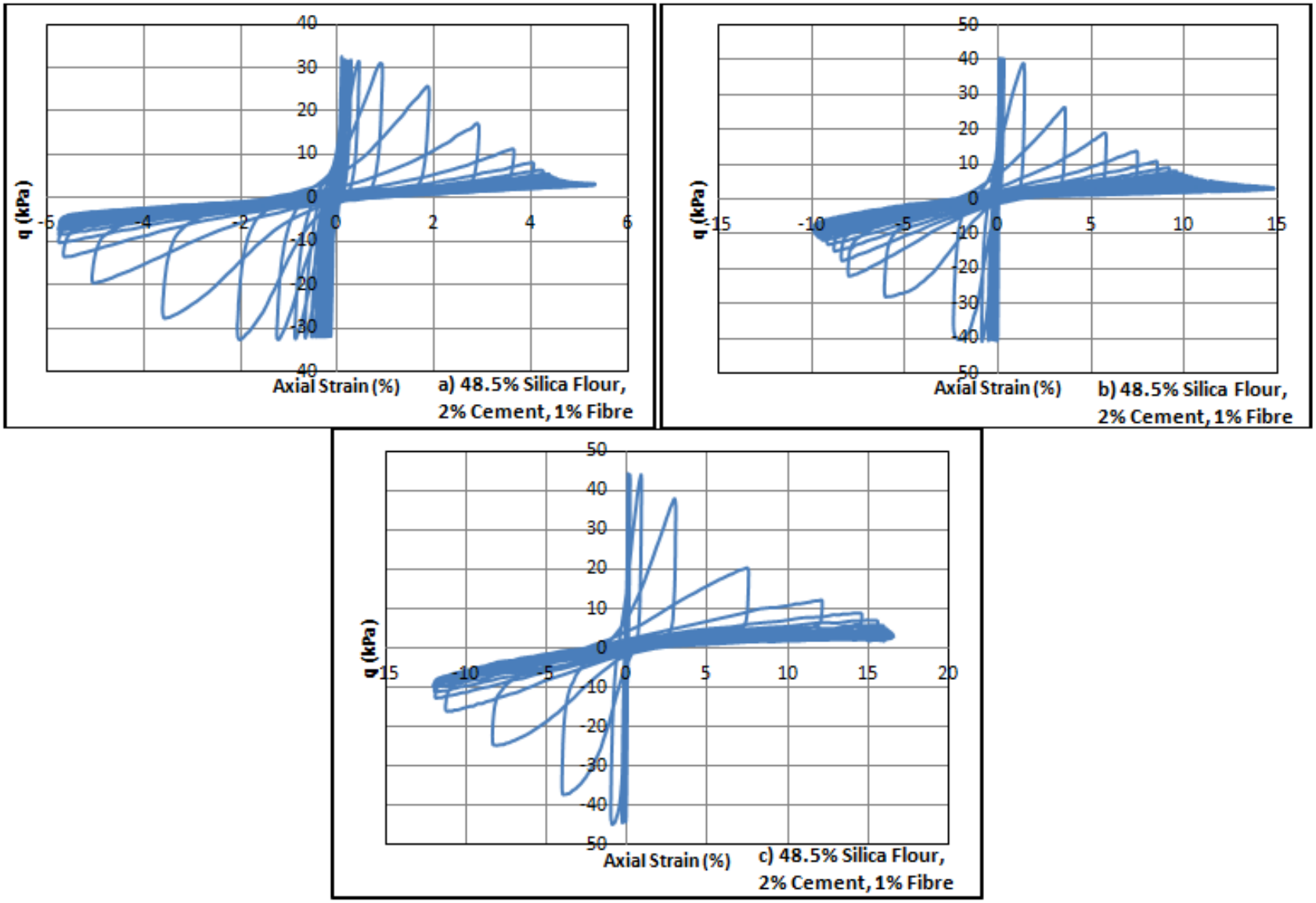

Figure 4.70. q vs. ε_a (%) for Toyoura sand with 48.5% silica flour, 2% cement, 1% fibre at D_r=60%, σ_c'=100kPa a) CSR=0.162; b) CSR=0.202; c) CSR=0.221

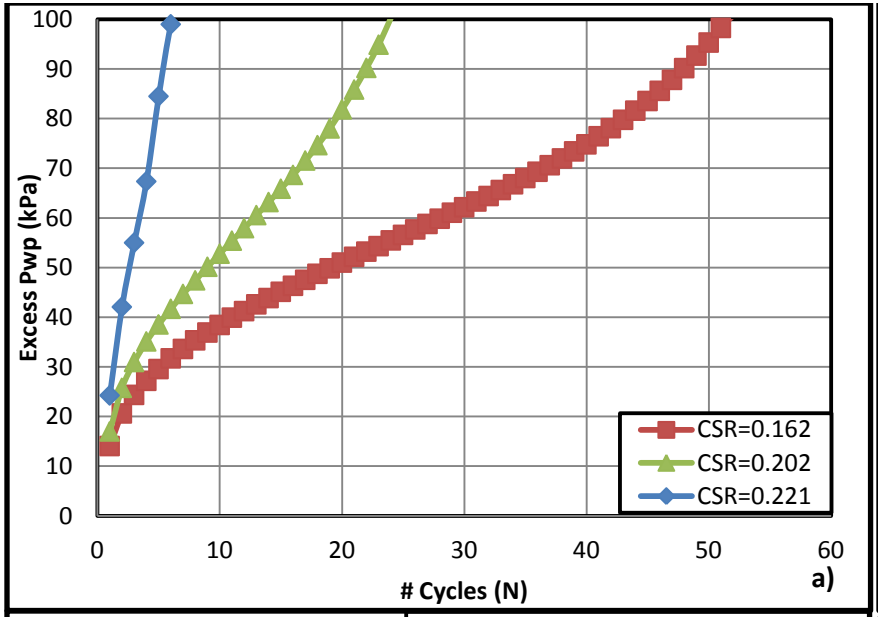
Excess Pwp (kPa)
# Cycles (N)
CSR=0.162
CSR=0.202
CSR=0.221
a)

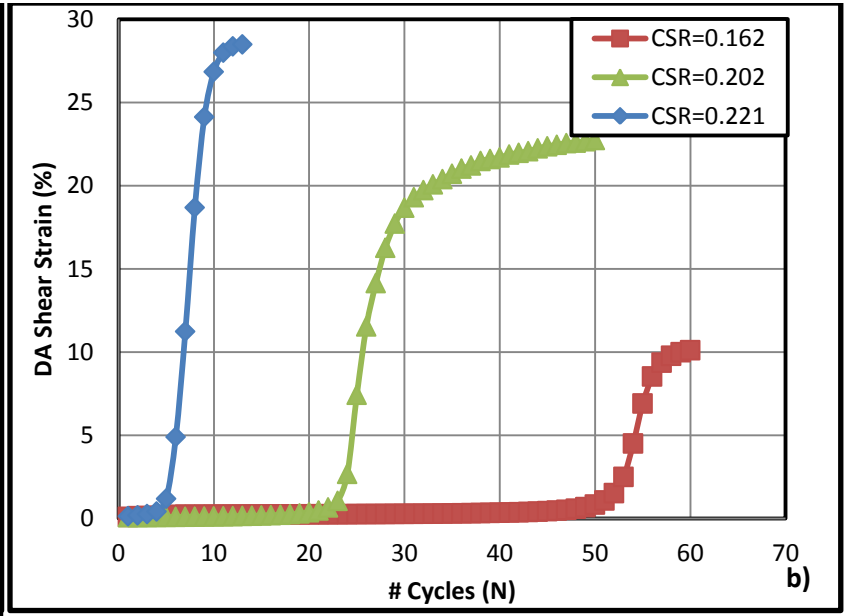
DA Shear Strain (%)
# Cycles (N)
CSR=0.162
CSR=0.202
CSR=0.221
b)

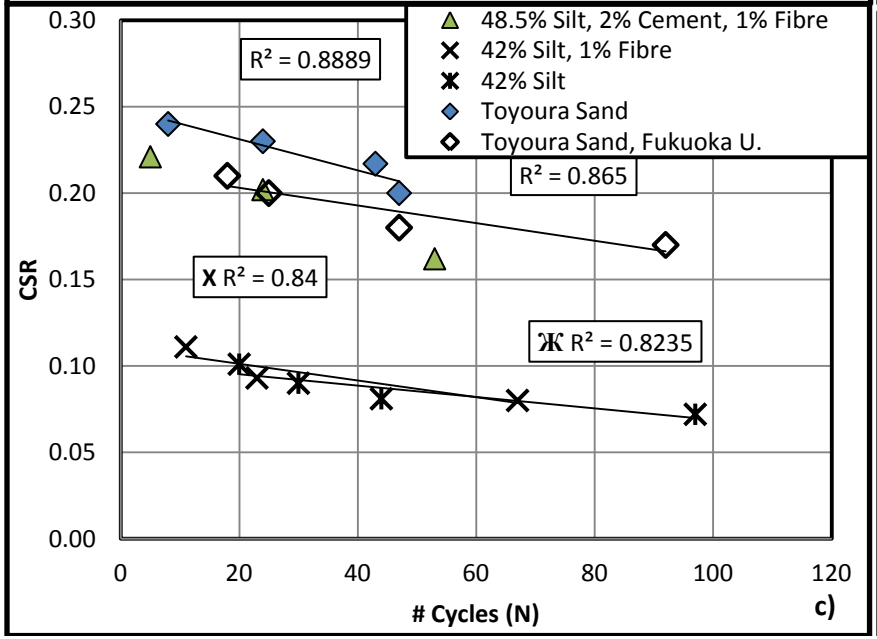
CSR
Cycles (N)
48.5% Silt, 2% Cement, 1% Fibre
42% Silt, 1% Fibre
42% Silt
Toyoura Sand
Toyoura Sand, Fukuoka U.
R² = 0.8889
R² = 0.865
X R² = 0.84
R² = 0.8235
c)

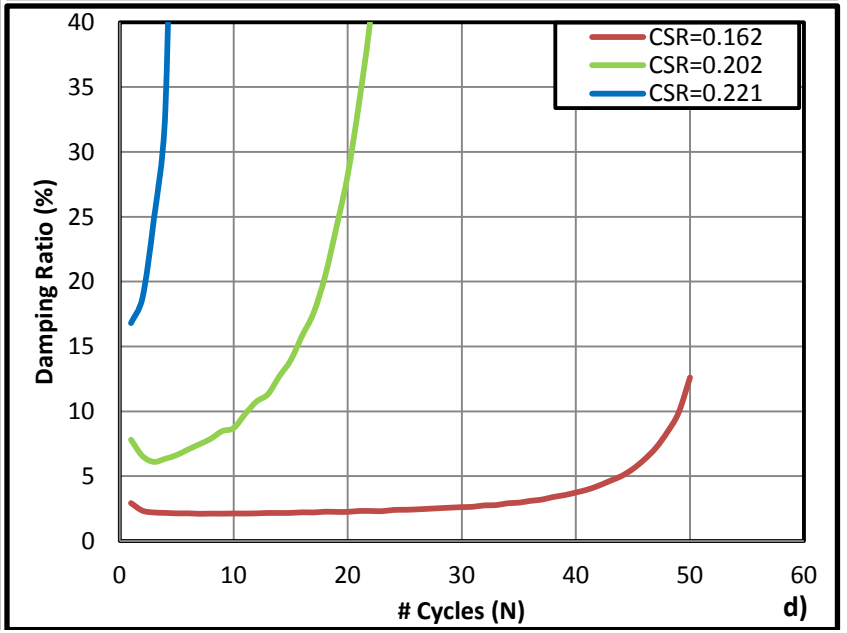
Damping Ratio (%)
# Cycles (N)
CSR=0.162
CSR=0.202
CSR=0.221
d)

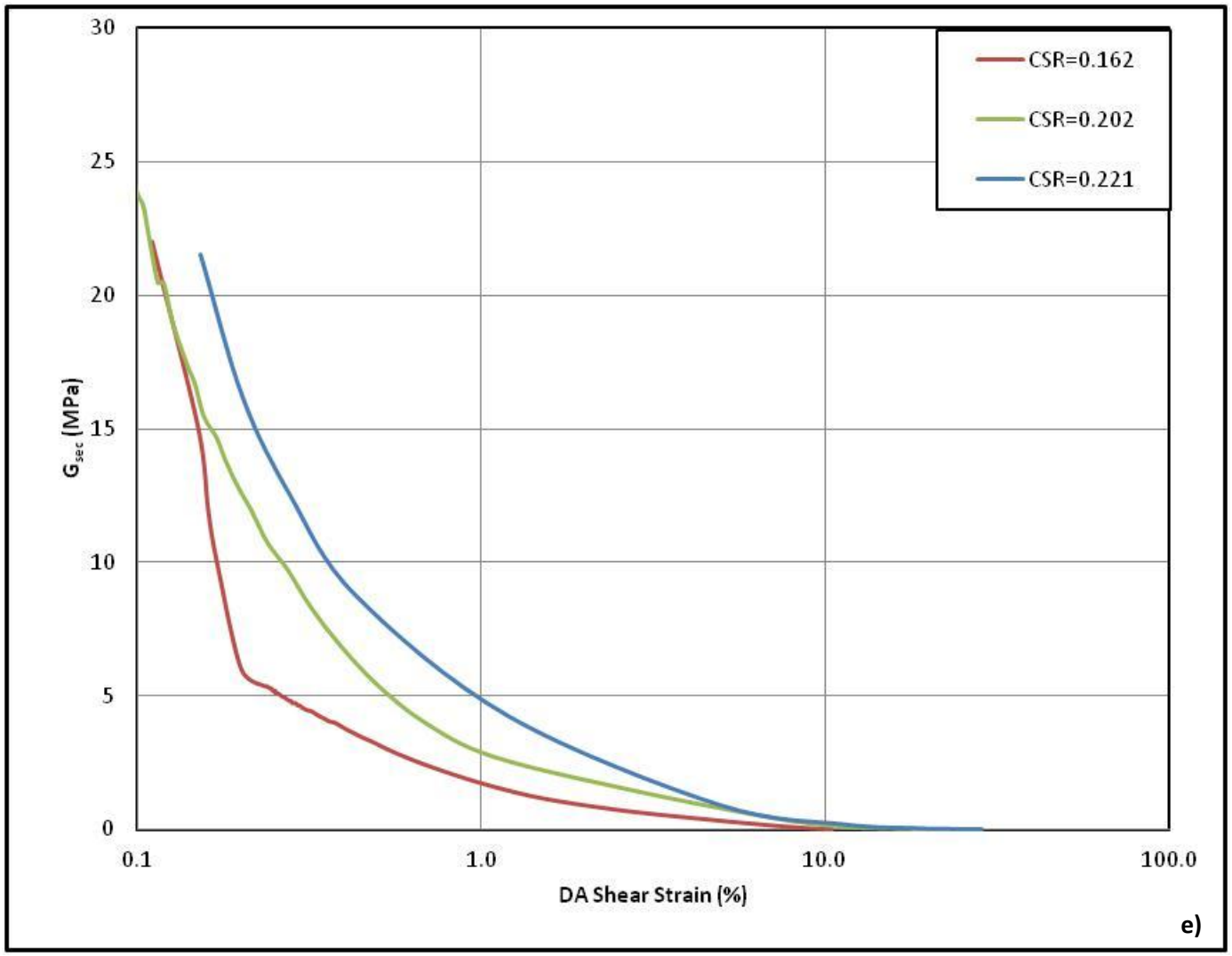

Figure 4.71. For Toyoura sand with 48.5% silica flour, 2% cement, 1% fibre at D_r=60%, σ_c'=100kPa a) excess pore pressure vs. N; b) DA shear strain vs. N; c) liquefaction resistance curve; d) damping ratio vs. N; e) G_{sec} vs. DA shear strain

4.7.5.3. Varying Silt, 2% Cement, 1% PVA Fibre, Various CSR

The effects of cement and fibre have been thoroughly and well documented in the literature. Trends from cyclic triaxial testing have matched closely with the results from other authors with respect to liquefaction resistance and plastic strain accumulation (Consoli et al., 2009; Nakamichi & Sato, 2013). The addition of silt to this mix has been examined far less, especially with respect to dynamic behaviour.

In the same manner as unstabilized silty sand the slope of the CSL for the Toyoura sand with 0-100% silica flour, 2% cement and 1% fibre decreases with increasing silica flour, from 2.30-1.50 in compression and 1.44-1.00 in extension, which is significantly higher than silt alone (Figure 4.72).

Using the same theories as were used for the Toyoura sand with 0-100% silica flour, 0-3% cement, and 0-2% fibre, a general idea of the behaviour of the combination of all three constituents can be formed. It is clear that the cement and fibre mixture provide significant improvement of the soil, hence the use of higher cyclic stress ratios. The addition of silt on the other hand was shown to reduce the liquefaction strength of the unstabilized samples and samples with 1% PVA fibre. This trend also held true for cemented, fibrous, silty Toyoura sand as shown in Figure 4.74c.

These tests were performed at B values ranging from 0.95-0.97. Examination of the excess pore water pressure build-up in Figure 4.74a shows the same initial jump seen in unstabilized silty Toyoura sand (Figure 4.41), followed by the linearly increasing trend of fibrous cemented samples indicating that the behaviours of the individual components can be essentially superimposed to estimate the behaviour of the combination (Kaniraj & Havanagi, 2001). This same principle of superposition holds true for the liquefaction strength with an increased CSR threshold, but a decreasing liquefaction resistance with increasing silt content.

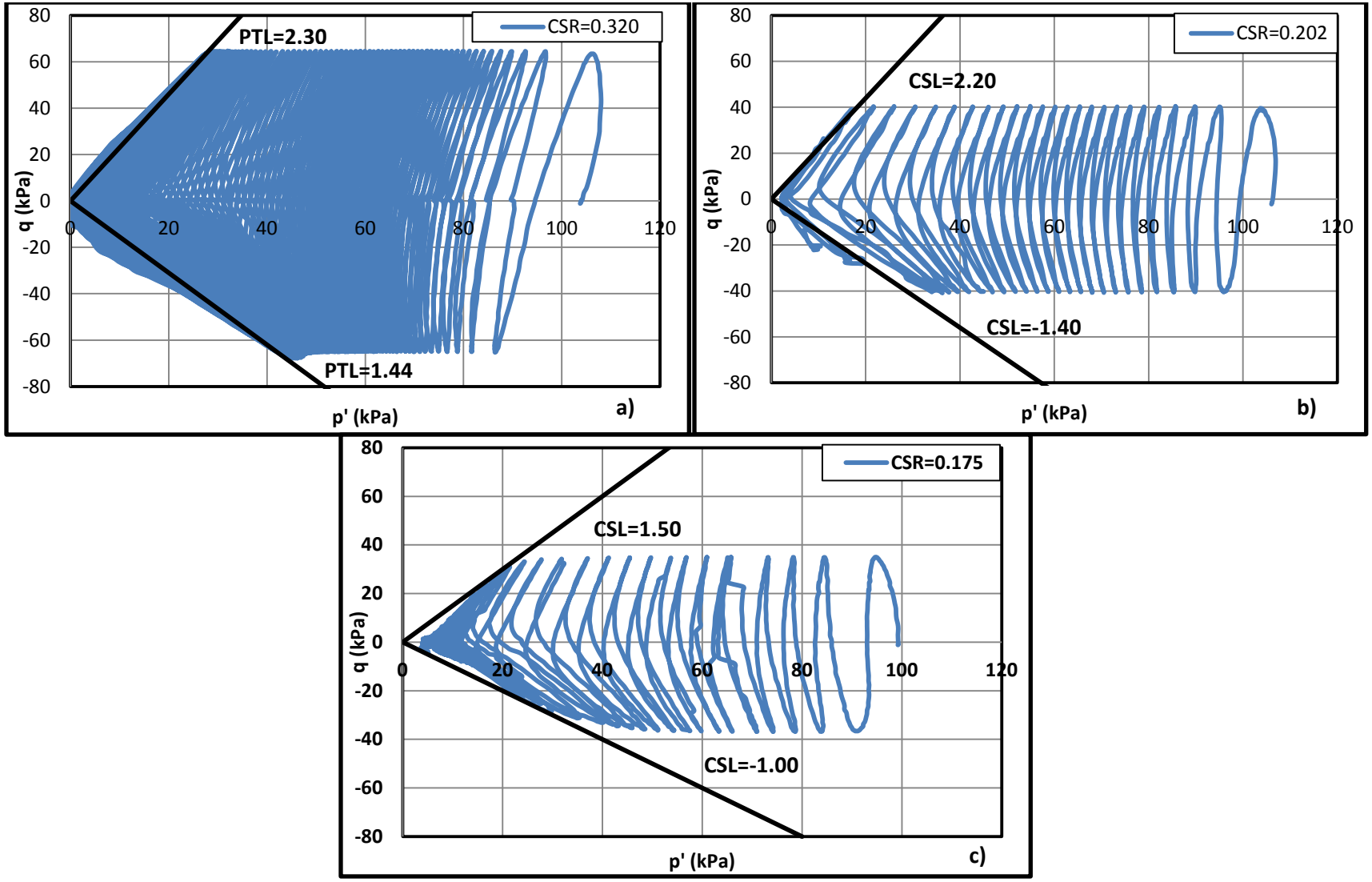

Figure 4.72. Deviator stress vs. Cambridge effective stress for Toyoura sand with 0-100% silica flour, 2% cement, 1% fibre at Dr=60%, σ_c'=100kPa
a) Toyoura sand, 2% cement, 1% fibre, CSR=0.320; b) 48.5% silica flour, 2% cement, 1% fibre, CSR=0.202; c) 100% silica flour, 2% cement, 1% fibre, CSR=0.175

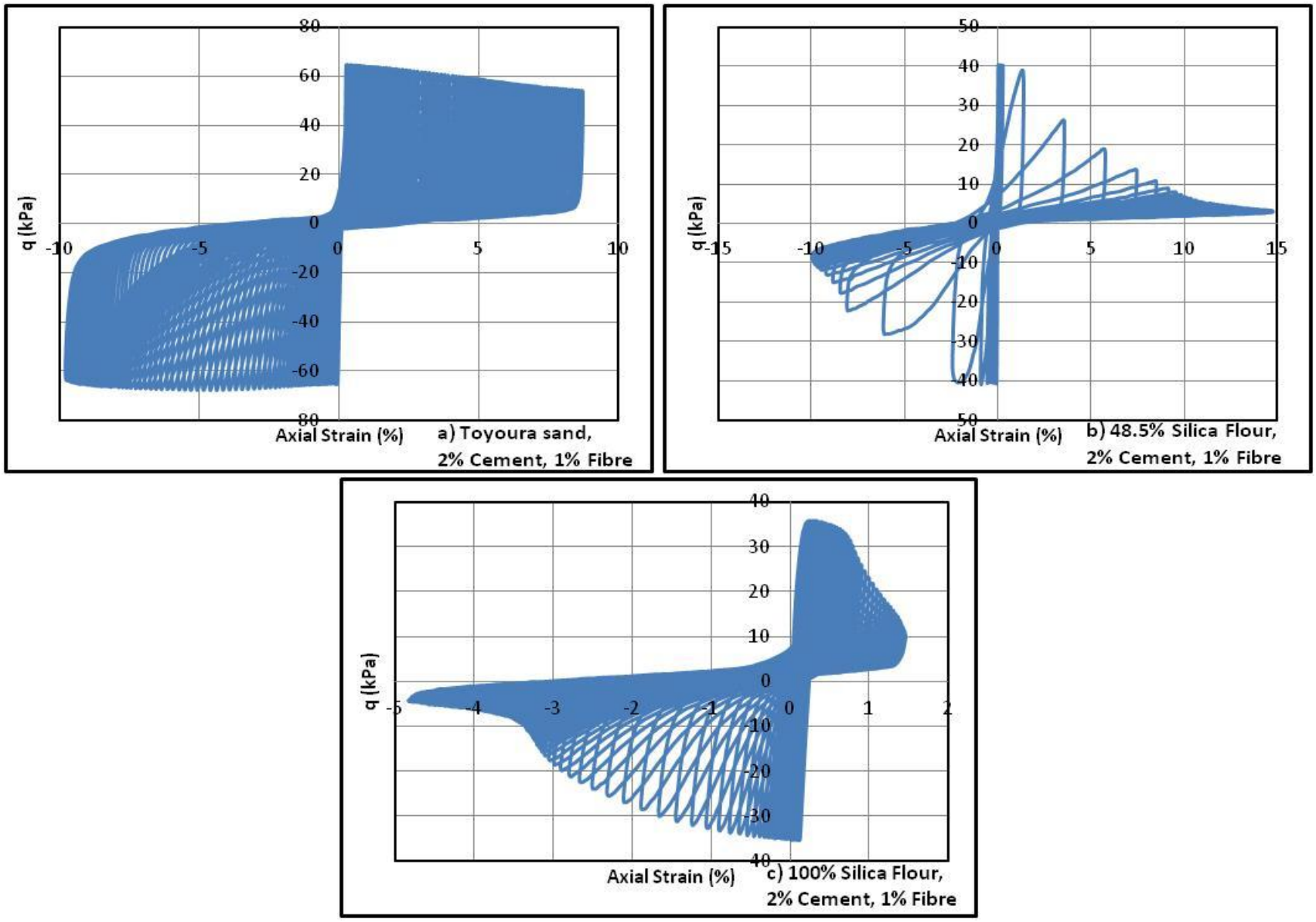

Figure 4.73. q vs. ε_a (%) for Toyoura sand with 0-100% silica flour, 2% cement, 1% fibre at Dr=60%, σc'=100kPa a) CSR=0.320; b) CSR=0.202; c) CSR=0.175

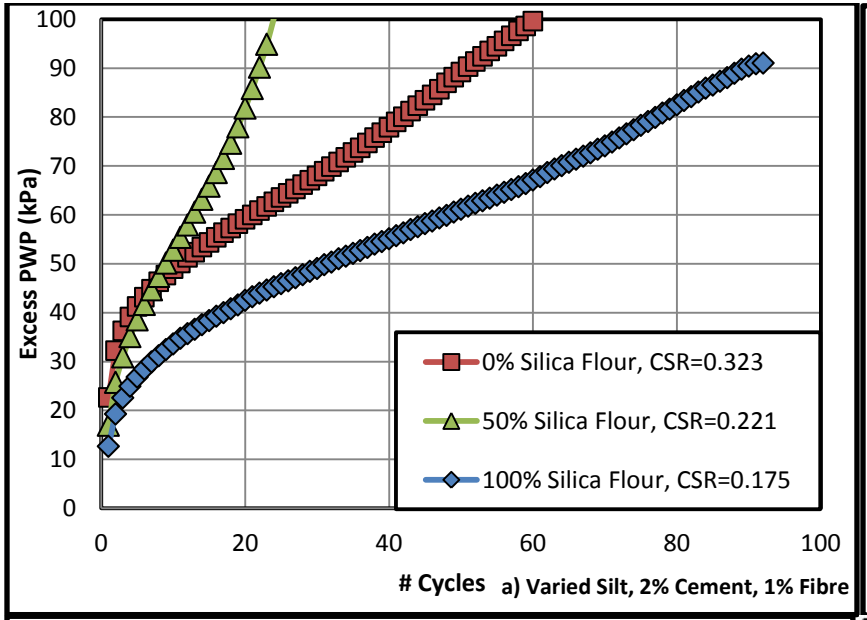
Excess PWP (kPa)
Cycles
a) Varied Silt, 2% Cement, 1% Fibre
0% Silica Flour, CSR=0.323
50% Silica Flour, CSR=0.221
100% Silica Flour, CSR=0.175

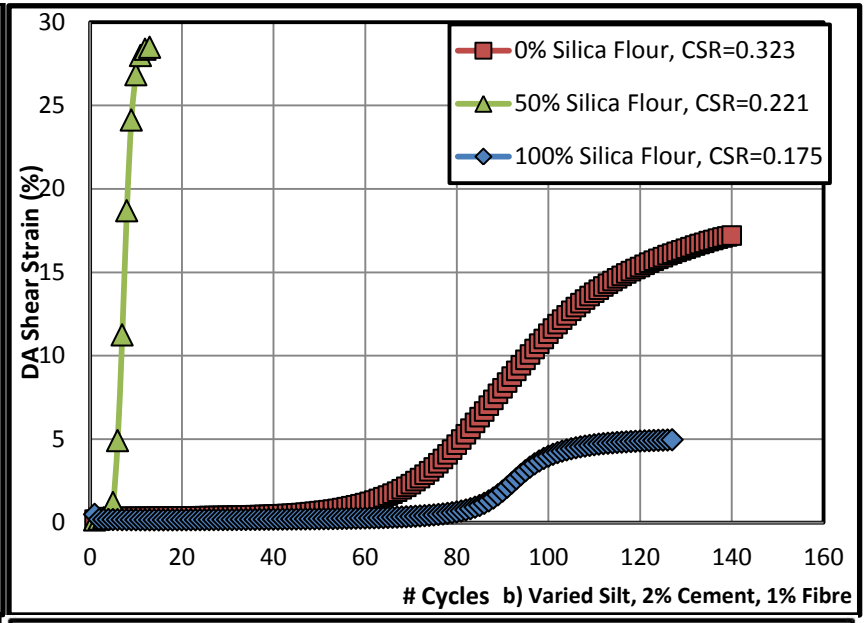
DA Shear Strain (%)
Cycles
b) Varied Silt, 2% Cement, 1% Fibre
0% Silica Flour, CSR=0.323
50% Silica Flour, CSR=0.221
100% Silica Flour, CSR=0.175

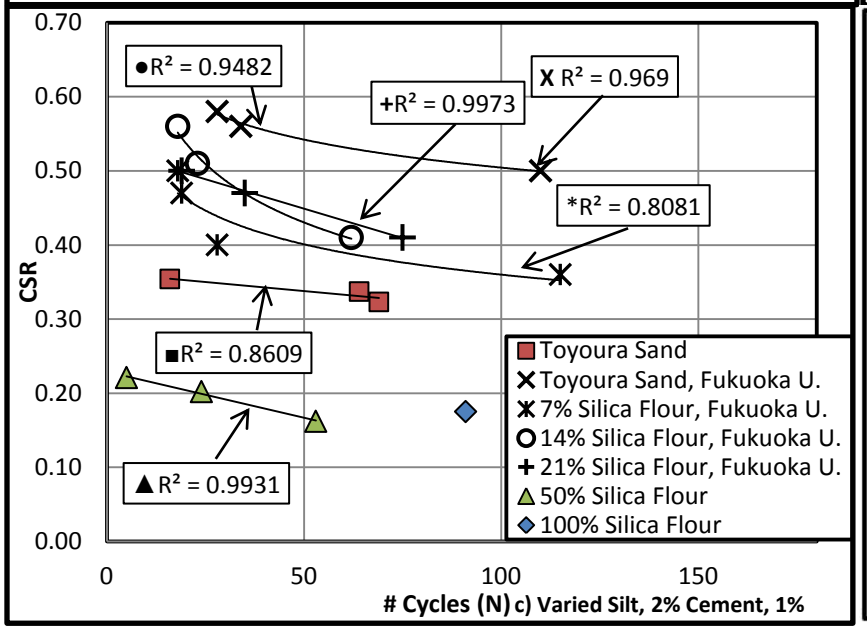
CSR
Cycles (N)
c) Varied Silt, 2% Cement, 1%
●R² = 0.9482
+R² = 0.9973
X R² = 0.969
*R² = 0.8081
■R² = 0.8609
▲R² = 0.9931
Toyoura Sand
Toyoura Sand, Fukuoka U.
7% Silica Flour, Fukuoka U.
14% Silica Flour, Fukuoka U.
21% Silica Flour, Fukuoka U.
50% Silica Flour
100% Silica Flour

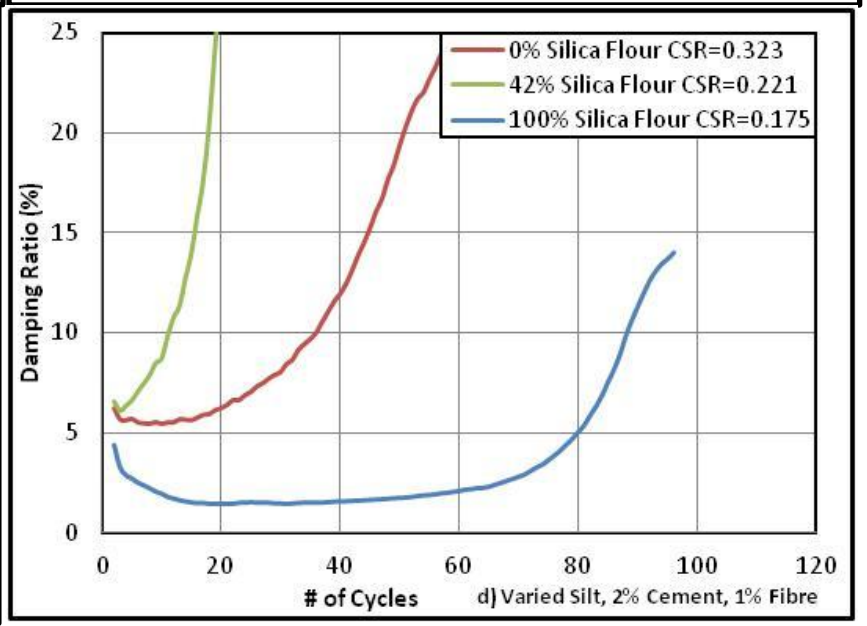
Damping Ratio (%)
# of Cycles
d) Varied Silt, 2% Cement, 1% Fibre
0% Silica Flour CSR=0.323
42% Silica Flour CSR=0.221
100% Silica Flour CSR=0.175

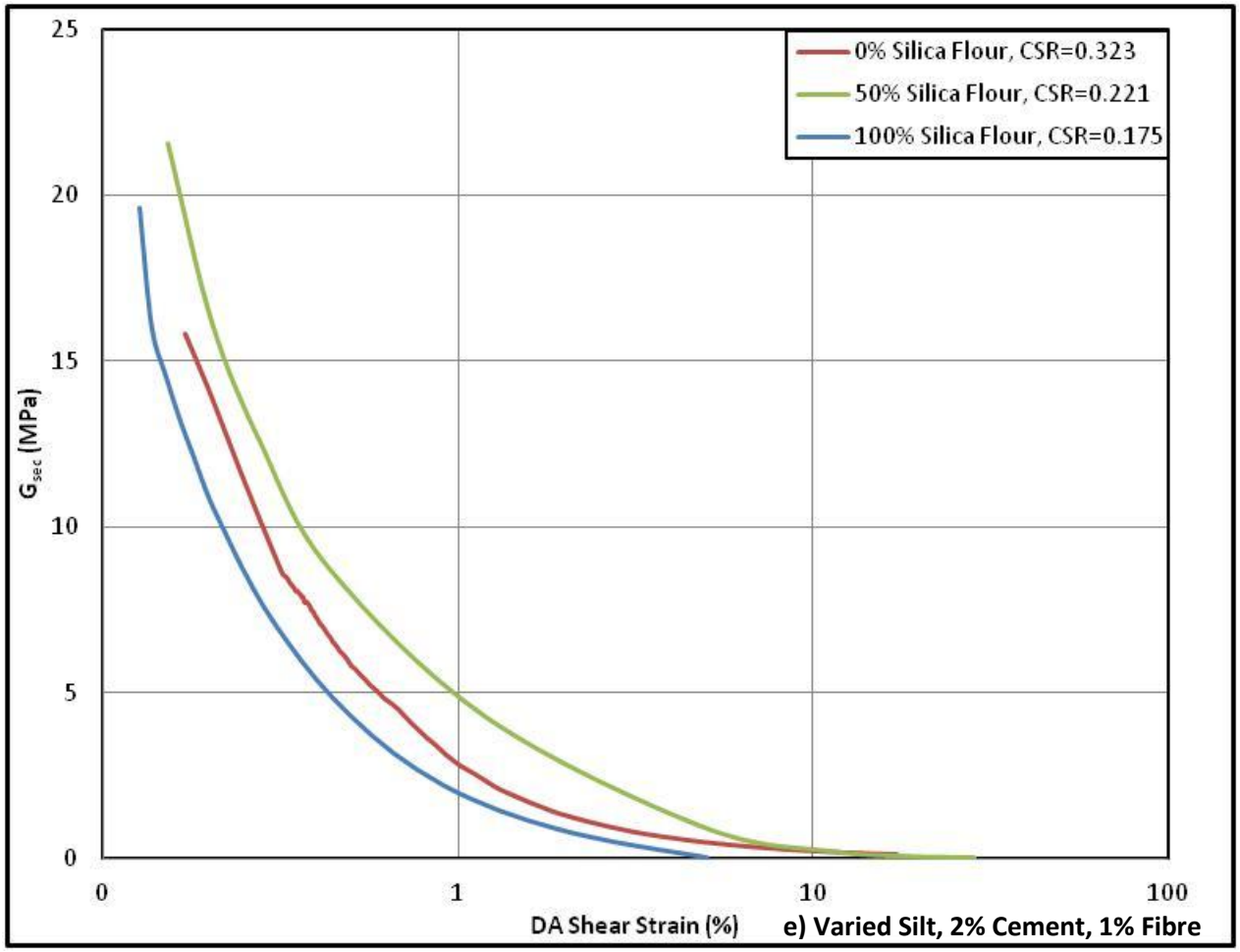

Figure 4.74. For Toyoura sand with 0-100% silica flour, 2% cement, 1% fibre at D_r=60%, σ_c'=100kPa a) excess pore pressure vs. N; b) DA shear strain vs. N; c) liquefaction resistance curve; d) damping ratio vs. N; e) G_{sec} vs. DA shear strain

4.8. Cyclic Triaxial Summaries

The following section summarizes the findings of Section 4.7. A series of normalized liquefaction resistance curves is presented for each data set to show the relative improvement over the base case of pure Toyoura sand. The cyclic stress ratio (CSR) is normalized over the CSR required to cause liquefaction in N=15 cycles (CSR/CSR_{15}).

The addition of the cement alone did not result in significant strength gain. The same was seen for increasing fibre addition, though a liquefaction resistance curve was not developed for the case of the Toyoura sand with 1% PVA fibre. Overall, it is clear that the combination of the cement and fibre additives is more effective for liquefaction mitigation than each component individually. This is represented by the higher CSR/CSR_{15} and the decreasing slope of the liquefaction resistance curve in Figure 4.75a. In terms of the damping ratio the addition of the cement caused a large increase, and a larger increase when combined with the cement and fibre. This increase was much larger for stabilized silty sand than for the pure Toyoura sand samples.

The addition of the silt was found to steadily decrease the liquefaction resistance of the Toyoura sand. At 42% silt addition, the peak concentration found in the Tokyo Bay region, the resistance was less than half that of the pure Toyoura sand as shown in Figure 4.75b. This same reduction was seen for the case of pure silt. In terms of the damping ratio the addition of the silt caused an initial decrease at 42% silt, followed by an increase at 100% silt. This matches the findings of (Kumar, Krishna, & Dey, 2013) who suggest that the damping continually decreases with an increase in silt content, though no research could be found on silt contents ranging from 0-100%.

When the cement and fibre additives were used to stabilize the silty Toyoura sand, a clear and significant improvement was seen (Figure 4.75c). As mentioned in Section 4.7, the effects of each

individual component were superimposed. The silt initially decreased the liquefaction resistance but the cement and PVA fibre addition then increased it closer to that of the pure Toyoura sand. In terms of the damping ratio, the addition of 42% silt lowered the initial value, whereas the cement increased it significantly. Again, the addition of the fibre as the sole stabilizer had minimal effect.

Finally, to summarize the effects of each individual additive (silt, cement, and PVA fibres) on the liquefaction resistance, the shear modulus, and the damping ratio, comparison graphs were developed in Figure 4.76-4.78. From Figure 4.76 it becomes clear that the fibre addition has a minimal effect on the liquefaction resistance and follows a parabolic curve for the number of cycles to reach a damping ratio of 5%. Figure 4.77 shows an improvement in liquefaction resistance with increasing cement, and a decreasing linear trend for the cycles to reach a damping ratio of 5%. When all of the additives are combined, the same principal of superposition discussed earlier applies. The liquefaction resistance decreases in a similar manner to that of silt. The shear modulus has a higher initial value but also decreases in the same way. Finally, the trend of the cycles to develop a damping ratio of 5% is decreasing as per the varied silt samples. It should be noted that the first two tests in Figure 4.78c were performed at a CSR of 0.20 whereas the rest were at a CSR of 0.10. The decreasing trend is still evident despite this fact.

Figures 4.79 and 4.80 show the effects of changing cement and silt content on the small-strain stiffness (Go), and reference CSRs (N=34) and damping ratios (5%).

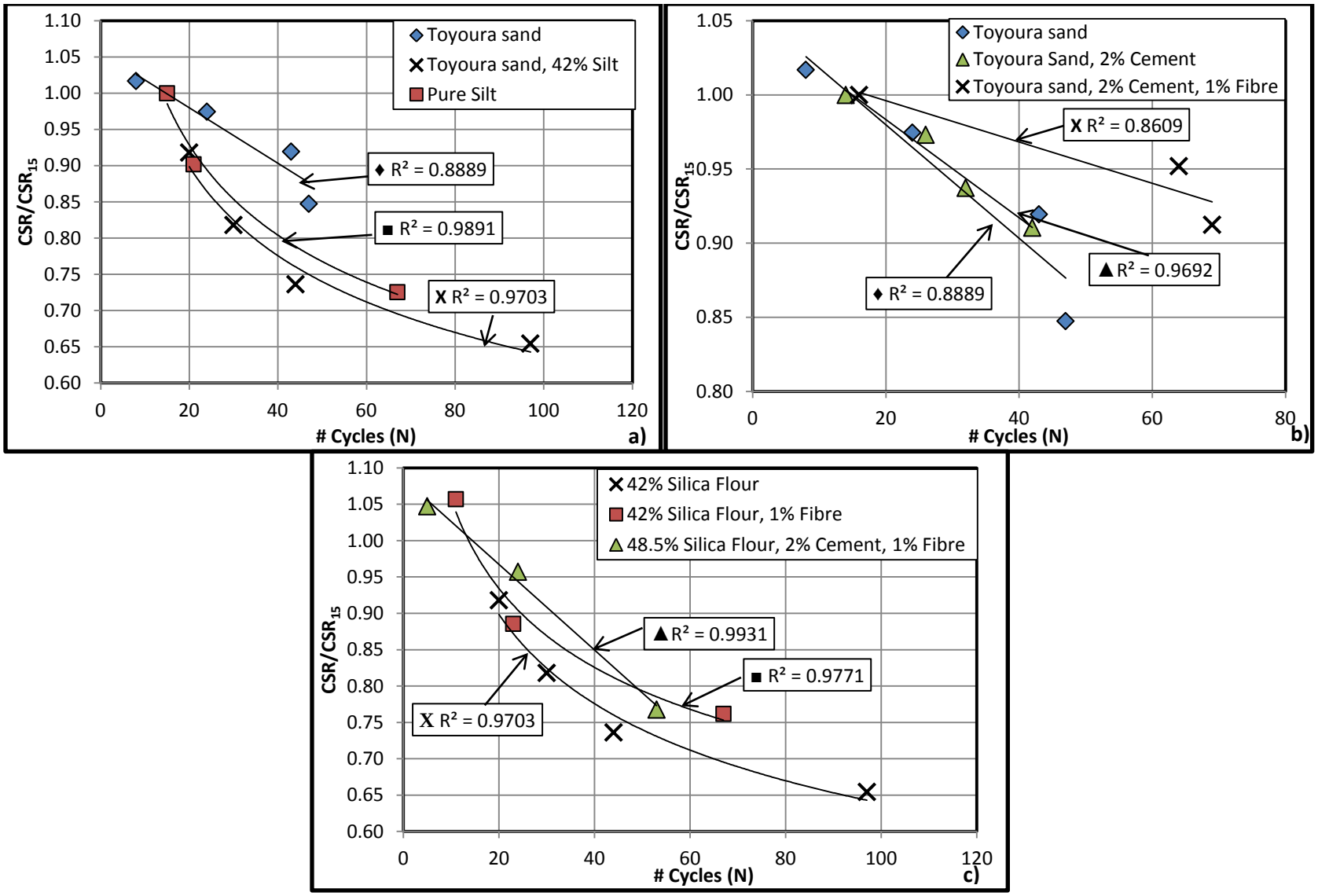

Figure 4.75. Normalized liquefaction resistance for Toyoura sand with a) varying silt; b) varying stabilizers c) 42% silt & varying stabilizers

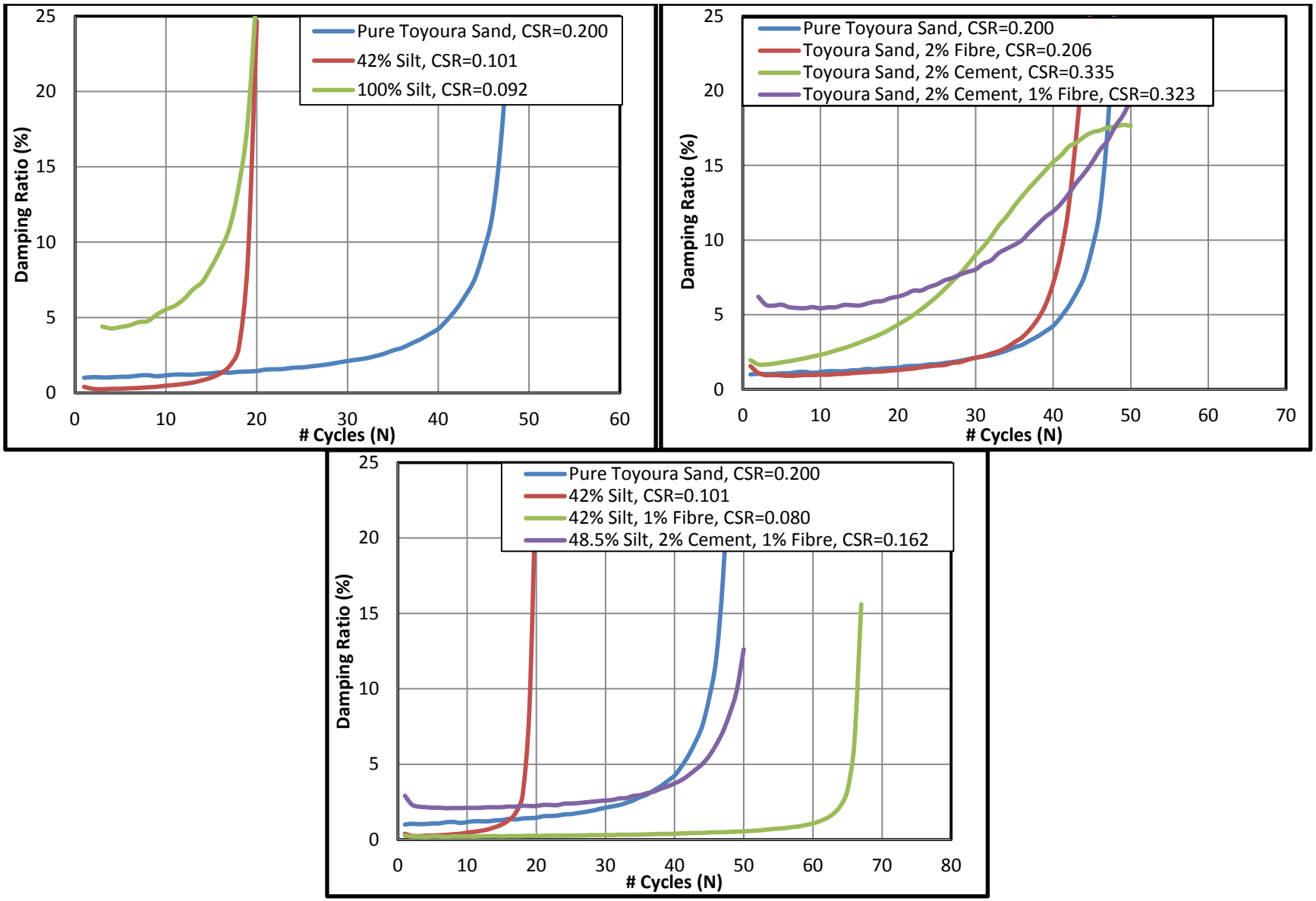

Figure 4.76. Damping ratio vs. N for Toyoura sand with a) varied silt; b) varying stabilizers; c) 42% silt & varying stabilizers

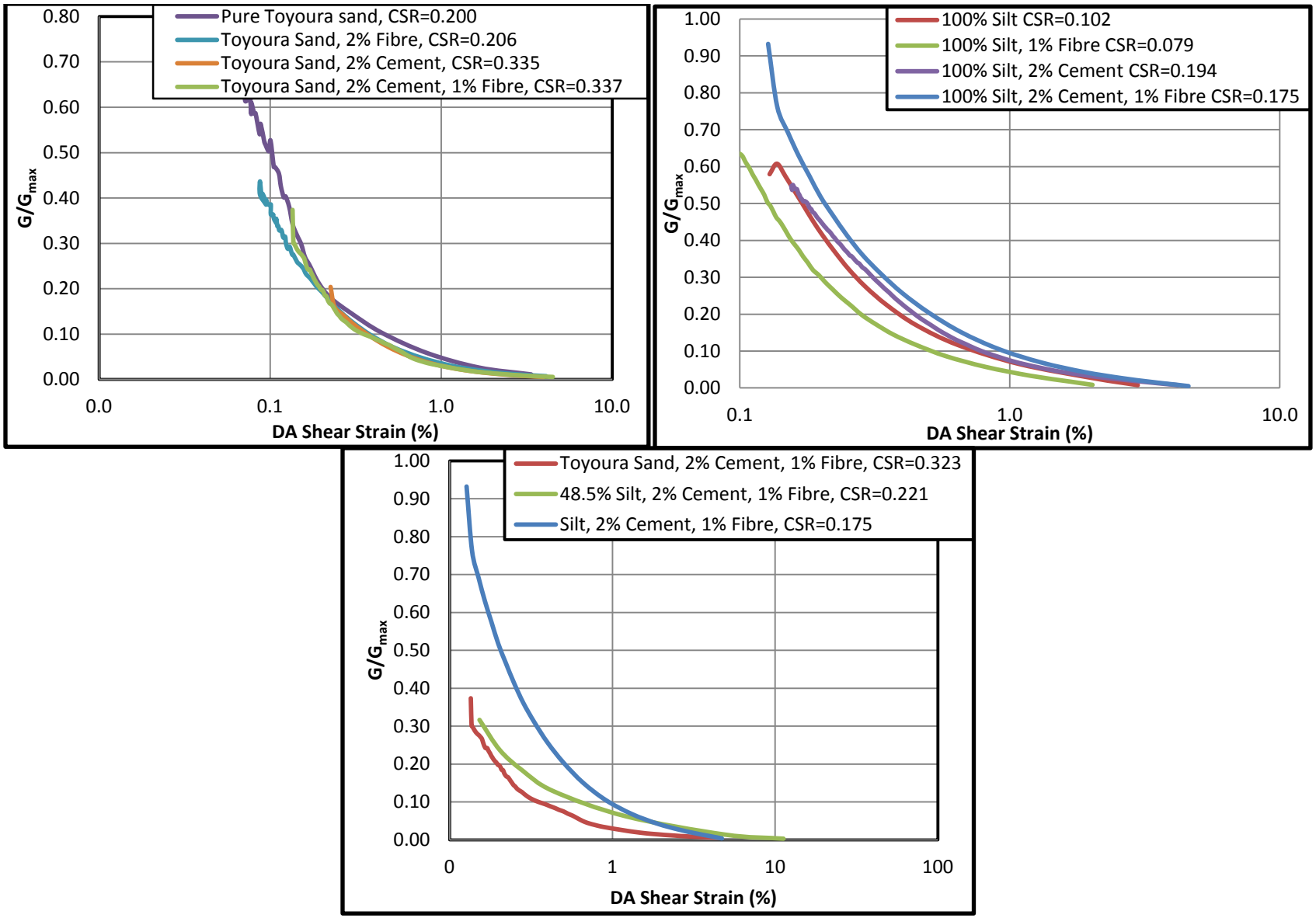

Figure 4.77. G/G_{max} vs. DA shear strain for a) Toyoura sand with varying stabilizers; b) 100% silt with varying stabilizers; c) varying silt & varying stabilizers

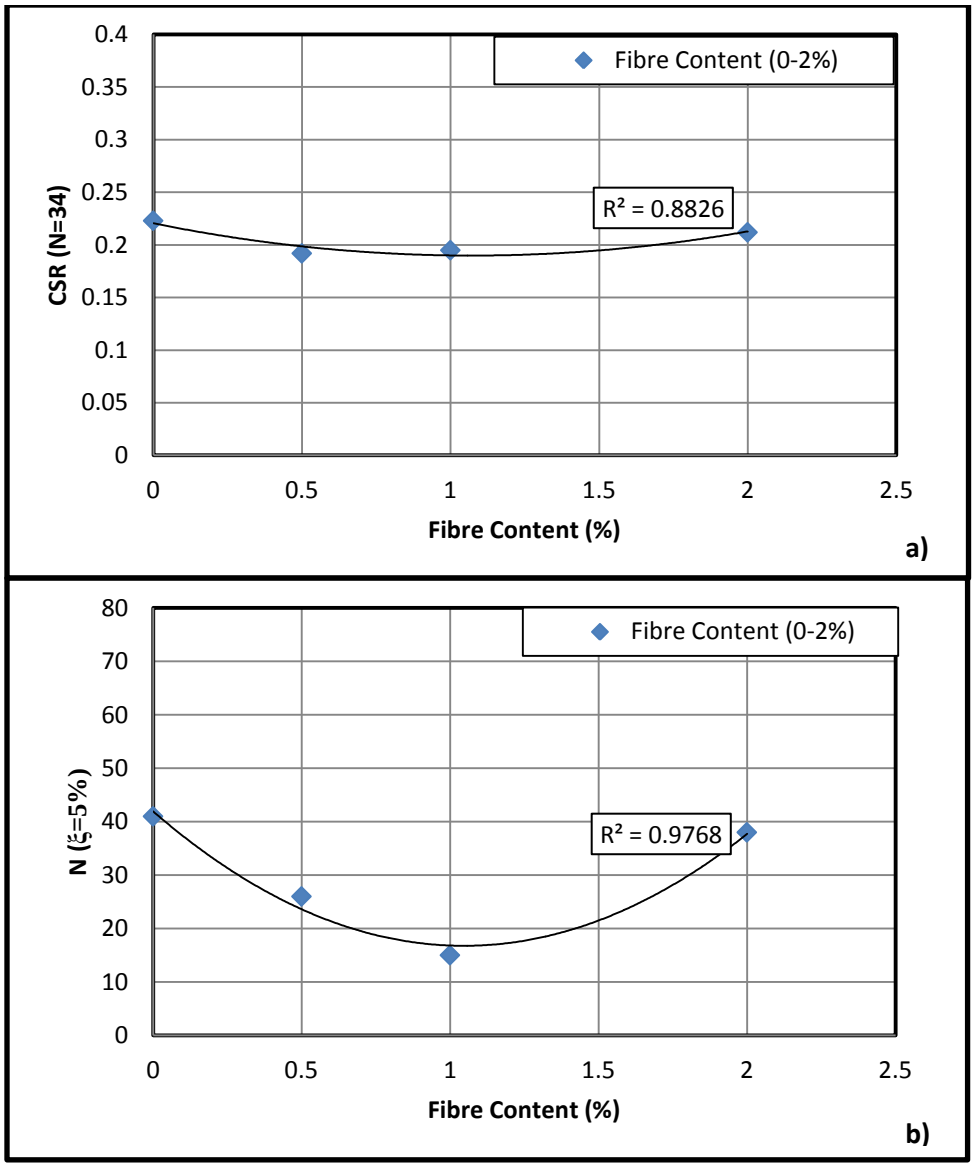

Figure 4.78. For Toyoura sand with 0-2% fibre a) $CSR_{N=34}$ vs. fibre content; b) N at ξ=5% vs. fibre content

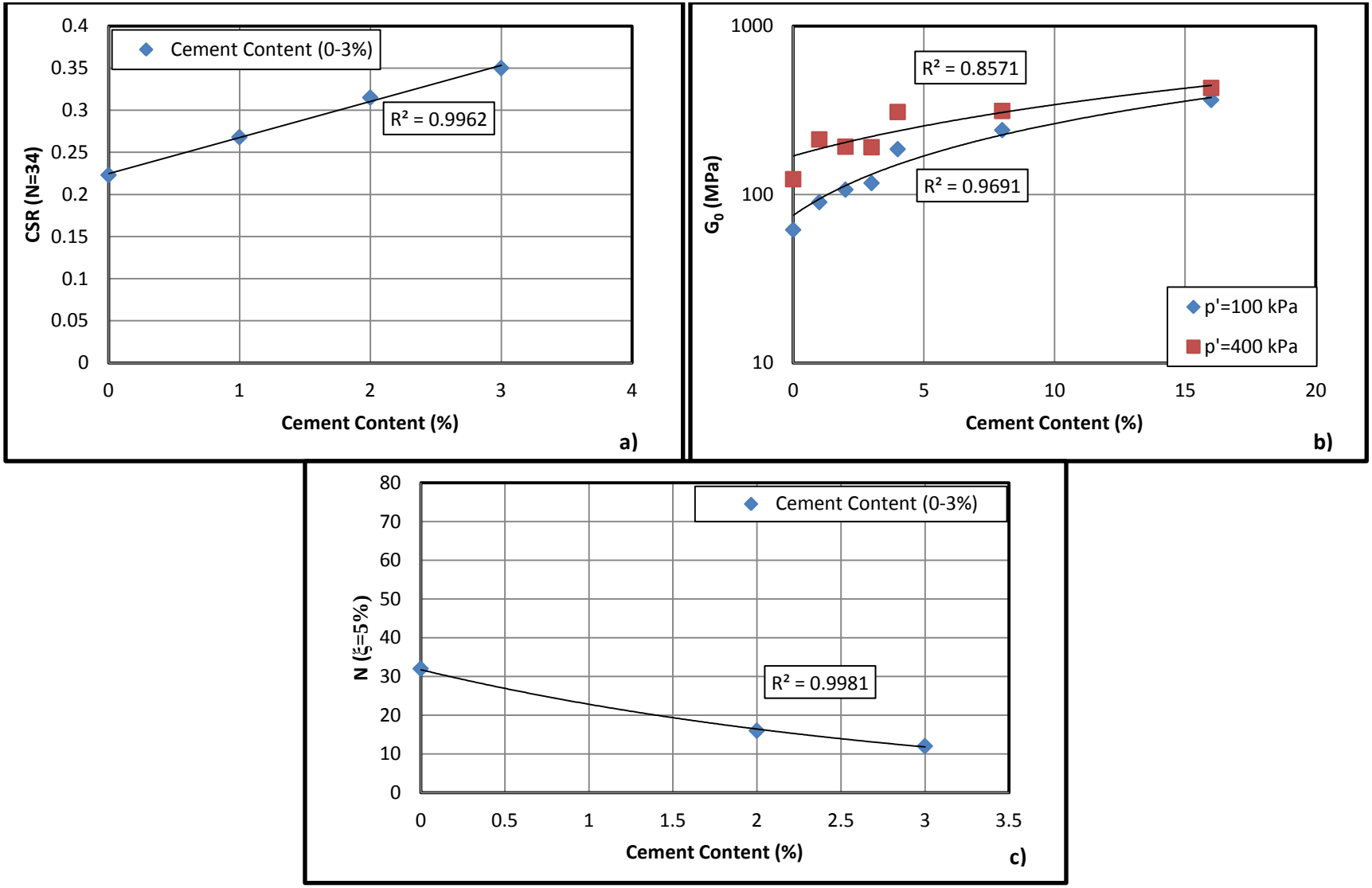

Figure 4.79. For 0-16% cement content a) $CSR_{N=34}$ vs. cement content; b) G_0 vs. cement content; c) N at ξ=5% vs. cement content

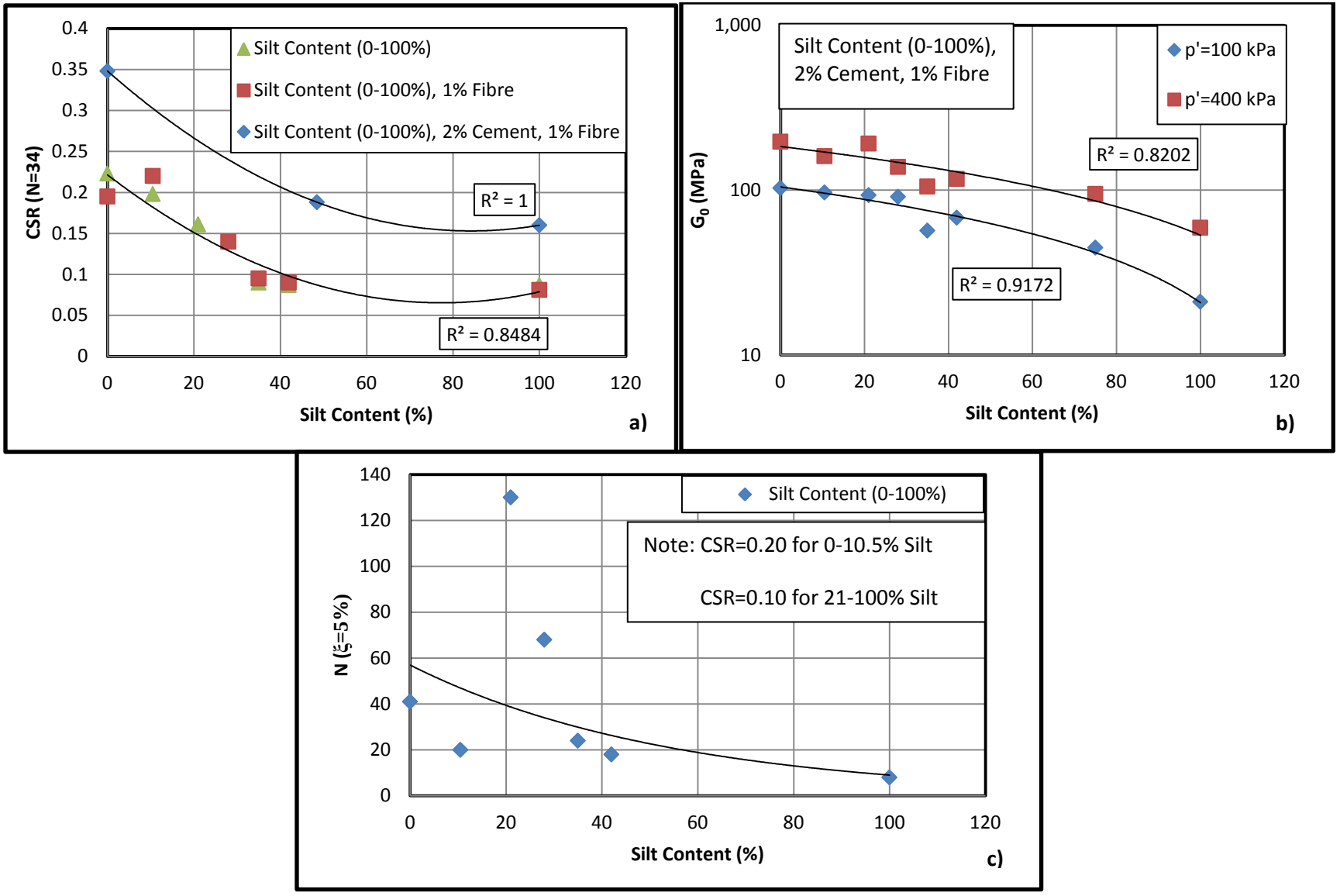

Figure 4.80. 0-100% silt content with and without cement and PVA fibre a) $CSR_{N=34}$ vs. cement content; b) G_0 vs. silt content; c) N at ξ=5% vs. silt content

Chapter 5: Conclusions and Future Work

5. Conclusions and Future Work

5.1. Introduction

The coastline of Japan, specifically the Tokyo Bay region, consists primarily of silty Toyoura sand; a highly liquefiable soil susceptible to loss of bearing strength and consequently large settlements and structural collapse. The mechanisms behind soil liquefaction have been studied since the 1910s, but mitigation of this phenomenon using recycled OPC and various natural and manmade fibres from disaster debris is a more recent development that has not been fully researched. The purpose of this thesis was to examine the microstructure of Toyoura sand with silt contents similar to those found in Tokyo Bay, and qualitatively examine how this changed when stabilized with OPC and PVA fibres. These microstructural changes were then related to the sort of macro scale behaviour that may have been witnessed during and after the Great East Japan Earthquake of 2011, via a regimen of lab testing consisting primarily of Rowe cell, bender element, and cyclic triaxial tests.

5.2. Findings of Study

From the SEM tests, direct shear tests, and CT scans it was found that both the Toyoura sand and the silica flour were angular to sub-angular soils with peak internal friction angles varying from 34.3° to 40.8°. When stabilized with Ordinary Portland Cement and PVA fibres, the cement coated the fibres and bonded them to the sand and silt, strengthening the soil despite the fact that the cement could not fully hydrate in the three day curing period used for this thesis. These nodules of unhydrated cement and the random fibre orientation would have caused some heterogeneity in the samples.

From the MIP testing of the cement and fibre stabilized silty sand, it became clear that the additives reduced pore diameter, and consequently pore volume and porosity. The addition of silt and cement caused the large pores to shrink and become micropores. This trend toward uniformity in the pore size distribution explained the increased tortuosity and decreased permeability of the silty and cemented samples and confirmed the trend seen in the maximum and minimum relative density of the silty sands.

In the large strain testing, each additive altered the behaviour of the Toyoura sand differently. In the Rowe cell testing, the silt addition decreased the constrained modulus until a concentration of 35% by mass, after which improvement was seen. This was due to the transference of the shear stresses from the granular structure to the silt matrix. The permeability constantly decreased with increased silt content due to the aforementioned increase in microporosity. This same trend was seen in oedometer testing and modelled using the approach of Pestana & Whittle (1995); though results for the constrained modulus were higher than those found in the Rowe cell. For the undrained shearing tests, this threshold was found to be closer to the 28% silt case. In static and dynamic testing, 100% silica flour was found to be the weakest soil, exhibiting low shear wave velocity, high compressibility (low α and high β), and low liquefaction resistance. In cyclic triaxial testing, the increasing proportion of silt constantly decreased the liquefaction resistance, shear modulus, and slope of the phase transformation line with no discernible threshold concentration. Increasing silt also prevented the pore water pressure ratio from reaching unity, though liquefaction based on other criteria still occurred.

Fibres improved the constrained modulus of the Toyoura sand at low concentrations (up to 1%) and increased compressibility at higher concentrations. In the bender element testing, the fibres caused virtually no change in the shear wave velocity, shear modulus or compressibility, though in undrained shearing the fibres were seen to increase compressibility and decrease the slope of the critical state line of the Toyoura sand. Contrary to the findings of Nakamichi & Sato (2013), the fibres reduced the

liquefaction resistance of the Toyoura sand, possibly due to the method of fibre addition. The fibres did, however, improve the resistance of the Toyoura sand to the development of large dynamic shear strains. The combination of the silt and fibres followed the same trends as mentioned above, with a slightly improved constrained modulus and the development of a yield point at 100 kPa, where the void ratio began to decline more rapidly. In samples of 100% silica flour, bender element testing and undrained shearing suggested that the fibres increase compressibility and decrease peak undrained shear strength slightly. There was no change in the build up of excess pore water pressure. In cyclic triaxial testing, the fibres slightly increased the slope of the PTL over that of the unstabilized silty sand and again reduce the speed of the build up of dynamic shear strains.

The addition of cement was found to have the least consistent behaviour, possibly due to the heterogeneity and the short curing time. For the Rowe cell tests, the cement addition provided little strength gain, though still reduced the permeability by an order of magnitude. In future testing, the experimental method should be optimized and matched more closely to that of Fukuoka University to establish a more accurate behavioural trend. Bender element results proved to establish a discernible trend due to the high range of tested cement concentrations. At 16% cement, the Toyoura sand was much stiffer and the shear wave velocity more than tripled, consequently dramatically improving the shear modulus as was suggested by Cha et al. (2014). Undrained shearing of the cemented sand increased the slope of the phase transformation and critical state line significantly, with large increases in undrained shear strength also developing. Results of cyclic triaxial testing suggested similar improvement, with the CSR increasing by over 50%, though not reaching the high values found by Nakamichi & Sato (2013). What was interesting to note was that the cemented samples no longer followed the sinusoidal build-up of excess pore water pressure, instead favouring a logarithmic trend. A suitable pore water pressure (damage) relationship could also be developed for this type of material.

5.3. Future Work

Although this thesis was quite comprehensive in its study of the effects of OPC and PVA fibres on the static and dynamic response of silty Toyoura sand, there is still a significant amount of research to be done in this area. Some of the issues that were encountered in this thesis led to assumptions that can be further clarified in future works. For example:

- Curing time for cemented soils should be increased to seven and thirty days to provide temporal estimates of soil strength;
- A more comprehensive examination of the volume of hydrated cement products should be performed to get a better estimate of the initial void ratio of cemented soils;
- Higher ranges of cement content should be tested to better complement the additive concentrations commonly used in the field and determine an optimum concentration;
- Higher ranges of fibre content should be tested to better optimize the additive percentage;
- Direct shear tests should be performed on Toyoura sand and silt with cement and/or fibre to determine the dilation angle and internal and critical state friction angles;
- Permeameter tests on Toyoura sand with cement and/or fibre should be performed to get a better estimate of initial permeability;
- Further collaboration with Fukuoka University in Japan should focus on silt contents ranging from 42-100% to acquire a full spectrum of soil behaviour.

Overall, this thesis tested a relatively narrow range of parameters for what could become a much larger project to optimize the stabilization of the silty Toyoura sand in and around the Tokyo Bay region of Japan. This thesis can be viewed as a starting point for the continuation of research into the cement and fibre stabilization of silty sands in similar materials around the world.

References

Abell, A. B., Willis, K. L., & Lange, D. A. (1999). MERCURY INTRUSION POROSIMETRY AND IMAGE ANALYSIS OF CEMENT-BASED MATERIALS. *Journal of Colloid and Interface Science* , 39-44.

Al-Attar, T. S. (2013). A Quantitative Evaluation of Bond Strength Between Coarse Aggregate and Cement Mortar in Concrete. *European Scientific Journal* , 46-61.

Amer, A., & Awad, A. (1974). Permeability of Cohesionless Soils. *Journal of Geotechnical and Geoenvironmental Engineering* , 1309-1316.

Amini, F., & Qi, G. (2000). Liquefaction Testing of Stratified Silty Sand. *Journal of Geotechnical and Geoenvironmental Engineering* , 208-217.

Andrews, D., & Martin, G. (2000). *Criteria for Liquefaction of Silty Soils.* 12WCEE.

Aon Benfield. (2011, August). *Tohoku Earthquake and Tsunami Event Recap Report.* Retrieved December 10, 2013, from Aon Benfield: http://thoughtleadership.aonbenfield.com/ThoughtLeadership/Documents/201108_ab_if_japan_eq_tsunami_event_recap.pdf

Askari, F., Dabiri, R., Shafiee, A., & Jafari, M. K. (2011). Liquefaction Resistance of Sand-Silt Mixtures Using Laboratory Based Shear Wave Velocity. *International Journal of Civil Engineering* , 135-144.

Askari, F., Dabiri, R., Shafiee, A., & Jafari, M. K. (2011). Liquefaction Resistance of Sand-Silt Mixtures Using Laboratory Based Shear Wave Velocity. *International Journal of Civil Engineering* , 135-144.

Atteberry, J. (2009, April 21). *How Scanning Electron Microscopes Work*. Retrieved December 5, 2014, from HowStuffWorks.com: http://science.howstuffworks.com/scanning-electron-microscope3.htm

Azuma, N. (2013). Audits in the Wake of the Great East Japan Earthquake. *International Journal of Government Auditing* .

Barden, L., McGown, A., & Collins, K. (1973). The Collapse Mechanism in Partly Saturated Soil. *Engineering Geology* , 49-60.

Bardet, J. (1997). *Experimental Soil Mechanics.* Upper Saddle River: Prentice-Hall.

Belkhatir, M., Arab, A., Della, N., & Schanz, T. (2012). Undrained monotonic pore presssure response of saturated silty sand soils. *Special Topics & Reviews in Porous Media* , 257-270.

Bellotti, R., Benoit, J., Fretti, C., & Jamiolkowski, M. (1997). Stiffness of Toyoura Sand from Dilatometer Tests. *Journal of Geotechnical and Geoenvironmental Engineering* , 836-846.

Bhattacharya, S., Hyodo, M., Goda, K., Tazoh, T., & Taylor, C. (2011). Liquefaction of soil in the Tokyo Bay area from the 2011 Tohoku (Japan) Earthquake. *Soil Dynamics and Earthquake Engineering* , 1618-1628.

Bolton, M. (1986). The Strength and Dilatancy of Sands. *Geotechnique* , 65-78.

Boulanger, R., & Idriss, I. (2004). *Evaluating the Potential for Liquefaction or Cyclic Failure of Silts and Clays.* Davis: Center for Geotechnical Modelling.

Boulanger, R., & Idriss, I. (2006). Liquefaction Susceptibility Criteria for Silts and Clays. *Journal of Geotechnical and Geoenvironmental Engineering* , 1413-1426.

Bray, J. D., Sancio, R. B., Durgunoglu, T., Onalp, A., Youd, T. L., Stewart, J. P., et al. (2004). Subsurface Characterization at Ground Failure Sites in Adapazari, Turkey. *Journal of Geotechnical and Geoenvironmental Engineering* , 673-685.

Builes, M., Garcia, E., & Riveros, C. A. (2008). *Dynamic and Static Measurements of Small Strain Moduli of Toyoura Sand.* Medellin, Colombia: GIGA Group, Faculty of Engineering, University of Antioquia.

Bullard, J. W., Jennings, H. M., Livingston, R. A., Nonat, A., Scherer, G. W., Schweitzer, J. S., et al. (2010). Mechanisms of Cement Hydration. *Cement and Concrete Research* , 1208-1223.

C.A.C. (2012). *Engineering Soil*. Retrieved May 22, 2014, from http://www.cement.ca/en/Engineered-Soil.html

Carraro, J., Bandini, P., & Salgado, R. (2003). Liquefaction Resistance of Clean and Non-Plastic Silty Sands Based on Cone Penetration Resistance. *Journal of Geotechnical and Geoenvironmental Engineering* , 965-976.

Carrier, W. D. (2003). Goodbye, Hazen; Hello, Kozeny-Carman. *Journal of Geotechnical and Geoevironmental Engineering* , 1054-1056.

Carter, M., & Bentley, S. (1991). *Correlations of Soil Properties.* London: Penetech Press Publishers.

CEB/FIB. (2000). *Stuctural Concrete: Textbook on Behaviour, Design and Performance.* Lausanne: Sprint-Druck Stuttgart.

Cha, M., Santamarina, J. C., Kim, H.-S., & Cho, G.-C. (2014). Small Strain Stiffness, Shear Wave Velocity, and Soil Compressibility. *Journal of Geotechnical and Geoenvironmental Engineering* .

Chapuis, R. P. (2004). Predicting the saturated hydraulic conductivity of sand and gravel using effective diameter and void ratio. *Canadian Geotechnical Journal* , 787-795.

Chaudhary, S. K., Kuwano, J., & Hayano, Y. (2013). Measurement of Quasi-Elastic Stiffness Parameters of Dense Toyoura Sand in HCA and Triaxial Apparatus with Bender Elements. *Geotechnical Testing Journal* , 1-13.

Chen, C.-W. (2006). *Drained and Undrained Behaviour of Fiber Reinforce Sand.* Columbia.

Chiaro, G., Koseki, J., & Sato, T. (2012). Effects of Initial Static Shear on Liquefation and Large Deformation Properties of Loose Saturated Toyoura Sand in Undrained Cyclic Torsional Shear Tests. *Soils and Foundations* , 498-510.

Cho, S.-W. (2012). Using Mercury Intrusion Porosimetry to Study the Interfacial Properties of Cement Based Materials. *Journal of Marine Science and Technology* , 269-273.

Clough, G., Iwabuchi, J., Rad, N., & Kuppusamy, T. (1989). Influence of cementation on liquefaction of sands. *Journal of geotechnical engineering* , 1102-1117.

Coduto, D. P., Yeung, M.-C. R., & Kitch, W. A. (2011). *2nd Edition Geotechnical Engineering Principles and Practices.* Upper Saddle River: Pearson Higher Education Inc.

Collins, R. W. (2011). *Stabilization of marginal soils using geofibres and nontraditional additives.* Fairbanks: University of Alaska Fairbanks.

Consoli, N., Bassani, M., & Festugato, L. (2010). Effect of Fiber Reinforcement on the Strength of Cemented Soils. *Geotextiles and Geomembranes* , 344-351.

Consoli, N., Vendruscolo, M., Fonini, A., & Dalla Rosa, F. (2009). Fibre reinforcement effects on sand considering a wide cementation range. *Geotextiles and geomembranes* , 196-203.

Cubrinovski, M., & Rees, S. (2008). Effects of Fines on Undrained Behaviour of Sands. *Geotechnical Earthquake Engineering and Soil Dynamics* , 1-11.

Dafalias, Y. F., & Taiebat, M. (2011, July). *Earthquake Liquefaction Hazards Assessments at Nuclear Power Plant Sites.* Retrieved April 2, 2013, from Democritus: http://www.demokritos.gr/library/downloads/docs/documents/events/dafalias.pdf

Dano, C., Hicher, P., & Tailliez, S. (2004). Engineering Properties of Grouted Sands. *Journal of Geotechnical and Geoenvironmental Engineering* , 328-338.

Day, R. W. (2006). *Foundation Engineering Handbook.* New York: McGraw-Hill.

De, S., & Basudhar, P. K. (2008). Steady State Strength Behaviour of Yamuna Sand. *Geotechnical and Geological Engineering* , 237-250.

Department of the Army Corps of Engineers. (1984). *Soil Stabilization for Pavements Mobilization Construction.* Washington: U.S. Army Corps of Engineers.

Derakhshani, A., Takahashi, N., Bahmanpour, A., Yamada, S., & Towhata, I. (2011). Experimental study on effects of underground columnar improvement on seismic behaviour of quay wall subjected to liquefaction. *Pan-Am CGS Geotechnical Conference.* Toronto: Canadian Geotechnical Society.

Dobry, R., Ladd, R., Yokel, F., Chung, R., & Powell, D. (1982). *Prediction of pore water pressure buildup and liquefaction of sands during earthquakes by the cyclic strain method.* Gaithersburg: NBS Building Science Series.

Dvorkin, J., & Yin, H. (1995). Contact laws for cemented grains: implications for grain and cement failure. *International Journal of Solids and Structures* , 2497-2510.

Dysli, M., & Steiner, W. (2011). *Correlations in Soil Mechanics.* PPUR.

Dyvik, R., & Madshus, C. (1985). Lab Measurements of GMax Using Bender Elements. *Advances in the Art of Testing Soils Under Cyclic Conditions* (pp. 186-196). Detroit: ASCE.

El Mohtar, C. (2009). Evaluation of the 5% double amplitude stain criterion. *The Academia and Practice of Geotechnical Engineering* (pp. 80-83). Alexandria: ICSMGE.

ElTakch, A. (2013). *Cyclic and Post-Cyclic Response of Silt and Sandy Silt Soils.* London: The University of Western Ontario.

Galle, C. (2011). Effect of drying on cement-based materials pore structure as identified by mercury intrusion porosimetry A comparative study between oven-, vacuum-, and freeze-drying. *Cement and Concrete Research* , 1467-1477.

GDS Instruments Internal Product Testing. (n.d.). GDS Bender Elements System. Hampshire, U.K.: GDS Instruments.

Ghassemi, A., & Pak, A. (2010). Pore Scale Study of Permeability and Tortuosity for Flow Through Particulate Media Using Lattice Boltzmann Method. *International Journal for Numerical and Analytical Methods in Geomechanics* .

Gray, D. H. (1988). *Constitutive Behaviour of Fiber Reinforced Sands.* Michigan: Air Force Office of Scientific Research.

Gray, D. H., & Refeai, T. A. (1986). Behaviour of Fabric vs. Fiber Reinforced Sand. *Journal of Geotechnical Engineering* , 804-820.

Gray, D., & Maher, M. (1989). Admixture Stabilization of Sands with Discrete, Randomly Distributed Fibers. *XII International Conference on Soil Mechanics and Foundation Engineering.* Rio, Brazil.

GUTIERREZ, G. A. (2007). *Influence of Late Cementation on the Behaviour of Reservoir Sands.* London.

Harris, C., Davies, M. C., & Etzelmuller, B. (2001). The Assessment of Potential Geotechnical Hazards Associated with Mountain Permafrost in a Warming Global Climate. *Permafrost and Periglacial Processes* , 145-156.

Head, K. H. (1986). *Manual of Laboratory Testing Volume 3: Effective Stress Tests.* New York: ELE International Limited.

Hecht, J. (2014, April 26). Slo-mo Tremors Make Big Tokyo Quake More Likely. New Scientist.

Heineck, K., Coop, M., & Consoli, N. (2005). Effect of microreinforcement of soils from very small to very large shear strains. *Journal of geotechnical and geoenvironmental engineering* , 1024-1033.

Helland, P., Huang, P.-H., & Diffendal Jr., R. (1997). SEM Analysis of Quartz Sand Grain Surface Texture Indicates Alluvial/Colluvial Origin of the Quaternary "Glacial" Boulder Clays at Huangshan (Yellow Mountain), East-Central China. *Quaternary Research , 48*, 177-186.

HongNam, N., Koseki, J., & Sato, T. (n.d.). Effect of Specimen Size on Quasi-Elastic Properties of Toyoura Sand in Hollow Cylinder Triaxial and Torsional Shear Tests. *Geotechnical Testing Journal* .

Hyodo, M., Tanimizu, H., Yasufuku, N., & Murata, H. (1994). Undrained Cyclic and Monotonic Triaxial Behaviour of Saturated Loose Sand. *Soils and Foundations* , 19-32.

Ibraim, E., & Fourmont, S. (2006). Behaviour of sand reinforced with fibres. Soil stress-strain behaviour: Measurement, Modeling and Analysis. *Geotechnical Symposium.* Roma.

Ibraim, E., Diambra, A., Russell, A., & Muir Wood, D. (2013). Fibre Reinforced Sands: From Experiments to Modelling and Beyond. *International Journal for Numerical and Analytical Methods in Geomechanics* , 2427-2455.

Idriss, I., & Boulanger, R. (2006). Semi-empirical procedures for evaluating liquefation potential during earthquakes. *Soil dynamics and earthquake engineering* , 115-130.

III, W. D. (2003). Goodbye, Hazen; Hello, Kozeny-Carman. *Journal of Geotechnical and Geoenvironmental Engineering* , 1054-1056.

Ingles, O., & Metcalf, J. (1973). *Soil Stabilization Principles and Practice.* New York: John Wiley and Sons.

Ishihara, K. (1993). Liquefaction and flow failure during earthquakes. *Geotechnique* , 46-72.

Ishitsuka, K., Tsuji, T., & Matsuoka, T. (2012). Detection and Mapping of Soil Liquefaction in the 2011 Tohoku Earthquake Using SAR Interferometry. *Earth Planets Space* , 1267-1276.

Jafarzadeh, F., & Sadeghi, H. (2012). Experimental Study On Dynamic Properties of Sand with Emphasis on the Degree of Saturation. *Soil Dynamics and Earthquake Engineering* , 26-41.

Japan MOE. (2014). *Progress on Treatment of Debris from the Great East Japan Earthquake.* Tokyo: Ministry of the Environment.

Jennings, H., & Pratt, P. (1979). An Experimental Argument for the Existence of a Protective Membrane Surrounding Portland Cement During the Induction Period. *Cem. Concr. Res* , 501-506.

Johnston, E. (2013, March 10). *Plummeting debris estimates belie pleas for disposal aid*. Retrieved December 19, 2014, from The Japan Times: http://www.japantimes.co.jp/news/2013/03/10/national/plummeting-debris-estimates-belie-pleas-for-disposal-aid/#.VJQmZF4BgA

Kalkan, E. (2011, March 24). *Top 5 Ground Motion Records of the March 11, 2011 M9.0 Tohoku Earthquake.* Retrieved Decemeber 10, 2013, from USGS: http://nsmp.wr.usgs.gov/ekalkan/Tohoku/Processed_Top_5_GMs.pdf

Kaniraj, S. R., & Havanagi, V. G. (2001). Behaviour of Cement-Stabilized Fiber-Reinforced Fly Ash-Soil Mixtures. *Journal of Geotechnical and Geoenvironmental Engineering* , 574-584.

Kaniraj, S., & Havanagi, V. (2001). Behaviour of cement-stabilization fibre-reinforced fly ash-soil mixtures. *Journal of geotechnical and geoenvironmental engineering* , 574-584.

Karkkainen, S., & Jensen, E. B. (2001). Estimation of Fibre Orientation from Digital Images. *Image Analysis and Stereology* , 199-202.

Katagiri, J., Matsushima, T., & Yamada, Y. (2010). Simple Shear Simulation of 3D Irregularly Shaped Particles by Image Based DEM. *Granular Matter* (pp. 491-497). Springer-Verlag.

Katz, A., & Thompson, A. (1986). Quantitative Prediction of Permeability in Porous Rock. *Physical Review B: Condensed Matter* , 8179-8181.

Kezdi, A. (1974). *Handbook of Soil Mechanics.* Amsterdam: Elsevier.

Kokusho, T. (1980). Cyclic Triaxial Test of Dynamic Soil Properties for Wide Strain Range. *Soils and Foundations* , 305-312.

Koseki, J., Kawakami, S., Nagayama, H., Sato, T., Hayano, K., & Torimitsu, M. (1999). *Liquefaction Tests of Toyoura Sand Measuring Change of Quasi Elastic Deformation Properties.* Tokyo: Bull ERS.

Kotake, N., Tatsuoka, F., Tanaka, T., Siddiquee, M., & Huang, C. (2001). FEM Simulation of The Bearing Capacity of Level Reinforced Sand Ground Subjected to Footing Load. *Geosynthetics International* (pp. 501-549). Roseville: Industrial Fabrics Association International.

Kramer, S. L. (2013). *Geotechnical Earthquake Engineering.* New Dehli: Pearson Education Inc. .

Krumbein, W., & Monk, G. (1942). Permeability as a Function of the Size Parameters of Unconsolidated Sand. *Petroleum Technology*, (pp. 153-163). Los Angeles.

Kumar, S. S., Krishna, A. M., & Dey, A. (2013). Parameters influencing dynamic soil properties: a review treatise. *National conference on recent advances in civil engineering* (pp. 1-9). Nirjuli: North eastern regional institute of science and technology.

Ladd, R. (1978). Specimen Preparation and Liquefaction of Sands. *Journal of Geotechnical Engineering Division* , 1180-1184.

Lade, P. V., & Ibsen, L. B. (1997). A Study of the Phase Transformation and the Characteristic Lines of Sand Behaviour. *Proceedings of the International Symposium on Deformation and Progressive Failure in Geomechanics* (pp. 353-359). Nagoya: AAU Geotechnical Engineering Group.

Lam, W.-K., & Tatsuoka, F. (1988). Effects of Initial Anisotropic Fabric and Sigma2 on Strength and Deformation Characteristics of Sand. *Soils and Foundations* , 89-106.

Lambe, W. T., & Whitman, R. V. (1969). *Soil Mechanics, SI Version.* New York: Wiley.

Lanzo, G., & D'Elia, B. (2003). Cyclic Properties of Toyoura Sand at Small to Medium Strains in Simple Shear Test. *Revista Italiana De Geotecnica* , 79-93.

Law, K., & Ling, Y. (1992). Liquefaction of granular soils with non-cohesive and cohesive fines. *Earthquake Engineering, Tenth World Conference*, (pp. 1491-1496). Balkema, Rotterdam.

Lawrence, G. (1977). Measurement of Pore Sizes in Fine-Textured Soils: A Review of Existing Techniques. *Journal of Soil Science , 28*, 527-540.

Lee, J., & Santamarina, J. (2005). Bender elements: performance and signal interpretation. *Journal of Geotechnical and Geoenvironmental Engineering* , 1063-1070.

Leonards, G. (1962). *Foundation Engineering.* McGraw Hill Book Company.

Li, C. (2005). *Mechanical Response of Fibre-Reinforced Soil.* Austin: The University of Texas at Austin.

Li, X., & Wang, Y. (1998). Linear Representation of Steady State Line for Sand. *Journal of Geotechnical and Geoenvironmental Engineering* , 1215-1217.

Ling, H. I., & Liu, H. (2003). Pressure Level Dependency and Densification Behaviour of Sand Through Generalized Plasticity Model. *Journal of Engineering Mechanics* , 851-860.

Ling, H. I., & Yang, S. (2006). Unified Sand Model Based on the Critical State and Generalized Plasticity. *Journal of Engineering Mechanics* , 1380-1391.

Liu, J.-C., & Znidarcic, D. (1991). Modelling One-Dimensional Compression Characteristics of Soils. *Journal of Geotechnical Engineering* , 162-169.

Lunne, T., Anderson, K. H., Low, H. E., Randolph, M. F., & Sjursen, M. (2011). Guidelines for offshore in situ testing and interpretation in deepwater soft clays. *Canadian Geotechnical Journal* , 543-556.

Mah, P., Reeves, T., & McDavid, W. (2010). Deriving Hounsfield units using grey levels in cone beam computed tomography. *Dentomaxillofacial Radiology* , 323-335.

Majarjan, M., & Takahashi, A. (2013). Centrifuge model tests on liquefaction-induced settlement and pore water migration in non-homogeneous soil deposits. *Soil Dynamics and Earthquake Engineering* , 161-169.

Marshall, T. (1958). A Relation Between Permeability and Size Distribution of Pores. *Journal of Soil Science* .

Materials, A. S. (2010, Decemeber 21). Standard Test Methods for One Dimensional Consolidation Properties of Soils Using Incremental Loading. *D2435-04* . West Conshohocken, Pennsylvania, USA: ASTM International.

Matsuoka, H., & Nakai, T. (1974). Stress Deformation and Strength Characteristics of Soil Under Three Different Principle Stresses. *Japan Society of Civil Engineers Conference*, (pp. 59-70).

McCarthy, D. F. (1998). *Essentials of Soil Mechanics and Foundations: Basic Geotechnics 5th Edition.* Prentice Hall.

Mehta, P. (1973). Mechanism of Expansion Associated with Ettringite Formation. *Cement and Concrete Research* , 1-6.

Mehta, P., & Monteiro, P. (2013). *Concrete: Microstructure, Properties, and Materials.* McGraw-Hill.

Meneses-Loja, J., Ishihara, K., & Towhata, I. (2000). Flow Failure of Saturated Sand Under Simultaneous Monotonic and Cyclic Stresses. *Journal of Geotechnical and Geoenviromental Engineering* , 131-138.

Michalowski, R., & Cermak, J. (1994). Strength anisotropy of fibre-reinforced sand. *Computers and Geotechnics* , 1166-1184.

Miura, H., Tokunaga, S., Kitazume, M., & Hirota, N. (2004). Laboratory permeability tests on cement treated soils. *Proc. of the International Symposium on Engineering Practice and Performance of Soft Deposits* (pp. 181-186). Toyonaka: Japanese Geotechnical Society.

Miura, N. (1979). A Consideration on the Stress Strain Relation of a Sand Under High Pressures. *Proceedings of the Japan Society of Civil Engineers* (pp. 127-130). JSCE.

Nakamichi, M., & Sato, K. (2013). A Method of Suppressing Liquefaction Using a Solidification Material and Tension Stiffeners. *International Conference on Soil Mechanics and Geotechnical Engineering.* Paris.

Neri, R. (2013). *Consideration of Bonding in the Behaviour of a Sand-Cement Mixture Simulating Jet Grouting.* Lisbon: Instituto Superior Tecnico.

Neville, A. (2011). *Properties of Concrete, 5th Edition.* Essex, England: Pearson Education Ltd.

News, B. (2012, March 11). *Japan Quake: Loss and Recovery in Numbers.* Retrieved May 6, 2014, from BBC News Asia: http://www.bbc.com/news/world-asia-17219008

Newson, T. (2013). *Advanced Soil Mechanics.* London: T. Newson.

Newson, T. (2013). Class Notes - CEE9522 Advanced Soil Mechanics. London, Ontario, Canada: T. Newson.

Oda, M. (1977). On the Influence of Progressive Failure on the Bearing Capacity of Shallow Foundations in Dense Sand. *Soils and Foundations* , 71-73.

Oda, M., Koishikawa, I., & Higuchi, T. (1978). Experimental Study of Anisotropic Shear Strength of Sand by Plane Strain Test. *Soils and Foundations* , 25-38.

Oda, M., Takemura, T., & Takahasi, M. (2004). Microstructure in Shear Band Observed by Microfocus Xray Computed Tomography. *Geotechnique* , 539-542.

Ojha, S., & Trivedi, A. (2013). Shear Strength Parameters for Silty-Sand Using Relative Compaction. *Electronic Journal of Geotechnical Engineering* , 81-99.

Oztoprak, S., & Bolton, M. (2013). Stiffness of sands through a laboratory test database. *Geotechnique* , 54-70.

Pestana, J., & Whittle, A. (1995). Compression Model for Cohesionless Soils. *Geotechnique* , 611-631.

Polito, C. P., & Martin II, J. R. (2001). Effects of Nonplastic Fines on the Liquefaction Resistance of Sands. *Journal of Geotechnical and Geoenvironmental Engineering* , 408-415.

Pradhan, T. B., Tatsuoka, F., & Horii, N. (1988). Strength and Deformation Characteristics of Sand in Torsional Simple Shear. *Soils and Foundations* , 131-148.

Rahman, M., Baki, M., & Lo, S. (2014). Prediction of undrained monotonic and cyclic liquefaction behaviour of sand with fines based on the equivalent granular state parameter. *International Journal of Geomechanics* , 254-266.

Rao, K. M., & Rao, K. M. (2007). Extraction and Tensile Properties of Natural Fibers: Vakka, Date and Bamboo. *Composite Structures* , 288-295.

Rasmussen, K. (2012). *An Investigation of Monotonic and Cyclic Behaviour of Leda Clay.* London: University of Western Ontario - Electronic Thesis and Dissertation Repository.

Rauch, A. F. *Chapter 2 Soil Liquefaction in Earthquakes.*

Reed, A. H., Briggs, K. B., & Lavoie, D. L. (2002). Porometric Properties of Siliciclastic Marine Sand: A Comparison of Traditional Laboratory Measurements With Image Analysis and Effective Medium Modeling. *IEEE JOURNAL OF OCEANIC ENGINEERING* , 581-593.

Robertson, P., & Fear, C. (1995). Liquefaction of Sands and its Evaluation. *Proceedings of the 1st International Conference on Earthquake Geotechnical Engineering.* Tokyo.

Romero, E., & Simms, P. H. (2008). Microstructure Investigation in Unsaturated Soils:A Review with Special Attention to Contribution of MercuryIntrusion Porosimetry and Environmental Scanning Electron Microscopy. *Geotechnical and Geological Engineering* , 705-727.

Roth, M., Mackey, J., Mackey, C., & Nyquist, J. (2002). A case study of the reliability of multielectrode earth resistivity testing for geotechnical investigations in karst terrains. *Engineering Geology* , 225-232.

Saettem, J., Rise, L., Rokoengen, K., & By, T. (1996). Soil investigations, offshore mid Norway: A case study of glacial influence on geotechnical properties. *Global and Planetary Change* , 271-285.

Salahuddin, Marri, A., & Kumar, A. (2013). Isotropic Compression Behaviour of Fibre Reinforced Cemented Sand. *Mehran University Research Journal of Engineering and Technology* , 381-390.

Salgado, R., Bandini, P., & Karim, A. (2000). Shear Strength and Stiffness of Silty Sand. 451-462.

Sanin, M. V. (2010). *Cyclic Shear Loading Response of Fraser River Delta Silt.* Vancouver: The University of British Columbia.

Saxena, S., Avramidis, A., & Reddy, K. (1988). Dynamic Moduli and Damping Ratios for Cemented Sands at Low Strains. *Canadian Geotechnical Journal* , 353-368.

Saxena, S., Reddy, K., & Avramidis, A. (1988). Liquefaction resistance of artificially cemented sand. *Journal of Geotechnical Engineering* , 1395-1413.

Seed, H., & Idriss, I. (1982). *Ground motions and soil liquefaction during earthquakes.* Oakland: Earthquake Engineering Research Institute.

Seed, H., & Lee, K. (1966). Liquefaction of saturated sands during cyclic loading. *Journal of soil mechanics and foundations division* , 105-134.

Seed, H., Martin, P., & Lysmer, J. (1975). *The generation and dissipation of pore water pressures during soil liquefaction.* California: EERC.

SEM/EDC of Cement and Concrete. (2014). *SEM cement training.* Retrieved December 15, 2014, from SEM imaging of cement and cementitious materials: http://semcementtraining.com/sem-cement-imaging/

Sfriso, A. O. *The Friction Angle and Critical State Void Ratio of Sands.* Buenos Aires: LMNI, University of Buenos Aires, & SRK Consulting.

Shafiq, N., & Nuruddin, M. F. (n.d.). Degree of Hydration of OPC and OPC/Fly Ash Paste Samples Conditioned at Different Relative Humidity. *International Journal of Sustainable Construction Engineering and Technology* , 47-56.

Shahir, H., Mohammadi-Haji, B., & Ghassemi, A. (2014). Employing a variable permeability model in numerical simulation of saturated sand behavior under earthquake loading. *Computers and Geotechnics* , 211-223.

Shepherd, R. G. (1989). Correlations of Permeability and Grain Size. *Groundwater* , 633-638.

Simoni, A., & Houlsby, G. T. (2006). The Direct Shear Strength and Dilatancy of Sand-Gravel Mixtures. *Geotechnical and Geological Engineering Journal* , 523-549.

Sitharam, T., GovindaRaju, L., & Srinivasa Murthy, B. (2004). Evaluation of Liquefaction Potential and Dynamic Properties of Silt Sand Using Cyclic Triaxial Testing. *Geotechnical Testing Journal* , 1-7.

Sladen, J., D'Hollander, R., & Krahn, J. (1985). The Liquefaction of Sands, a Collapse Surface Approach. *Canadian Geotechnical Journal* , 564-578.

Spangler, M. G., & Handy, R. (1982). *Soil Engineering, 4th edition.* New York: Harper and Row Publishers.

Stroeven, P. (1977). The Analysis of Fibre Distributions in Fibre Reinforced Materials. *Journal of Microscopy* , 283-295.

Sybico Jr., A. K. (1992). Post-liquefaction settlement of sand. *Wroth Memorial Symposium.* Oxford: Oxford University.

Sze, H. Y., & Yang, J. (2014). Failure modes of sand in undrained cyclic loading: impact of sample preparation. *Journal of geotechnical and geoenvironmental engineering* , 152-169.

Taira, A. (2001). Tectonic Evolution of the Japanese Island Arc System. *Annual Review Earth Planetary Science* , 109-134.

Tao, M., Figueroa, J., & Saada, A. (2004). *Influence of Nonplastic Fines Content on the Liquefaction Resistance of Soils in Terms of Unit Energy.* London: Taylor and Francis Group.

Tarnawski, V., Momose, T., & Leong, W. (2011). Thermal Conductivity of Standard Sands II. Saturated Conditions. *International Journal of Thermophsyics* , 984-1005.

Tatsuoka, F., Nakamura, S., Huang, C.-C., & Tani, K. (1990). Strength Anisotropy and Shear Band Direction in Plane Strain Tests of Sand. *Soils and Foundations* , 35-54.

Tatsuoka, F., Toki, S., Miura, S., Kato, H., Okamoto, M., Yamada, S.-I., et al. (1986). Some factors affecting cyclic undrained triaxial strength of sand. *Soils and foundations* , 99-116.

Terashi, M., & Juran, I. (2000). Ground Improvement - State of the Art. *ISRM Conference* (pp. 1-59). ISRM.

Terzaghi, K., & Peck, R. (1948). *Soil Mechanics in Engineering Practice.* New York: Wiley.

The World Bank. (2014). *Learning from Megadisasters: Lessons from the Great East Japan Earthquake.* Washington, D.C.: International Bank for Reconstruction and Development/ The World Bank.

Thevanayagam, S. (1998). Effect of Fines and Confining Stress on Undrained Shear Strength of Silty Sands. *JOURNAL OF GEOTECHNICAL AND GEOENVIRONMENTAL ENGINEERING* , 479-491.

Toki, S., Tatsuoka, F., Miura, S., Yoshimi, Y., Yasuda, S., & Makihara, Y. (1986). Cyclic Undrained Triaxial Strength of Sand by a Cooperative Test Program. *Soils and Foundations , 26* (3), 117-128.

Toutanji, H. A., Xu, B., Lavin, T., & Gilbert, J. A. (2010). Properties of Poly(vinyl alcohol) Fibre Reinforced High-performance Organic Aggregate Cementitious Material. *International Congress on Polymers in Concrete*, (pp. 1-8). Funchal.

Towhata, I. (2008). *Geotechnical Earthquake Engineering.* Berlin: Springer.

Treatise, P. I. (2013). Shiv Shankar Kumar; A. Murali Krishna; Arindam Dey. *National Conference on Recent Advances in Civil Engineering* (pp. 1-10). Nirjuli: North Eastern Regional Institute of Science and Technology.

Troncoso, J. (1986). Critical state of Tailing Silty Sands for Earthquake Loading. *Soil dynamics and earthquake engineering , 5* (3), 248-252.

USGS. (2012, April). *Historic World Earthquakes*. Retrieved December 17, 2013, from USGS Earthquake Hazards Program: http://earthquake.usgs.gov/earthquakes/world/historical_country_mag.php#japan

Uygunoglu, T. (2008). Investigation of microstructure and flexural behavior of steel-fibre reinforced concrete. *Materials and structures* , 1441-1449.

Viggiani, G., & Atkinson, J. (1995). Interpretation of Bender Element Tests. *Geotechnique* , 149-154.

Wang, Z.-L., Dafalias, Y. F., Li, X.-S., & Makdisi, F. I. (2002). State Pressure Index for Modelling Sand Behaviour. *Journal of Geotechnical and Geoenvironmental Engineering* , 511-519.

Washburn, E. W. (1921). The Dynamics of Capillary Flow. *The Physical Review* , 273-283.

Webb, P. A., & DeSousa, T. (2010). *Mercury Intrusion Porosimetry.* Micromeritics Instrument Corp.

West, T. (1995). *Geology Applied to Engineering.* Prentice Hall.

Whitlow, R. (2001). *Basic Soil Mechanics.* Dorchester: Pearson Education Ltd.

Wood, D. M. (1990). *Soil Behaviour and Critical State Soil Mechanics.* Cambridge: Cambridge University Press.

Xenaki, V., & Athanasopolous, G. (2003). Liquefaction Resistance of Sand-Silt Mixtures: An Experimental Investigation of the Effect of Fines. *Soil Dynamics and Earthquake Engineering* , 183-194.

Xenaki, V., & Athanasopolous, G. (2003). Liquefaction Resistance of Sand-Silt Mixtures: An Experimental Investigation of the Effects of Fines. *Soil Dynamics and Earthquake Engineering* , 183-194.

Yamamuro, J. A., & Lade, P. V. (1998). Steady-state concepts and static liquefaction of silty sands. *Journal of geotechnical and geoenvironmental engineering* , 868-877.

Yamamuro, J. A., & Lade, P. V. (1998). Steady-State Concepts and Static Liquefaction of Silty Sands. *Journal of Geotechnical and Geoenvironmental Engineering* , 868-877.

Yang, J., Savidis, S., & Roemer, M. (2004). Evaluating Liquefaction Strength of Partially Saturated Sand. *Journal of Geotechnical and Geoenvironmental Engineering* , 975-979.

Yang, Z., Li, X., & Yang, J. (2008). Quantifying and modelling fabric anisotropy. *Geotechnique* , 237-248.

Yasuda, S., Haradai, K., Ishikawa, K., & Kanemaru, Y. (2012). Characteristics of Liquefaction in Tokyo Bay Area by the 2011 Great East Japan Earthquake. *Soils and Foundations* , 793-810.

Yasuda, S., Haradai, K., Ishikawa, K., & Kanemaru, Y. (2012). Characteristics of Liquefaction in Tokyo Bay Area by the 2011 Great East Japan Earthquake. *Soils and Foundations* , 793-810.

Yoder, E., & Witczak, M. (1975). *Principles of Pavement Design, 2nd Edition.* New York: John Wiley and Son, Inc.

Yoshimine, M., & Koike, R. (n.d.). *Liquefaction of Clean Sand with Stratified Structure Due to Segregation of Particle Size*. Retrieved February 28, 2014, from Soil Mechanics; Tokyo Metropolitan University: http://geot.civil.ues.tmu.ac.jp/~my/publications/jcasand/

Youd, T., & Idriss, I. (2001). Liquefaction resistance of soils: summary report from the 1996 NCEER and 1998 NCEER/NSF workshops on evaluation of liquefaction resistance of soils. *Journal of geotechnical and geoenvironmental engineering* , 297-313.

Youn, J.-U., Choo, Y.-W., & Kim, D.-S. (2008). Measurement of small-strain shear modulus Gmax of dry and saturated sands by bender element,resonant column, and torsional shear tests. *Canadian Geotechnical Journal* , 1426-1438.

ZHANG, F., YE, B., & YE, G. (2011). *Unified Description of Sand Behavior.* Nagoya, Japan: Higher Education Press and Springer-Verlag Berlin Heidelberg.

Appendix

A. Sample calculations

Appendix A presents a sample calculation of the fibres per unit volume and the equivalent earthquake magnitude for the cyclic triaxial samples. The calculated and empirically determined CSR values are representative of magnitude 7.5 and magnitude 9.0 earthquakes.

$G_{s\ fibre} = 1.3$
$D_{fibre} = 0.115mm$
$L_{fibre} = 12mm$
$V_{sample} = 196.35cm^3$
$M_{fibres} = 5.85g$

$$V_{fibre} = \frac{\pi}{4} D_{fibre}^2 L_{fibre} = 1.246x10^{-4} cm^3$$
$$V_{fibre\ in\ sample} = \frac{M_{fibres}}{G_{s\ fibre}} = 4.5cm^3$$
$$\#fibres = \frac{V_{fibre\ in\ sample}}{V_{fibre}} = 36{,}115\ fibres$$

Table A.1. Equivalent Earthquake Magnitudes for Stabilized and Unstabilized Silty Toyoura Sand

EQUIVALENT EARTHQUAKES		
Sample Name	**Magnitude 7.5 Earthquake (CSR to cause failure in 15 cycles)**	**CSR for Magnitude 9.0 Earthquake (CSR to cause failure in 34 cycles)**
Toyoura sand	0.235	0.219
Silica Flour	0.102	0.087
2% Cement	0.335	0.314
2% Cement, 1% Fibre	0.354	0.346
42% Silt, 1% Fibre	0.104	0.095
42% Silt	0.110	0.090
48.5% Silt, 2% Cement, 1% Fibre	0.210	0.188

B. Direct Shear Results

Appendix B contains results from direct shear tests on Toyoura sand and silica flour. It has the graphs of vertical displacement vs. horizontal displacement and shear stress vs. horizontal displacement for the tests at normal stresses ranging from 25 kPa to 300 kPa.

B.1. Direct Shear Tests on Silica Flour

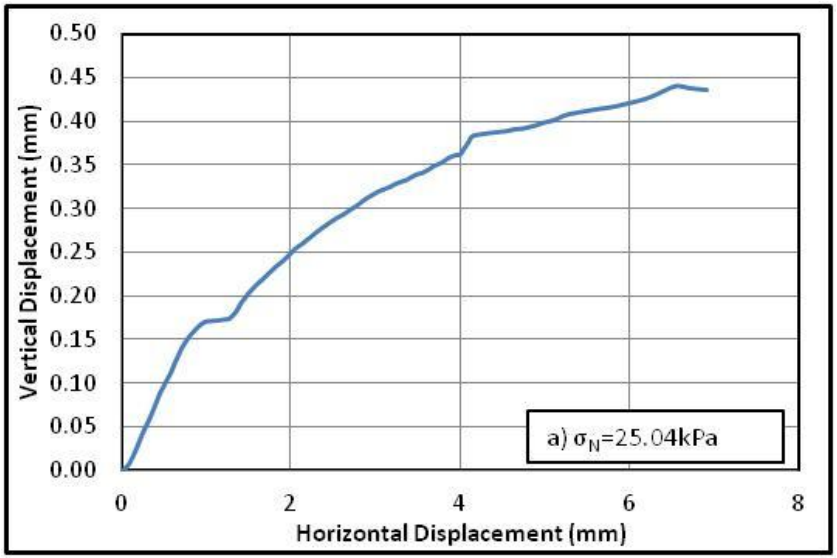

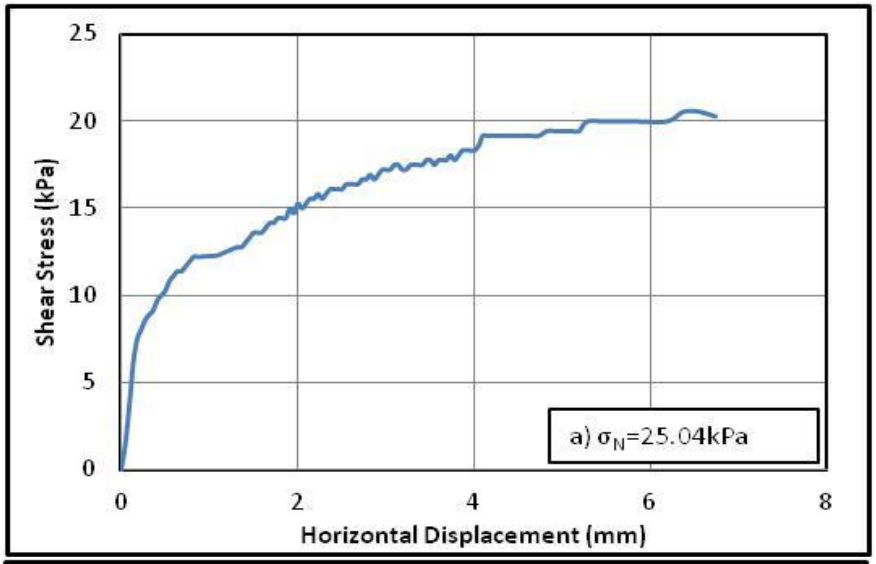

NO DATA

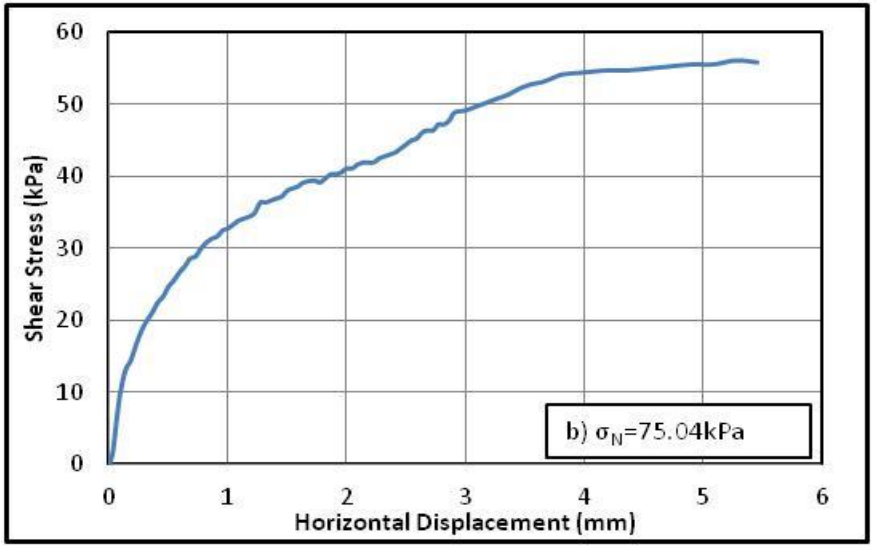

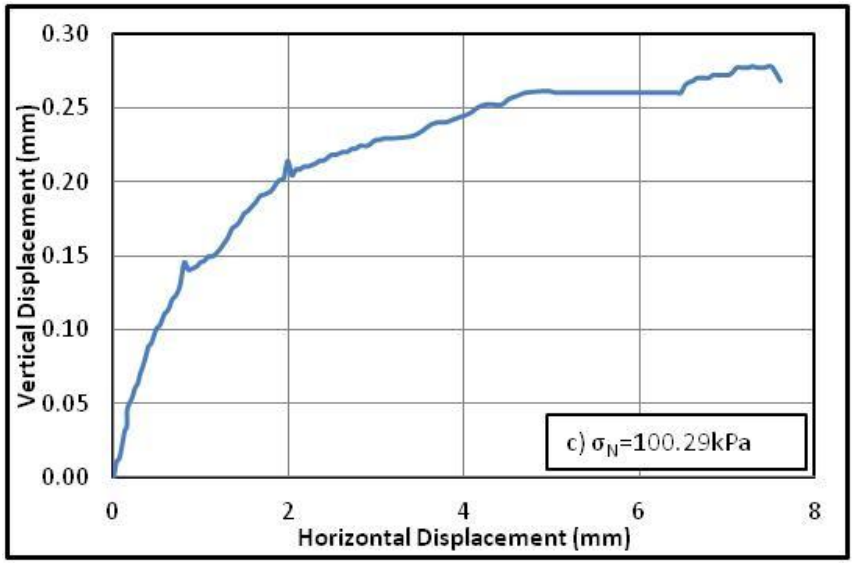
Vertical Displacement (mm)
0.30
0.25
0.20
0.15
0.10
0.05
0.00
0
2
4
6
8
Horizontal Displacement (mm)
c) σN=100.29kPa

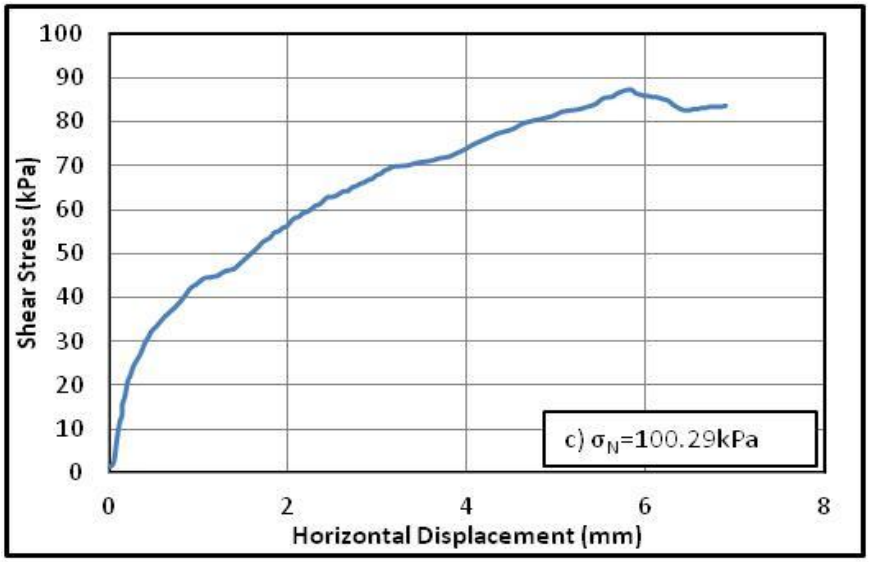
Shear Stress (kPa)
100
90
80
70
60
50
40
30
20
10
0
0
2
4
6
8
Horizontal Displacement (mm)
c) σN=100.29kPa

NO DATA

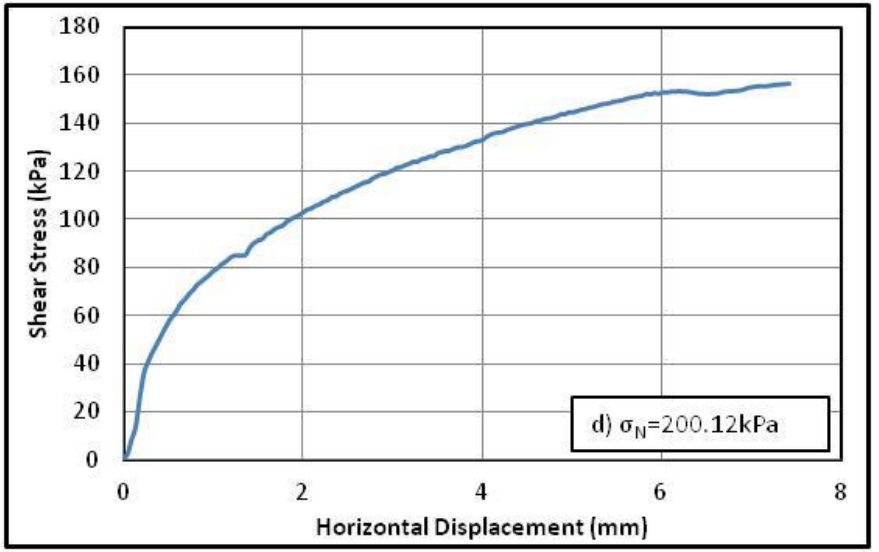
Shear Stress (kPa)
180
160
140
120
100
80
60
40
20
0
0
2
4
6
8
Horizontal Displacement (mm)
d) σN=200.12kPa

NO DATA

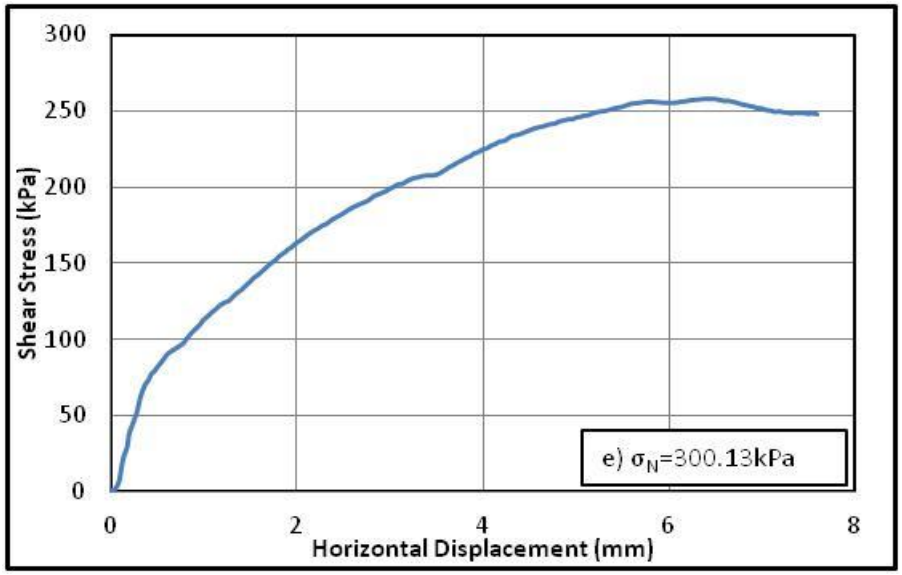

Figure B.1. Silica flour: Vertical vs. horizontal displacement and shear stress vs. horizontal displacement for a) σ_N=25.04 kPa; b) σ_N =75.04 kPa; c) σ_N =100.29 kPa; d) σ_N =200.12 kPa; e) σ_N =300.13 kPa

B.2. Direct Shear Tests on Toyoura Sand

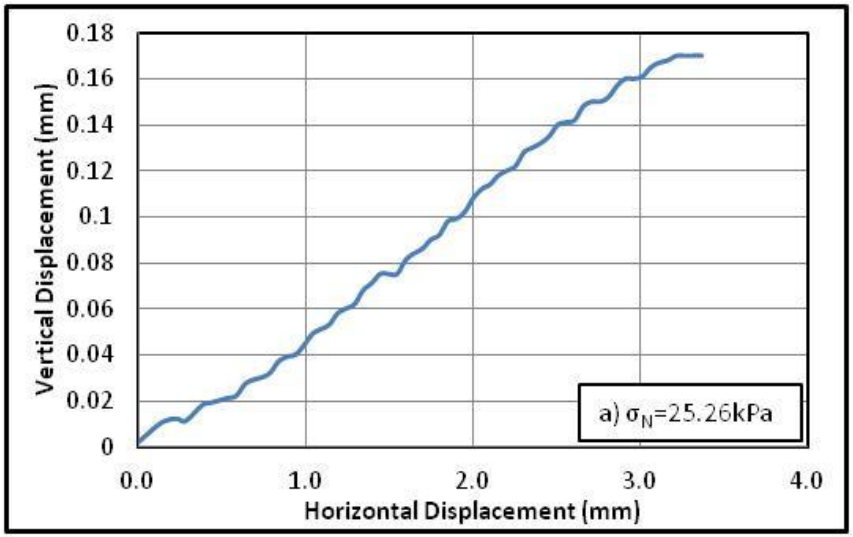

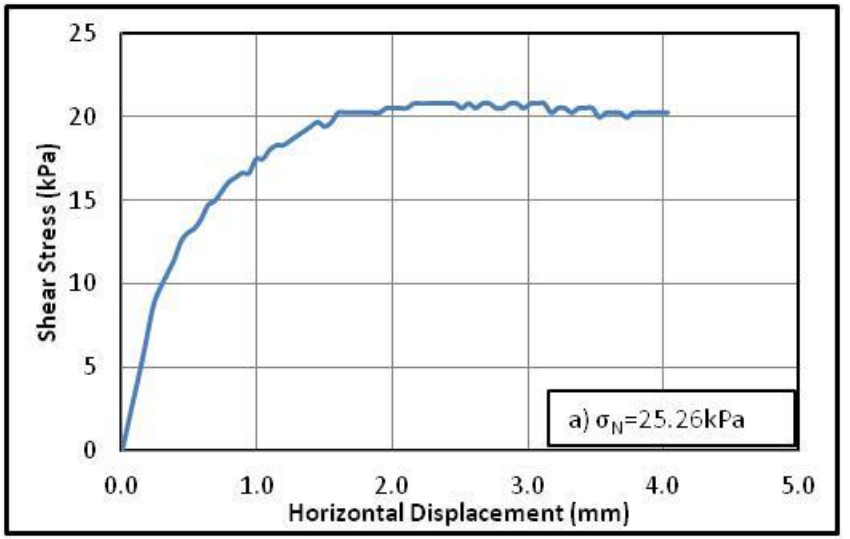

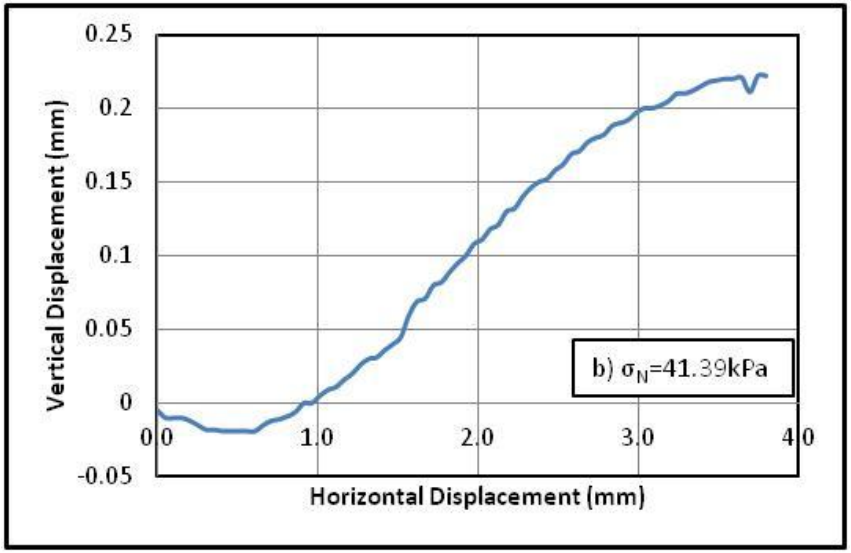

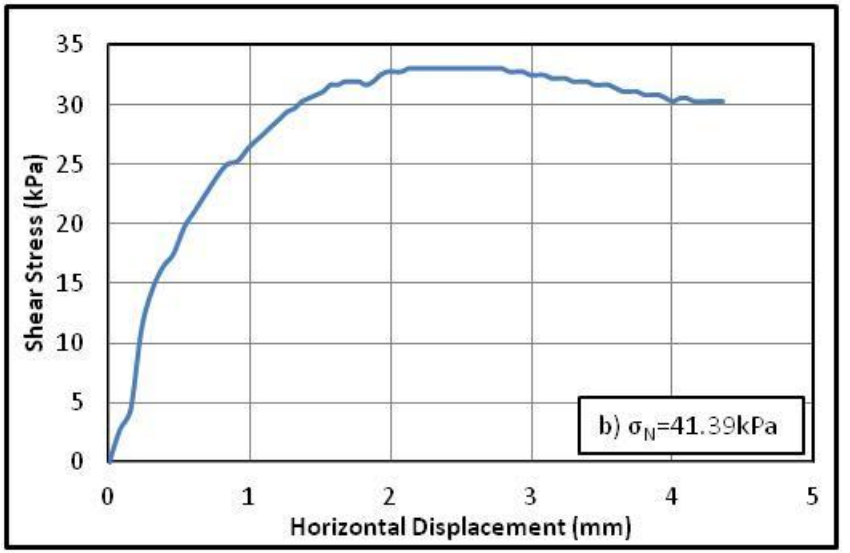

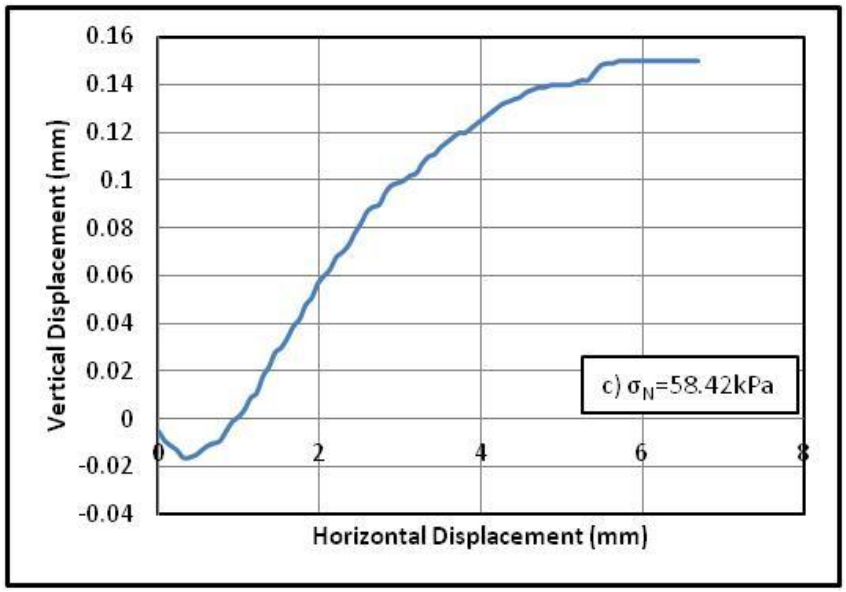
Vertical Displacement (mm)
0.16
0.14
0.12
0.1
0.08
0.06
0.04
0.02
0
-0.02
-0.04
0
2
4
6
8
Horizontal Displacement (mm)
c) σN=58.42kPa

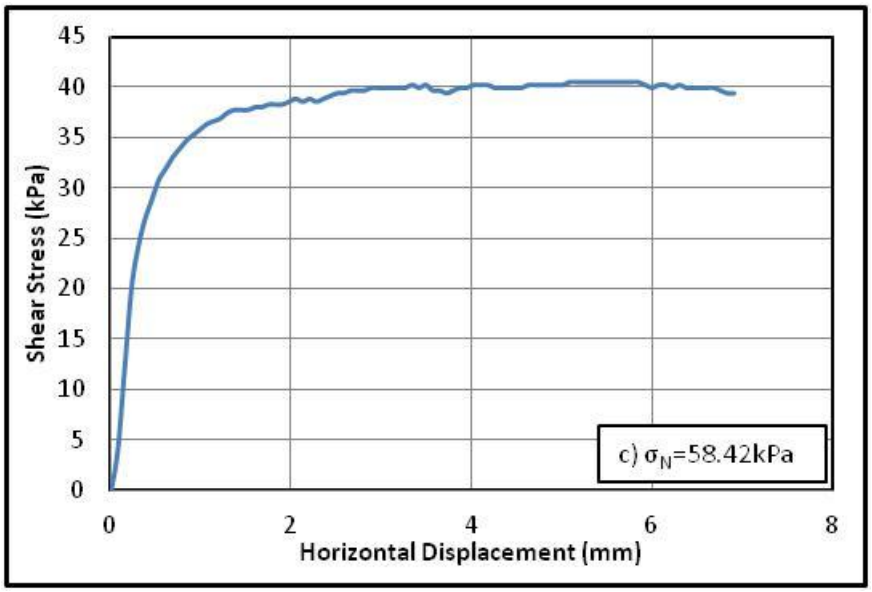
Shear Stress (kPa)
45
40
35
30
25
20
15
10
5
0
0
2
4
6
8
Horizontal Displacement (mm)
c) σN=58.42kPa

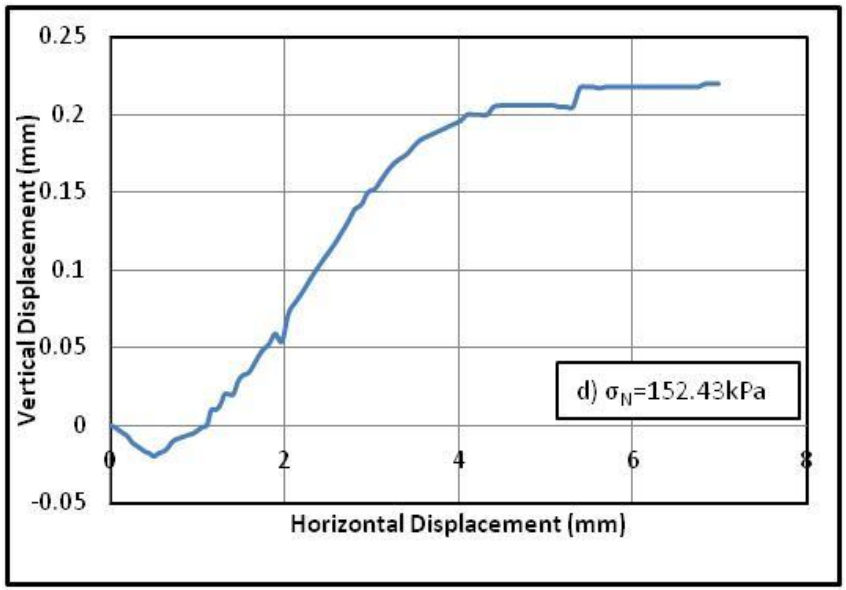
Vertical Displacement (mm)
0.25
0.2
0.15
0.1
0.05
0
-0.05
0
2
4
6
8
Horizontal Displacement (mm)
d) σN=152.43kPa

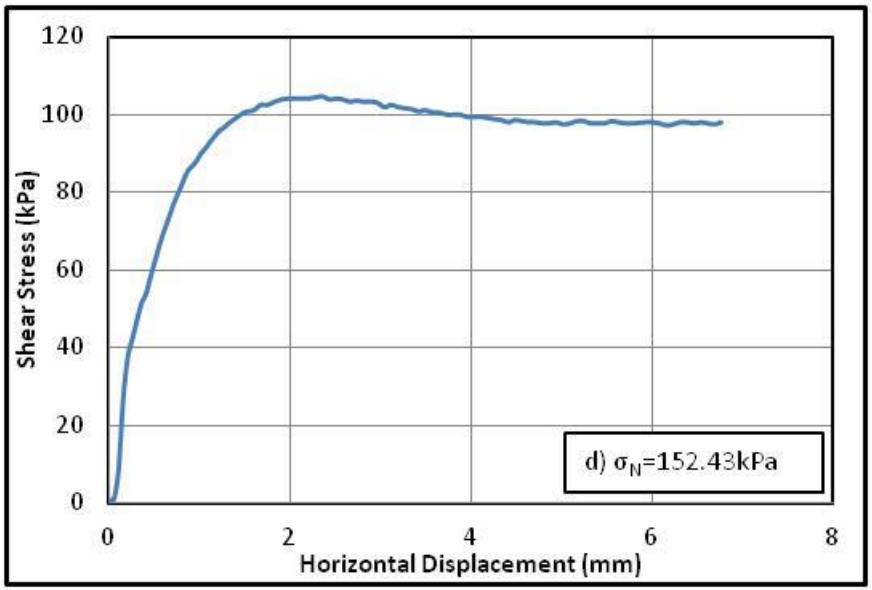
Shear Stress (kPa)
120
100
80
60
40
20
0
0
2
4
6
8
Horizontal Displacement (mm)
d) σN=152.43kPa

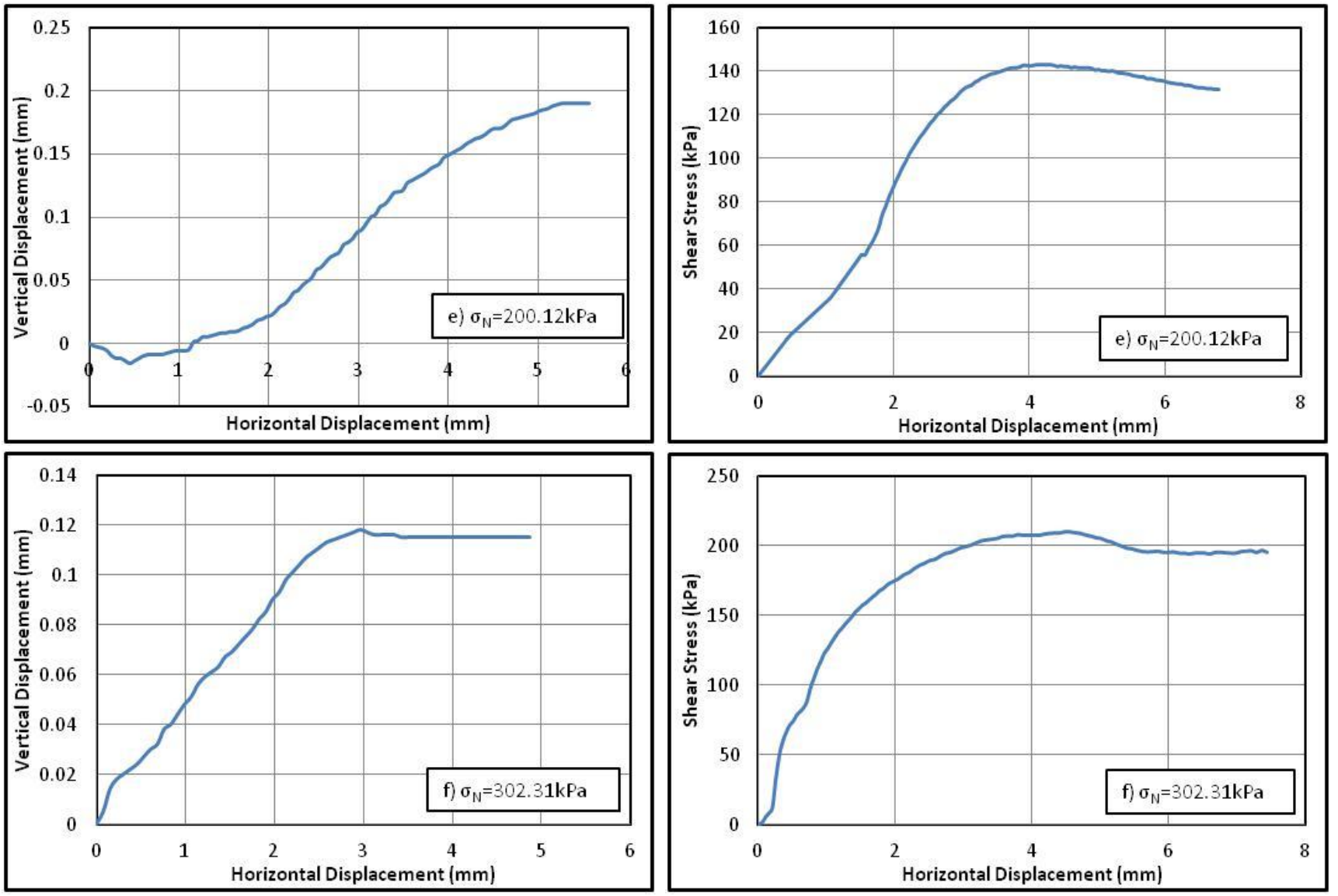

Figure B.2. Toyoura sand: Vertical vs. horizontal displacement and shear stress vs. horizontal displacement for a) N=25.26 kPa; b) N=41.39 kPa; c) N=58.42 kPa; d) N=152.43 kPa; e) N=200.12 kPa; f) N=302.31 kPa

C. Cyclic Triaxial Results

Appendix C contains cyclic triaxial test results for pure silt stabilized with varying concentrations of cement and PVA fibres. Each individual test is presented in Section 4.7. with an outline of the trends and behaviours of the samples. The content of this section is summary graphs of those results.

C.1. Pure Silt: 1% Fibre, 2% Cement, 1% Fibre & 2% Cement, Same CSR

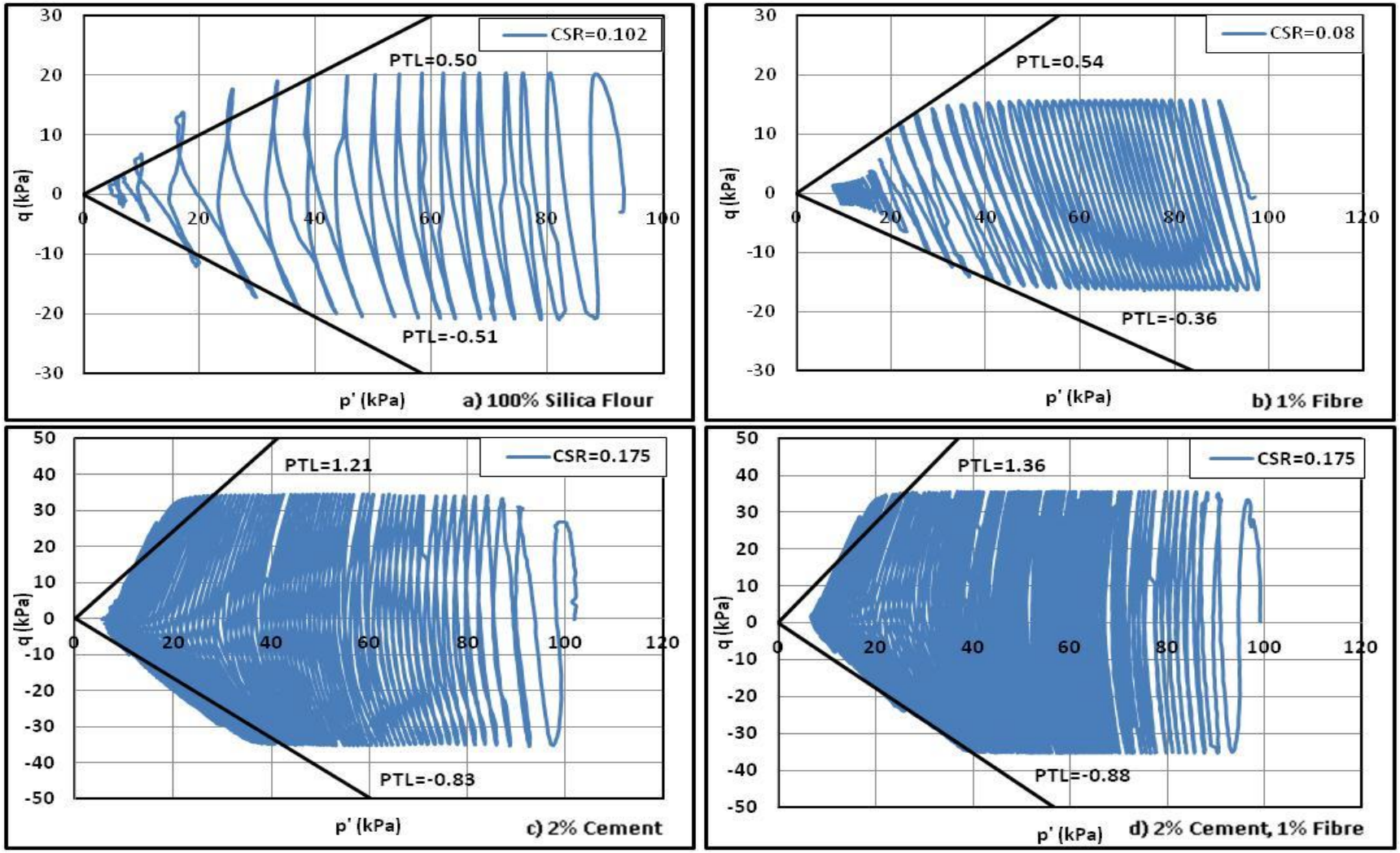

Figure C.1. Deviator stress vs. Cambridge effective stress for 100% silica flour with and without stabilizers at D_r=60%, σ_c'=100kPa a) 100% Silica Flour, CSR=0.102; b) 1% Fibre, CSR=0.080; c) 2% Cement, CSR=0.175; d) 2% Cement, 1% Fibre, CSR=0.175

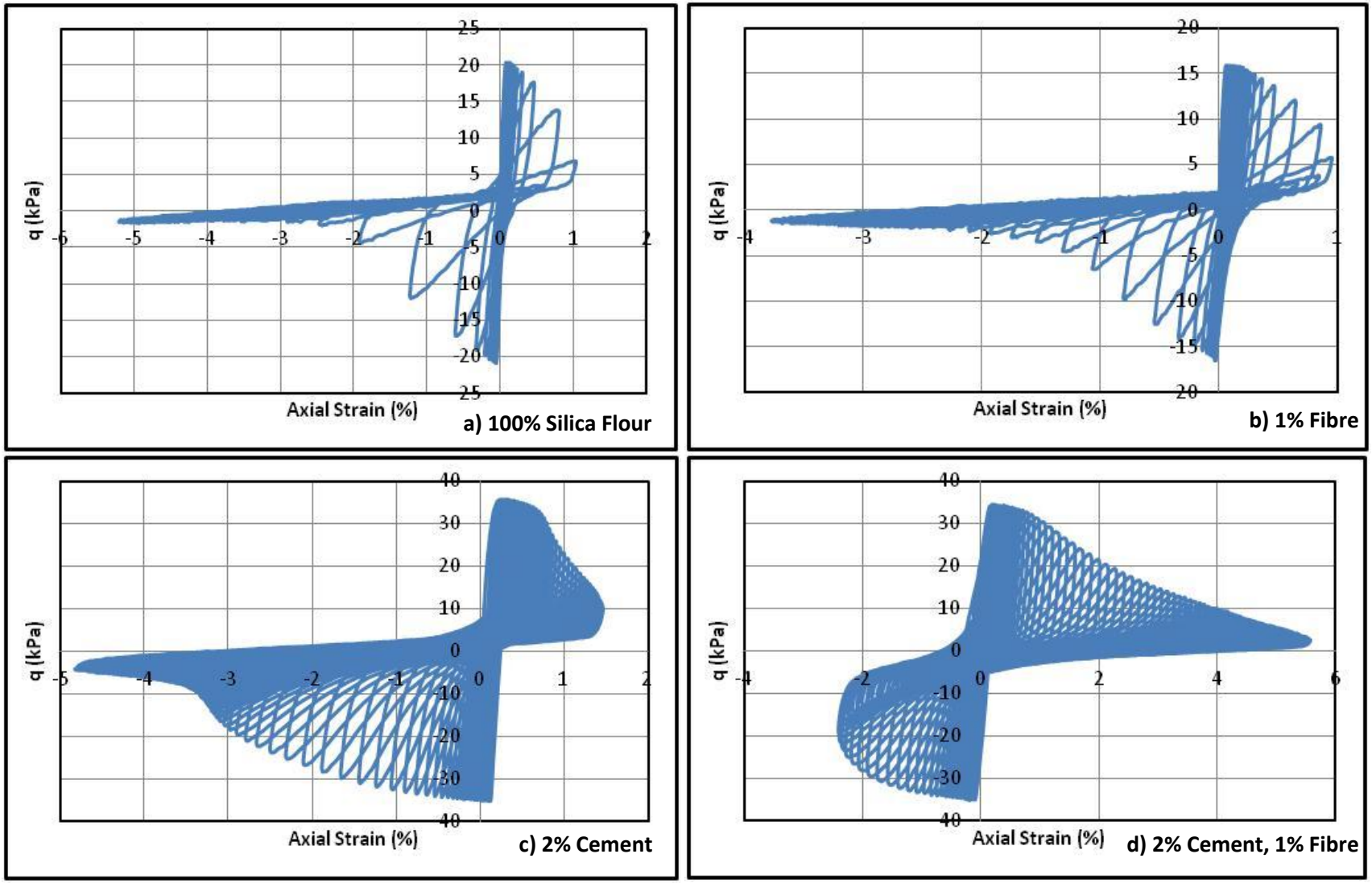

Figure C.2. q vs. ε_a for 100% silica flour with and without stabilizers at D_r=60%, σ_c'=100kPa a) 100% Silica Flour, CSR=0.102; b) 1% Fibre, CSR=0.080; c) 2% Cement, CSR=0.175; d) 2% Cement, 1% Fibre, CSR=0.175

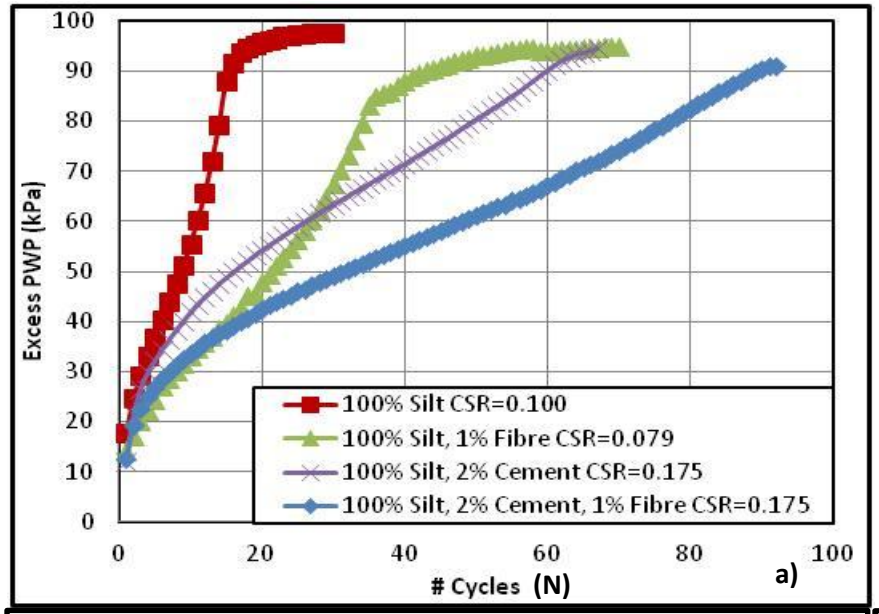
Excess PWP (kPa)
Cycles (N)
a)
100% Silt CSR=0.100
100% Silt, 1% Fibre CSR=0.079
100% Silt, 2% Cement CSR=0.175
100% Silt, 2% Cement, 1% Fibre CSR=0.175

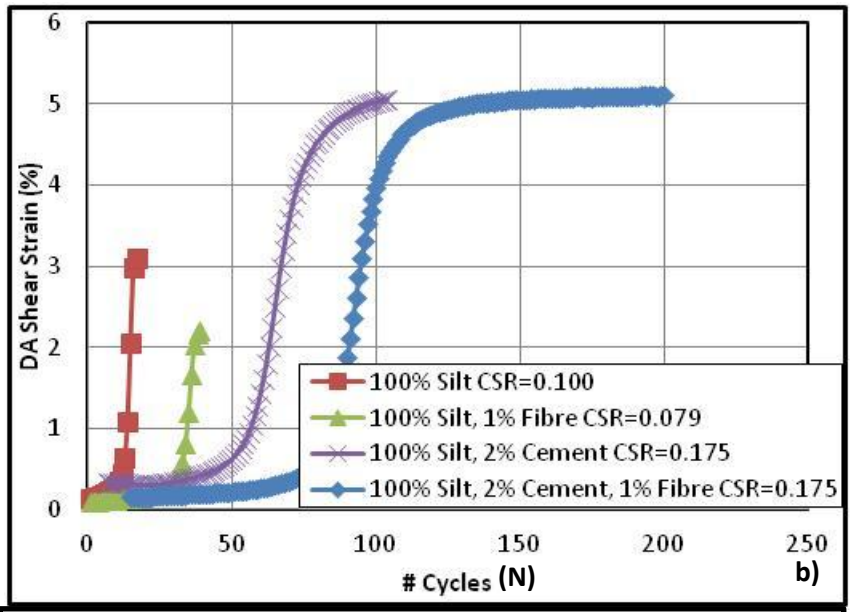
DA Shear Strain (%)
Cycles (N)
b)
100% Silt CSR=0.100
100% Silt, 1% Fibre CSR=0.079
100% Silt, 2% Cement CSR=0.175
100% Silt, 2% Cement, 1% Fibre CSR=0.175

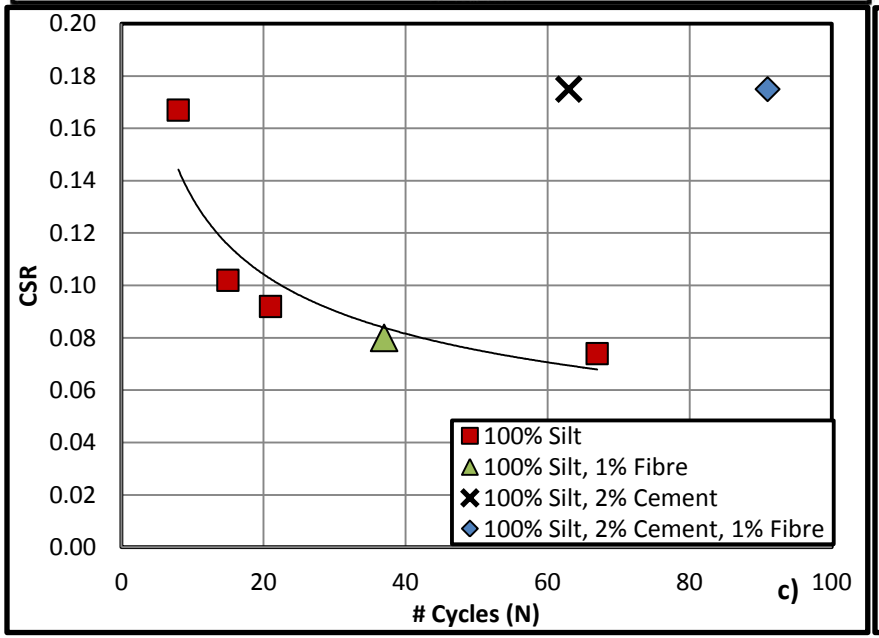
CSR
Cycles (N)
c)
100% Silt
100% Silt, 1% Fibre
100% Silt, 2% Cement
100% Silt, 2% Cement, 1% Fibre

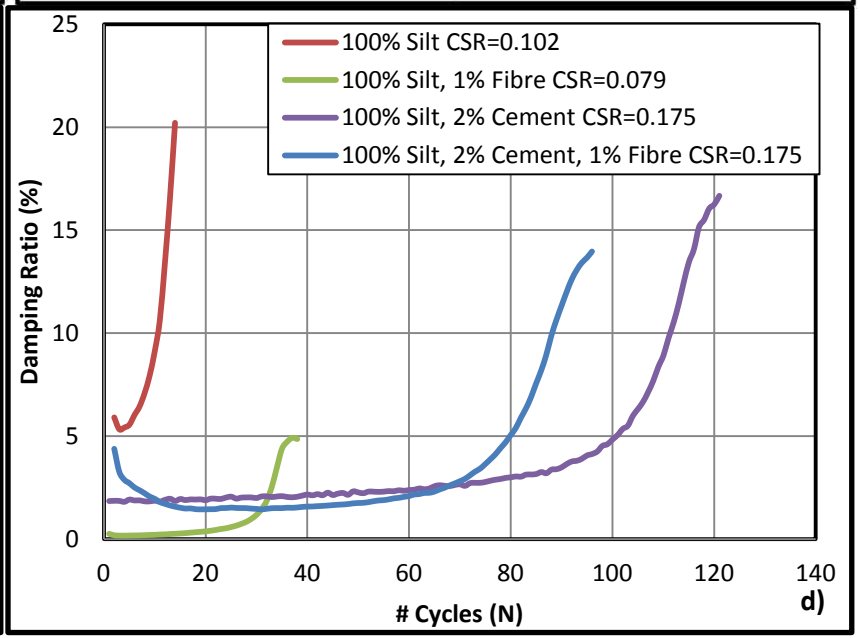
Damping Ratio (%)
Cycles (N)
d)
100% Silt CSR=0.102
100% Silt, 1% Fibre CSR=0.079
100% Silt, 2% Cement CSR=0.175
100% Silt, 2% Cement, 1% Fibre CSR=0.175

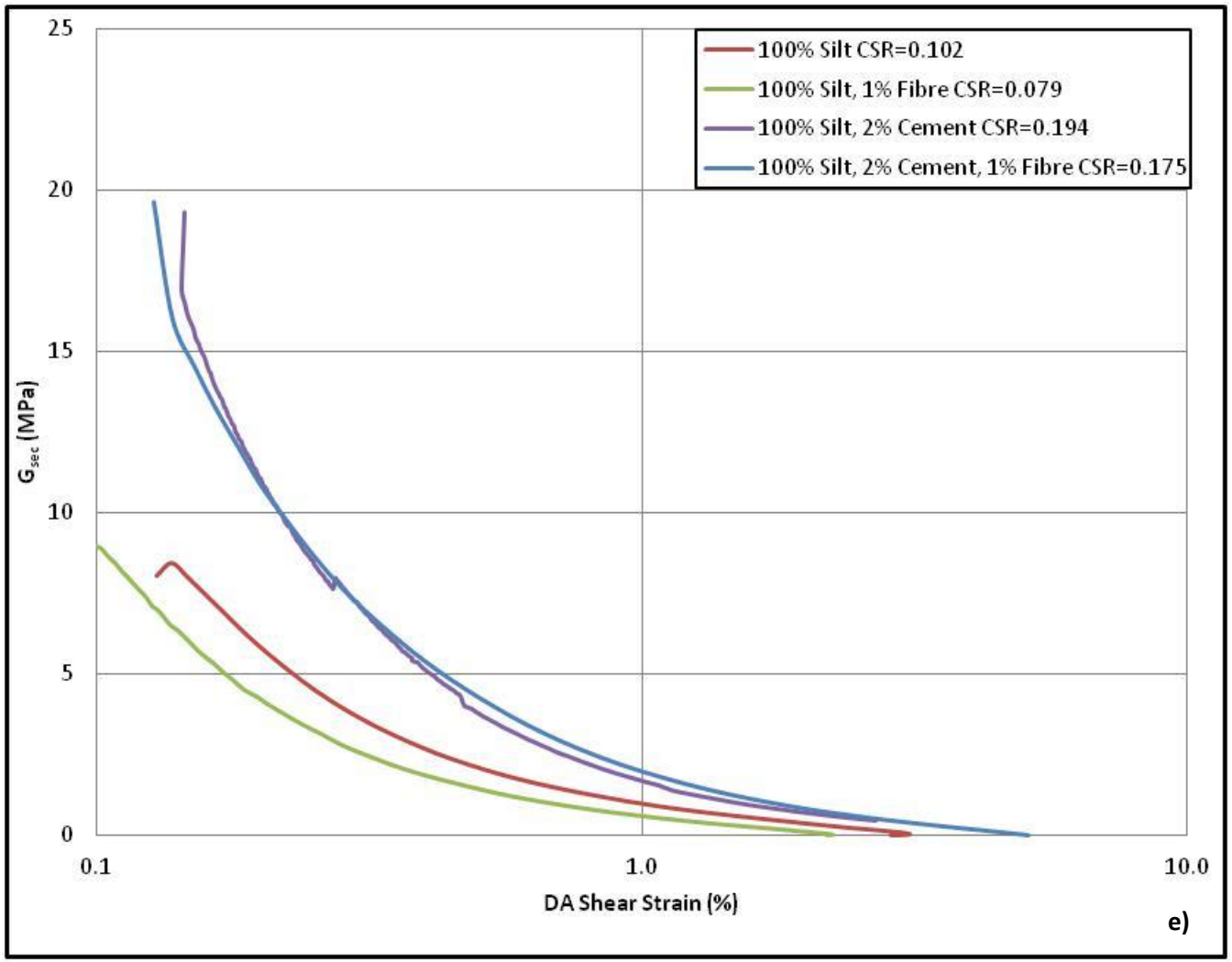

Figure C.3. For 100% silica flour with and without stabilizers at D_r=60%, σ_c'=100kPa a) excess pore pressure vs. N; b) DA shear strain vs. N; c) liquefaction resistance curve; d) damping ratio vs. N; e) G_{sec} vs. DA shear strain

COLIN SCHMIDT

EDUCATION

Master of Engineering Science: Geotechnical and Geoenvironmental Engineering ***2012-2015***
Western University, London

Bachelor of Engineering Science: Civil & Environmental Engineering ***2008-2012***
Western University, London

THESIS AND ACADEMIC PROJECTS

Static and Dynamic Response of Silty Toyoura Sand with PVA Fibre and Cement Additives ***2012-2015***
Master of Engineering Science Thesis
Western University, London

- Developed and implemented a testing regimen and schedule for laboratory testing
- Analyzed and interpreted laboratory test data using Excel and GDS software
- Determined liquefaction potential, permeability, and shear strength parameters and assessed trends in the data

City of London Design Competition – 4th Year Design Project (3rd place) ***2011-2012***
Western University, London

- Third place winner out of eleven participating groups
- Designed chemically enhanced primary treatment system for Greenway Pollution Control Center
- Used monthly wastewater volume statistics to plan a partial-treatment rerouting system for high flow events

Engineering Competition – 2nd Year Engineering Communication Project (1st place) **Nov. *2011***
Western University, London

- Effectively worked as a team to optimize traffic flow at a major London intersection
- Discussed and evaluated current traffic patterns control infrastructure with MTO officials and established cost estimates for improvements

ENGINEERING EXPERIENCE

Geotechnical Engineer in Training ***2015-present***
exp Services Inc.

- Effectively wrote concise and detailed borehole logs identifying soil type and characteristics
- Utilized class and laboratory experience for elevation surveying and determining soil moisture contents
- Planned and organized engineering project elements such as asphalt coring, rock coring, topsoil sampling, borehole drilling, surveying and water sampling

Researcher ***2012-2015***
Dept. of Civil Engineering; Western University, London

- Competently performed direct shear, cyclic triaxial, Rowe and Barden Cell, oedometer, relative density, specific gravity, and sieve tests
- Applied understanding of basic and advanced soil mechanics concepts to interpret lab results
- Scheduled and managed experiments to meet deadlines

COLIN SCHMIDT

Teaching Assistant for Case Studies for Civil Engineers Course ***Winter 2013, 2014***
Dept. of Civil Engineering; Western University, London

- Evaluated performance of 60-80 students and provided constructive feedback on course work
- Led one hour class discussion on civil engineering practices in international development pertaining to the use of wood as a construction material in Peru

Teaching Assistant for Project Management and Engineering Cases Course ***Fall 2012, 2013***
Dept. of Civil Engineering; Western University, London

- Led help sessions on critical path method individually and for groups of 10-20 students
- Utilized knowledge of project management procedures and practices to develop answer keys to assignments and midterms

Researcher ***Winter 2013***
Joint Venture Panama; Western University, London

- Performed one-dimensional consolidation tests on mine tailings to obtain compressibility and permeability data
- Worked within a specified deadline to provide accurate test results

Tour Guide – Western University Green Tours ***2011-2013***
Western University, London

- Presented Western University L.E.E.D. and sustainability initiatives to faculty, students and clubs
- Effectively communicated benefits and shortcomings of environmental initiatives in civil engineering construction works on campus

ADDITIONAL WORK EXPERIENCE

Bartender and Server ***Summer 2011-2012***
Novotel Hotel, Toronto

- Networked with international business men and women
- Used my knowledge of the restaurant industry to assist in the creation of promotional offers

Deputy Returning Officer (DRO) for Provincial Election ***Oct. 2011***
Government of Ontario, Toronto

- Responsible for registering voters, addressing complaints and resolving conflicts
- Managed and monitored voter and poll clerk conduct

COLIN SCHMIDT

VOLUNTEER EXPERIENCE

Representative for International Development Program ***Jan. 2011***
Undergraduate Engineering Society; Western University, London

- Communicated course requirements and civil engineering attributes required to pursue a career in international development

Tour guide - Western Engineering Bonanza ***Mar. 2011***
Undergraduate Engineering Society; Western University, London

- Marketed Western engineering to prospective incoming students

Canada World Youth Volunteer ***Jan 2008***
Canada World Youth; San Francisco De Yojoa, Honduras

- Mixed concrete and built formwork and roadways for a developing township
- Enhanced my international development skills by partnering with Honduran skilled laborers and representatives

SOFTWARE SKILLS

Experienced in:

- Microsoft Office Suite
- GDS Software
- Slope/W
- DEEPSOIL
- AutoCAD
- Gint

TECHNICAL SKILLS

- Geotechnical lab testing
- Writing technical reports
- Soil classification
- Lecturing and public speaking
- Managing teams
- Site surveying

CLUBS AND ASSOCIATIONS

Western Engineering Concrete Canoe Association member ***2012-2014***
Western University

- Aided in design, construction, modelling, analysis and testing of a concrete canoe
- Led team of students in concrete mix design to improve strength and decrease density
- Individually, and in small groups, raised over $2,000 for the team

Co-founder of Western Engineering Association for International Development (WEAID) ***Fall 2012***
Western University

- Increased awareness of the international development program at Western University
- Collaboratively organized fundraisers to send students overseas for civil engineering projects

Captain/co-captain of intramural volleyball team ***2008-2014***
Soccer, ultimate frisbee, trivia club, salsa club ***2012-2014***